

# Seismic Performance and Damage Assessment of Hungarian Road Bridges

by

József Simon

Supervisor:

László Gergely Vigh, PhD

PhD dissertation

Budapest, Hungary, 2016





M Ű E G Y E T E M 1 7 8 2

Budapest University of Technology and Economics

# Seismic Performance and Damage Assessment of Hungarian Road Bridges

PhD dissertation

*(v.2 – modified according to the Reviewers' opinion)*

**József Simon**

Supervisor:

László Gergely Vigh, PhD

Budapest University of Technology and Economics

Department of Structural Engineering

Budapest, 2016

## ***Declaration of authenticity***

I declare that all material presented in this dissertation are either my own work or fully and specifically acknowledged wherever adapted from other sources.

In Hungarian:

Kijelentem, hogy ezt a doktori értekezést magam készítettem és abban csak a megadott forrásokat használtam fel. Minden olyan részt, amelyet szó szerint vagy azonos tartalomban, de átfogalmazva más forrásból átvettem, egyértelműen, a forrás megadásával megjelöltem.

Budapest, February 2<sup>nd</sup> 2016

József Simon

## *Acknowledgements*

I would like to express my deepest appreciation to my supervisor Dr. László Gergely Vigh for his guidance, advice, criticism and insight throughout the study. He encouraged me to start this research, and ensured that I will have experiences and opportunities that will provide a solid foundation for my future.

I would like to thank to Dr. Mohammed Hjjaj and Dr. Hugues Somja from Institut National des Sciences Appliquées de Rennes for their great help during my stay in France. I would also like to thank to Dr. Paolo Franchin, Dr. Paolo Emilio Pinto and Dr. Francesco Cavalieri from Sapienza Università di Roma for their comments and supports during my study in Rome.

I appreciate the help of the members of the Hungarian Transportation Administration for providing the raw data of the database of existing road bridges; and also the help of the members of Hungarian bridge design companies (Főmterv Zrt., MSc Mérnöki Tervező és Tanácsadó Kft., Speciálterv Építőmérnöki Kft., Uvaterv Zrt.) for their advice and for providing bridge plans and bridge data.

I would certainly like to extend my gratitude to the staff of the Department of Structural Engineering, especially to Bettina Badari, Tamás Balogh, Dr. Viktor Budaházy, Eduardo Charters, Dr. László Dunai, Kitti Gidófalvy, Dr. László Horváth, Dr. Mátyás Hunyadi, Dr. Levente Katula, Dr. Tamás Kovács, Dr. Balázs Kövesdi, Árpád Rózsás, Dr. István Völgyi, Dr. Ádám Zsarnóczay with whom I had the opportunity to have several conversations about both professional and personal issues. I have been fortunate to be surrounded by an excellent group of colleagues.

Finally, I am truly grateful for the unconditional and endless support of my family. They deserve special thanks for their help and kindness.

The research work is completed under the support of the following projects and programs:

- Talent care and cultivation in the scientific workshops of BME project supported by the grant TÁMOP-4.2.1/B-09/1/KMR-2010-0002 and TÁMOP-4.2.2/B-10/1-2010-0009.
- Campus Hungary Program supported by the grant TÁMOP-4.2.4.B/1-11/1-2012-0001.
- János Bolyai Research Scholarship of the Hungarian Academy of Sciences.

## *Abstract*

Recent studies showed that Hungary can be characterized by moderate seismicity. In the pre-Eurocode era, most bridges were built without seismic design; their seismic behavior is not known. Bridges are key elements of the transportation network, therefore it is an important issue to evaluate their seismic performance to estimate the economic and financial consequences due to the developing damages caused by a seismic event.

State of the art vulnerability assessment methods are based on fragility analysis. The fragility curves of the structure are conditional probability functions which give the probability of a bridge attaining or exceeding a particular damage level for an earthquake of a given intensity level. Fragility curves are useful tools in both pre- and post-earthquake situations to work out retrofit strategies and to plan emergency routes. They can also be used to calculate the probability of failure if the hazard of the design site is known.

The long-term goal of the research is to carry out a nationwide seismic performance evaluation of road bridges in Hungary. For this reason, an automatic performance evaluation framework is worked out. Unfortunately, the existing bridge database does not provide sufficient information for reliable numerical modeling of each structure. Thus, bridges are grouped into 8 bridge classes based on their contribution to the whole inventory and on their various structural attributes; then a portfolio of 30 structures representing typical bridge types in Hungary is created for further analysis.

Before the fragility analyses, a preliminary study is carried out to understand the seismic behavior, and to highlight critical configurations and bridge components. The fragility evaluation is conducted with detailed 3-D numerical models subjected to hazard consistent earthquake ground motions with various intensity levels using non-linear time-history analysis. The results show that the insufficient pier shear resistance is a typical problem considering all bridge types, and that the monolithic joints are highly vulnerable in case of precast multi-girder and slab bridges. Comparing the reliability of the structures, it is also shown that precast multi-girder bridges and bridges with conventional bearings perform better, while slab bridges and precast multi-girder bridges with elastomeric bearings have worse behavior. In certain cases, the improperly chosen structural configuration and the lack of seismic design lead to an unacceptable low reliability level.

As a last step, different possible retrofit strategies are evaluated and proposed for vulnerable bridge configurations. Based on the results of the research, seismic design concepts for new bridges are also provided.

## *Összefoglalás*

A legújabb kutatások szerint Magyarország mérsékelt szeizmicitással jellemezhető. Az Eurocode bevezetése előtt a hidak többsége szeizmikus tervezés nélkül épült, szeizmikus viselkedésük nem ismert. A hidak az infrastruktúra kulcsfontosságú elemei, így szeizmikus teljesítőképességük kiértékelése elsődleges feladat, hogy becslni lehessen egy esetleges földrengés során kialakuló károk pénzügyi és gazdasági következményeit.

A korszerű károsodáselemzési eljárások törékenységi vizsgálaton alapulnak. A szerkezet törékenységi görbéi feltételes valószínűséget reprezentálnak, megadják egy adott károsodási határállapot túllépésének valószínűségét a földrengés intenzitásának függvényében. A törékenységi görbék hatékonyan alkalmazhatóak mind földrengés előtti, mind utáni helyzetekben megerősítési tervek vagy elérhetőségi útvonalak kidolgozásához. Segítségükkel számítható a szerkezet tönkremeneteli valószínűsége is, amennyiben rendelkezésre áll a tervezési helyszínrre vonatkozó szeizmikus veszélyeztetettség.

A kutatás hosszú távú célja a közúti hidak szeizmikus teljesítőképességének kiértékelése az egész ország területén. Ennek érdekében egy automatizált kiértékelő keretrendszert dolgoztam ki. A meglévő adatbázisban lévő adatok nem elégségesek a hidak megbízható modellezéséhez, így a hidakat 8 osztályba soroltam fontosságuk és szerkezeti jellemzőik szerint, majd egy 30 reprezentatív hídból álló portfóliót hoztam létre további vizsgálatokra.

A törékenységi vizsgálatok előtt egy közelítő előzetes vizsgálatot végeztem, hogy megismerjem a hidak szeizmikus viselkedését és a kritikus komponensek, kialakítások körét. A törékenységi vizsgálatot fejlett 3 dimenziós numerikus modelleken nemlineáris időtörténeti analízissel hajtottam végre, melyhez a veszélyeztetettséggel konzisztens, többféle intenzitású földrengésrekordokat alkalmaztam. Az eredmények szerint a pillérek elégtelen nyírési teherbírása általános probléma, míg a monolit kapcsolat nagyon kritikus sűrűbordás és lemezhidak esetén. A hidak megbízhatóságát összehasonlítva kimondható, hogy a sűrűbordás és hagyományos sarus hidak jobban, míg a lemezhidak és elasztomer sarus sűrűbordás hidak rosszabbul viselkednek. Egyes esetekben a nem megfelelő szerkezeti kialakítás és a szeizmikus tervezés hiánya miatt a megbízhatósági szint elfogadhatatlanul alacsony.

Utolsó lépésként különböző lehetséges megerősítési módokat hasonlítottam össze és elemeztem azok hatékonyságát a kritikus hídszerkezetek esetén. A kutatás eredményei alapján szeizmikus tervezési koncepciókat fogalmaztam meg új hidak gazdaságos és megfelelő biztonságú tervezéséhez.

# Table of contents

<b>Chapter 1</b>	<b>Introduction .....</b>	<b>4</b>
1.1	<i>Problem description .....</i>	4
1.2	<i>State of the art seismic vulnerability assessment .....</i>	5
1.3	<i>Methodology and primary tasks .....</i>	6
1.4	<i>Organization of the thesis .....</i>	8
<b>Chapter 2</b>	<b>Seismic Hazard in Hungary .....</b>	<b>9</b>
2.1	<i>Seismicity of Hungary .....</i>	9
2.2	<i>Seismic design in Hungary .....</i>	10
2.3	<i>Probabilistic seismic hazard analysis .....</i>	11
2.3.1	Introduction .....	11
2.3.2	Hazard curve and disaggregation .....	12
2.3.3	Uniform Hazard Spectrum .....	13
2.4	<i>Application of PSHA for Hungarian sites .....</i>	13
2.4.1	Introduction .....	13
2.4.2	Description of the implemented procedure .....	14
2.4.3	Comparison of UHS and standard spectra .....	15
2.5	<i>Determination of the seismic load .....</i>	16
2.5.1	Artificial record generation .....	16
2.5.2	State of the art record selection method .....	18
2.5.3	Generated and selected records for further analysis .....	19
2.6	<i>Summary .....</i>	21
<b>Chapter 3</b>	<b>Bridge Inventory of Hungary .....</b>	<b>22</b>
3.1	<i>Database of existing bridges .....</i>	22
3.2	<i>Aspects of regional damage evaluation .....</i>	22
3.2.1	Knowledge Levels .....	22
3.2.2	Evaluation of the whole inventory .....	23
3.3	<i>Extension of the database .....</i>	23
3.4	<i>Statistical evaluation of the database .....</i>	24
3.4.1	Bridge classification .....	24
3.4.2	Statistical analysis of the bridge classes .....	26
3.4.3	Representative structural types .....	29
3.5	<i>Summary .....</i>	31
<b>Chapter 4</b>	<b>Numerical Model Development .....</b>	<b>32</b>
4.1	<i>Numerical modeling aspects .....</i>	32
4.2	<i>General illustration of the developed numerical model .....</i>	33
4.3	<i>Modeling of bridge components .....</i>	34
4.3.1	Superstructure, pier cap beam .....	35
4.3.2	Superstructure-substructure joints .....	35
4.3.3	Piers .....	40
4.3.4	Abutments and backfill soil .....	41
4.3.5	Foundation .....	43
4.4	<i>Summary .....</i>	44
<b>Chapter 5</b>	<b>Preliminary Seismic Analysis of Existing Bridges .....</b>	<b>45</b>
5.1	<i>Review of the parametric analysis of continuous girder bridges .....</i>	45
5.2	<i>Applied procedure for parametric seismic analysis .....</i>	46
5.3	<i>Parametric analysis of integral precast multi-girder (PMG-I) bridges .....</i>	46
5.3.1	Description of PMG-I bridges .....	46
5.3.2	Numerical modeling issues .....	48
5.3.3	Modal analysis results .....	48
5.3.4	Effect of the soil structure interaction .....	49
5.3.5	Calculated seismic demands .....	50
5.3.6	Critical components and layouts .....	53
5.4	<i>Parametric analysis of reinforced concrete slab (SLAB) bridges .....</i>	54
5.4.1	Description of SLAB bridges .....	54
5.4.2	Numerical modeling issues .....	55
5.4.3	Modal analysis results .....	55

5.4.4	Effect of the soil structure interaction .....	56
5.4.5	Calculated seismic demands .....	56
5.4.6	Critical components and layouts .....	58
5.5	<i>Estimation of critical bridges based on the preliminary study</i> .....	58
5.6	<i>Summary</i> .....	59
<b>Chapter 6</b>	<b>Seismic Fragility Assessment of Existing Bridges .....</b>	<b>61</b>
6.1	<i>Examined bridge configurations</i> .....	61
6.2	<i>Adopted method for fragility analysis</i> .....	61
6.3	<i>Damage limit states</i> .....	63
6.4	<i>Uncertainties applied during the analysis</i> .....	64
6.5	<i>Aspects of the modeling and analysis assumptions</i> .....	64
6.6	<i>Parametric fragility analysis of PMG-I bridges</i> .....	66
6.6.1	Calculated demands .....	66
6.6.2	Optimal intensity measure .....	68
6.6.3	Fragility curves .....	68
6.7	<i>Fragility analysis of portfolio bridges</i> .....	70
6.7.1	Optimal intensity measure .....	70
6.7.2	Fragility curves .....	71
6.8	<i>Calculated reliability of the structures</i> .....	75
6.8.1	Introduction .....	75
6.8.2	Reliability of PMG-I bridges .....	76
6.8.3	Reliability of the portfolio bridges .....	77
6.9	<i>Comparison of intensity and reliability based evaluation methods</i> .....	79
6.10	<i>Application of fragility curves</i> .....	80
6.10.1	Pre-earthquake actions and prioritization of retrofit strategies .....	80
6.10.2	Post-earthquake evaluation of bridges .....	81
6.11	<i>Summary</i> .....	82
<b>Chapter 7</b>	<b>Proposed Retrofit Methods and Design Concepts .....</b>	<b>83</b>
7.1	<i>Possible retrofit methods</i> .....	83
7.1.1	Conventional strenghtening methods .....	83
7.1.2	Application of anti-seismic devices .....	84
7.2	<i>Evaluation of possible retrofit methods</i> .....	85
7.2.1	Conventional strengthening .....	85
7.2.2	Application of anti-seismic devices .....	86
7.3	<i>Simplified analysis method for conceptual retrofit design</i> .....	89
7.3.1	Equivalent linear analysis method .....	89
7.3.2	Limitations of the equivalent linear method .....	90
7.3.3	Conceptual seismic retrofit design of M0 Háros highway bridge .....	92
7.4	<i>Proposed design concepts</i> .....	95
7.4.1	Bridges with monolithic joints .....	95
7.4.2	Bridges with conventional bearings .....	96
7.5	<i>Summary</i> .....	97
<b>Chapter 8</b>	<b>Summary and Conclusions .....</b>	<b>98</b>
8.1	<i>Primary results and impact</i> .....	98
8.2	<i>Recommendations for future work</i> .....	99
8.3	<i>New scientific results</i> .....	99
8.4	<i>Publications of the author on the subject of the thesis</i> .....	102
<b>References</b>	.....	<b>103</b>
<b>Appendix A:</b>	<b>Ground motion prediction and correlation equations, calculation of intensity measures ...</b>	<b>110</b>
<b>Appendix B:</b>	<b>Extension of the existing road bridge database .....</b>	<b>112</b>
<b>Appendix C:</b>	<b>Fundamental periods of the examined bridges .....</b>	<b>116</b>
<b>Appendix D:</b>	<b>MAPGA values for PMG-I and SLAB bridges .....</b>	<b>119</b>
<b>Appendix E:</b>	<b>Detailed description of portfolio bridges .....</b>	<b>126</b>
<b>Appendix F:</b>	<b>Damage limit states for the examined bridges .....</b>	<b>157</b>
<b>Appendix G:</b>	<b>Fragility parameters of the examined bridges .....</b>	<b>159</b>
<b>Appendix H:</b>	<b>New scientific results in Hungarian .....</b>	<b>161</b>

## List of symbols

AI	Arias Intensity	STU	Shock Transmission Unit
ASI	Acceleration Spectrum Intensity	TG	Technical Guide
CAV	Cumulative Absolute Velocity	UHS	Uniform Hazard Spectrum
CFRP	Carbon Reinforced Fiber Polymer	ULS	Ultimate Limit State
COD	Coefficient of Determination	VSI	Velocity Spectrum Intensity
COV	Coefficient of Variation		
CS	Conditional Spectrum		
CSUS	Central and Southeastern United States		
DC	Demand-Capacity ratio		
DSI	Displacement Spectrum Intensity		
ECDF	Empirical Cumulative Distribution Function		
ELA	Equivalent Linear Analysis		
EQ	Seismic Load Combination		
FEM	Finite Element Method		
GCIM	General Conditioned Intensity Measure		
GM	Ground Motion		
GMPE	Ground Motion Prediction Equation		
IBD	Integrated Bridge Database		
IDA	Incremental Dynamic Analysis		
IM	Intensity Measure		
KL	Knowledge Level		
KS	Kolmogorov-Smirnov		
LN	Lognormal		
LNSTD	Lognormal Standard Deviation		
LS	Limit State		
MAPGA	Maximum Acceptable Peak Ground Acceleration		
MLN	Multivariate Lognormal		
MMRSA	Multi-Modal Response Spectrum Analysis		
MSA	Multiple Stripes Analysis		
MSC	Mercalli-Sieberg-Cancani intensity scale		
NLTHA	Nonlinear Time-History Analysis		
PDF	Probability Density Function		
PGA	Peak Ground Acceleration		
PGV	Peak Ground Velocity		
PSDM	Probabilistic Seismic Demand Model		
PSHA	Probabilistic Seismic Hazard Analysis		
RC	Reinforced Concrete		
RCSM	Relative Cost of Safety Measure		
Sa	Spectral Acceleration		
SDOF	Single Degree of Freedom		
SI	Seismic Isolator		
SSI	Soil-Structure Interaction		

# Chapter 1

## Introduction

### 1.1 Problem description

Bridges are key elements of the infrastructure. Damages induced by severe seismic events (San Fernando 1971; Northridge 1971 and 1994; Kobe 1995; Chi-Chi 1999; Haiti 2010) showed that bridges are the most vulnerable components of the transportation system. Their failure causes significant economic consequences: disruption to the traffic, transportation and emergency routes as well as economic loss and repair costs. In high seismicity regions (such as the West Coast of the US, Japan, the Mediterranean region of Europe etc.), people are aware of significant earthquakes, lessons learnt from previous devastating seismic events induced the improvement of seismic design and also the application and evaluation of retrofit strategies. In moderate or low seismic areas (e.g. eastern part of the US, northern parts of Europe etc.), seismic risk mitigation efforts have lagged, because in these regions large earthquakes are infrequent and may not have been experienced for over a century while modern design methodologies and codes have been developed (Elnashai and Di Sarno 2008). Most bridges were designed with no seismic consideration; and due to inadequate detailing, even moderate earthquakes might cause severe damage (Nielson 2005). For this reason, the uniform European standard (CEN 2008a,b) prescribes the seismic design of new and retrofitted structures even in moderate and low seismic regions.

Hungary had been considered a region of low seismicity throughout the past century. Per the formal Hungarian road bridge standard (ÚT 2004), only bridges with spans over 50 m had to be designed for seismic actions regardless of their other (often more relevant) parameters. Moreover, the standard did not propose any particular seismic design methodology, it only stated that the design shall be carried out “based on acknowledged earthquake engineering principles”, but did not specify further details. Unfortunately, this resulted in inadequate seismic detailing of several road bridges. Along with the replacement of the national seismic regulations with the European standard, the seismic hazard of Hungary was revised by the Georisk Earthquake Research Institute releasing a new peak ground acceleration (PGA) map (Tóth et al. 2006). The region is characterized with moderate seismicity with 0.08-0.15g PGA values (for the seismic hazard associated with 10% probability of exceedance in 50 years).

The moderate seismicity and the lack of seismic design raise the question whether Hungarian road bridges are able to retain their structural integrity after a design seismic event

or may suffer significant damage. Experience with existing and new structures in the last decade (Vigh et al. 2006, Simon and Vigh 2012), and parametric study on continuous girder bridges (Zsarnóczy et al. 2014) showed that a large portion of road bridges may be vulnerable to earthquake loads. Therefore, it is an urgent and important issue to evaluate the seismic performance and vulnerability of conventional road bridges in Hungary.

## 1.2 State of the art seismic vulnerability assessment

State of the art seismic vulnerability assessment is based on analytical fragility curves (Billah and Alam 2015) created with non-linear time-history analysis (NLTHA). Fragility curves are conditional probability statements giving the probability of reaching a particular limit state (LS) for a given intensity measure (IM) level (Fig. 1.1). For the unconditional probability of failure, the IM exceedance rate for the reference period is needed, which is provided by the seismic hazard curve of the site (Vigh et al. 2016). Note that failure does not necessary mean collapse, it only shows that the structure reached a predefined LS. Fragility analysis is a useful tool, since it enables retrofit decisions regarding economical and financial aspects. Besides, fragility curves can be used for other pre- and post-earthquake situations. Comparing the seismic performance via fragility curves, vulnerable bridge types and configurations can also be highlighted, retrofit prioritization can be made. They can also be used to assign a level of functionality to each bridge after a seismic event that is essential for the determination of emergency routes and recovery planning (Basoz and Kiremidjian 1996).

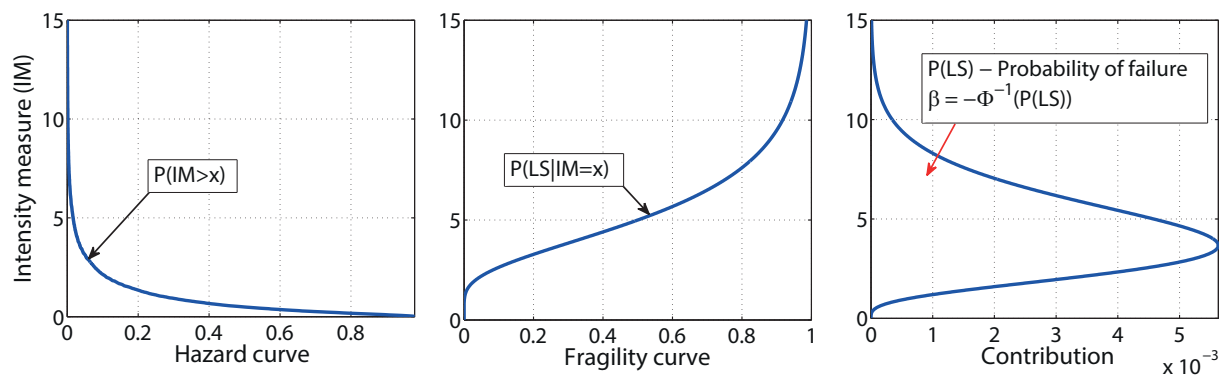


Fig. 1.1 Illustration of the probability of failure.

Comprehensive seismic fragility evaluation of road bridges has been carried out in Central and Southeastern US (CSUS) (Nielson 2005), Italy (Borzi et al. 2015), Greece (Moschonas et al. 2009), Turkey (Avşar et al. 2011) and Algeria (Kibboua et al. 2014), but to the best of my knowledge, there is no such regional study on road bridges in a moderate seismic zone in Europe. The mentioned studies can be used to presume the seismic behavior of Hungarian bridges, however, there are several reasons why they cannot be adapted directly: 1) the higher

seismicity of the mentioned countries in Europe results in different design traditions, the structural characteristics and details may be different; 2) Hungarian multi-span bridges are dominantly continuous, while simply supported versions are equally preferred in other countries; 3) the vulnerability is dependent on the seismic action determined in accordance with the seismic characteristics of the site, thus results are expected to differ in Hungary.

In recent studies, investigation of the seismic performance of road bridges was carried out applying two different approaches: 1) bridge classification and the analysis of archetype bridges; 2) individual bridge analysis. In the CSUS (Nielson 2005) typical bridge types were chosen with the statistical evaluation of the National Bridge Inventory database (FHWA 2002). The classification was in line with the proposal of HAZUS (NIBS 1999). Evaluation of the seismic performance was carried out by creating analytical fragility curves of the chosen bridge types with sophisticated numerical models and NLTHA. A more complex classification method was applied in Greece (Moschonas et al. 2009) and Turkey (Avşar et al. 2011). In the first case, static pushover, while in the second study NLTHA is used for fragility analysis. In a recent study in Italy (Borzi et al. 2015), prior to the nationwide seismic performance evaluation, an extensive data collection (e.g. geometry, material of each bridge) was performed providing a solid basis for standalone bridge fragility evaluation. The bridge-by-bridge analysis showed great variance of fragilities even for bridges in the same typological class, questioning the validity of typological classification for fragility derivation.

In conclusion, it is recognized that reliable fragility curves are required to obtain a realistic picture about the seismic performance of the whole transportation network in case of both pre- and post-earthquake situations. This is feasible through the analysis of individual bridges using NLTHA with highly detailed nonlinear numerical models.

### **1.3 Methodology and primary tasks**

The main goal of the research is to determine the probability of failure of conventional road bridges in Hungary based on analytically derived fragility curves. The assessment of the whole bridge inventory requires an evaluation framework where automatization is of great importance due to the large number of structures. The proposed framework is presented in Fig. 1.2. Individual bridge analysis demands a database of all the essential data for reliable numerical modeling. Probabilistic Seismic Hazard Analysis (PSHA) is used to obtain hazard curves and to predict the expected spectral and other IMs for a site. An artificial record generation and a record selection module are needed to provide either artificial or recorded real ground motions for NLTHA. The modeling of thousands of bridges is not feasible by

manual numerical model building, therefore, an automatic model generation is required that communicates with the database and inquires data for the model. Using the automatically created numerical models, the fragility analysis along with the post-processing are also automatized. The fragility curves can be applied to evaluate retrofit strategies, to plan post-earthquake actions and to calculate the probability of failure related to pre-defined limit states.

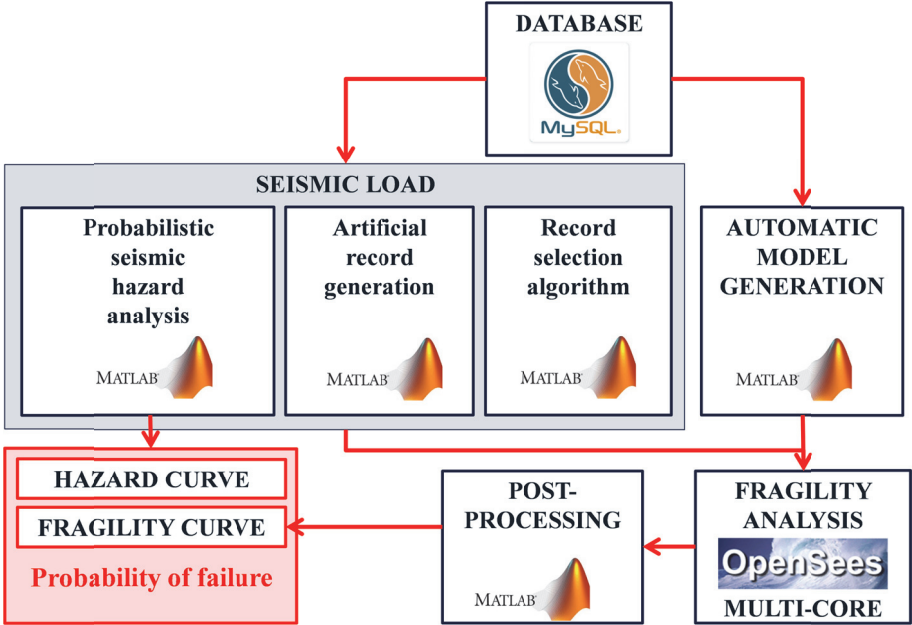


Fig. 1.2. Framework for automatic seismic performance evaluation.

The existing bridge database (Integrated Bridge Database; IBD) operated by the Hungarian Transport Administration (HTA 2015) is created for road management and maintenance purposes. It is not sufficient for a detailed description of the structures, thus individual analysis is not a feasible option. Despite the lack of data, the framework is established in a way that after an extensive data collection phase, the evaluation could be carried out automatically for the whole road network. Meanwhile, the research is started with typical bridge configurations to provide insight about the seismic performance of typical road bridges.

Before carrying out fragility analysis, preliminary analysis is needed to understand the seismic behavior of the most common bridge types with a wide range of different layouts. A simplified parametric study was carried out for continuous girder bridges with conventional bearings in (Zsarnóczay et al. 2014). However, there is a need for the analysis of concrete bridge types with monolithic joints (e.g. precast multi-girder and slab bridges), the seismic behavior of which may be significantly different. Precast multi-girder and slab bridges are extremely popular on primary roads. Their main parameters (e.g. number of spans, pier cross-

section etc.) can be described with a compact parametric field, while the diversity of the structural attributes of other bridge classes makes a parametric analysis impractical.

The following primary tasks are set out considering the observations above:

- Review the seismicity and seismic design in Hungary. Characterize the seismic hazard and employ an artificial record generation and a record selection algorithm for Hungarian circumstances.
- Examine the structure of the existing bridge database; determine the missing data required for reliable seismic analysis, then work out the possible extension. Choose typical bridge classes for further analysis and determine their most important structural attributes. Compile a portfolio of representative bridges for further analysis.
- Create an automatic numerical model generation module. Review the numerical modeling of bridge components and work out non-linear numerical models for each bridge class.
- Conduct a preliminary seismic analysis to reveal critical components and layouts of typical road bridges in Hungary. Estimate the number of critical bridges in the bridge stock considering the most typical bridge classes.
- Carry out fragility analysis; highlight the most critical bridge components and configurations; determine the probability of failure.
- Propose concepts for new bridge design. Review and suggest possible retrofit methods for vulnerable bridges. Evaluate retrofit strategies with fragility analysis of the retrofitted configurations. Provide a simplified analysis for conceptual retrofit design.

#### **1.4 Organization of the thesis**

The dissertation consists of eight chapters as follows. Characterization of the seismic hazard in Hungary along with the artificial record generation module and the implemented record selection method are presented in Chapter 2. Chapter 3 illustrates the evaluation of the existing road bridge database. Proposal is given for the extension. Bridge classification and statistical analysis of the database are also presented in this chapter. This is followed by the presentation of the detailed 3 dimensional numerical models in Chapter 4. Chapter 5 and 6 provide detailed description and results of the preliminary and the fragility analysis, respectively. Design concepts and the evaluation of retrofit strategies are presented in Chapter 7, where a proposal for a simplified analysis method for conceptual seismic retrofit design can also be found. Summary, conclusions and future recommendations are given in Chapter 8.

## Chapter 2

### Seismic Hazard in Hungary

#### 2.1 Seismicity of Hungary

Hungary lies in the Pannonian Basin and as part of the Pannonian region, it is situated between the Mediterranean area and the Eastern European platform. The former is one of the most seismically active regions in the world, while the latter is practically an aseismic area. The tectonics of the region is rather complex, caused by the collision of the Eurasian and African plates (Horváth 1988). Deformations are caused by the movements of the Adria microplate relative to the European plate (Bada et al. 1999).

One of the key steps of the seismic characterization in Hungary was the compilation of a comprehensive earthquake catalogue of the Pannonian region containing more than 20.000 events from 456 to 1995 (Zsíros 2000). Despite the fact that devastating earthquakes are extremely rare, there are some information available about past damaging earthquakes. The oldest known severe earthquake is from the Roman times in 456, which ruined the city of Savaria. The first event documented with more details is the Komárom earthquake in 1763 (Szeidovitz 1990). Table 2.1 shows historical Hungarian earthquakes with higher magnitudes.

Table 2.1. Historical earthquakes with higher magnitudes in Hungary.

Area	Szombathely	Komárom	Mór	Érmellék	Eger	Dunaharaszti	Berhida	Oroszlány
Year	456	1763	1810	1834	1925	1956	1985	2011
Magnitude	6.1	6.3	5.4	6.2	5	5.6	4.9	4.7

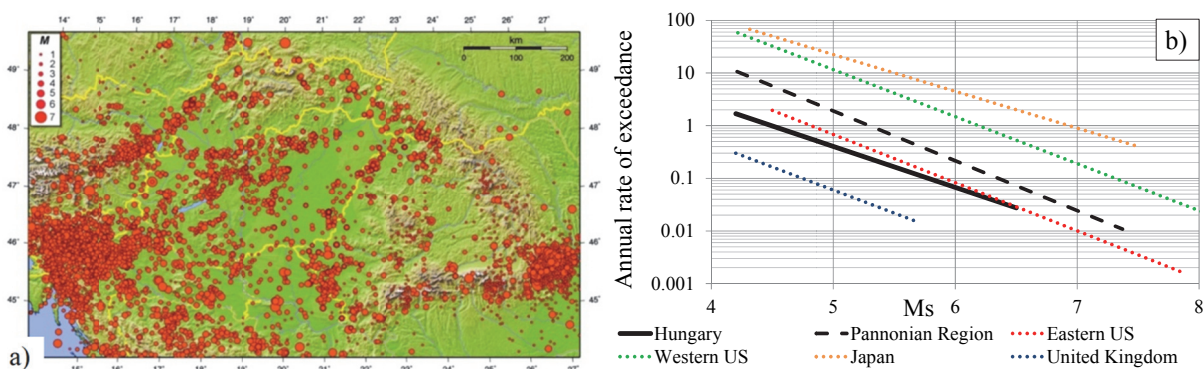


Fig. 2.1 a) Distribution of earthquake epicenters with different magnitudes in the Pannonian region. b) Annual rate of magnitude exceedance in various regions of the world (normalized to  $10^6 \text{ km}^2$ ) (Tóth et al. 2006).

Based on the catalogue, spatial distribution of the epicenters of different magnitudes in the Pannonian region is presented in Fig. 2.1a (Tóth et al. 2006). The region is a typical example of distributed seismicity. Most earthquakes are hard to associate with a certain fault due to the lack of accurate seismic and geological information especially in case of events with magnitudes lower than 4. The spatial distribution of epicenters is diffused, however, there are

some areas where the occurrences show higher proneness (e.g. Komárom, Mór, Kecskemét, Dunaharaszti, Nagykanizsa). In such areas (e.g. Hungary), where the proper characterization of underlying faults is not feasible, Poisson process is used per current practice to represent the temporal occurrence of seismic events. The annual rate of exceedance ( $\lambda_m$ ) of different magnitudes ( $m$ ) can be characterized by an exponential distribution as suggested by Gutenberg and Richter (1944) with  $a$  and  $b$  constants:

$$\log_{10}\lambda_m = a - bm, \quad (2.1)$$

Fig. 2.1b shows the seismic activity rate of Hungary and some other regions for comparison. The seismicity of Hungary is similar to that of the Eastern part of the United States. Both the Pannonian Basin and the whole region are between the high (e.g. Japan, Western part of the United States) and low (e.g. United Kingdom) seismic areas, it can be characterized with moderate seismicity. Return periods of magnitude 6 and 5 earthquakes in Hungary are around 100 and 20 years, respectively. Based on high sensitivity monitoring data, Tóth et al. (2004) concluded that the average number of magnitude 4 earthquakes is around 4 per year; while the annual number of magnitude 2 earthquakes is about 30. The expected highest magnitude is approximately 6.5 in Hungary. The hypocentral depths are in the range of 6-15 km; thus this region can be characterized with shallow crustal seismicity.

## 2.2 Seismic design in Hungary

The first Technical Specification ME-95-72 related to seismic design was published in 1972 (ÉVM 1972) dealing with the design of block houses with precast elements. The rules were based on rough estimations, the seismic load was determined using the Mercalli-Sieberg-Cancani (MSC) intensity scale. The specification did not explain how to define this intensity at the design site. In 1978, a Technical Guideline (TG) MI-04.133 (ÉTK 1978) was released still using the MSC scale, however an intensity map was given to help the designers. The application of the TG was not obligatory, it was meant to be a design aid for engineers. In the following decades, Hungarian building (HSI 1986a) and road bridge design codes (HSI 1986b) mentioned earthquakes as extreme loads but did not give any instructions only referred to the MI-04.133 TG. Other codes such as foundation design (HSI 1987) or railway bridge design (HSI 1990) regulations did not mention seismic effects at all.

In 1998, a new Building Act came into force prescribing the seismic design as an obligatory task in case of new or retrofitted structures in accordance with EC8. The intensity based approach of EC8-1 and EC8-2 prescribe no-collapse and damage limitation criteria at the hazard level of 10% probability of exceedance in 50 and 10 years, respectively. The

hazard is described with the PGA on rock sites. The standard response spectrum (Fig. 2.2) considers the dominant magnitude, soil condition and the damping or energy dissipation of the structure. Afterwards, the MSZ-ENV 1998-1-1 (HSI 1998a) was released. The MSC intensity based calculation was replaced by a PGA hazard map with three zones (Fig. 2.3a) with 0.06-0.10 g PGA values. In 2006, a new seismic hazard map (Fig. 2.3b) was created by Tóth et al. (2006) based on a state-of-the-art PSHA showing increased hazard (PGA of 0.08-0.15 g) in some areas compared to previous values.

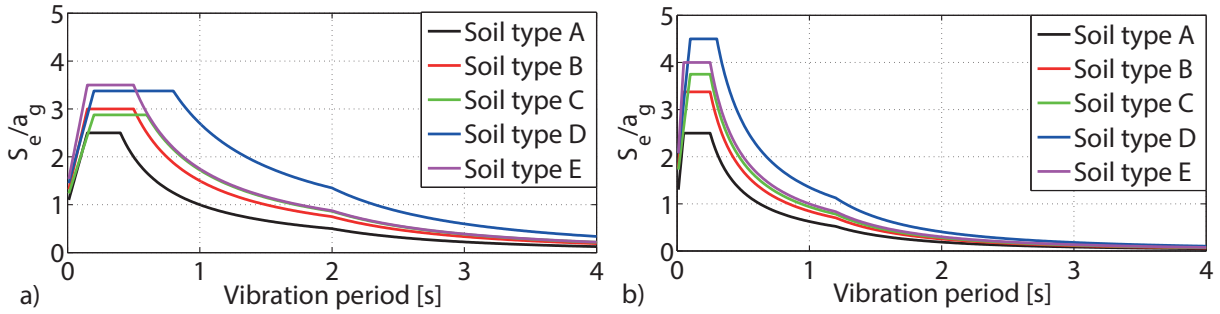


Fig. 2.2. Standard elastic response spectra (EC8-1) for different soil types (A,B,C,D,E). a) Type 1 spectra for dominant magnitudes over 5.5; b) Type 2 spectra for  $M < 5.5$ .

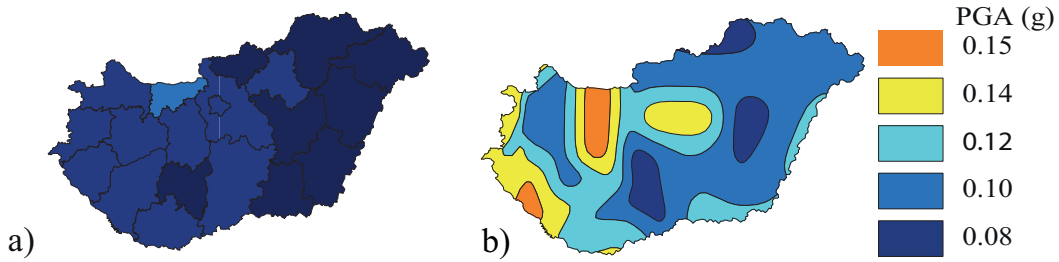


Fig. 2.3. Seismic zone map of Hungary (10% probability of exceedance in 50 years for PGA) per: a) MSZ-ENV 1998-1-1; b) National Annex to MSZ-EN 1998-1-1 (HSI 2008; Tóth et al. 2006).

## 2.3 Probabilistic seismic hazard analysis

### 2.3.1 Introduction

PSHA is a tool to quantify uncertainty about the location, size, and resulting shaking intensity of future earthquakes (Cornell 1968). It aims to consider all possible earthquake events and resulting ground motions, along with their associated probabilities of occurrence. PSHA is carried out in five steps (see Fig. 2.4; Baker 2008): 1) identify all earthquake sources capable of producing damaging ground motions; 2) characterize the distribution of earthquake magnitudes for each source:  $f_M(m)$ ; 3) characterize the distribution of source-to-site distances associated with potential earthquakes:  $f_R(r)$ ; 4) estimate the resulting distribution of ground motion intensity as a function of earthquake magnitude ( $M$ ), distance ( $R$ ) and other rupture characteristics (e.g. faulting style, soil conditions etc.;  $\Theta$ ); 5) combine the uncertainties using the total probability theorem to calculate the probability of an IM exceeding a given level ( $x$ ):

$$P(IM > x) = \int_{m_{min}}^{m_{max}} \int_{r_{min}}^{r_{max}} P(IM > x | m, r, \theta) f_M(m) f_R(r) dr dm. \quad (2.2)$$

The discrete form of Eq. (2.2) can be efficiently used for numerical calculation:

$$P(IM > x) = \sum_{j=1}^{n_M} \sum_{k=1}^{n_R} P(IM > x | m_j, r_k, \theta) P(M = m_j) P(R = r_k), \quad (2.3)$$

The first term in Eq. (2.2) can be determined as follows. The ground motion prediction (or attenuation) equation (GMPE) provides the mean ( $\overline{\ln(IM)}$ ) and standard deviation ( $\sigma_{\ln IM}$ ) of the lognormally distributed IM at the site for a seismic event with a specific magnitude ( $m_j$ ), distance ( $r_k$ ) and other characteristics ( $\theta$ ). The exceedance probability is then given as:

$$P(IM > x | m_j, r_k, \theta) = 1 - \Phi\left(\frac{\ln(x) - \overline{\ln(IM)}}{\sigma_{\ln IM}}\right). \quad (2.4)$$

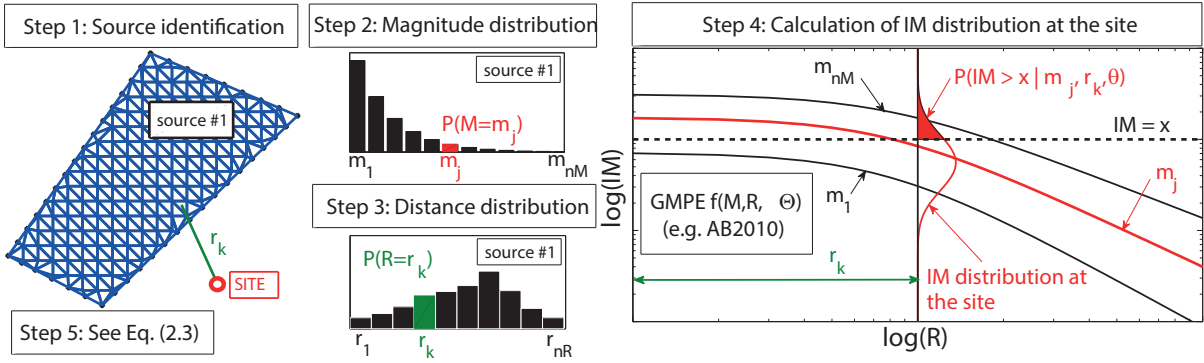


Fig. 2.4 Five steps of the PSHA procedure.

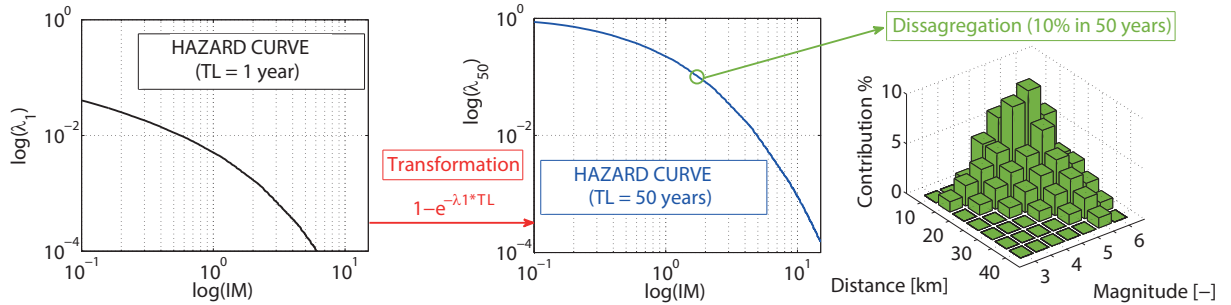


Fig. 2.5 Hazard curves for 1 year and 50 years. Dissaggregation for a specific hazard level.

### 2.3.2 Hazard curve and disaggregation

The seismic hazard at the site can be characterized by the seismic hazard curve. It can also be used to calculate the probability of failure of the examined structure if the corresponding fragility curve is available. Eq.(2.3) gives the probability of  $IM > x$ , however no information is provided on the annual exceedance rate. The annual rate of  $IM > x$  can be calculated as:

$$\lambda_1(IM > x) = \sum_{i=1}^{n_{source}} \lambda_m(M_i > m_{min}) \sum_{j=1}^{n_M} \sum_{k=1}^{n_R} P(IM > x | m_j, r_k, \theta) P(M_i = m_j) P(R_i = r_k), \quad (2.5)$$

where the first term is the annual occurrence rate of earthquakes greater than  $m_{min}$  (applied due to the lack of engineering importance of lower magnitudes; and the lack of available data) for the source (see Eq.(2.1)); and  $n_{source}$  is the number of relevant sources considered. The ground motion intensity against the annual rate of exceedance can be determined using

Eq.(2.5) at several  $x$  values (Fig. 2.5); the obtained curve is the seismic hazard curve.  $\lambda$  can be calculated for other reference periods ( $T_L$ ) by applying a Poisson model:

$$\lambda_{T_L} = 1 - e^{-\lambda_1 T_L}. \quad (2.6)$$

The hazard curve is aggregated from the hazards of multiple possible earthquakes. Seismic hazard disaggregation shows which values of earthquake properties (typically magnitude and distance) contribute most to a specific hazard level (see Fig. 2.5)

### 2.3.3 Uniform Hazard Spectrum

The typical representation of the seismic action is the acceleration response spectrum showing the spectral accelerations of a single degree of freedom (SDOF) system at various fundamental periods. Different earthquakes have different frequency contents, therefore the calculated response spectra may vary as well. To account for this variance, structural design is usually conducted with an envelope spectrum of all possible earthquakes at the site. The determination of such spectrum can be carried out as follows (see Fig. 2.6): 1) determine the hazard curve for spectral acceleration values at several fundamental periods; 2) obtain the spectral acceleration values corresponding to the same hazard level of  $\lambda_{T_L}$  for all fundamental periods (e.g. design  $\lambda_{T_L}$  per EC8-1 is 10% for  $T_L=50$  years); 3) plot the spectral acceleration values against the corresponding fundamental periods. This spectrum is called the Uniform Hazard Spectrum (UHS), for all spectral values belong to the same hazard level. The standard spectrum is a conservative estimation of the UHS in many design codes (e.g. in EC8).

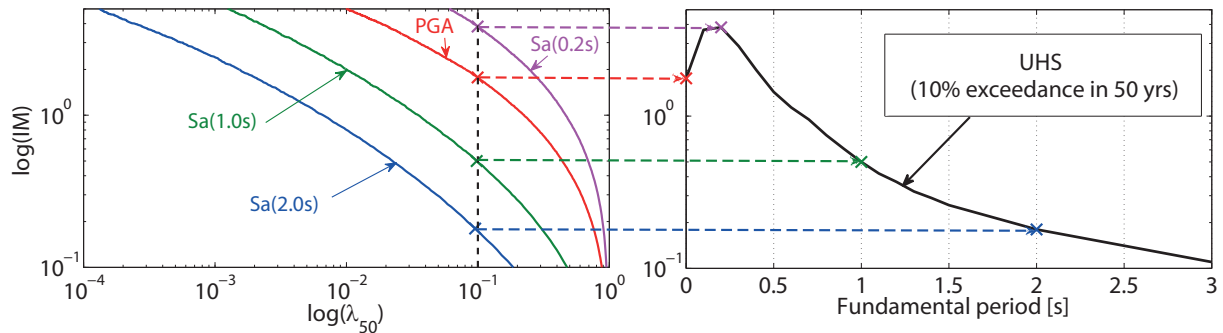


Fig. 2.6 Determination of the Uniform Hazard Spectrum.

## 2.4 Application of PSHA for Hungarian sites

### 2.4.1 Introduction

There is a European project (Seismic Hazard Harmonization in Europe; SHARE; <http://www.share-eu.org/>) aiming to establish seismic hazard harmonization between countries in the European Union by a close cooperation of leading European geologists, seismologists and engineers. In the European Facility for Earthquake Hazard and Risk website (<http://www.efehr.org/>) (EFEHR 2015), it is possible to inquire data about hazard curves and

UHS for European sites. However, it provides information only on PGA and spectral acceleration ( $S_a$ ) values, and the soil condition is restricted to rock. Besides, disaggregation is not included yet, which would provide the basic information for modern record selection methods. Therefore, the discrete form of the PSHA is implemented in the seismic performance evaluation framework to: 1) create hazard curves at a site for different soil conditions and intensity measures; 2) create site-specific spectra; 3) provide information (e.g. disaggregation) for record selection. The procedure is applicable for all sites where the seismicity can be characterized well with area sources (typical moderate seismic regions).

## *2.4.2 Description of the implemented procedure*

### *2.4.2.1 Identification of all earthquake sources*

In Hungary, proper characterization of underlying faults is not feasible; area sources are used for earthquakes that are not associated with any specific fault. The earthquake area sources (Fig. 2.7a) are obtained from the EFEHR website.

### *2.4.2.2 Characterization of earthquake magnitude distributions*

The constants for the Gutenberg-Richter recurrence law (see Eq. (2.1)) are also obtained from the EFEHR website. The recurrence law can be used to construct the distribution of earthquake magnitudes for each source (Baker 2008). The distribution is discretized between  $m_{min}$  (taken as 3.0 for all sites) and  $m_{max}$  (provided estimation by the EFEHR website for the largest expected magnitude of the source) with 0.2 magnitude steps.

### *2.4.2.3 Characterization of source-to-site distance distributions*

The discretization of source-to-site distances is carried out with Delaunay triangulation (see Fig. 2.4, Step 1) with a 5 km mesh size. An area source is assumed to produce earthquakes randomly and with equal likelihood anywhere inside the area, therefore, the probability of each distance is weighted with the ratio of the triangle area to the total area.

### *2.4.2.4 Prediction of the resulting distribution of ground motion intensity at the site*

The probability of  $IM > x$  for an earthquake with a specific magnitude and distance (and other characteristics) can be calculated with GMPEs. The calculated probability may be highly dependent on the applied GMPE; it should represent well the seismic and tectonic characteristics of the area. Hungary is an active region of shallow crustal seismicity; the EFEHR website applies a logic tree with four different GMPEs for these regions to consider epistemic uncertainty. In the implemented PSHA procedure, only the GMPE with the highest weight (Akkar and Bommer 2010) (AB2010) is incorporated. There are three reasons for this: 1) the GMPE with the highest weight is assumed to describe the hazard well; 2) the AB2010

GMPE gives conservative results in the examined Hungarian sites (10 different sites were investigated, some examples are shown in Fig. 2.7b-c); 3) including a logic tree with multiple GMPEs in the ground motion selection procedure is a complex and time-consuming task, therefore it is out of scope in this study.

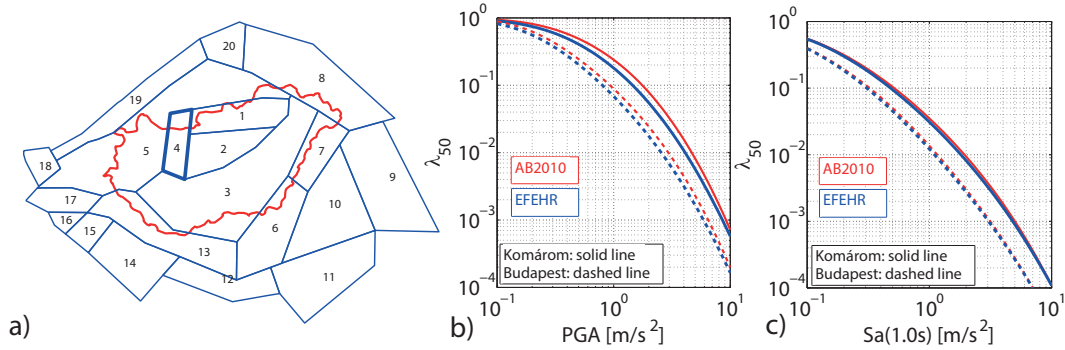


Fig. 2.7 a) Area sources considered in the study. b-c) Comparison of hazard curves calculated with AB2010 GMPE or determined with multiple GMPEs applying the logic tree of the EFEHR website.

### 2.4.3 Comparison of UHS and standard spectra

An example application of the PSHA is presented for Komárom (area of highest seismicity in Hungary). Fig. 2.8a shows the hazard curves ( $T_L=50$  years) for PGA and  $Sa(T=0.5s)$  considering soil type C (average shear wave velocity  $v_{s30}<360$  m/s per EC8-1). Disaggregation for PGA is also shown in Fig. 2.8b. It can be concluded that relatively small source to site distances ( $<10$  km) and moderate magnitudes ( $<5.5$ ) contribute most to the hazard at the observed return period (design PGA level). According to EC8-1, if the earthquakes that contribute most to the seismic hazard have a surface-wave magnitude not greater than 5.5, it is recommended that the Type 2 spectrum is adopted.

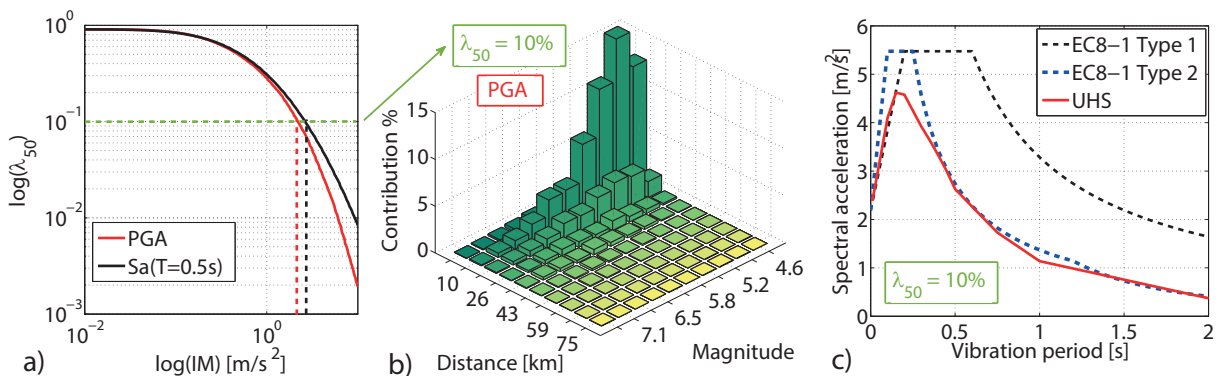


Fig. 2.8 PSHA results for Komárom: a) hazard curves; b) disaggregation of the PGA hazard (10% in 50 years); c) UHS and standard spectra (hazard level: 10% in 50 years).

The above statement is valid for the site of Komárom which is confirmed by Fig. 2.8c showing the UHS and standard spectra (Type 1 and 2 per EC8-1) for comparison. The UHS can be estimated better with the Type 2 than with the Type 1 spectrum (note also that the standard spectrum gives conservative  $Sa$  values compared to the UHS).

Fig. 2.9a presents UHS (normalized to PGA) near the bigger cities of Hungary validating the appropriateness of the Type 2 spectrum<sup>1</sup>. Even so, Type 1 spectral shape is proposed by the Hungarian National Annex to EC8, thus its modification is suggested. To illustrate the influence of the replacement of the Type 1 with the Type 2 spectrum, the ratios of Type 2 to Type 1 spectral values are shown in Fig. 2.9b. An increase of ~15% or ~35% in the Sa values can be observed at lower (<0.5 s) fundamental periods depending on the soil type, while a high reduction of ~40-60% can be obtained at high vibration periods.

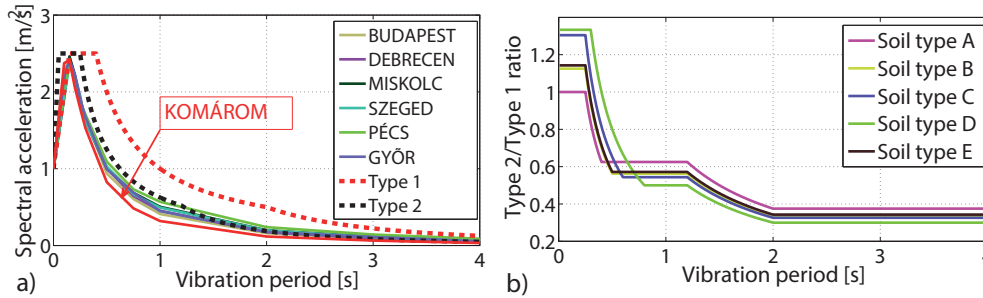


Fig. 2.9 a) Comparison of UHS and standard spectra for various Hungarian sites normalized to PGA. b) Ratio of Type 2 and Type 1 standard spectral values.

## 2.5 Determination of the seismic load

To create the fragility function of a structure, advanced modeling and NLTHA using either artificial or recorded and selected ground motions (GM) are required.

### 2.5.1 Artificial record generation

Artificial ground motions are usually generated to match a target response spectrum (typically the UHS or the standard spectrum) and they are obtained as the output from filters and the evaluation of an SDOF system response from a white noise input. Artificial records generally have an excessive number of cycles of strong motion and unrealistically high energy content. To account for other characteristics (such as duration) of an artificial spectrum-compatible record, it is necessary to obtain supplementary information about the expected earthquake motion besides the acceleration response spectrum. In spite of these facts, these records can be easily applied for linear time-history analysis, where the unrealistic characteristics do not have significant influence on the response. There are also several examples where fragility analysis is carried out with artificial records (e.g. Borzi et al. 2014). Numerous software exist which provide artificial ground motion generation tools, however the implemented algorithms in these programs are rather complex. For instance, SIMQKE-II (Vanmarcke et al. 1999) generates the power spectral density function from the input response

<sup>1</sup> UHS for the presented areas are also inquired from the EFEHR website for validation. The results confirmed the conclusions drawn from the results of this research.

spectrum and uses this to derive the amplitudes of sinusoidal waves with random phase angles which build up the artificial ground motion. The TARSCTHS (Papageorgiou et al. 2000) uses non-stationary stochastic vector processes and iteration in frequency domain.

An artificial record generation software is created as part of the research for 3 reasons: 1) the automatic performance evaluation framework requires a built-in record generation module; 2) there is a need for a fast and easily programmable algorithm; 3) there is no free software available for practicing engineers (the mentioned software are not free to use). Although common methods are based on minimizing the differences between the artificial motions and the target spectrum in a least-square sense, the idea of the developed algorithm is based on the work of Gasparini and Vanmarcke (1979) to define the amplitude vector ( $A$ ) with an iteration procedure. The ground acceleration is assumed to be the sum of independent cosine waves with different frequency, amplitude and random period shift:

$$a(t) = I(t) \sum_{i=1}^n A_i \cos\left(\frac{2\pi}{T_i} t + \varphi_i\right), \quad (2.7)$$

where  $A_i$  is the amplitude of the  $i^{th}$  cosine wave (initially 1.0 for each member),  $T_i$  is the natural period defined in advance;  $\varphi_i$  is the random period shift ( $0-2\pi$ ),  $I(t)$  describes the intensity change of the ground motion during the seismic event. Once the  $a(t)$  function is created, the acceleration response ( $S_{GM_i}^k$ ) at different natural periods ( $i$ ) in the  $k^{th}$  iteration can be calculated with Newmark- $\beta$  method. The values are compared to the target values ( $S_{Target_i}^k$ ) and the  $A$  vector is corrected as follows:

$$A_i^{k+1} = A_i^k \left[ S_{Target_i}^k / S_{GM_i}^k \right]. \quad (2.8)$$

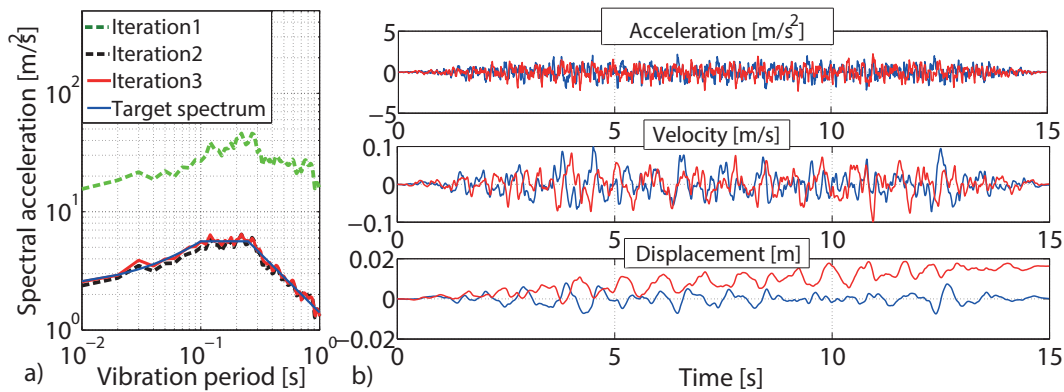


Fig. 2.10 Artificial record generation: a) iteration procedure; b) a generated record before (red) and after (blue) using the high pass filter.

The iteration is continued until the ratios of the compared Sa values are close to 1 with a predefined tolerance. At the end of the iteration process, adjustments have to be made to the  $a(t)$  artificial record to ensure that the residual velocity and displacement are zero.

The corrected acceleration record ( $\ddot{z}(t)$ ) is obtained as the solution of the differential equation describing a high-pass filter based on the corner frequency ( $\omega_c$ ) related to the geometry of the seismic source and the shear-wave velocity (Rezaeian and Der Kiureghian 2010):

$$\ddot{z}(t) + 2\omega_c\dot{z}(t) + \omega_c^2z(t) = a(t). \quad (2.9)$$

The iteration steps can be seen in Fig. 2.10a; while Fig. 2.10b shows the final fitted artificial record with or without the correction per Eq.(2.9). The algorithm is efficient, 3 iteration steps are sufficient to achieve results with negligible error. The developed artificial record generation program is freely available upon request.

### 2.5.2 *State of the art record selection method*

Selection of appropriate ground motions is crucial for the reliability of the fragility curves. Recorded accelerograms should be selected from the earthquake ground motions specific to the respective region. However, this is not always feasible (especially in moderate seismic regions); in several cases record-to-record variability cannot be represented with the limited available data. To bridge over this problem, selection is typically carried out using strong motion databases which contain recorded GMs from all over the world.

Simple selection approaches consider only the basic earthquake characteristics at the site. For example in (Avşar et al. 2011) the selection is arbitrary, but it is restricted to earthquakes with magnitudes, source-to-site distances and other characteristics (e.g. faulting style, soil condition) representative to the site. More advanced approaches explicitly account for a target response spectrum; selecting GMs the mean spectrum of which represent well the UHS (or the standard spectrum) is the most common method (e.g. Moschonas et al. 2009).

The UHS conservatively implies that large-amplitude spectral values will occur at all periods within a single ground motion (Baker 2011) and provides the envelope spectrum for all possible earthquakes at the site. The correlation of spectral ordinates at different vibration periods were acknowledged by Baker and Cornell (2006). They proposed the Conditional Spectrum (CS) approach where the effect of this correlation is taken into account. It is validated by Jayaram and Baker (2008) that spectral accelerations at multiple vibration periods have a multivariate lognormal (MLN) distribution. The CS approach provides the conditional distribution of spectral acceleration ordinates conditioned commonly on the occurrence of a specific value of a single spectral period, the record selection is therefore directly linked to the PSHA. Jayaram et al. (2011) and Wang (2011) propose the following selection method using the CS approach. Firstly, random realizations from the multivariate distribution of spectral accelerations are obtained for a given seismic event, then ground motions with the best match for each realization are selected.

The primary limitation of the CS is that only spectral accelerations are considered, while other important ground motion characteristics influencing the seismic response (e.g. frequency content and duration) are not accounted for. Bradley (2010a and 2012a) extended the idea of the CS. The General Conditional Intensity Measure (GCIM) record selection procedure is similar to that presented in (Baker 2011), deriving the distribution of a vector of IMs conditional on the main IM from their joint distribution. The novelty of the GCIM method is that the IM vector can consist of not only  $S_a$  values but also other IMs (such as energy content or duration measures). The conditional distribution provides the theoretical distribution of potential ground motions which may be observed at the site, therefore ground motion selection can be carried out fully consistently with the hazard. The limitation of the GCIM approach is that the GMPEs for all the IMs and the empirical correlation functions between the conditioning IM and the other selected IMs should exist. Bradley (2012a) proposed a selection procedure similar to that of Jayaram et al. (2011): a number of random realizations are generated from the theoretical distribution, then GMs with the smallest residual for each realization are selected. Additionally, Bradley (2012a) suggested that multiple realization sets should be generated, and finally the ground motion pack with the smallest Kolmogorov-Smirnov (KS) test statistic (which defines the difference between the target distribution and the empirical distribution of the GM set) should be selected.

The GCIM approach is a state of the art record selection method; fragility curves and the probability of failure can be determined with high reliability using hazard compatible recorded ground motions. For this reason, this method is chosen to be incorporated in the performance evaluation framework as part of this research. The steps of the record selection: 1) select the conditioning IM (fragility curve will be created as the function of this IM); 2) select other IMs on which the selection is based; 3) determine the conditional MLN distribution of the IMs using the corresponding GMPEs and empirical correlation equations; 4) sample random realization sets from the MLN distribution to create multiple vectors of random IM values; 5) select records for each realization with the smallest residual; 6) calculate the KS test statistics for the selected GM sets and choose the most appropriate one.

### *2.5.3 Generated and selected records for further analysis*

Ground motions are generated and selected prior to the analyses accelerating the fragility evaluation. Two soil categories A and C (most common in Hungary) and three areas are considered: Komárom (highest seismicity), Debrecen (lowest seismicity) and Budapest (capital of Hungary). The standard Type 1 and Type 2 spectra and the site-specific UHS are

used for the generation, while selection is carried out with the GCIM method. The PGA range is 0.25:0.25:10.00 m/s<sup>2</sup> and 50 ground motions are generated and selected at each PGA level.

As noted by Bradley (2012d), consistent ground motion selection with the GCIM method ensures that the demand hazard will be statistically independent of the conditioning IM (note that the conditional probability, therefore the fragility curves may differ). The conditioning IM is the PGA in this study, since it is the most widely used IM, thus interpretation of the results is convenient. The main aim of the study is to create the analytical fragility curves of typical road bridges in Hungary. To obtain reliable results, all relevant IMs should be incorporated in the record selection. The bridge inventory is diverse, therefore it is most advantageous to select a vector of IMs that measure different properties of the GM and correlate well with the seismic response of a wide range of different bridge configurations. PGA and Sa at T0={0.1, 0.2, 0.3, 0.4, 0.5, 0.6, 0.7, 0.8, 1.0, 2.0, 3.0, 4.0} s) are considered to account for ground motion intensity over a wide range of vibration periods; and additionally, acceleration spectrum intensity (ASI), peak ground velocity (PGV) as well as velocity spectrum intensity (VSI), and displacement spectrum intensity (DSI) are included for acceleration, velocity and displacement sensitive structures, respectively. These parameters represent peak responses, however, to describe cumulative phenomena, absolute velocity (CAV) – which accounts for the amplitude, frequency content and duration of ground motion in a cumulative manner (Campbell and Bozorgnia 2010) – and significant duration (Ds<sub>575</sub> and Ds<sub>595</sub>) – which approximately indicate durations of body, and body + surface waves, respectively (Bommer and Martinez-Pereira 1999) – are also incorporated. Therefore the IM vector consists of 20 elements: {PGA, Sa(T0), PGV, ASI, VSI, DSI, CAV, D<sub>s575</sub>, D<sub>s595</sub>}<sup>2</sup>. According to Bradley (2012a), the importance of different IMs should be taken into account by assigning different weights to them. The weights are set equally, thus the total weight of the most important IMs related to peak responses is 0.7, while a total weight of 0.3 is assigned to the other IMs associated with cumulative behavior.

An example record selection is presented for Komárom: the theoretical distributions (conditioned on the design PGA level: 10% probability of exceedance in 50 years) of some selected IMs and the empirical CDF (ECDF) of the selected 50 GMs are shown in Fig. 2.11a, and Fig. 2.11b presents the spectrum of the selected records. The selected records represent well the theoretical distributions, ECDFs are always inside the 0.1 confidence interval of the KS test (proposed by Bradley 2012a).

---

<sup>2</sup> References to the GMPEs and correlation equations, and the IM definitions are presented in Appendix A.

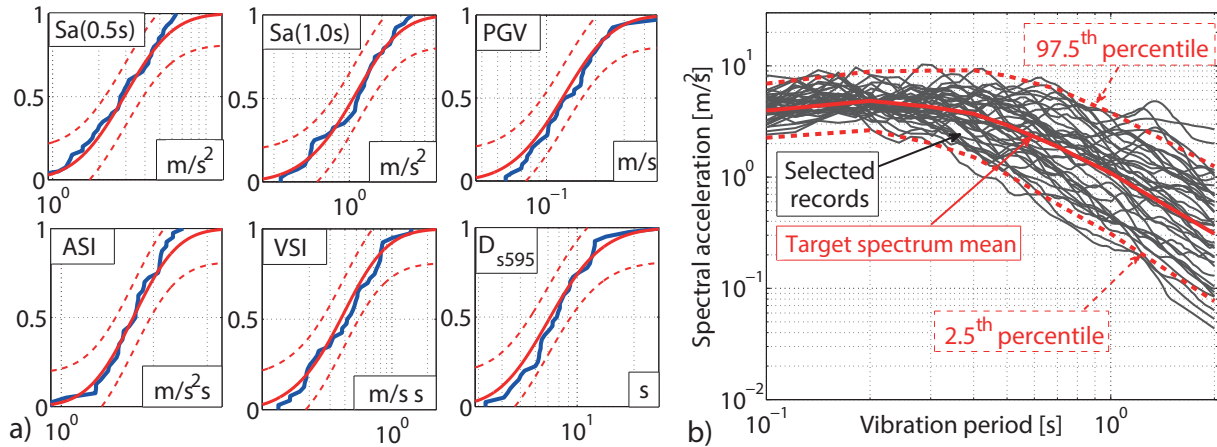


Fig. 2.11 a) Theoretical distribution of some IM conditioned on PGA (solid red line). Red dashed line: KS bounds (0.1 confidence level); solid blue line: empirical distribution of the selected GMs. b) Acceleration response spectra of the selected records.

The theoretical distributions are also useful to analyze the expected earthquake characteristics. For instance, the median significant duration is only  $\sim 7$  s. The distribution is consistent with the disaggregation results (see Fig. 2.8b) showing that earthquakes with short distance have the highest contribution to the hazard at the design PGA level, and the duration is proportional with distance (Kempton and Stewart 2006). Several other areas are investigated and it can be concluded that earthquakes in Hungary can be characterized with short duration. Per EC8-1, the minimum duration of the stationary part of the artificial records should be at least 10 s. Considering the expected characteristics of possible earthquakes leads to a decreased duration of the seismic load ( $P[D_{s595} < 10 \text{ s}] = \sim 75\%$ ) and less conservative seismic demands, especially in the case of structures with rapid rates of cyclic deterioration and accumulating plastic deformations (Chandramohan et al. 2015).

## 2.6 Summary

In this chapter, the seismic design and the seismicity in Hungary are reviewed. A PSHA, an artificial record generation and a state of the art record selection procedure are implemented in the developed seismic performance evaluation framework. It is shown, that the standard Type 2 spectrum describes well the UHS in Hungarian sites. Besides, the expected characteristics of possible earthquakes in Hungary are also investigated. As the last step, a database of selected and generated ground motions is created for the fragility analyses. I summarized the conclusions of this chapter in my Thesis I.

The next step of the research is to characterize the road bridge inventory of Hungary. The following chapter presents this characterization conducting statistical analysis of the available bridge data.

## Chapter 3

### Bridge Inventory of Hungary

#### 3.1 Database of existing bridges

The IBD existing bridge database is created for road management purposes; therefore it contains only limited information. The database stores basic data (location, main dimensions, structural system, construction materials, road category, designer); geometric and technical parameters (number of spans, span lengths, surface area of the deck, deck width); and bridge condition ratings (year of inspection, current condition). It also provides additional technical data compared to other conventional road management databases (such as the National Bridge Inventory; FHWA 2002). Information is stored about each span and each support meaning that the spans (system, material, length, structural height), abutments and piers (type of support: single, multi column or wall type; bearing type: conventional or monolithic; dilatations and foundations) can be characterized individually. Note that the pier height is not stored directly, the vertical underclearance (which is not even provided for all bridges) can be used to assume this parameter. More details about the database can be found in Appendix B.

#### 3.2 Aspects of regional damage evaluation

The IBD has been already used in a previous study by Vigh and Kollár (2006) who worked out an approximate analysis method for permitting procedures of overweight vehicles. Although only the superstructure was included in the structural model and analysis, shortcomings were revealed in some cases (e.g. arch bridges) due to the lack of essential data. Assumptions were needed to carry out the analysis. The seismic response is highly dependent on the actual layout and type of the substructure, the foundation system and soil characteristics. The reliability of the results is significantly influenced by the Knowledge Level (KL) (e.g. more alternatives should be studied when several assumptions are made). Regarding the global geometry and the material properties, three KLs are determined in accordance with EC8-3 (CEN 2011a).

##### 3.2.1 Knowledge Levels

In case of KL-1, the minimum required data should be sufficient to estimate the real geometry and possible cross sections based on typical configurations and considering the construction year and the official code used for the design. The required data describes the global geometry (mechanical system, number of spans, span lengths and construction material); the abutment and pier type, height, size; the foundation system. In this level, it is

sufficient to determine the bearing type (e.g. monolithic or conventional). The size of the dilatation can be estimated by simplified calculations. Material properties (e.g. concrete and steel grade) can be assumed based on the construction year. Due to the lack of data, the soil-structure interaction should be estimated in a conservative way (for each bridge component).

In KL-2, the global geometry should be refined. The skew angle and the alignment of the bearings are known; the global sizes of the structural elements (pier height, abutment height and type, foundation type) are known and the cross-sections can be characterized with an average cross-section. The bearing type and size; layout of the monolithic joints and the material properties are known from plans. The soil classification is available for the seismic analysis.

In KL-3, the exact geometry (with even horizontal curvature) of the superstructure is known, the structural elements are divided into segments with individual cross-sections. Material properties and soil conditions are determined via in-situ testing.

### *3.2.2 Evaluation of the whole inventory*

Reliable fragility analysis requires detailed numerical models with high fidelity to the real structure. In current state, the IBD provides only KL-1 or lower knowledge level (since pier height is missing for several bridges). Accordingly, it is not conducive to carry out individual bridge analysis due to the necessity of several assumptions. Bridge classes should be determined to represent typical bridge types and configurations. The seismic performance and failure probabilities can be estimated with the seismic analysis of these typical bridges. The results also provide guidance on which configurations are critical and need further investigation; which parameters influence most the seismic performance of typical bridges and which data should be collected for more sophisticated analyses. Dealing with only one specific bridge, the highest knowledge level can be attained with little effort (e.g. data collection from drawings, measuring real geometry and material properties), but for a bridge stock of thousands of structures, this can be accomplished only through a relative costly data collecting project. The structure of the extended database for higher level analysis is designed, while the research is started with typical configurations to evaluate their seismic performance.

## **3.3 Extension of the database**

Due to the high expenditure of the data collection, a three-phase extension is suggested in accordance with the KLS presented earlier (Simon and Vigh 2015a). The data required for each extension phase and the plan of extension is presented in Appendix B. Most of the data can be obtained from drawings, thus the KL can be increased easily with an organized data

collection without any work or in-situ tests at the site. The extension phases are determined in a way to include as many bridges as possible in the automatized evaluation framework. The statistical analysis of the database shows that most of the bridges are straight in plan girder bridges; while the number of curved and special bridges (e.g. arches, suspension or cable stayed bridges) is negligible compared to the whole inventory. The extended database and the automatic numerical model generation should be consistent, therefore, special structures are excluded from the framework for simplification. The new database structure is defined in a way that new tables and attributes can be attached easily to the existing ones at each extension phase.

### **3.4 Statistical evaluation of the database**

#### *3.4.1 Bridge classification*

The raw data of the IBD was provided by the Hungarian Transport Administration. A database is created in SQLite (<http://www.sqlite.org/>) for the seismic performance evaluation framework as part of the research. Although the information provided in the IBD is not sufficient for a detailed description of each bridge, general classification can be made with the following benefits: 1) it can be observed which types have dominant presence in the inventory; 2) a parametric field can be determined to describe bridges in each class; 3) bridges are expected to follow the same behavior in the same class having the same significant attributes, i.e. interpolation and extrapolation of analysis results may provide approximate results. The main aim of the classification is to choose representative structural types to cover as many bridges as possible in Hungary.

The aspects of the classification are as follows: 1) road category; 2) structural and material type; 3) relative number; 4) relative value. There are about 12 000 bridges in the database (see Fig. 3.1a), the relative contribution to the total number of single and multi-span bridges on primary and secondary roads are shown in Table 3.1. Most of the bridges are on secondary roads (roads between small towns or villages) with less frequent traffic, while the number of bridges on primary roads (highways and autoroutes) is only about one third of the total amount. The majority of the bridges on secondary roads are single span bridges (~7700) which usually show low vulnerability against seismic loads. If bridges with shorter spans (<10 m) are excluded due to their low vulnerability, the relative number of primary road bridges increases to 54% (see Fig. 3.1b). Table 3.1 also shows the relative value of existing structures, confirming the importance of primary roads. 80-85% of the total bridge value is associated with primary road bridges; where the contribution of longer multi-span bridges is dominant

(73%). Besides, primary roads are essential elements of the transportation system to reach regions of interest as fast as possible. Accordingly, in the rest of the study only primary road bridges (~3200) are investigated, secondary road bridges are excluded from the evaluation.

Table 3.1 Relative number and value in % of single and multi-span bridges on primary and secondary roads.

		All bridges		Span length > 5 m		Span length > 10 m	
Road category		Primary	Secondary	Primary	Secondary	Primary	Secondary
Rel. number [%]	Single span	16	64	17	51	18	26
	Multi span	11	9	18	14	36	20
<b>Sum</b>		<b>27</b>	<b>73</b>	<b>35</b>	<b>65</b>	<b>54</b>	<b>46</b>
Rel. value [%]	Single span	8	6	7	5	6	3
	Multi span	73	13	75	13	78	13
<b>Sum</b>		<b>81</b>	<b>19</b>	<b>82</b>	<b>18</b>	<b>84</b>	<b>16</b>
Total number			11949		6912		3270

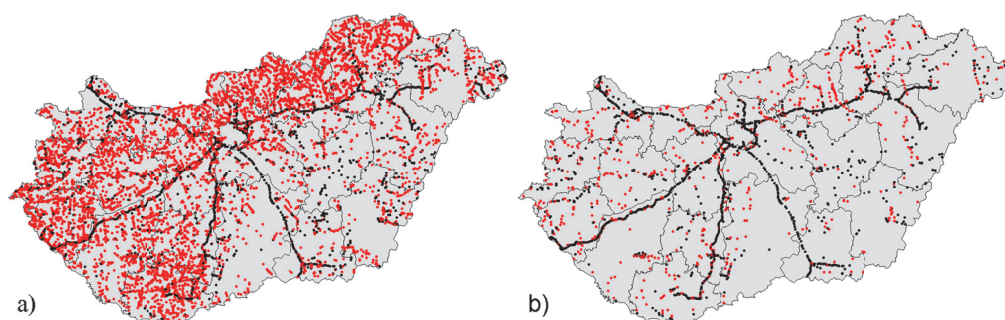


Fig. 3.1 Existing bridges in Hungary (red – simple span; black – multi-span bridges). a) All the bridges; b) bridges with maximum span length over 10 m.

Table 3.2 Classification of primary road bridges based on structural type, relative number and value.

Structural type	Number (%)	Value (%)
<b>Reinforced concrete</b>	<b>83.1</b>	<b>44.4</b>
Precast multi-girder	49.9	32.6
Monolithic slab	24.1	5.5
Monolithic frame	7.6	0.8
Prestressed box girder	0.7	4.2
One or two-box girder	0.7	1.3
<b>Steel</b>	<b>1.0</b>	<b>12.4</b>
Riveted steel truss	0.4	4.7
Welded girder	0.4	3.5
Welded box with orthotropic deck	0.2	4.2
<b>Composite</b>	<b>1.3</b>	<b>5.7</b>
Composite girder	1.0	1.7
Composite box girder	0.3	4.0
<b>Concrete or stone arch - tubosiders</b>	<b>9.0</b>	<b>1.2</b>
Tubosider	5	0.9
Concrete, RC pipe	3	0.2
Stone or masonry arch	1	0.1
<b>Special bridges (e.g. Duna bridges)</b>	<b>2.3</b>	<b>33.9</b>

The next step is to classify the bridges based on their construction material and structural type. The relative number and relative value are calculated for each bridge class; and bridge classes with a contribution of at least 1% to the relative number or value are presented in Table 3.2. The majority (>83%) of the selected bridges are reinforced concrete bridge, moreover the approximate value of RC bridges is more than 40% of the total value. Steel and composite girders and also special bridges (such as large span river bridges; e.g. over the Danube river) have significant contribution to the overall value, however their number is not

considerable (<5%). Although, the number of masonry and stone arches, RC pipes and tubosiders is high, they cannot be regarded as conventional bridges, therefore they are left out from the analysis. Special bridges are also excluded from the evaluation despite their significant value (over 33%) for the following reasons: 1) the database does not store sufficient information, also the structural type is marked as various (mostly because long span river bridges typically consist of flood and river bridge parts); 2) each special bridge should be modeled with high fidelity and rigorous seismic analysis method should be applied because of their importance; 3) these bridges are too specific, general results cannot be drawn.

The most commonly used structural type is the precast multi-girder bridge with a number of about 1600 bridges (~50%) followed by slab bridges (~24%), while typically the others are single span or multi-span continuous girders. The inclusion of only conventional girders in the framework is proven to be correct, other structural types are far less common or represent low relative value of the whole inventory. The selected bridges are illustrated in Fig. 3.2a.

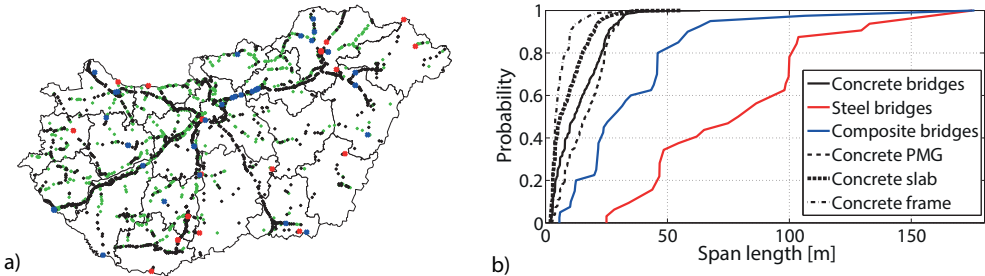


Fig. 3.2 a) Bridge classes on primary roads. Black – precast multi-girder bridges; green – other concrete bridges; blue – composite bridges; red – steel bridges. b) ECDFs for the maximum span lengths.

### 3.4.2 Statistical analysis of the bridge classes

To obtain general idea of the typical configurations, statistical analysis of each bridge class is made. Note that only precast multi-girder, slab and RC frame bridges have a relatively high number to regard the sample size as representative. To increase the number of data, other bridges are grouped based on material type only: concrete, composite and steel.

#### 3.4.2.1 Number of spans

Histograms showing the relative frequency of the number of spans are presented in Fig. 3.3. RC bridges are built typically with single span and more than 95% of the RC bridges have 4 or less spans, while the most common is the 3 span bridge among multiple-span versions. If we observe separately the three most common RC classes, it can be concluded that RC frames are dominantly single span constructions, the popularity of multi-span versions are increased for slab and precast multi-girder classes. The dominance of the 3 span layout can also be observed for composite and steel bridges, however, the distribution is more scattered; note the relatively high contribution of bridges with more spans.

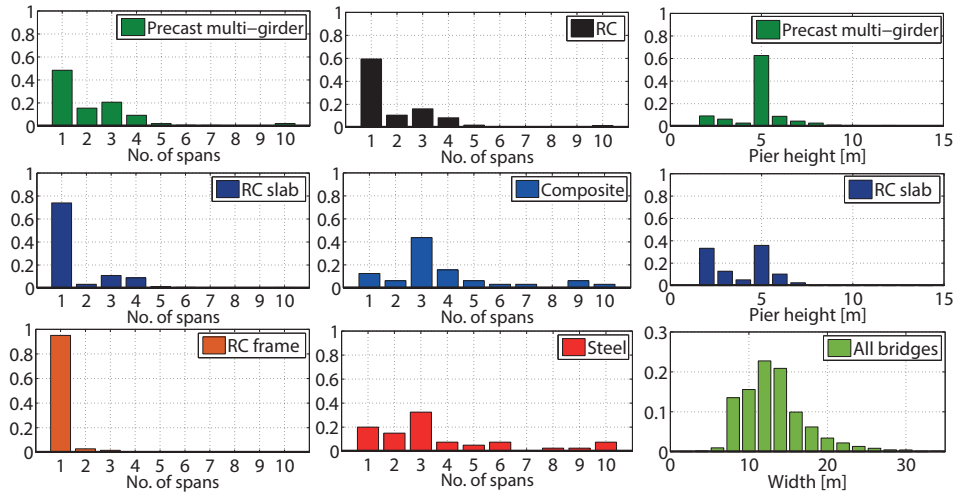


Fig. 3.3 Histograms for the number of spans, pier height and deck width.

### 3.4.2.2 Maximum span length

Besides the number of spans, the global geometry can be characterized well with the maximum span length illustrated with the help of ECDF in Fig. 3.2b. The maximum span length of RC frames is dominantly (>90%) around 5-8 m, while nearly half of the slab bridges have a maximum span length under 5 m then nearly equally distributed up to 25 m. The versatile applicability of precast multi-girder bridges is implied by the nearly uniform distribution of maximum span lengths up to 30 m. Composite and steel bridges are applied for longer spans. The majority of bridges have maximum span lengths between 20 m and 60 m; and between 40 m and 120 m for composite and steel bridges, respectively. The ECDFs show that the distributions are neither uniform nor unimodal; there are typical span lengths for both composite (around 20 m and 45 m) and steel (around 45 m and 100 m) bridges.

### 3.4.2.3 Deck width

The deck width is also an important parameter of the global geometry, since it is heavily correlated with the number of lanes; the total weight of the superstructure; the number of piers in the transverse direction; the lateral bending stiffness of the superstructure etc. It is assumed that the deck width is independent of the structural type and it is more related to the road category. Therefore, the histogram with the relative frequency of the deck width is calculated and shown in Fig. 3.3 for all the bridges. The deck width is at least 8 m which presumably belongs to overpass bridges of less significant roads crossing the highways, but generally the deck width is between 8 and 20 m, while 11-15 m is the most commonly used value for typical highway bridges with 2+1 lanes.

### 3.4.2.4 Pier height

The pier height is one of the most important structural parameter with respect to the seismic behavior of the bridge. Unfortunately, the IBD does not store the pier height directly;

it contains only the vertical underclearance of certain bridges. Besides, most of the cases this information is simply left out during the input phase and it is set to zero in the database. The vertical underclearance is known only for a limited number of multi-span bridges; representative results can be obtained only for precast multi-girder and RC slab classes (see Fig. 3.3). The most common value in both cases is ~5 m belonging to typical overpass bridges on highways. Lower vertical underclearance (mostly present in case of slab bridges) is possibly related to bridges crossing other obstacles (e.g. brooks).

3.4.2.5 Skew angle

The skew angle may significantly influence the seismic behavior as it is acknowledged by Avşar et al. (2011). The skewness limit to specify whether the skewness has significant influence varies per different codes (e.g. Caltrans 2013 or AASTHO 2012). The limit is usually between 20° and 30°. Bridges are not typical to be built with high skew angles. More than ~80% and 95% of the bridges are constructed with a skew angle under the 20° and 30° limit, respectively. Therefore skew angle is not regarded as a primary structural attribute here.

3.4.2.6 Year of construction and condition ratings

The construction year can give an insight into typical structural layouts; relevant design codes; the consideration of seismic loads. However this data alone is not sufficient to make general inferences about the structural condition. The IBD stores the condition ratings (5 level scale with 1 being excellent condition and 5 being extensive damages) of the bridge superstructure, substructure and pavement (Fig. 3.4). This information is updated on a yearly basis providing solid a basis for condition evaluation.

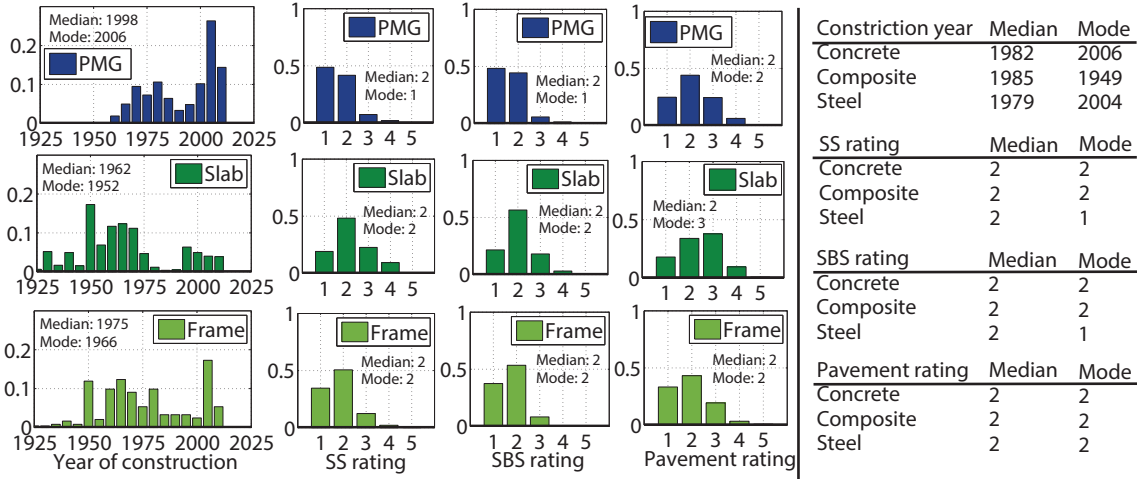


Fig. 3.4 Histograms, mode and median values for the year of construction and condition ratings. SS – superstructure; SBS – substructure.

Among the three RC bridge classes, PMG bridges are the newest with a median construction year of 1998, while slab bridges seem to be the oldest structures. The average

age of the structures is reflected in the condition ratings. Most of the PMG bridges have a superstructure and substructure rating of 1 representing excellent condition, while the worst condition can be associated with slab bridges. Note that the deterioration rate of the deck and pavement is higher than that of the main structural elements due to the shorter design working life and planned reconstructions. If bridges are grouped based on construction material, steel bridges are the oldest, composite bridges are the newest per the median value.

According to the condition ratings, the median values show good condition for structural elements without significant deterioration in strength or stiffness. This is an expected condition of the structures, since they are on primary roads, where maintenance and planned recovery are of high priority and a basic requirement.

### *3.4.3 Representative structural types*

The bridge classification is carried out taking into account only the significance of the bridge and the type and material of the superstructure. However representative structural types should be selected considering other structural attributes. To focus on the most important and possibly critical structures, some bridge classes are excluded from the analysis, while some of them are integrated into one class. RC frames are concluded to be dominantly single span bridges with short span lengths (<10 m), thus such configurations are unlikely to be critical. Riveted steel truss is one of the oldest structural type with great uncertainty associated with their actual condition, stiffness of the members, pier construction etc. Therefore, this type is not included either. Additionally, prestressed and normal RC box girder bridges are integrated into one class. Finally, seven bridge classes are used to formulate representative bridges.

Besides the type of superstructure, usually other parameters are used to distinguish bridge types with possibly different seismic behavior. HAZUS (NIBS 1999) classifies bridges according to: seismic design, number of spans (single vs multiple span bridges), superstructure type (concrete, steel, others), pier type (multiple column bents, single column bents and pier walls), abutment type, bearing type (monolithic vs non-monolithic; high rocker bearings, low steel bearings and neoprene rubber bearings), span continuity (continuous, discontinuous and simply supported). The classification results in a total of 28 classes. In the work of Avşar et al. (2011) the following primary structural parameters are identified for ordinary highway bridges in Turkey: span number (single vs multiple), bent column number (single vs multiple), and skew angle (negligible vs significant). Moschonas et al. (2009) analyzed and classified Greek highway bridges on a selected primary highway. The aspects of classification were: deck type (slab, box-girder, simply supported prefabricated-prestressed

girders with continuous RC slab), pier type (single-column cylindrical, rectangular, multiple column, wall-type) and deck-to-pier connection (monolithic, bearings and combination). This leads to 36 possible typologies.

After multiple consultations with Hungarian bridge design companies and thorough investigation of existing bridge configurations, the eight representative structural types shown in Table 3.3 and Fig. 3.5 are selected taking into account classification approaches mentioned above. The relative frequency of each representative bridge type is also indicated in Table 3.3.

Table 3.3 Selected representative bridge types on primary roads.

No.	Class type	Abbreviation	Bearing type	Typical bent type	Relative frequency (%)
1	Precast multi-girder	PMG-I	Monolithic	Multi-bent	45.0
2	Precast multi-girder	PMG-NI	Elastomeric + monolithic	Multi-bent	5.0
3	RC slab	SLAB	Monolithic	Multi-bent	24
4	RC box girder	RC-B	Conventional bearing	Single bent	1.4
5	Composite girder	COMP-I	Conventional bearing	Multi-bent	1
6	Composite box girder	COMP-B	Conventional bearing	Multi-bent	0.3
7	Steel girder	STEEL-I	Conventional bearing	Single bent	0.4
8	Steel box girder	STEEL-B	Conventional bearing	Single bent	0.2

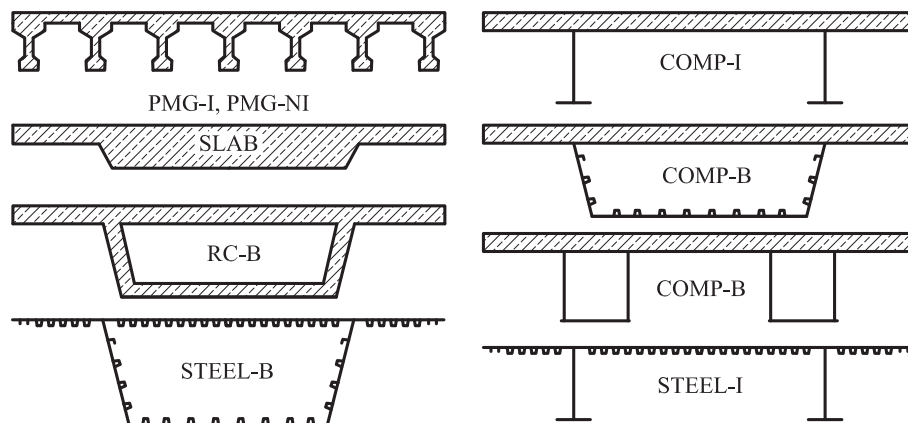


Fig. 3.5 Typical cross-sections for each bridge class.

It should be emphasized that only PMG and SLAB bridges are sufficiently high in number to draw a reliable parametric field for the most important structural attributes. Accordingly, parametric analysis is carried out and presented in Chapter 5 and 6 for PMG-I and SLAB bridges only. Other bridge types are evaluated as part of a bridge portfolio that is a result of multiple consultations with leading bridge designer companies. It contains bridges that are typical, commonly used or represent an important element of the transportation system.

The bridge portfolio and the most important structural attributes are presented in Table 3.4. Besides the identified main structural parameters (number of spans, span lengths, pier height and deck width) other important characteristics are also summarized: e.g. pier cross section and reinforcement, number of piers in the transverse direction etc. More detailed description of each portfolio bridge is presented in Appendix E.

Table 3.4 Structural attributes of the portfolio bridges (referred to with bridges number, e.g. BR25).

No.	Class	NS	Span lengths	TL	W	NFIX	NP	PCS	PH	ROS	FIW	SW	AW	SSW	JOINT
BR01	PMG-I	2	25-25	50	10	3	3 C	0.8 0.8	5.5	1	10	100	1571	18275	MJ1
BR02	PMG-I	2	25-25	50	18	3	5 C	0.8 0.8	8	2.45	10	100	1571	32700	MJ1
BR03	PMG-I	3	25-30-25	80	14	4	4 R	0.9 0.6	5.5	0.85	12	200	1131	32200	MJ1
BR04	PMG-I	3	18-30-18	66	14	4	3 R	0.9 0.6	9	1.15	16	150	2681	28950	MJ1
BR05	PMG-I	4	13-18-18-13	62	10	5	3 R	0.9 0.6	5.5	1.05	12	150	1508	17745	MJ1
BR06	PMG-I	4	15-17.5-17.5-15	65	15	5	4 R	0.9 0.6	7.5	1.05	12	150	1508	24635	MJ1
BR07	PMG-I	4	19-22-22-19	82	9	5	2 R	0.9 0.6	8	3	12	200	1131	14710	MJ1
BR08	PMG-I	6	11-15-17-17-15-11	86	12	7	3 C	0.8 0.8	6	1	10	100	1571	20232	MJ1
BR09	PMG-NI	3	35-45-35	115	14	2	4 C	1.2 1.2	4.5	0.87	12	200	1131	29795	MJ1+EB
BR10	PMG-NI	5	25-32-33-32-25	147	14	2	4 C	1.2 1.2	7	0.67	10	150	1047	29535	MJ1+EB
BR11	PMG-NI	6	30-4x45-30	240	14	3	3 C	1.2 1.2	7	1	12	100	2262	32155	MJ1+EB
BR12	PMG-NI	7	20-5x24-20	160	14	2	4 R	0.9 0.9	7	1.1	12	200	1131	28850	MJ1+EB
BR13	SLAB	2	25-25	50	9	3	2 R	0.9 0.6	8.5	2	12	150	1508	19650	MJ1+MJ2
BR14	SLAB	4	13-23-23-13	72	15	5	3 R	2.5 0.9	6	0.8	10	200	2356	34780	MJ1+MJ2
BR15	SLAB	4	12-22-22-12	68	12	5	2 R	0.9 0.6	6.5	1.16	12	200	1131	26200	MJ1+MJ2
BR16	SLAB	6	12-14-18-18-14-12	88	13	7	3 C	0.6 0.6	8	2.78	10	100	1571	29050	MJ1+MJ2
BR17	PC-B	5	5x34	170	11	1	1 R	6.0 2.0	14	0.5	16	200	4021	27800	CB
BR18	PC-B	6	37.5-4x50-37.5	275	14	1	1 R	4.9 2.0	15	0.45	12	200	4524	32500	CB
BR19	PC-B	7	36-5x45-36	297	17	1	1 R	6.0 2.8	24	1	12	150	3016	36485	CB
BR20	COMP-I	3	40-60-40	140	14	1	1 R	7.3 1.4	8	0.4	20	200	9425	21300	CB
BR21	COMP-I	3	75-90-75	240	14	1	1 R	12.0 3.3	7	0.15	16	150	22368	19700	CB
BR22	COMP-I	4	35-45-45-35	160	11	1	2 R	2.4 1.2	4.5	0.45	16	150	5362	18200	CB
BR23	COMP-B	3	24-36-24	84	14	4	4 R	1.1 0.6	4.5	2.25	16	100	4021	23700	MJ1+CB
BR24	COMP-B	3	35-45-35	115	14	1	2 C	1.6 1.6	5.5	1	16	200	2011	22000	CB
BR25	COMP-B	9	40-7x48-40	416	14	2	2 C	1.4 1.4	6.5	0.4	12	200	1131	22000	CB
BR26	STEEL-I	5	5x50	250	14	1	2 R	2.0 1.2	5.5	1.25	16	150	8042	15500	CB
BR27	STEEL-I	9	22.5-3x45-60-3x45-22.5	375	14	2	2 R	2.0 1.2	5.5	1.25	16	150	8042	15500	CB
BR28	STEEL-B	2	80-80	160	15	1	2 R	1.5 1.5	11.5	1.3	16	150	8043	16500	CB
BR29	STEEL-B	3	3x110	330	22	1	1 R	13.0 3.5	16.5	0.15	16	250	4826	17500	CB
BR30	STEEL-B	8	60-6x80-60	600	14	1	2 R	1.5 1.5	11	1.3	16	150	8043	16500	CB

Notation

NS – number of spans; TL – total length [m]; W – width [m]; NFIX – number of fixed bearings in the longitudinal direction; PCS – pier cross section size [m] (C: circular; R: rectangular); PH – pier height [m]; ROS – pier longitudinal reinforcement ratio [%]; FIW, SW and AW – pier shear reinforcement diameter and distance [mm], total area [mm<sup>2</sup>]; SSW – superstructure mass [kg/m]; JOINT – joint type (see Chapter 4): MJ1 and MJ2 – monolithic joint T type 1 and 2; EB – elastomeric bearing; CB – conventional bearing.

### 3.5 Summary

The existing bridge database does not contain sufficient data for reliable numerical modeling required for a nationwide seismic performance evaluation. Therefore, bridges are classified, important structural attributes are determined and 30 representative bridges are selected for further studies. Additionally, the possible database extension is designed. I formulated my Thesis II related to the evaluation of the database and the established automatic performance evaluation framework.

As the next step, I worked out the numerical models of each bridge type. These models are presented in detail in the next chapter.

## Chapter 4

### Numerical Model Development

#### 4.1 Numerical modeling aspects

Numerical model is the link between real structure and simulation, characterized by a duality: it should be reliable, but also time-efficient. It is inevitable to make certain simplifications and assumptions which should be given special attention. Based on a comprehensive literature review, the following conclusions can be drawn for numerical modeling issues:

- Bridges require 3 dimensional models for the reliable estimation of the combined effect of the ground motion in both transverse and longitudinal directions (Hwang et al. 2000, Zhu et al. 2002, Nielson 2005, Aviram et al. 2008, Avşar et al. 2011).
- It is sufficient to use structural component modeling level using simple beam elements and springs with properly chosen material models, while detailed models can be used to examine local effects (Nielson and DesRoches 2006, Padgett 2007, Padgett and DesRoches 2008, Tavares et al. 2012).
- In most cases the superstructure remains elastic (Choi et al. 2004, Nielson 2005), the seismic reaction forces and moments are generally lower than those obtained from conventional design situations (e.g. from traffic loads).
- The piers probably suffer plastic deformations; second order effects should be taken into account (Choi et al. 2004, Nielson 2005, Padgett 2007).
- The non-linear behavior of the bearings has great influence on the response. Bi-linear modeling of bearings is commonly used (Nielson 2005, Padgett 2007, Haque et al. 2010).
- Pounding between the superstructure and the abutment wall should be taken into account. In this case, the longitudinal movements of the bridge are limited which also has influence on the structural response (Nielson 2005, Avşar et al. 2011).
- The soil-structure interaction is a very sensitive point: flexible supports can radically change the response (Saadeghvaziri et al. 2000).
- Seismic isolation is commonly constructed with isolation bearings. In most cases they can be modeled with simple bi-linear characteristic (Haque et al. 2010, Caltrans 2013).
- Special isolation and other seismic devices show more complex behavior. Material models are proposed for these devices based on laboratory tests (Dicleli and Mansour 2003, Eröz and DesRoches 2008, Gosh et al. 2011, Wei et al. 2011).

The actual elements and material models incorporated in the numerical model are highly dependent on the applied analysis method. According to EC8-2, there are two main analysis aspects: 1) static or dynamic; 2) linear or non-linear. In this study, the following methods are employed: 1) due to its time-efficiency, linear multi-modal response spectrum analysis (MMRSA) for preliminary parametric studies in Chapter 5; 2) non-linear time-history analysis to derive fragility curves in Chapter 6; 3) equivalent linear analysis as well as NLTHA in Chapter 7 for the evaluation of the feasibility of the equivalent linear approach.

## 4.2 General illustration of the developed numerical model

A 3 dimensional beam element model is implemented in the OpenSees FEM environment (McKenna et al. 2010). OpenSees is a powerful open source platform for seismic analysis: 1) it has a large variety of material models and element types especially for seismic analysis; 2) bridge models are defined through input code files, thus changing some parameters of the bridge can be performed easily; 3) multi-core processors can be utilized. It is effectively employed for the simultaneous analysis of different modes for MMRSA or for the application of multiple ground motions for the same structure during fragility analysis in this study.

The main aspect is to create an automatic model generation algorithm for conventional girder bridges. Special bridges (arches, cable stayed and suspension) are out of scope. The developed algorithm queries information from the bridge database to build the model based on structural type, global geometry and element types with specific material models. A schematic illustration of the beam element model is shown in Fig. 4.1.

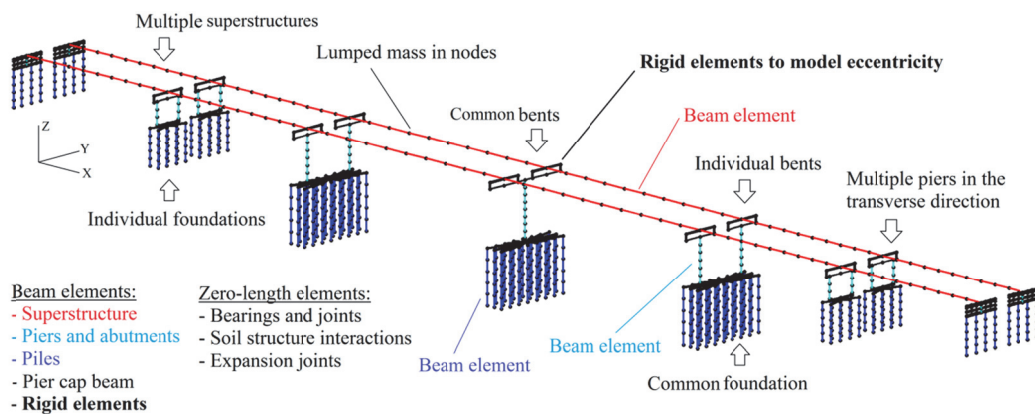


Fig. 4.1 Schematic illustration of the general beam element model.

The main structural elements (piers, superstructure, abutments etc.) are modeled with two-node 3D beam elements with 6 degrees of freedom per node, while nonlinear springs are used to model the flexible supports, the soil-structure interaction and the bearings. The beam elements are placed in the center of mass, eccentricity between the member axes – such as axes of the superstructure and pier cap – is bridged over with rigid elements. A convergence



The main difference between the bridge classes is the superstructure-substructure joint type. PMG-I and SLAB bridges are constructed with monolithic joints (MJ1 and MJ2) both at the piers and abutments. PMG-NI bridges have monolithic joints (MJ2) usually at the middle piers, however elastomeric bearings (EB) are used at other piers and at the abutments, where expansion joints (EJ) are also applied to allow girder displacements in the longitudinal direction. Other girder bridges (RC-B, COMP-I, COMP-B, STEEL-I, STEEL-B) are usually constructed with conventional bearings free or fixed in one or two horizontal directions (generally on one or just some of the piers in the longitudinal, while on all the piers in the transverse direction).

Pier cap beams (PC) are used for PMG-I and PMG-NI bridges to provide proper support for the precast beams, while piers are joined directly to the deck in case of SLAB bridges. The application of pier cap and also tie beams is common for other bridge classes as well where multiple piers are applied in the transverse direction.

The abutment is integral type with monolithic joints (MJ2) for PMG-I and SLAB bridges; and seat type for other bridge classes with the application of elastomeric (EB) or conventional bearings (CB) and expansion joints (EJ). In the following sections, the detailed modeling of these components is presented.

#### *4.3.1 Superstructure, pier cap beam*

Excessive damage of the superstructure is not expected as it is concluded for typical girder bridges in Hungary (Zsarnóczy et al. 2014) (and later in Chapter 5 for PMG-I and SLAB bridges), therefore linear elastic behavior is assigned to this component (*elasticBeamColumn* element). Section analysis is carried out for all the analyzed bridges considering different modulus of elasticity in case of composite sections.

Pier cap beams are applied for bridges with multiple piers in the transverse direction to increase the strength and the stiffness of the bent; and also to extend the width of the bent to provide proper support for the superstructure. Cap beams are common for PMG bridges in Hungary and constructed as part of the monolithic joint the strength of which is relatively high; therefore excessive damage is not expected. For this reason, linear elastic beam element (*elasticBeamColumn* element) is used to model this component as well.

#### *4.3.2 Superstructure-substructure joints*

The superstructure-substructure joints have a significant effect on the seismic behavior, since their characteristics define the amount of internal forces transferred from the superstructure to the abutment and piers. Moreover, failure of these components may lead to

unseating of the girders. The joints can be classified by type (monolithic or conventional) and by the continuity of the superstructure. Typical joint configurations implemented in the numerical model generation can be seen in Fig. 4.3.

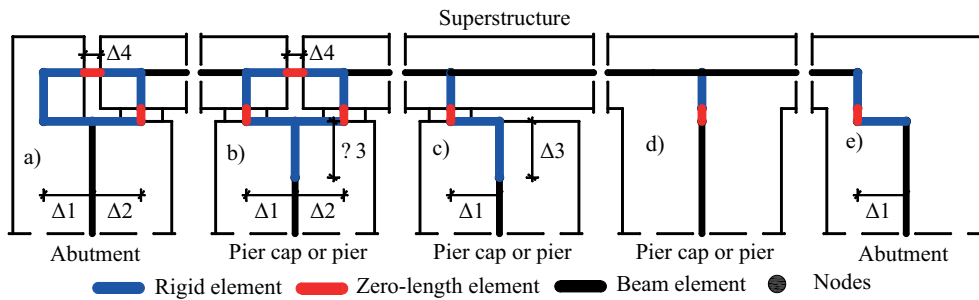


Fig. 4.3 Superstructure-substructure joints: a) abutment with expansion joint and conventional bearing; b) pier or pier cap with expansion joint and conventional bearings; c) pier or pier cap with continuous superstructure; d) pier or pier cap with monolithic joint; e) abutment with monolithic joint.

Rigid elements are used to model eccentricities between the member axes, and the eccentricity of the bearings ( $\Delta 1$  and  $\Delta 2$ ). The behavior of the bearings is taken into account with spring elements (*ZeroLength* element) with appropriate constitutive models (force-deformation relationships) assigned in specific degrees of freedom. In case of conventional bearings, spring elements are placed at each bearing position, while continuous monolithic joints are approximated with discrete contact points with concentrated constitutive models calculated from the corresponding contact lengths (Fig. 4.4). The discretization length should be lower than 0.2 m to properly follow the distribution of contact forces along the deck width.

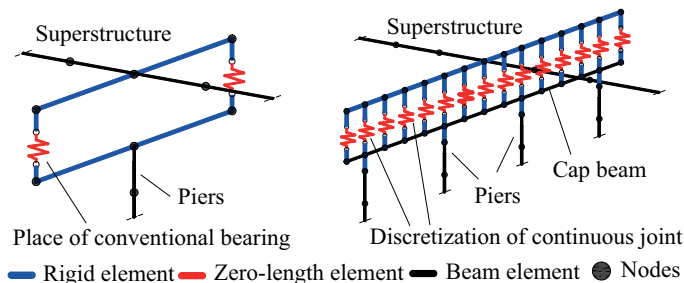
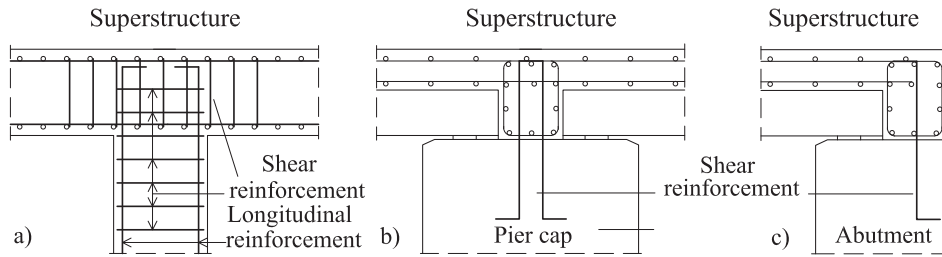


Fig. 4.4 Modeling of bearings: a) conventional bearings; b) discretization of continuous monolithic joints.

Discontinuity of the superstructure at the pier (Fig. 4.3b) or the expansion joints at the abutment (Fig. 4.3a) should be modeled if pounding between the adjacent elements (e.g. girder to abutment) is expected. The pounding is incorporated in the model with non-linear springs (*ZeroLength* element). The constitutive models for bearings and expansion joints are presented in the following subsections.

#### 4.3.2.1 Monolithic joints

There are two typical monolithic joints (Fig. 4.5): 1) piers are joined directly to the deck in case of SLAB bridges (MJ1); 2) vertical reinforcement is applied to transfer lateral forces for PMG bridges (MJ2). MJ2 is commonly used for SLAB bridge abutment joints as well.



4.5 Typical monolithic joints. a) Piers are joined directly to the deck (MJ1). Shear reinforcement is applied between: b) the deck and the pier cap (MJ2); c) the deck and the abutment (MJ2).

MJ1 joints can be characterized with complex behavior transferring both shear forces and bending moments from the superstructure to the piers. Design and verification of such joints are based on the limitation of maximum shear stress in the middle point. MJ1 monolithic bridge joints was studied with laboratory tests by many researchers (detailed literature can be found in Timosidis et al. 2015), however there are only a few suggestions for the modeling. The most rigorous approach uses volume elements (Naito et al. 2001), while a simpler method is the application of a shear panel model (Lowes et al. 2003). Even for this simplified model, at each interface three material models representing the shear behavior and the upper and lower bar slip behavior are required leading to a total number of 10 material models (including the shear panel itself). Timosidis and Pantazopoulou (2009) proposed a uniaxial backbone curve for the shear stress-shear deformation relationship in case of monolithic bridge joints, however the proper determination of the input parameters still holds a lot of uncertainties. Moreover, degradation and other cyclic parameters are needed for proper modeling. In typical bridge configurations, MJ1 joints show significantly higher resistance<sup>3</sup> compared to the pier. This implies that focus should be laid on the pier resistance rather than on the joint behavior. For this reason, and also due to the uncertainties in the input parameters and modeling, MJ1 monolithic joints are incorporated as rigid connections both for displacements and rotations.

The behavior of MJ2 joints is simpler. Since only shear reinforcement is applied, they can be characterized with semi-rigid flexural behavior. The flexural stiffness is negligible compared to that of the adjacent structural elements, thus it is best approximated as hinged (Fennema et al. 2005). It is sufficient to characterize only the lateral behavior (i.e. the relationship between the shear forces and lateral deformations). During the rotation of the

<sup>3</sup> If a typical RC slab bridge is considered with: 0.8 x 0.8 m pier with 20 $\phi$ 20 longitudinal reinforcement and  $\phi$ 12/15 stirrups. The normal force is 1000 kN in the pier. Mean material properties:  $f_{cm} = 38$  MPa;  $f_{ctm} = 2.9$  MPa;  $f_{sym} = 590$  MPa. The calculated joint shear resistance is: 3350 kN, 3710 kN and 9500 kN for cracking, rebar yielding and crushing of concrete, respectively. Pier shear resistance is: 1200 kN.

joint, cracks may appear between the concrete-concrete surface. For this reason, reliable estimation of the concrete shear strength cannot be given.

MJ2 joints are modeled with two material models working parallel to take into account the cyclic behavior of the vertical rebars and the friction between the two concrete surfaces, while the adhesion is neglected. The friction between the concrete surfaces is modeled using a bi-linear model (*Steel01* material) presented in Fig. 4.6a. The yielding force is calculated as the normal force ( $F_z$ ) times the frictional coefficient ( $\mu$ ) and the  $K_0$  equals to  $F_y$  divided by  $d_y$  determined as per (FIB 2008) as follows:

$$d_y[\text{mm}] = 0.15 \sqrt{\sigma_N[\text{MPa}]}, \quad (4.1)$$

Based on laboratory test results of pinned connections with  $2\phi 16$  vertical rebars (Psycharis and Mouzakis 2012), material model calibration (*Pinching4* material) is carried out to model the cyclic behavior of the shear reinforcement (Fig. 4.6b). The input parameters of the material model are the force-deformation points of the monotonic backbone curve (available from the tests); parameters controlling the pinching behavior ( $rD$ ,  $rF$ ,  $uF$ ); and parameters controlling the degradation of the unloading stiffness ( $gK1$ - $gK4$ ,  $gKlim$ ), the reloading stiffness ( $gD1$ - $gD4$ ,  $gDlim$ ) and the strength ( $gF1$ - $gF4$ ,  $gFlim$ ); and the last two parameters ( $gE$  and  $dmgType$ ) define the maximum energy dissipation under cyclic loading and the type of algorithm for damage estimation. The damage type is chosen to be “energy” type, where the damage indices are defined to be a function of both displacement history and energy accumulation (Lowes et al. 2003).

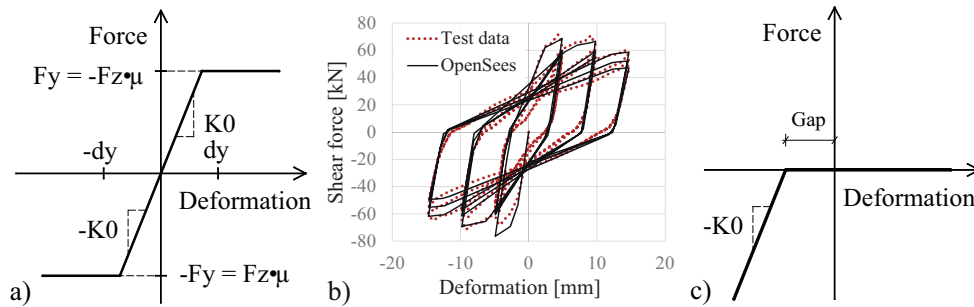


Fig. 4.6 MJ2 monolithic joint model: a) bi-linear model for the friction; b) test data and calibrated Pinching4 material model for the cyclic behavior of the shear reinforcement. c) Constitutive model for expansion joints.

Table 4.2 Calibrated Pinching4 material model parameters for MJ2 monolithic joint.

Pinching behavior			Energy dissipation		Unloading stiffness degradation				
$rD$	$rF$	$uF$	$gE$	$dmgType$	$gK1$	$gK2$	$gK3$	$gK4$	$gKlim$
<b>0.63</b>	<b>0.88</b>	<b>0.00</b>	<b>2.26</b>	<b>Energy</b>	<b>0.05</b>	<b>0.55</b>	<b>0.95</b>	<b>0.95</b>	<b>0.42</b>
Reloading stiffness degradation				Strength degradation					
$gD1$	$gD2$	$gD3$	$gD4$	$gDlim$	$gF1$	$gF2$	$gF3$	$gF4$	$gFlim$
<b>0.92</b>	<b>0.94</b>	<b>0.44</b>	<b>0.55</b>	<b>0.50</b>	<b>0.62</b>	<b>0.53</b>	<b>0.63</b>	<b>0.54</b>	<b>0.89</b>

The calibrated model shall approximate the measured response history (occurring forces), when subjected to the same cyclic test protocol. Due to the relatively large number of 19

unknown parameters and the non-linearity of the problem genetic algorithm can be efficiently invoked which is a heuristic optimum search method (Goldberg 1989). The applied fitness function is calculated from the weighted sum of square errors of the tested and calculated load values. The calibrated model parameters are shown in Table 4.2.

#### 4.3.2.2 Expansion joint

The gap in the expansion joint can be modeled directly with separate components and contact elements to recognize pounding. It is a difficult task to set proper parameters for the contact stiffness while avoiding convergence problems. Moreover, these elements tend to increase the calculation time. A simpler approach is followed: the gap is integrated into the constitutive model characterized by high stiffness (to model rigid contact) and infinite strength (*ElasticPPGap* material) (Fig. 4.6c).

#### 4.3.2.3 Conventional bearings

The most commonly used bearing type is the elastomeric bearing. Usually internal steel plates (shims) are placed in the elastomer to reduce the lateral bulging of the bearing and increase its vertical stiffness considerably (see Fig. 4.7a).

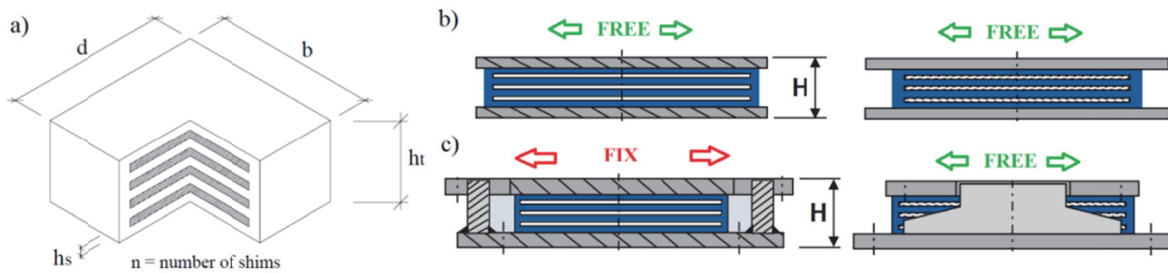


Fig. 4.7 Elastomeric bearings. a) General structure. b) Horizontally free-deforming in all directions. c) Horizontally fixed with steel restraints in one direction.

Elastomeric bearings are used as expansion bearings mainly for PMG-NI bridges (Fig. 4.7b); and they are also applied in case of multi-span continuous RC-B, COMP and STEEL girders to provide free movements in a specific horizontal direction, while in the other direction a keeper or guiding plate minimize the displacements (Fig. 4.7c).

The behavior in the free horizontal direction can be characterized with a bi-linear curve (similar to the one in Fig. 4.5b). The stiffness is associated with that of the shear stiffness of the rubber bearing. The lateral shear capacity is calculated either from the dynamic friction capacity between the surface of the bearing and of the pier or superstructure; or the shear resistance of the bearing itself. The friction coefficient is 0.4 for concrete and 0.35 for steel surface (Caltrans 2013). The initial stiffness of the elastomeric bearing (see Fig.4.7a):

$$K_0 = GA/h_{rt}; A = d * b; h_{rt} = h_t - n h_s, \quad (4.2)$$

where  $G$ ,  $A$  and  $h_{rt}$  are the shear modulus, area and the total rubber height of the elastomeric bearings, respectively. The shear modulus usually ranges between 0.65 MPa and 2.00 MPa AASHTO (2012); in this study 0.9 MPa is used which complies with the average shear modulus according to EN 1337-3 (CEN 2005).

In a fixed direction, the behavior is highly dependent on the actual configuration and restrainer components. Ultimate resistance of the bearings can be estimated from the design forces from ultimate limit state (ULS), however cyclic but even post yielding behavior are unpredictable without laboratory tests or detailed finite element models. For this reason, a simplified modeling is followed: bearing stiffness is fully rigid in the restrained direction, while their failure is not incorporated in the model (infinite strength is assumed). The same assumption applies for other conventional bearing (e.g. spherical, pot) in this study. Note that the decreased stiffness due to yielding leads to lower seismic demands of the piers, abutments and foundations, therefore this modeling technique is a conservative approach with regard to these important components maintaining the structural integrity of the structure.

### 4.3.3 Piers

Piers are modeled with nonlinear beam elements (*dispBeamColumn* element), material nonlinearity is taken into account with fiber sections (Taucer et al. 1991), while geometric nonlinearity (P- $\Delta$  effect) is also incorporated. The fiber discretization of reinforced concrete pier cross-sections can be seen in Fig. 4.8a. Each fiber has its own uniaxial stress-strain relationship, force-deformation relationship is obtained with integration over the cross-section assuming plane cross-section after deformation. This approach takes into account the interaction of biaxial bending and normal force. Uniaxial constitutive models assigned to the fibers of inelastic pier elements are the Scott-Kent-Park (Kent and Park, 1971 and Scott et al., 1982) concrete model (*Concrete01* material) and bilinear steel model (*Steel01* material).

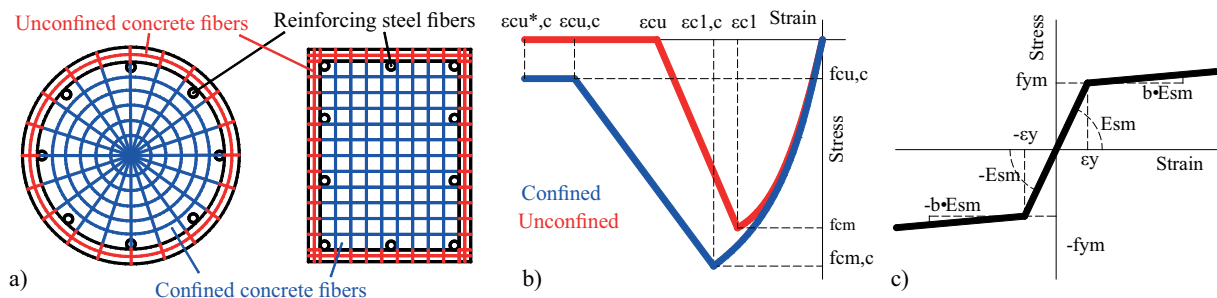


Fig. 4.8 a) Fiber discretization of reinforced concrete pier sections. b) Concrete material models. c) Reinforcing steel material model assigned to the corresponding fibers.

The bilinear steel material model (Fig. 4.8c) can be described with three parameters: yielding strength ( $f_{ym}$ ), initial stiffness ( $E_{sm}$ ) and post-yield stiffness (to take into account the

strain hardening effect). The post-yield to initial stiffness ratio ( $b$ ) is taken as 0.01 in the analyses. Four parameters are used to construct the concrete stress-strain relationship presented in Fig. 4.8b. The tensile strength is neglected in this model, the required parameters on the compression side are: maximum compressive strength ( $f_{cm}$ ); corresponding compressive strain ( $\epsilon_{c1}$ ); ultimate strain ( $\epsilon_{cu}$ ) and corresponding residual stress ( $f_{cu}$ ). The ultimate strain is 0.035 and the residual stress is zero in case of normal concrete, other parameters depend on the actual concrete strength and grade (e.g.  $f_{cm}$  and  $\epsilon_{c1}$  are 38 MPa and 0.002 for C30/37 concrete).

The normal parameterization of the concrete is valid for the unconfined outer concrete layer. The confining effect of the transverse reinforcement can be taken into account in case of the core concrete. As it is shown in Fig. 4.8b, confinement improves both the maximum compressive strength and also the ductility of the concrete material. Confined concrete properties are calculated as per EC8-2 Annex E. The maximum strength is:

$$f_{cm,c} = f_{cm} \lambda_c, \text{ where } \lambda_c = 2.254 \sqrt{1 + 7.94 \sigma_e / f_{cm}} - 2 \sigma_e / f_{cm} - 1.254, \quad (4.3)$$

where  $\sigma_e$  is the effective confining stress. The strain at maximum strength is:

$$\epsilon_{c1,c} = 0.002 [1 + 5(f_{cm,c} / f_{cm} - 1)]. \quad (4.4)$$

The effective confining stress is calculated from the confining reinforcement ratio ( $\rho_w$ ):

$$\sigma_e = \beta \alpha \rho_w f_{ym}, \quad (4.5)$$

where  $\beta$  is 0.5 for circular and 1.0 for rectangular hoops;  $\alpha$  is the confinement effectiveness factor (assumed to be 1.0). Two other parameters are left to describe the concrete stress-strain relationship. The residual stress at ultimate strain ( $f_{cu,c}$ ) is 20% of the maximum strength, while the ultimate strain of the confined concrete can be obtained with the following formula:

$$\epsilon_{cu,c} = \epsilon_{c1} (f_{cm,c} / f_{cm})^2. \quad (4.6)$$

Note that due to the low shear reinforcement ratio usually applied in Hungary (<0.75%), the increase of strength and ductility of the confined concrete is not significant (<10%).

#### 4.3.4 *Abutments and backfill soil*

The abutment-backfill soil system can significantly affect the seismic behavior. The backfill soil under compression exerts reaction forces due to the developing passive earth pressure (Fig. 4.9a), therefore it provides extra support in addition to the stiffness of the abutment. Its influence on the seismic response is dominant in the longitudinal direction especially in case of bridges with monolithic abutment-superstructure joints. Even in the case of free bearings and expansion joints, it can alter the responses if pounding occurs between the superstructure and the abutment.

The abutment can be regarded as a rigid block, stability failure is more possible than failure due to inadequate strength. Therefore, abutments are modeled with simple linear elastic behavior (*elasticBeamColumn* element). The complex behavior of the backfill soil under compression was investigated by several researchers (e.g. Wilson 1988; Wilson and Tan 1990; Goel and Chopra 1997; Duncan and Mokwa 2001; Wilson and Elgamal 2010) and suggestions were made on the stiffness and the ultimate resistance. As part of the Caltrans seismic research program, full-scale abutment field experiments were conducted (Romstad et al. 1995; Maroney et al. 1995). The test results showed hyperbolic force-deformation behavior of the abutment-backfill soil system subjected to monotonic longitudinal loading (Shamsabadi et al. 2007). Based on the results, a bilinear approximation is proposed in Caltrans (2013) which is adopted in this study.

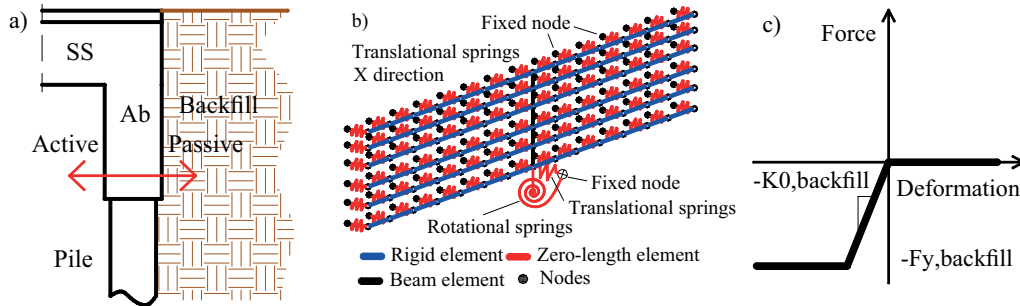


Fig. 4.9 Abutment-backfill soil system. a) Active and passive action in the longitudinal direction. b) Details of the numerical model. c) Constitutive model assigned to the backfill soil spring elements.

This bilinear behavior is modeled with the help of spring elements (*ZeroLength* elements): one end is attached to the nodes of a rigid grid modeling the surface of the abutment; the other end is attached to fixed nodes (Fig. 4.9b). The initial stiffness is calculated per Caltrans (2013) from a stiffness value ( $K_i$ ) of 28.7 kN/mm/m determined for the entire width ( $w$ ) of the bridge. The stiffness is adjusted to the backwall height ( $H$ ) lumped into the nodes proportionally to the corresponding areas ( $A$ ):

$$K_{0,backfill} = K_i w (H/1.7m) / A. \quad (4.7)$$

The yielding force is lumped into the surface nodes in the same way, where 368 kPa maximum passive soil pressure is utilized for dynamic loads per Caltrans (2013):

$$F_{y,backfill} = 368 \text{ kPa} (H/1.7m) \cdot A. \quad (4.8)$$

The post-yielding stiffness of this model is zero, and the model is defined to work only in compression (*ElasticPPGap* material; see Fig. 4.9c). The participating mass of the backfill soil is also incorporated (lumped to the abutment surface nodes); it is calculated considering the critical length ( $L_c$ ) of the embankment according to Zhang and Makris (2002):

$$L_c \cong 0.7 \sqrt{SB_c H} \quad (4.8)$$

where  $B_c$  and  $B_b$  are the crest and base width (at the bottom of the backwall) of the embankment, and  $S = 2H/(B_b - B_c)$  is its slope.

#### 4.3.5 Foundation

The seismic responses of a flexibly-supported structure fundamentally differ from those calculated assuming rigid foundation. Former practice usually neglected the effects of flexible support, while fragility analyses of bridges are also often conducted with rigid boundary conditions (Borzi et al. 2015; Avşar et al. 2011). Two modeling techniques are implemented in the automatic model generation algorithm: 1) lumped parameter model; 2) Beam on Non-Linear Winkler Foundation (BNLWF) method.

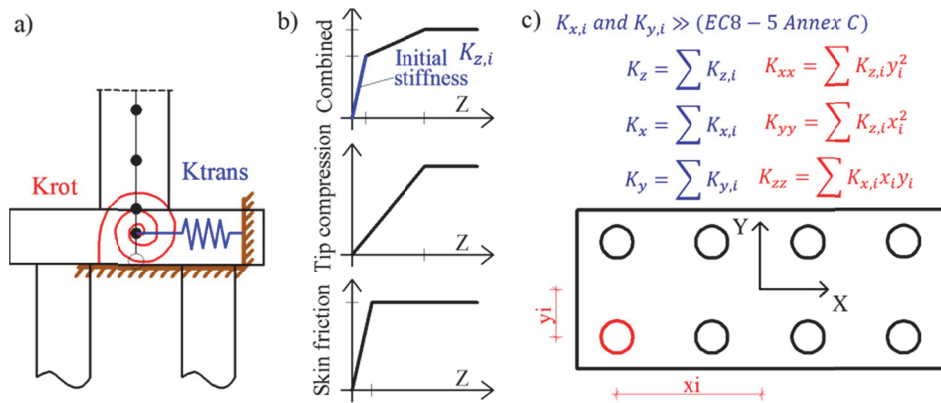


Fig. 4.10 a) Numerical model with integrated linear springs. b) Tri-linear vertical behavior of piles. c) Calculation method of the stiffness of the whole pile foundation system.

In the first sub-structuring model, dynamic impedance of the soil-foundation system is approximated through assemblies of springs, dashpots and fictitious masses (Wolf 1985). The complex impedance is frequency-dependent, where the complex part represents radiation damping in the soil. As a conservative approach, both radiation and material damping of the soil is neglected in this study. Linear springs are used (*ZeroLength* element) to take into consideration the translational and flexural stiffness of the shallow or pile foundation (Fig. 4.10a). Spring stiffness values for shallow foundations are calculated per ASCE 41-13 (ASCE 2014). The vertical stiffness of an individual pile is determined as the initial stiffness of a simplified tri-linear behavior (Fig. 4.10b), representing the combined behavior of skin friction and tip resistance; and the estimation of the horizontal stiffness is given according to EC8-5 Annex C (CEN 2009a). The translational and rotational stiffness of the foundations is calculated directly from the vertical and horizontal stiffness of the individual piles considering the actual layout of the pile foundation system. The calculation is explained in Fig. 4.10c.

In case of the second, more advanced BNLWF modeling approach, piles are modeled either with simple elastic beam elements (*elasticBeamColumn* element), or if plastic deformations are expected in the piles, the behavior can be modeled by using fiber sections

with non-linear beam elements (*dispBeamColumn* element) as well. Rigid elements are applied to create the pile cap; the mass and the moment of inertia of the pile cap is concentrated into the pile cap node. The division of the piles, thus the number of nodes along the pile length is important, since the soil-structure interaction is modeled with concentrated contact points. At each pile node, a fixed node is placed and they are connected with non-linear springs representing the non-linear force-displacement relationships for skin friction (t-z), the tip in compression (q-z) and lateral behavior (p-y) (*TzSimple1*, *QzSimple1*, *PySimple1* materials) based on the work of Boulanger et al. (1999). The pile foundation numerical model is illustrated in Fig. 4.11.

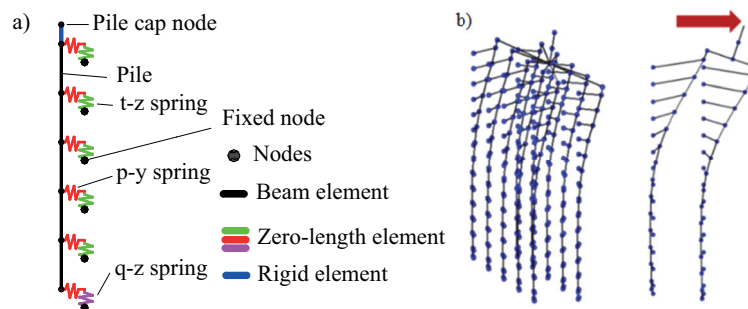


Fig. 4.11 Pile foundation. a) BNLWF modeling approach. b) Numerical model in OpenSees.

The definition of the t-z, q-z and p-y material model parameters is elaborated as part of this research considering the EC7-1 (CEN 2015) regulations and Hungarian design practice in accordance with Szepesházi (2011). Details can be found in (Simon 2013). Using the BNLWF method increases the computational time more than three times compared to the simpler sub-structuring approach (note that a high number (~30000) of NLTHA carried out as part of the fragility evaluation). Besides, reliable data about the soil layers are required for this model. For these reasons, this approach is not used in this study, however with the implementation in the automatic model generation module, specific bridges can be analyzed in an advanced manner if information on the soil layers and characteristics is available.

#### 4.4 Summary

Based on a comprehensive literature review, an automatic numerical model generation module is created. In addition to the detailed component modeling (e.g. calibration of cyclic model for monolithic joints), the global model is elaborated to handle several geometric situations. The numerical models are used for both linear and non-linear analyses; thus their contribution appears in my Thesis III and IV.

Before the fragility analysis, preliminary analysis is needed to determine the seismic behavior of typical road bridges and to reveal critical bridge configurations and components. This preliminary analysis is presented in the following chapter.

## Chapter 5

### Preliminary Seismic Analysis of Existing Bridges

#### 5.1 Review of the parametric analysis of continuous girder bridges

In the work of Zsarnóczy et al. (2014) a parametric study was carried out using linear MMRSA for thousands of continuous girder bridge configurations with conventional bearings. A set of eight parameters was used: span length (5-140 m); number of spans (2-9); pier height (5-50 m); number of fix bearings in the longitudinal direction (1-8); pier reinforcement ratio (0.5-2.5 %); proportions of the piers' rectangular cross-section (1:1 and 1:3); soil stiffness ( $10^{10}$ - $10^{13}$  N/m<sup>3</sup>); type of superstructure (cast-in-situ concrete, precast concrete, concrete box, composite girder, regular steel girder and steel box girder).

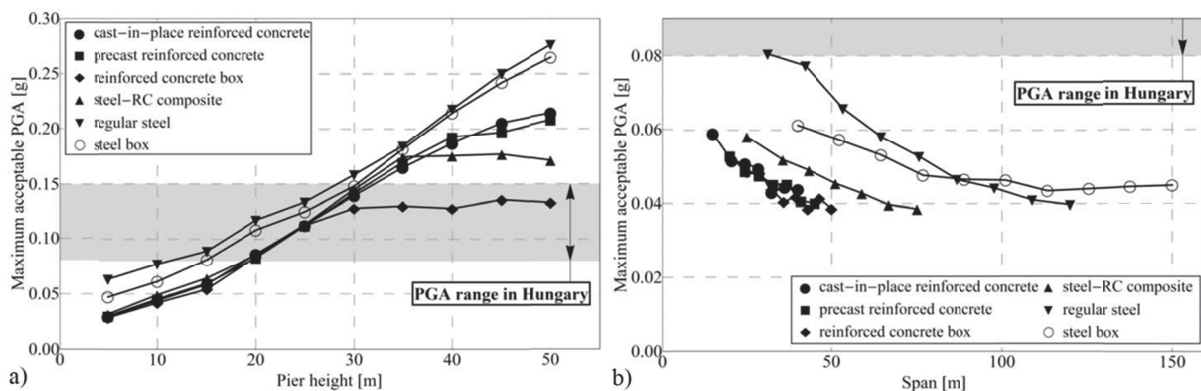


Fig. 5.1 Maximum acceptable PGA values for five span bridges with one fix bearing in the longitudinal direction: a) with 40 m span length; and b) 10 m pier height. (Zsarnóczy et al. 2014).

The bridges were designed without considering any seismic loads to mimic the design of existing structures. MMRSA was carried out using soil type B and PGA of  $1.0 \text{ m/s}^2$ . Demand-capacity (DC) ratios and maximum acceptable PGA values (MAPGA; DC ratio is divided with the applied PGA) were calculated for each bridge component. The following conclusions were drawn: 1) the superstructure is not critical; 2) longitudinal vibration is dominant; 3) vertical excitation has negligible effect on the pier demands; 4) torsion of the piers can be neglected; 5) critical components are the piers and bearings.

It was also shown that earthquake loads are dominant in case of every structural type if the piers are lower than 20 m; and that DC ratios of both bearings and piers may be as high as 2-3 in case of even lower piers (<10 m). MAPGA values in Fig. 5.1a indicate that bridges with shorter piers are heavily affected by earthquakes due to their increased stiffness. Another example from the study can be seen in Fig. 5.1b where different bridge classes with 10 m pier height are shown. The figure confirms that bridges with such short piers can be characterized with extremely low MAPGA values.

The study provides suggestions for increased seismic performance: 1) application of multiple fix bearings in the longitudinal direction can cause more favorable distribution of seismic demands among piers; 2) by increasing the pier reinforcement ratio in the design phase the same load bearing capacity may be attained while arriving to smaller cross-sections and slender piers, which in return decreases the stiffness and possibly the seismic forces as well. More details about the results can be found in (Zsarnóczy 2010).

## **5.2 Applied procedure for parametric seismic analysis**

The bridge types investigated by Zsarnóczy et al. (2014) can be associated with the PMG-NI, RC-B, COMP-I and COMP-B, STEEL-I and STEEL-B classes of this study. In this research, a similar intensity based approach is applied for preliminary parametric analysis for two bridge classes with monolithic joints (PMG-I and SLAB). Time-efficient MMRSA is programmed using OpenSees to compute seismic demands (Simon and Vigh 2014). Although MMRSA cannot capture non-linear behavior and generally provides conservative results compared to more rigorous methods (e.g. NLTHA), the short computational time gives the opportunity to cover a wide multi-dimensional parametric field and it can provide the order of magnitude of the seismic demands to highlight possible critical components and configurations. The applied elastic spectrum assumes the most common soil type C and Type 2 spectral shape (Type 2 standard spectrum is used based on the conclusions of Chapter 2). The highest PGA value of  $1.5 \text{ m/s}^2$  in Hungary for EC8-1 no-collapse criteria (the hazard is computed at 10% exceedance in 50 years for rock sites) is applied. The bridges are considered as ordinary bridges of normal importance, thus an importance factor of 1.0 is used to determine the seismic load. A behavior factor  $q=1.0$  is applied as it is suggested by EC8-2 for bridges with a deck connected to both abutments with monolithic joints. After careful investigation of the available data and the details of selected existing PMG and SLAB bridges, relevant design parameters are determined. Main variable parameters are: number of supports, span length, deck width and pier height. These parameters are determined with the statistical analysis of the existing bridge database presented in Chapter 3.

## **5.3 Parametric analysis of integral precast multi-girder (PMG-I) bridges**

### *5.3.1 Description of PMG-I bridges*

Fig. 5.2a shows the general layout of PMG-I bridges. They are constructed as follows. In the first construction steps, the substructure is created (piles, pile cap, abutments and piers, and finally the pier cap beam); vertical reinforcements are extended from the abutment and pier cap. Precast beams are placed on the pier cap beam and on the abutments. The last step is

to position the reinforcements of the deck, then the monolithic joints and the concrete deck are constructed with cast-in-situ concrete. PMG-I bridges with a few exceptions are built as continuous integrated (instead of simply supported) systems. Typical shear reinforcements of the monolithic Type 2 joints are  $\phi 16/150$  at the abutment and  $2\phi 16/150$  at the piers.

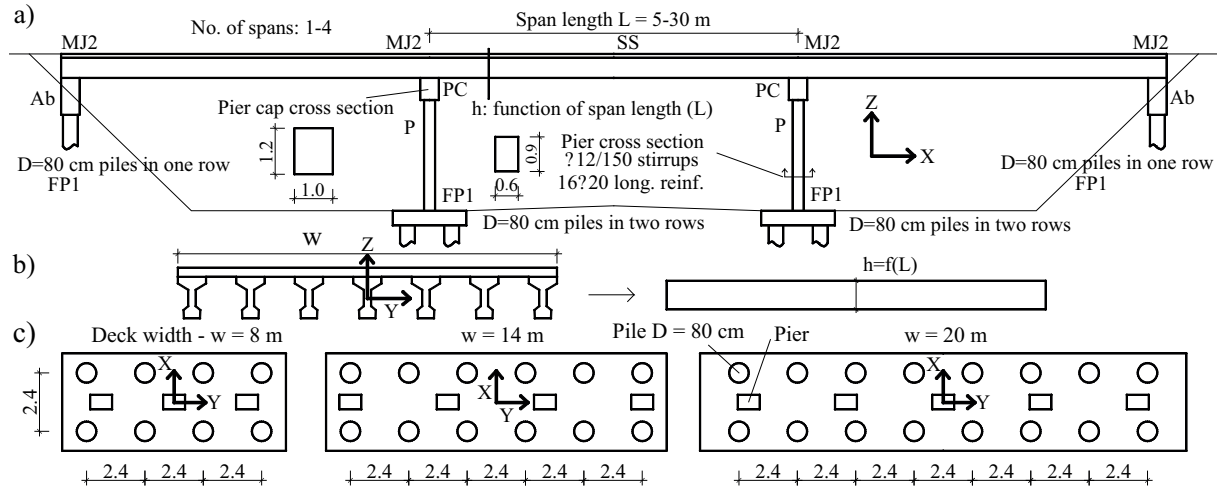


Fig. 5.2 General layout of PMG-I bridges: a) side-view of the bridge; b) typical cross section; c) applied pile foundation arrangements for different bridge widths.

Table 5.1 Input parameters for the parametric study (parameters for fragility analysis are marked with red fonts) and notations for different configurations (e.g. a 3 span bridge with 14 m width, 6 m pier height and 20 m span length is referred to as W14S3P06L20).

Parameter	Width			Notations
	8 m	14 m	20 m	
No. of spans		1-2-3-4		W08-W14-W20 S1-S2-S3-S4
Pier height		2-4-(5)-6-8-10 m		P02-P04-(P05)-P06-P08-P10
Span length (L)		5-10-15-20-25-30 m		L05-L10-L15-L20-L30
SS height	$h_{ss} = -0.0004(L-5)^2 + 0.035(L-5) + 0.4$ [m]			-
No. of piers in the transverse direction	3	4	5	-
Foundation - abutment	1x4 D=80 cm	1x6 D=80 cm	1x8 D=80 cm	-
Foundation - pier	2x4 D=80 cm	2x6 D=80 cm	2x8 D=80 cm	-

The structural height of the girder is determined as the function of the span length (an equivalent slab is considered taking into account stiffness and mass properties; see Table 5.1 and Fig. 5.2b). Additional permanent load of the superstructure is  $\sim 750$  kg/m railing and  $\sim 400$  kg/m<sup>2</sup> pavement. Piers are constructed as multi-column bents with 3-4 m transverse distance. Longitudinal reinforcement ratio is typically  $\sim 1\%$ , while minimal shear reinforcement (mostly  $\phi 12/150$ ) is applied due to the low shear forces in conventional design situations (e.g. traffic loads). Since these bridges are extremely popular on highways, cross section of the piers (0.6 m x 0.9 m) and the pier cap (1.0 m x 1.2 m) and the dimensions of the abutments (1.0 m x 2.0 m) are more or less the same for all structures for the efficient reusability of formwork. Accordingly, pier and cap beam cross-section, abutment geometry are considered fixed during the studies. The foundation system is mostly pile foundation, the assumed layouts for different deck widths are shown in Fig. 5.2c. The input parameters of the parametric study are

presented in Table 5.1 where the notations for different configurations are also indicated (e.g. a 3 span bridge with 14 m width, 6 m pier height and 20 m span length is referred to as W14S3P06L20).

### 5.3.2 Numerical modeling issues

The numerical model is the one presented for PMG-I bridges in Chapter 4 except that geometric non-linearity is not incorporated, and initial stiffness values are used due to the linear nature of the analysis method. The analysis cannot take into account that the backfill soil work only in compression, it assigns the same initial stiffness in the tension zone as well. The examined bridges have both longitudinal and transverse axes of symmetry, thus the longitudinal vibration mode with movements toward one abutment is identical to the one moving toward the other abutment. For this reason, during linear MMRSA spring elements are applied at only one of the abutments to model the effect of the backfill soil only in compression. In the preliminary phase, effective pier stiffness (~65% of the uncracked stiffness) is not taken into account, stiffness values are calculated using concrete Young modulus of 30 GPa to obtain conservative seismic demands for the piers.

Table 5.2 Stiffness values of the foundation springs.  $k_x$ ,  $k_y$  and  $k_z$  denote translational stiffness along the x, y and z axis (see Fig. 5.2); while  $k_{xx}$ ,  $k_{yy}$ ,  $k_{zz}$  represent rotational stiffness values around the same axes, respectively.

Width	Span	$E_{soil}$ MPa	Abutment						Pier					
			$k_x$	$k_y$ $10^9$ N/m	$k_z$	$k_{xx}$	$k_{yy}$ $10^9$ Nm/rad	$k_{zz}$	$k_x$	$k_y$ $10^9$ N/m	$k_z$	$k_{xx}$	$k_{yy}$ $10^9$ Nm/rad	$k_{zz}$
W14	L05	10	0.28	0.28	0.19	5.14	1.99	1e4	0.56	0.56	0.38	10.29	4.52	1e4
		100	1.72	1.72	0.19	6.69	3.54		3.43	3.43	0.38	13.39	7.63	
	L30	10	0.28	0.28	0.75	14.59	1.99		0.56	0.56	1.50	29.19	6.14	
		100	1.72	1.72	0.75	16.14	3.54		3.43	3.43	1.50	32.29	9.25	

The calculation of foundation spring stiffness of the lumped parameter model is presented in Chapter 4. For sensitivity analysis, lower and upper values are also determined considering the Young modulus of the soil as either 10 MPa or 100 MPa (typical range from soft to stiff clay and from loose to compact sand). Results for W14 deck width are illustrated in Table 5.2.

### 5.3.3 Modal analysis results

Typical vibration modes of different configurations are illustrated in Fig. 5.3a-d. The modal analysis results show the high stiffness and thus low fundamental periods of these structures. In the case of shorter, less flexible bridges (Fig. 5.3e), the fundamental period is often lower than the  $T_c$  period, thus it falls onto the plateau of the applied spectrum. This indicates that high base shear forces are expected and that these bridges are possibly vulnerable against seismic actions. The fundamental periods are summarized in Appendix C.

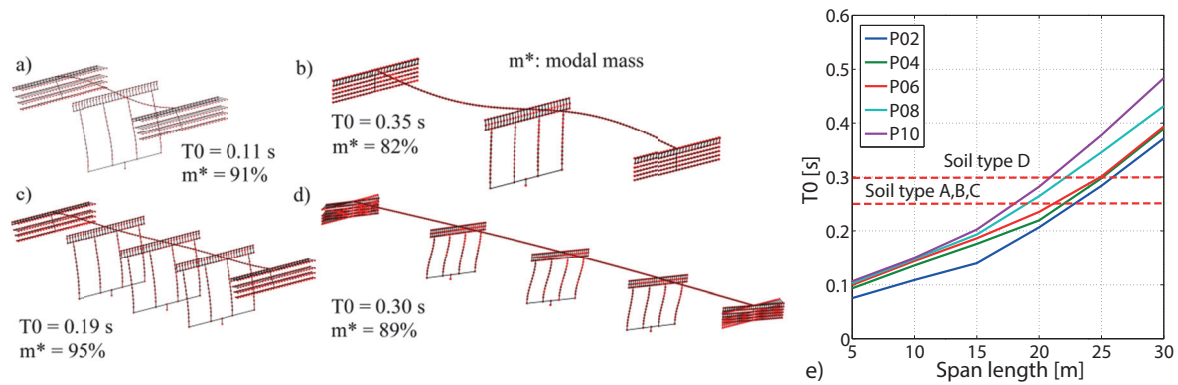


Fig. 5.3 First vibration modes and fundamental periods for different typical layouts for W14P06 bridges. a) S2L10; b) S2L25; c) S4L10; d) S4L25. e) Fundamental periods for W14S4 bridges ( $T_C$  periods: red dashed line).

### 5.3.4 Effect of the soil structure interaction

Since PMG-I bridges are built with monolithic joints, the seismic resistance is provided by both piers and abutments, thus the soil-structure interaction (SSI) can significantly influence the seismic behavior. In this case, the use of upper and lower bound estimates of the soil stiffness (Table 5.2) is recommended to obtain conservative demands for each bridge component. The effect of the backfill soil is also investigated with two different stiffness values (28.7 and 14.35 kN/mm/m) (Caltrans 2013). Three cases are examined: in each case one of the three components (backfill soil - 100, abutment foundation - 010, pier foundation - 001) is characterized with its higher, while the other two components have their lower stiffness value. In Table 5.3 representative results are illustrated for two different layouts.

Table 5.3 Sensitivity of MMRSA results to different SSI stiffness. P06L20 bridges: a) W8S2; b) W20S4.  $\Delta$  denotes the relative difference between maximum and minimum value in %.

a)											
Code	Pier internal forces				Joint sh. force (abut.)		Joint sh. force (pier)		Earth pres.. $\sigma$ [kPa]	Girder disp. [mm]	
	$F_x$ [kN]	$F_y$ [kN]	$M_x$ [kNm]	$M_y$ [kNm]	$F_x$ [kN]	$F_y$ [kN]	$F_x$ [kN]	$F_y$ [kN]		$d_x$	$d_y$
100	25	153	456	122	2218	<b>1370</b>	30	387	<b>63</b>	3	<b>6</b>
010	23	125	368	103	<b>2295</b>	1355	17	293	26	3	5
001	<b>32</b>	<b>172</b>	<b>514</b>	<b>163</b>	2202	1336	<b>46</b>	<b>440</b>	38	<b>4</b>	6
$\Delta$ %	39	38	40	58	4	3	167	50	145	56	25
b)											
Code	Pier internal forces				Joint sh. force (abut.)		Joint sh. force (pier)		Earth pres.. $\sigma$ [kPa]	Girder disp.[mm]	
	$F_x$ [kN]	$F_y$ [kN]	$M_x$ [kNm]	$M_y$ [kNm]	$F_x$ [kN]	$F_y$ [kN]	$F_x$ [kN]	$F_y$ [kN]		$d_x$	$d_y$
100	59	250	745	310	<b>8398</b>	4756	281	1164	<b>121</b>	7	<b>7</b>
010	45	192	571	204	8082	<b>4802</b>	213	894	49	5	6
001	<b>70</b>	<b>261</b>	<b>781</b>	<b>377</b>	8303	4621	<b>340</b>	<b>1217</b>	76	<b>8</b>	7
$\Delta$ %	57	36	37	85	4	4	59	36	147	64	20

Conservative pier internal forces and pier joint shear forces are obtained considering the pier foundation as the stiffest element of the SSI (code: 001). The same behavior can be observed in case of the abutment-backfill soil system. The increased stiffness of these components (code: 100 or 010) can slightly affect the abutment joint shear forces; while the passive earth pressure is significantly dependent on the stiffness of the backfill soil (code: 100). Observing the girder displacements, both longitudinal and transverse movements are controlled by the stiffness of the abutment foundation (code: 010). As confirmed by Table 5.3

using non-conservative variation may lead to ~60% underestimation of specific demands. Therefore, in this study analyses are carried out with all the three variations to calculate conservative results for each component.

### 5.3.5 Calculated seismic demands

#### 5.3.5.1 Superstructure

In Fig. 5.4b vertical girder bending moments of the W14S4P06L25 configuration are illustrated. The moments from dead load are dominantly sagging due to the composite construction technology (considerable dead load is carried by the simply supported girders, since continuity is created after the hardening process of the concrete slab). A significant contribution can be observed from the longitudinal vibration (EQX) compared to the vertical one (EQZ). This can be explained as follows. Horizontal forces are transferred with eccentricity from the substructure. The longitudinal movement of the piers can develop only if the girders are bent (Fig. 5.4a). The high stiffness of the whole system implies significant bending moments; besides, the intensity of the horizontal ground motion is usually higher.

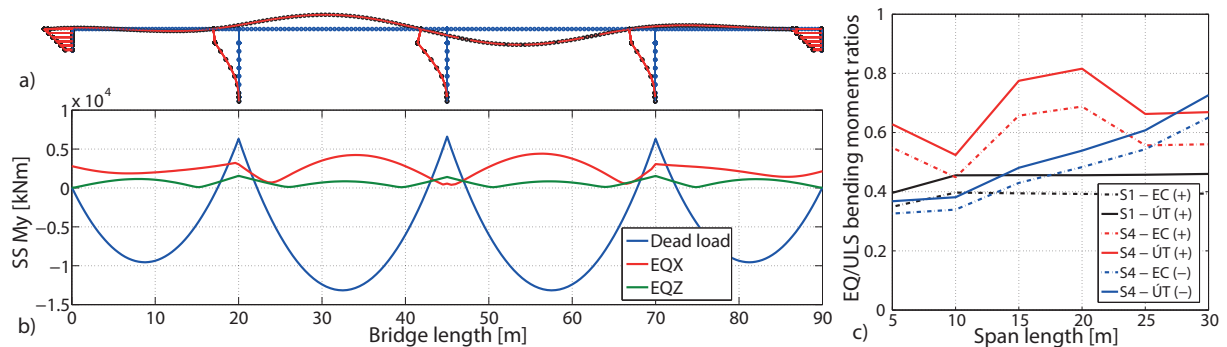


Fig. 5.4 a) Dominant vibration mode in the longitudinal direction. b) Vertical bending moments ( $M_y$ ) of the superstructure for the W14S4P06L25 configuration<sup>4</sup>. c) EQ/ULS  $M_y$  ratios for W14P06 bridges.

Evaluation of the superstructure is carried out as follows. Even though the girders are not designed for seismic action, they should withstand the demands in ULS. Internal forces are determined both in ULS and in seismic combination (EQ). In Fig. 5.4c, ratios of maximum bending moments calculated in accordance with the former Hungarian standard ÚT and with EC0-1 (CEN 2011b) are shown. The two standards differ in the partial factor of the dead load (1.1 and 1.35 in ÚT and EC, respectively) leading to a significant difference in the superstructure capacity. The induced additional safety per EC results in higher capacity and better seismic performance. The EQ/ULS ratios indicate that single span bridges are less

<sup>4</sup> Note that seismic demands obtained with MMRSA are always positive due to the combination of modal responses, however negative signed values are also valid because of the bi-directional nature of earthquakes.

vulnerable; and even for multi-span bridges the critical ratio of 1.0 (failure of the girders) for either sagging (+) or hogging (-) moments is not reached.

Transverse bending moments of the superstructure may be higher than those from ULS, however the flexural capacity is still an order of magnitude greater, failure is not expected. For instance, the compressive stress in the external concrete fiber is around 2-5 MPa.

### 5.3.5.2 Superstructure-substructure joints

In Fig. 5.5a-c resultant joint shear forces are shown. Increasing demands with increasing span length is a general tendency due to the higher applied mass. Shear forces are higher at the superstructure-abutment joint as a result of the relatively high stiffness of the abutment-backfill soil system. At the abutment joint (Fig. 5.5a), increase is observed at lower piers (<4 m), while the tendency is reversed at the pier joint (Fig. 5.5b). The effect of the deck width is illustrated in Fig. 5.5c showing that the results are nearly the same for 14 m and 20 m width, while slightly increased demands are obtained for 8 m.

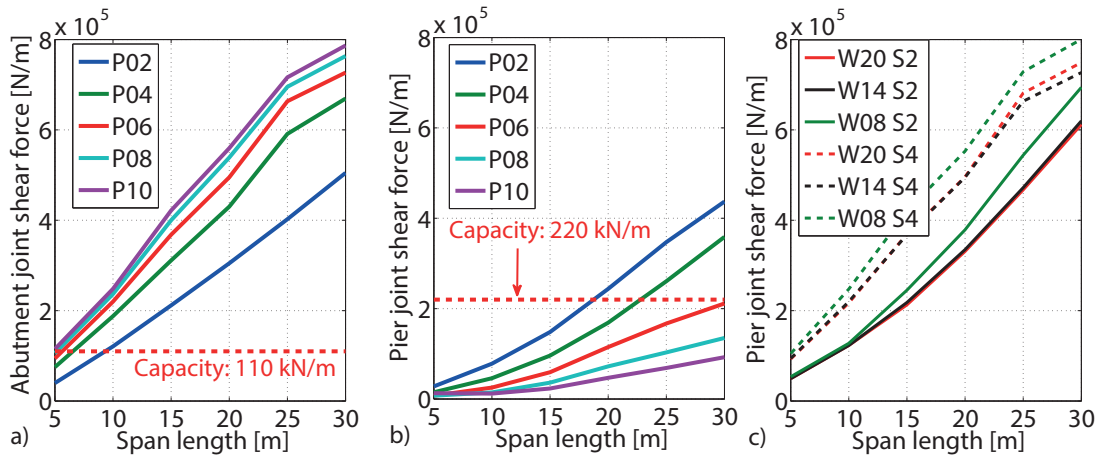


Fig. 5.5 Resultant joint shear forces (normalized to deck width): a) at the abutment (W14S4 configurations); b) at the pier (W14S4 configurations); c) for different deck widths.

To evaluate critical configurations, the shear resistance of the joints ( $R_u$ ) is determined with the formula presented in (Psycharis and Mouzakis 2012):

$$R_u = 1.1 n D^2 \sqrt{f_{cd} f_{sd}} / \gamma_R, \quad (5.1)$$

where  $n$ ,  $D$  and  $f_{sd}$  are the number, diameter and design strength of the rebars;  $f_{cd}$  is the design strength of the concrete and  $\gamma_R$  is the safety factor of 1.3. A conservative estimation neglecting the frictional resistance and considering C20/30 concrete and S500B rebars leads to a normalized resistance of  $\sim 110$  kN/m at the abutment (with  $\phi 16/150$ ) and  $\sim 220$  kN/m at the piers (with  $2\phi 16/150$ ). The resistance at the abutment is definitely insufficient even for shorter spans. The lower demands and the higher resistance of the pier joint lead to a lower vulnerability (critical only at shorter piers). Note, however, that after a possible failure of the abutment joint, redistribution of the forces may risk the failure of this component as well.

### 5.3.5.3 Piers

Results for the piers are depicted in Fig. 5.6a-c. Demands are lower in the longitudinal direction which stems from the longitudinal support provided by the high stiffness of the abutment and the backfill soil. The longitudinal shear forces ( $V_x$ ), the corresponding  $M_y$  bending moments and the transverse shear forces ( $V_y$ ) have the same tendency (Fig. 5.6a) of being increased for shorter piers. However, in Fig. 5.6b, the maximum values of transverse bending moments ( $M_x$ ) do not correspond to the lowest 2 m pier height, instead, a peak can be observed at 4 m. The pier height does not only influence the relative stiffness and thus the transferred lateral forces but also the lever arm of these forces. The pier should be high enough to minimize the developing seismic shear forces in a way that the governing bending moments are decreased as well.

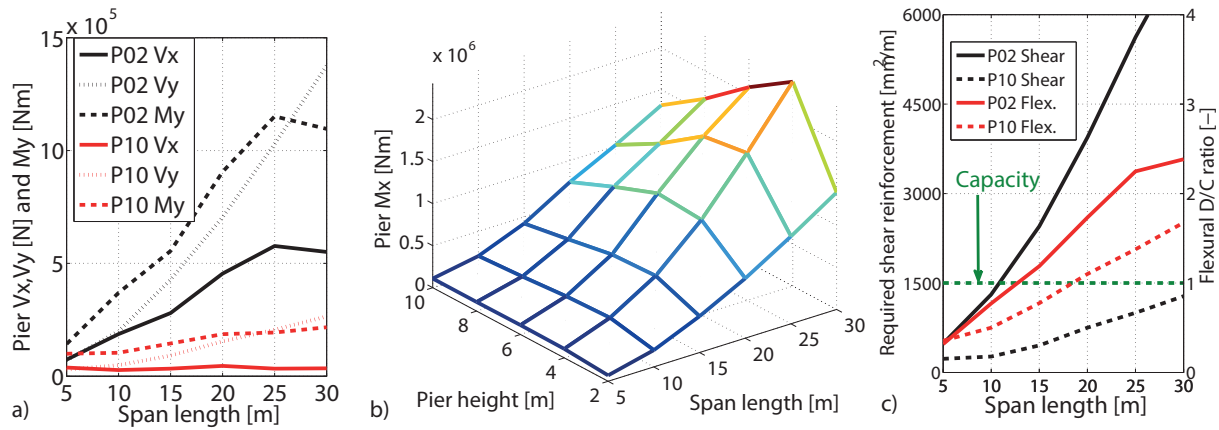


Fig. 5.6 Results for W14S4 configurations: a) pier shear forces ( $V_x, V_y$ ) and vertical bending moments ( $M_y$ ); b) pier transverse bending moments ( $M_x$ ). c) required shear reinforcements and flexural DC ratio of the pier.

The required shear reinforcement ( $A_{sw}/s_w$ ) and the flexural DC ratio are calculated per EC2-2 (CEN 2009b) and EC8-2:

$$A_{sw}/s_w = \gamma_{Bd} V_{Ed} / (z f_{ywd} \cot \theta) \text{ and} \quad (5.2)$$

$$DC_{fl} = (M_{xEd}/M_{xRd})^a + (M_{yEd}/M_{yRd})^a, \quad (5.3)$$

where  $\gamma_{Bd}$  is a partial factor for brittle failure;  $V_{Ed}$  is the resultant shear force;  $z$  is the lever arm of internal forces;  $f_{ywd}$  is the design strength of the stirrups;  $\theta$  is the angle of the concrete compression strut;  $M_{xEd}$ ,  $M_{yEd}$  and  $M_{xRd}$ ,  $M_{yRd}$  are the design moments and flexural resistance in each direction and the exponent  $a$  takes into account the normal force in the element. Typical cross-section and material properties<sup>5</sup> are used for the calculations. According to Fig. 5.6c short piers show high vulnerability against shear forces (maximum applicable span

<sup>5</sup> 0.6x0.9 m cross section;  $\phi 12/150$  stirrups ( $\sim 1500 \text{ mm}^2/\text{m}$ );  $\sim 1\%$  longitudinal reinforcement ratio ( $16\phi 20$ ); S500B steel and conservative concrete grade C20/30.

length is <10 m), while flexural behavior is inadequate for higher piers (but the span length can be much longer <17 m in this case).

#### 5.3.5.4 Piles

The pile foundation is incorporated in the model with simple integrated springs. Detailed analysis of the individual piles is out of scope in this study, however forces transferred to the pile head can be calculated using the foundation layout and the reaction forces. Pile normal forces are calculated (Fig. 5.7a) to estimate whether compressive resistance failure occurs. The typical pile resistance is around 2000-2500 kN; therefore failure is not expected.

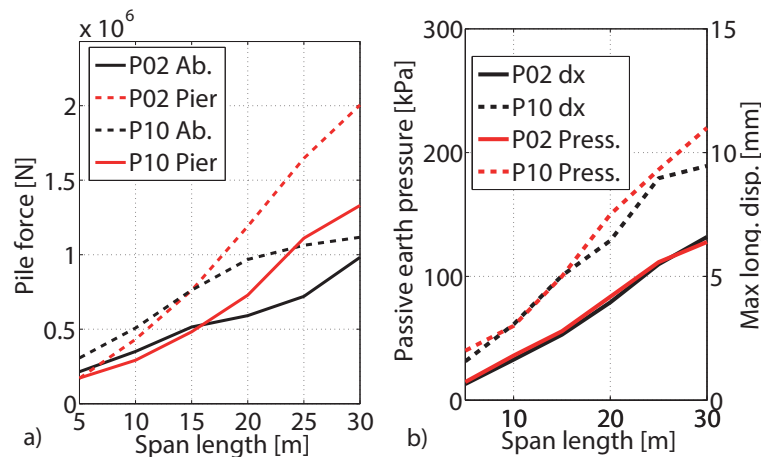


Fig. 5.7 Results for W14S4 configurations: a) pile normal forces; b) maximum passive earth pressure and maximum longitudinal displacements.

#### 5.3.5.5 Abutment and backfill soil

Two other components, the abutment and backfill soil demands are shown in Fig. 5.7b. The abutments are considered as rigid blocks, therefore only global stability failure is taken into consideration. Demands are determined as the maximum longitudinal displacement that can possibly cause stability failure, while the backfill soil demands are measured with the maximum passive earth pressure. These demands are in high correlation, since passive earth pressure is caused by the longitudinal movements of the abutment. It can be concluded that the probability of failure is low. Passive earth pressure never reaches ~430 kPa (ultimate failure threshold per Caltrans), while the displacements are always under 30 mm (recommended limit for bridges of importance class III per EC8-2).

#### 5.3.6 Critical components and layouts

To highlight critical components and layouts, maximum acceptable PGA is calculated for each component of each configuration. These MAPGA values are presented in detail in Appendix D, only some tendencies are illustrated here. The capacities of the components are the ones presented in the previous subsections.

Fig. 5.8 presents the dependency of MAPGA on the pier height and deck width. The pier height highly influences the pier internal forces (especially shear), thus the MAPGA values as well (Fig. 5.8a-b). As confirmed by Fig. 5.8c-d, the results are less sensitive to the deck width, pier height and the length of the superstructure are far more important structural attributes.

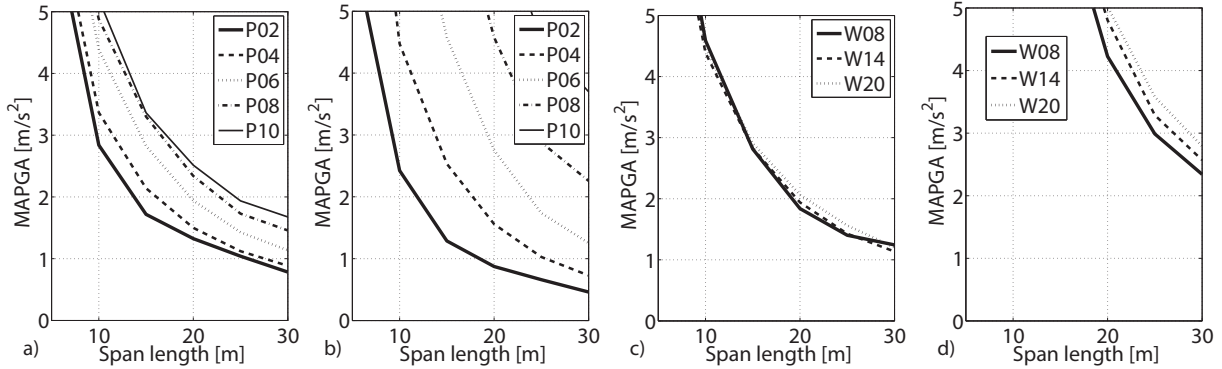


Fig. 5.8 MAPGA values of S3 bridges. Different pier heights and W14: a) pier bending; b) pier shear. Different widths and P06: d) pier bending; e) pier pile compression. PGA values in Hungary: 0.8-1.5  $m/s^2$ .

It is assumed that the failure of one component can initiate the failure of the whole system (series system). It is important to understand which component is the most vulnerable for different layouts. In Fig. 5.9, MAPGA results for the most vulnerable components are illustrated for W14S3 configurations. High vulnerability of the abutment joint is confirmed, this component is the most critical for every configuration. Failure of the pier is characterized by shear or flexural failure for shorter or higher piers, respectively. Note that flexural capacity can be characterized with at least a limited ductile behavior. This indicates the sensitivity of piers to shear forces for pier heights typically used in case of highway bridges (up to  $\sim 5-6$  m).

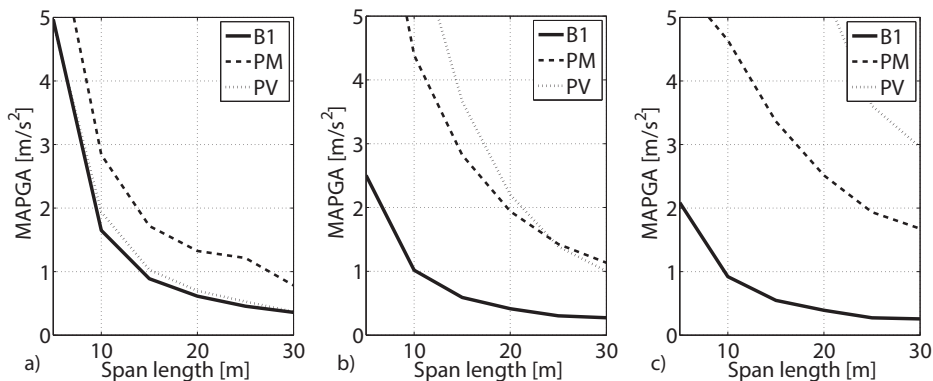


Fig. 5.9 Critical components for W14S3 configurations: a) P02; b) P06; c) P10. (B1-abutment joint; PM – pier flexural failure; PV – pier shear failure). PGA values in Hungary: 0.8-1.5  $m/s^2$ .

## 5.4 Parametric analysis of reinforced concrete slab (SLAB) bridges

### 5.4.1 Description of SLAB bridges

SLAB bridges are cast-in-situ monolithic reinforced concrete structures commonly constructed as highway overpass bridges along with PMG bridges. Their construction requires

stand- and formwork, thus the construction time is longer than in case of PMG bridges. The general layout is shown in Fig. 5.10a. The global geometry is usually the same as of PMG-I bridges, thus the examined configurations and the parametric space are assumed to be the same in this study.

However, fundamental differences affecting the behavior of SLAB bridges should be highlighted. Note that there is no pier cap, piers are connected directly to the deck with a monolithic joint which can transfer not only shear forces but also moments (monolithic joint Type 1). However, the joints at the abutments are constructed with one layer of vertical bars only, characterized by a similar behavior as PMG bridge joints (monolithic joint Type 2). The stiffness and mass of the deck is calculated considering typical SLAB bridge cross-sections for different deck widths (Fig. 5.10b). The structural height is determined as the function of span length. Additional permanent load is  $\sim 750$  kg/m railing;  $\sim 400$  kg/m<sup>2</sup> pavement.

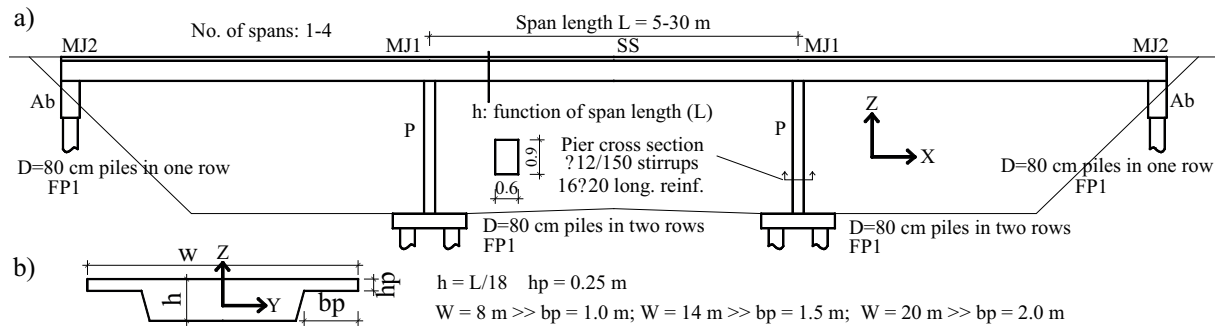


Fig. 5.10 General layout of SLAB bridges: a) side-view of the bridge; b) general cross-section.

Since the behavior is not expected to be significantly different from that of PMG-I bridges, the following sections focus on the main conclusions and remarkable differences.

#### 5.4.2 Numerical modeling issues

The modeling assumptions are the same as for PMG-I bridges. Geometric linear analysis with initial stiffness values (foundation stiffness is presented in Table 5.2) is used.

#### 5.4.3 Modal analysis results

Fig. 5.11a shows the typical vibration modes of the W8S4L30P06 configuration. The figure illustrates well the high level of interaction between the longitudinal and vertical vibration modes; pier shear and bending also occur during vertical vibration due to the integrate monolithic joint type. Similarly to PMG-I bridges, SLAB bridges can also be characterized by high vibration frequencies.

The fundamental periods are often on the plateau of the applied spectrum, moreover other vibration modes (which are more important for the piers, for instance) can be characterized

with even higher frequencies as it is shown in Fig. 5.11a where the dominant longitudinal vibration mode is only the third one with a fundamental period of  $\sim 0.3$  s.

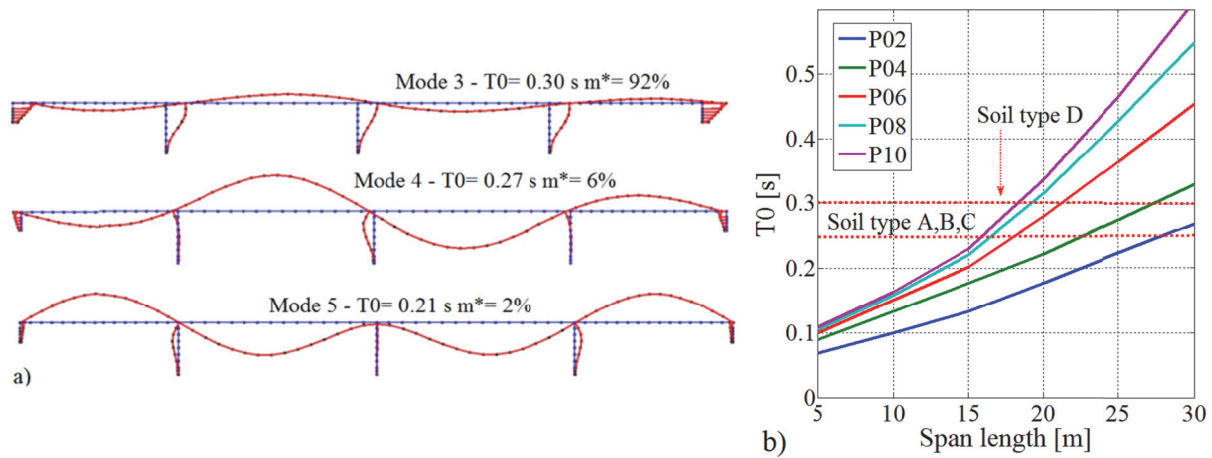


Fig. 5.11 a) Typical vibration modes and fundamental periods for the W8S4L30P06 configuration. b) Fundamental periods of W14S4 configurations ( $T_C$  periods: red dashed line).

#### 5.4.4 Effect of the soil structure interaction

Similarly to the analysis of PMG-I bridges, the effect of the SSI is also investigated. In Table 5.4 representative results are presented for two different layouts. The results are similar to the ones observed in case of PMG-I bridges, however note that pier internal forces are increased compared to PMG-I bridges with the same configurations. As confirmed again by Table 5.4, using non-conservative variation may lead to significant underestimation of specific demands in case of SLAB bridges as well.

Table 5.4 Sensitivity of MMRSA results to different SSI stiffness. L20P06: a) W8S2; b) W20S4.  $\Delta$  denotes the relative difference between maximum and minimum value in %.

a)		Pier internal forces				Joint sh. force (abut.)		Joint sh. force (pier)		Earth pres..	Girder disp. [mm]	
Code	$F_x$ [kN]	$F_y$ [kN]	$M_x$ [kNm]	$M_y$ [kNm]	$F_x$ [kN]	$F_y$ [kN]	$F_x$ [kN]	$F_y$ [kN]	$\sigma$ [kPa]	$d_x$	$d_y$	
100	89	221	661	257	<b>3110</b>	<b>1629</b>	200	577	<b>85</b>	4	<b>8</b>	
010	64	189	562	178	2905	1602	128	478	32	3	7	
001	<b>106</b>	<b>247</b>	<b>738</b>	<b>315</b>	2889	1585	<b>253</b>	<b>654</b>	48	<b>5</b>	8	
$\Delta$ %	67	30	31	77	8	3	98	37	166	65	19	
b)		Pier internal forces				Joint sh. force (abut.)		Joint sh. force (pier)		Earth pres..	Girder disp. [mm]	
Code	$F_x$ [kN]	$F_y$ [kN]	$M_x$ [kNm]	$M_y$ [kNm]	$F_x$ [kN]	$F_y$ [kN]	$F_x$ [kN]	$F_y$ [kN]	$\sigma$ [kPa]	$d_x$	$d_y$	
100	269	440	1311	752	<b>13224</b>	8316	815	1449	<b>192</b>	10	<b>11</b>	
010	231	321	955	635	12977	<b>8669</b>	672	1034	80	8	9	
001	<b>295</b>	<b>461</b>	<b>1375</b>	<b>842</b>	11160	8202	<b>916</b>	<b>1524</b>	103	<b>11</b>	11	
$\Delta$ %	27	43	44	33	18	6	36	47	140	32	22	

#### 5.4.5 Calculated seismic demands

##### 5.4.5.1 Superstructure

In Fig. 5.12a vertical bending moments are illustrated (W14S4P06L25 configuration). The contribution of the longitudinal vibration (EQX) is still as significant as the vertical one (EQZ). However, the total seismic effect is negligible compared to the dead load. This is also confirmed by Fig. 5.12b where the EQ/ULS ratios (calculated per  $\dot{U}T$ ) are presented. The

ratio remains under 0.7 indicating low vulnerability. Moreover, if the bridge was designed in line with EC8-2, the possibility of superstructure failure would be even lower.

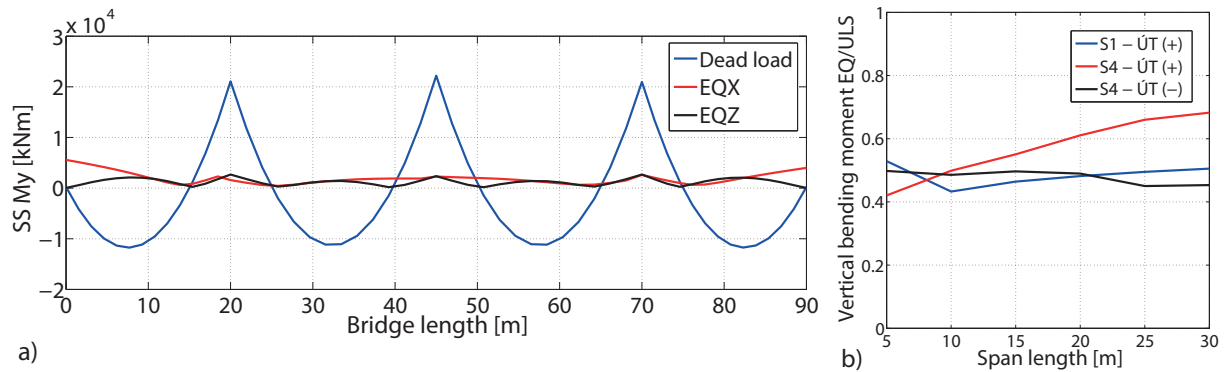


Fig. 5.12 a) Vertical bending moments ( $M_y$ ) of the superstructure of the W14S4P06L25 configuration. b) Ratios of vertical bending moments calculated in EQ and ULS for W14P06 bridges.

#### 5.4.5.2 Superstructure-substructure joints

Normalized abutment joint shear forces (Fig. 5.13a) indicate that this component may be critical for SLAB bridges as well. Using Eq.(5.1) to calculate the resistance of a typical joint with  $\phi 16/150$  shear reinforcement results in  $\sim 110$  kN/m shear capacity showing that there is a high probability that this component fails even in case of shorter spans. The deck to pier joints are less vulnerable due to the lower shear forces, besides, it is shown in Chapter 4 that pier shear failure is much more likely to occur prior to the failure of the monolithic joint.

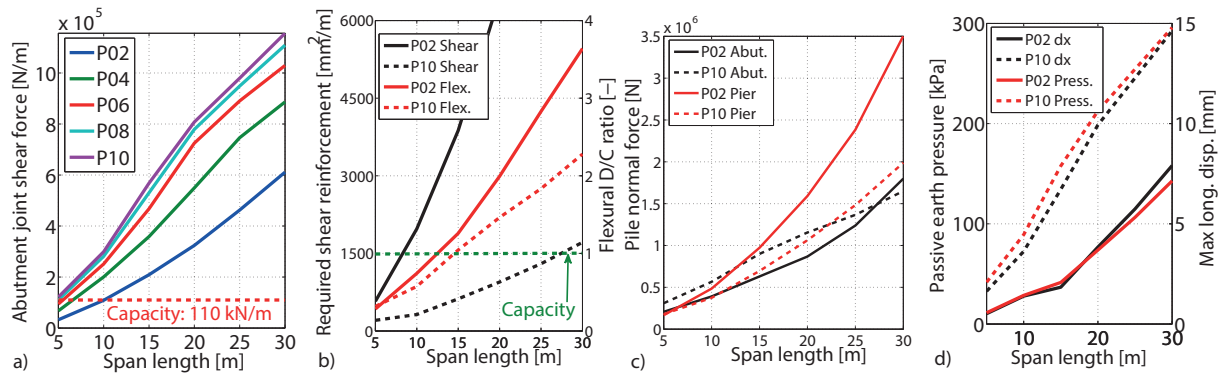


Fig. 5.13 Results for W14S4 bridges. a) abutment joint shear forces; b) required shear reinforcement and flexural DC ratio of the pier; c) pile normal forces; d) passive earth pressure and longitudinal displacements.

#### 5.4.5.3 Substructure

Required shear reinforcement and flexural DC ratio of the pier are shown in Fig. 5.13b. SLAB bridge piers show higher vulnerability than PMG-I bridges against shear forces and flexural failure as well. The maximum applicable span length for short piers is under 8 m, for instance. Fig. 5.13c illustrates pile normal forces. Considering typical pile resistance ( $\sim 2500$  kN) failure is not expected except for extremely short piers and long spans. The low probability of either backfill soil or abutment failure can also be concluded (Fig. 5.13d).

### 5.4.6 Critical components and layouts

MAPGA values are calculated for SLAB bridges as well (see Appendix D). The dependencies on the deck width and pier height are similar to those presented in Fig. 5.8 in case of PMG-I bridges, while the critical components are also identical for the same configurations. However, pier internal forces are generally higher in case of SLAB bridges for the same arrangement due to the different monolithic joint type (MJ2) transferring not only shear forces but also bending moments. Besides, the mass of the SLAB bridges is also higher causing higher seismic demands. Table 5.5 illustrates the differences for pier flexural and shear failure of W14S4 bridges. Worse performance can be observed for both bridge classes if the piers are shorter and the spans are longer. Note the better performance of PMG-I bridges in case of a typical highway overpass configuration (P06 and L20-25).

Table 5.5 MAPGA values for pier flexural and shear failure for W14S4 bridges.

SLAB						PMG-I						Span length/Pier height [m]	Component
5	10	15	20	25	30	5	10	15	20	25	30		
6.9	2.6	1.5	1.0	0.7	0.5	6.2	2.5	1.6	1.1	0.9	0.8	2	Flexural
5.1	1.9	1.0	0.6	0.5	0.4	5.8	2.7	1.6	1.2	0.8	0.7	4	
5.6	2.3	1.2	0.8	0.6	0.5	6.7	3.4	2.0	1.3	0.9	0.8	6	
6.3	2.9	1.5	1.1	0.8	0.7	6.8	3.9	2.3	1.5	1.2	1.0	8	
6.2	3.4	1.9	1.3	1.1	0.9	5.5	3.9	2.5	1.8	1.4	1.2	10	
3.9	1.1	0.6	0.3	0.2	0.2	4.6	1.7	0.9	0.6	0.4	0.3	2	
5.2	1.7	0.8	0.4	0.3	0.2	7.2	2.8	1.4	0.8	0.5	0.4	4	
7.9	3.1	1.4	0.8	0.6	0.5	10.3	4.6	2.2	1.2	0.8	0.7	6	
10.6	5.0	2.3	1.4	1.0	0.8	12.3	6.8	3.5	1.9	1.4	1.1	8	
10.9	7.1	3.6	2.4	1.7	1.3	9.8	8.4	5.0	3.0	2.2	1.8	10	
5	10	15	20	25	30	5	10	15	20	25	30		

## 5.5 Estimation of critical bridges based on the preliminary study

Due to the lack of essential data for other classes, preliminary performance evaluation is conducted only for PMG-I and SLAB bridges. The evaluation is carried out as follows: 1) Essential parameters of the bridge are obtained from the database (bridges without sufficient input parameters are excluded). 2) MAPGA values are determined with linear interpolation on the parametric results for each structural component. 3) The MAPGA values are modified with a factor reflecting bridge condition (from condition 1 to 5 a factor of 1.0-0.6 is applied). 4) PGA value for the bridge site is determined. 5) Possible failure of each component is calculated comparing the PGA and the corresponding MAPGA.

To illustrate the utilization of each bridge component regarding all the bridges, empirical cumulative distributions (representing non-exceedance) of the component DC ratios are created (Fig. 5.14). For example, the PV curve in Fig. 5.14a shows that 30% of the bridges have inadequate pier shear resistance.

In case of single span bridges only the abutment joint is critical. In 22% of the observed 1313 bridges, there is a possibility that this component fails (Table 5.6). The percentage is

lower for slab bridges because they are often constructed for shorter spans. Failure of this component is highly probable for multi-span bridges as well, more than 90% of the bridges have inadequately detailed abutment joint.

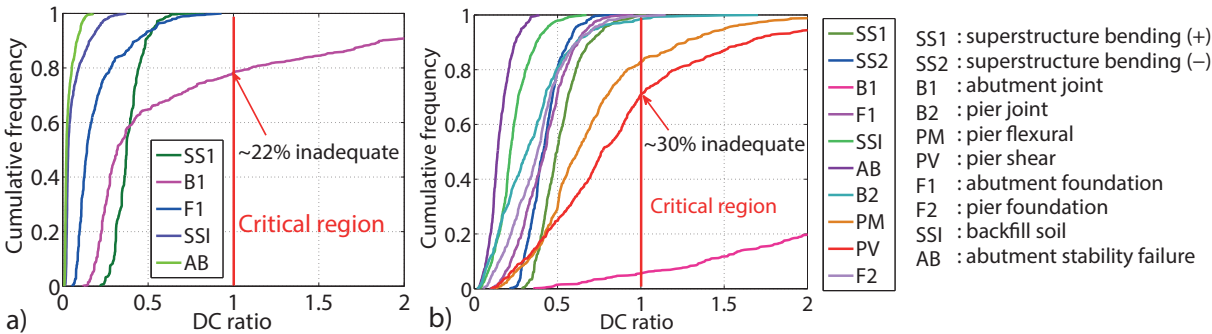


Fig. 5.14 Critical bridge component of single (a) and multi-span (b) bridges in %.

Table 5.6 Relative number of critical bridge components.

	Single span bridges		Multi span bridges			
	Abutment joint	Total number	Abutment joint	Pier flexural failure	Pier shear failure	Total number
PMG-I	29 %	758	94 %	1 %	22 %	602
SLAB	12 %	555	96 %	4 %	51 %	166
ALL	22 %	1313	95 %	2 %	28 %	768

The joint failure does not necessary cause progressive collapse in case of multi-span bridges; pier failure is far more dangerous. Table 5.6 also shows the relative number of bridges where collapse occurs either with pier flexural or shear failure. According to Table 5.5 pier shear failure is critical for the most commonly used typical highway overpass layout (P06 and L20-25). This is reflected in the results: pier shear failure is more likely to occur regarding the whole bridge stock. Note also that a significant portion of slab bridges may suffer pier failure even though they are usually constructed with shorter spans.

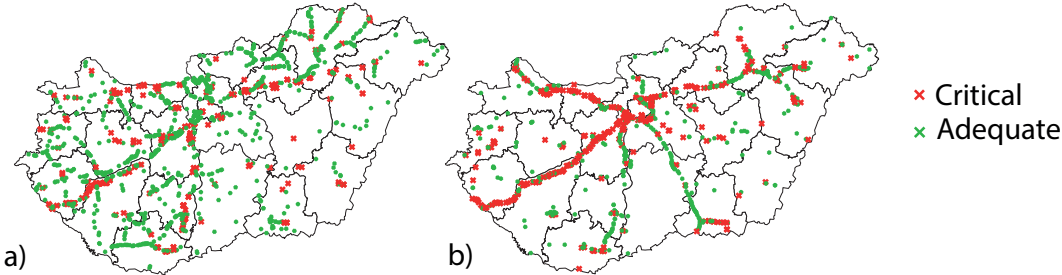


Fig. 5.15 Critical bridges. a) Single span - abutment joint failure. b) Multi span - pier failure (shear or flexural).

In Fig. 5.15a-b, single span bridges with possible abutment joint and multi-span bridges with pier failure (causing collapse) are illustrated. These maps are useful tools to identify critical bridges and to select regions of interest for a possible retrofiting project.

### 5.6 Summary

A preliminary parametric seismic analysis is conducted for typical slab and integral precast multi-girder bridges with monolithic joints. It is shown that the abutment joints are highly

vulnerable; besides, pier failure (causing progressive collapse) may also occur in case of multi-span configurations. The evaluation of the whole inventory indicates that the pier and monolithic joint shear resistance are not sufficient for several existing bridges. Note that these results are obtained with conservative assumptions (both for capacities and demands), thus the number of critical structures may be lower in reality. I summarized the presented results in my Thesis III.

The linear MMRSA is useful to highlight the critical components and configurations, however, it cannot follow the nonlinear behavior and thusly the redistribution of internal forces after yielding. To capture the post-elastic behavior and to predict the developing damage in the structures, fragility analysis is conducted and presented in Chapter 6.

# Chapter 6

## Seismic Fragility Assessment of Existing Bridges

### 6.1 Examined bridge configurations

Parametric fragility analysis would be beneficial for each bridge class to determine the seismic performance of a wide range of different structural types and configurations. There are two factors limiting this demand: 1) the computational time for one bridge can be excessive; 2) only PMG-I and SLAB bridges can be described by a reliable parametric field for the most important structural attributes. Considering these limitations, parametric fragility analysis is carried out only for PMG-I bridges regarding their most significant contribution to the inventory, while other classes are evaluated as part of the bridge portfolio presented in Chapter 3. Accordingly, the fragility evaluation is divided into two main parts:

- 1) Parametric analysis of PMG-I bridges (bridges are referred to with the configuration notation e.g. W14S4P04L30). Due to the longer computational time, the parametric field is reasonably smaller than in the preliminary study (see Table 5.1).
- 2) Individual analysis of 30 representative bridges in the portfolio (bridges are referred to with the bridge number; e.g. BR25; see Table 3.4).

### 6.2 Adopted method for fragility analysis

Widely applied methods exist for fragility analysis such as Incremental Dynamic Analysis (IDA) (Vamvatsikos and Cornell 2002) and Multiple Stripes Analysis (MSA) (Jalayer and Cornell 2009). In this study, MSA is adopted since it is proved to be more efficient fragility estimates than IDA for a given number of structural analyses (Baker 2015). Moreover, it allows for different ground motions to be used at varying intensity levels, to represent the differing characteristics of low and high intensity shaking. The steps of the MSA procedure are presented in Fig. 6.1a.

At each intensity level a number of ground motions are selected for each horizontal direction. Maximum demands are registered during NLTHA, then assuming LN distribution the median and the coefficient of variation (COV) are calculated for the demands. A single fragility point at an intensity level is obtained as follows:

$$P[(D > C_{LSi})|IM] = \int_0^{\infty} P(D > \alpha|IM) P(C_{LSi} = \alpha) d\alpha, \quad (6.1)$$

where  $D$  is the calculated seismic demand;  $C_{LSi}$  is the capacity associated with the  $i^{\text{th}}$  LS; the second function is the probability density function of the capacity and  $\alpha$  denotes integration over the demand parameter. The total probability for a component  $LS_i$  can be computed as:

$$p_i = \int_{IM} P[(D > C_{LSi})|IM] d\lambda(IM), \quad (6.2)$$

where  $d\lambda$  is the derivative of the hazard curve (Fig. 6.1b). In this study, the reliability index ( $\beta$  calculated with the inverse standard normal CDF) is used to compare the seismic performance of different bridge configurations:

$$\beta_i = -\phi^{-1}(p_i). \quad (6.3)$$

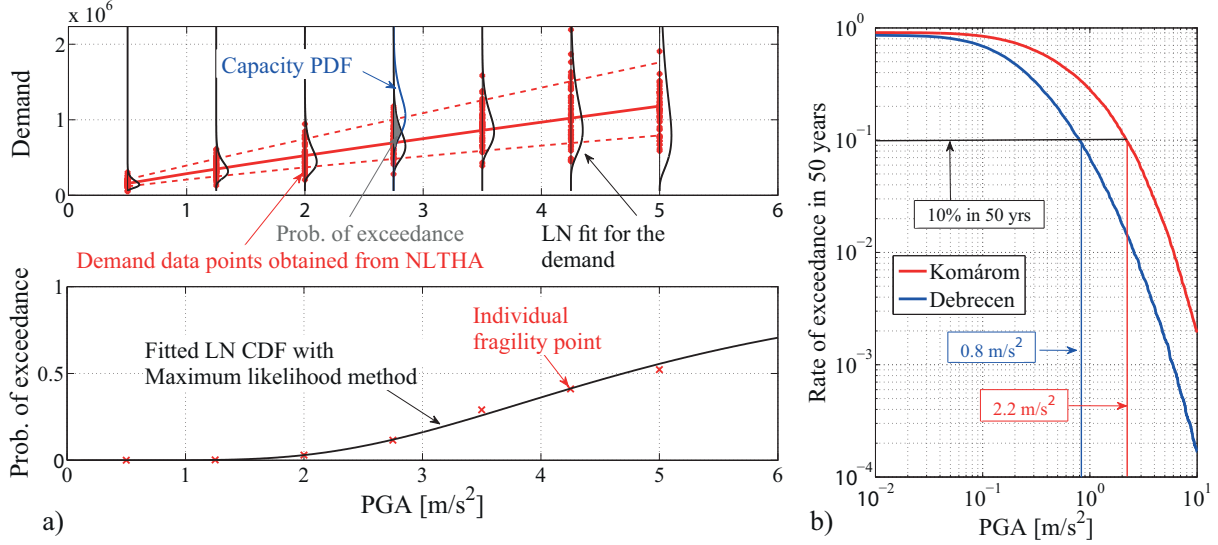


Fig. 6.1 a) Procedure of the Multiple Stripes Analysis. b) PGA hazard curve for Komárom and Debrecen considering soil type C.

The component fragility curves are useful to highlight critical components, and to calculate the probability of component failure, however, a system fragility curve is required to determine the probability related to the whole structure. It is assumed that bridges compose series systems (system failure is associated with the failure of any component). Using first-order reliability theory, a simple lower and upper bound on the system fragility ( $P_{sys}$ ) can be determined for an  $m$  component system with  $P_i$  component probabilities at a given IM level:

$$\max_{i=1:m} P_i \leq P_{sys} \leq 1 - \prod_{i=1}^m [1 - P_i]. \quad (6.4)$$

The lower bound represents a system where the components are fully stochastically dependent (un-conservative estimate), while the upper bound assumes that the components are all statistically independent (conservative estimate) (Nowak and Collins 2000).

Additionally, MC simulation is applied to give a better estimation based on the joint distribution of the demands and capacities assumed to be multivariate LN (MLN) distributions (Nielson 2005). At each IM level, the marginal distribution of the component demands are obtained during the MSA procedure, then the cross-correlation is computed to fully describe the distribution of the demands. The capacities are also estimated with an MLN distribution, but in this case the correlation between each component capacity is not known. Accordingly, two cases are examined: full correlation or no correlation at all (regarding the

capacities). The idea of the simulation is to generate a large number of random samples from the demand and capacity MLN distributions, then  $P_{sys}$  is determined by taking the ratio of the cases of failure and the number of simulated cases. This can be done for various IM levels to compose the individual points of the system fragility curve.

In the study, PGA is selected as the intensity measure for two reasons: 1) theoretically the probability of failure is independent of the chosen IM if hazard compatible ground motions are selected with the GCIM approach (Bradley 2012d); 2) comparison between fragility curves are easier with a general IM such as PGA. 7 (0.50:0.75:5.00 m/s<sup>2</sup>) and 10 (0.5:0.5:5 m/s<sup>2</sup>) intensity levels are chosen for the analysis of PMG-I bridges and the portfolio bridges, respectively. Finally, 50 tri-directional ground motions<sup>6</sup> (two horizontal and one vertical component) are selected for each level in all cases considering soil type C.

Table 6.1 Limit states and associated capacities. VA – various values for different configurations. Detailed information on the limit state median values can be found in Appendix F.

Component	Measure	Definition			Median			COV		
		LS1	LS2	LS3	LS1	LS2	LS3	LS1	LS2	LS3
Pier flexural	Steel or concrete strain	Yielding of rebars	Spalling of concrete	Crushing of concrete	0.28%	0.3% <sup>1</sup>	VA <sup>2</sup>	0.25	0.30	0.35
Pier shear <sup>3</sup>	Shear force	Shear failure	Shear failure	Shear failure	VA <sup>4</sup>	VA	VA	0.25	0.25	0.25
Type 2 monolithic joint <sup>5</sup>	Deformation	Yielding	Strength degradation	Unseating <sup>6</sup>	2 mm	50 mm	VA	0.25	0.30	0.35
Elastomeric bearing <sup>7</sup>	Deformation	Yielding	Girder falls off from pedestal <sup>8</sup>	Unseating	70 mm <sup>8</sup>	VA	VA	0.25	0.30	0.35
Conventional bearing <sup>9</sup> – free <sup>10</sup>	Deformation	Girder falls off from pedestal	Girder falls off from pedestal	Unseating	VA	VA	VA	0.25	0.30	0.35
Backfill soil <sup>12</sup>	Deformation	Yielding	Minor damage	Abutment instability	30 mm	60 mm	300 mm	0.25	0.30	0.35

Notes:

- 1 - Priestley et al. (1996).
- 2 - Determined with moment-curvature analysis of the pier cross-section.
- 3 - Brittle failure mode. Only one limit state is defined.
- 4 - Calculated according to Priestley et al. (1996) considering the contributions from concrete resistance, axial force and transverse steel.
- 5 - Used for PMG-I, PMG-NI and SLAB bridges with the presented capacities based on the cyclic behavior.
- 6 - Depends on the dimensions of the support. Measured as the closest distance from the supporting axis to the edge of the support.
- 7 - Used for PMG-NI bridges.
- 8 - Calculated from typical bearing properties applied for PMG-NI bridges.
- 9 - Depends on the dimensions of the support. Measured as the closest distance from the supporting axis to the edge of the pedestal.
- 10 - Used for RC-B, COMP-I, COMP-B, STEEL-I and STEEL-B bridges to model unrestrained horizontal behavior.
- 11 - Due to the uncertainty of the actual capacities, this component is not evaluated in the fixed direction.
- 12 - Capacity values are in accordance with EC8-2 (yielding, damage control limit, excessive deformation).

### 6.3 Damage limit states

Three damage limit states per Priestley et al. (1996) are considered that can be associated with the Damage Limitation (LS1), Significant Damage (LS2) and Near Collapse (LS3) LSs

<sup>6</sup> A preliminary fragility analysis is conducted for several bridges with 10, 20, 30, 40, 50 and 100 ground motions. It is concluded that using 50 ground motions per each intensity level is a rational choice, leading to reasonable computational time and negligible difference in the calculated fragility curves.

of EC8-3 (Table 6.1). The capacities of the bridge components are assumed to follow a LN distribution per EC0. In case of shear failure, COV value is assigned according to Biskinis et al. (2004). The other LSs are determined in a prescriptive manner (the thresholds are defined by the analyst) with assigned COV values of 0.25, 0.30 and 0.35 (Nielson 2005).

## 6.4 Uncertainties applied during the analysis

MSA can be regarded as a simplified MC simulation, where the capacity distribution is known and the distributions of the demands are determined independently from a reasonably large number of time-history analyses at each intensity level. The uncertainty of the demands are controlled mainly by the seismic load. However, to take into account other uncertainties in the phase of determining the demands, material properties and other input parameters are considered as random variables (Table 6.2). For each time-history analysis, a random sample is used to create the numerical model of the bridge.

Table 6.2 Random variables applied to sample input for the numerical model. VA – various values.

Variable	Distribution	Mean/median	STD/COV	Reference
Pier cross section	Uniform <sup>1</sup>	VA	± 20 mm	-
Pier height	Uniform	VA	± 50 mm	-
Superstructure mass	Normal	VA	0.1	Nowak and Collins (2000)
Reinforcement ratio	Uniform	1%	± 0.3%	-
Expansion joint gap	Uniform	VA	± 65% <sup>2</sup>	-
Concrete compressive strength	Lognormal	VA <sup>3</sup>	0.15	Ellingwood et al. (1980)
Reinforcing steel yielding	Normal	598 MPa <sup>4</sup>	0.1	Ellingwood et al. (1980)
Friction coefficient (concrete-concrete) <sup>5</sup>	Uniform	0.4	± 0.1	-
Elastomeric bearing shear modulus	Uniform	0.9 MPa	± 50%	Nielson (2005)
Elastomeric bearing friction coefficient	Lognormal	VA <sup>6</sup>	0.1	Dutta (1999)
Foundation stiffness	Uniform	VA	± 50%	Nielson (2005)
Backfill soil stiffness	Uniform	21.6 kN/mm/m	± 7.2 kN/mm/m <sup>7</sup>	Nielson (2005)
Earthquake direction	Uniform	$\pi/4$ rad	± $\pi/4$ rad	Nielson (2005)

### Notes

1- When sufficient information on probability distributions is not available, it is acceptable to assume a uniform distribution with reasonable upper and lower limits to roughly account for uncertainty (Nielson 2005).

2 - Assumption: the expected thermal movements are between ± 65% of the designed gap value.

3 - During the parametric analysis of PMG-I bridges a C20/25 concrete grade is assumed with a median strength value of 26 MPa. Bridges in the portfolio are usually built with C30/37 or C35/45 concrete with a median of 38 MPa and 44 MPa, respectively.

4 - S500 steel grade is assumed for all the bridges.

5 - Used in case of Type 2 monolithic joints.

6 - 0.35 and 0.4 for steel and concrete superstructure, respectively.

7 - Based on the upper and lower value of 14.4 and 28.8 kN/mm/m proposed by Caltrans (2013).

## 6.5 Aspects of the modeling and analysis assumptions

Two modeling issues are investigated: monolithic joints and expansion joints. Fig. 6.2 shows the NLTHA results for a PMG-I example bridge with or without modeling the non-linear behavior of the monolithic joints. Fig. 6.2b indicates that due to the high seismic demands, strength degradation of the shear reinforcement occurs and eventually the resistance is reduced, only frictional forces develop. This degradation leads to the redistribution of seismic demands: pier demands (Fig. 6.2a) and shear forces in the pier joint (Fig. 6.2c) are

increased significantly compared to the model where the joint is modeled as a rigid connection.

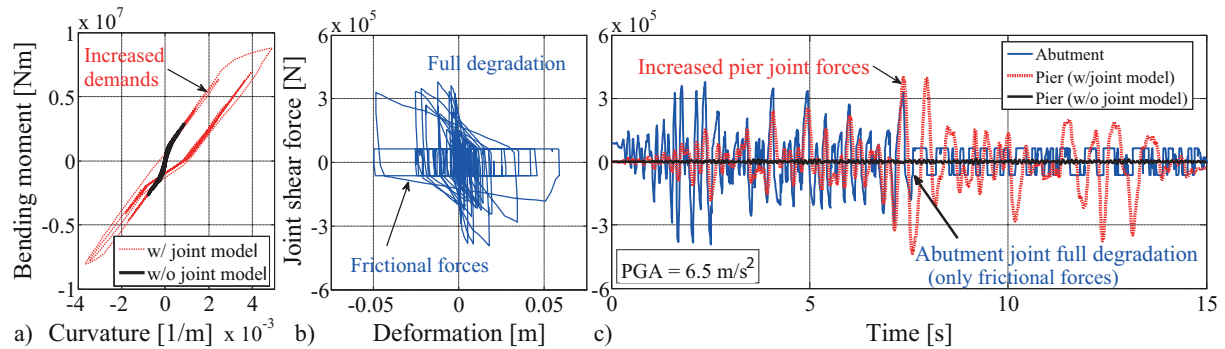


Fig. 6.2 NLTHA results with or without modeling the Type 2 joint behavior for a PMG-I example bridge (BR03). a) Pier moment-curvature diagram. b) Abutment joint behavior. c) Abutment and pier joint shear forces.

In case of bridges with expansion joints, the pounding between the abutment and the superstructure may significantly alter the seismic response. The phenomenon is illustrated in Fig. 6.3 for a composite bridge with 65 mm expansion joint gap. The pounding may decrease the demands of the piers: excessive displacements, thus the second order effects are reduced, while a portion of the seismic force is transferred to the abutment-backfill soil system (Fig. 6.3a). Fig. 6.3b shows that the pounding limits the expansion joint compressive deformations, while in Fig. 6.3c a pulse like peak can be observed in the backfill soil deformation when collision occurs.

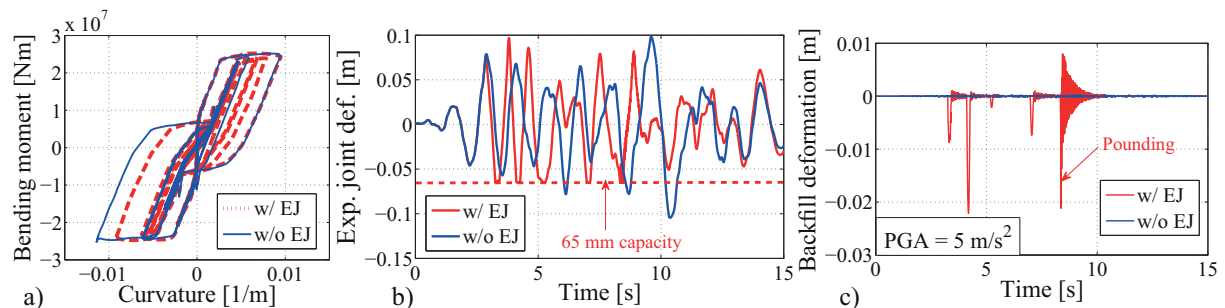


Fig. 6.3 NLTHA results with or without modeling the expansion joint (EJ) behavior for a COMP-I example bridge (BR20). a) Pier moment-curvature diagram. b) Expansion joint deformation. c) Backfill soil deformation.

As a second step, fragility curves are created considering different analysis assumptions: 1) using different spectra; 2) considering different sites; 3) considering uncertainties in the input parameters. The derived fragility curves are highly dependent on the spectral shape (Fig. 6.4a). Artificial records<sup>7</sup> are generated for two standard spectra (EC8 Type 1 and 2) and GCIM selection is carried out for two site specific UHS. Chapter 2 concludes that the Type 2 standard spectrum is a better description of the UHS. It is confirmed by Fig. 6.4a showing that

<sup>7</sup> Artificial records are nearly exactly matched to the spectra. To take into account the uncertainty in the seismic load, a conservative approach is followed: their amplitude is multiplied with a random factor with a lognormal distribution of 1.0 median and 0.5 standard deviation (Jernigan and Hwang 2002).

the fragility curve derived with Type 2 spectrum is closer to the site specific ones. It can also be observed that there is only a slight difference between fragility curves created for different sites. It implies that the general seismic characteristics are just slightly different and the difference stems from the different standard deviation of spectral values (median is nearly the same), therefore it might be sufficient to derive fragility curves for only one site and use it for other areas in Hungary without introducing significant error in the results.

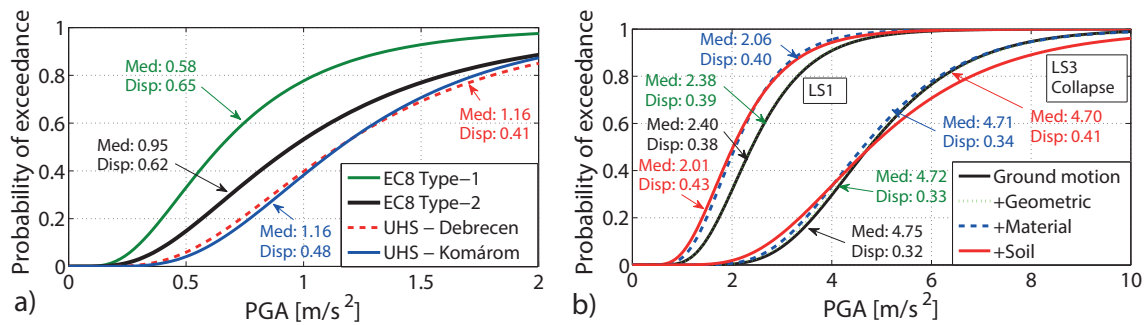


Fig. 6.4 Comparison of fragility curves for pier shear failure: a) using different spectra and sites for BR24; b) taking into account ground motion direction, geometric, material and soil uncertainties for BR01.

In Table 6.2, random variables applied to sample input for the numerical model are presented. The effect of these uncertainties is illustrated in Fig. 6.4b. Fragility curves are created for LS1 and LS3 for an integral PMG-I bridge by considering only ground motion direction uncertainty, then additional geometric, material and soil uncertainties, respectively. It is shown that the geometric uncertainty has negligible effect, while the material and soil uncertainties may significantly influence the calculated probability of failure. The material uncertainty is dominant when the LS is associated with yielding and plastic deformations (e.g. LS1 in Fig. 6.4b is controlled by the yielding of the abutment joint); while in case of LS with dominant brittle failure mode (e.g. LS3 in Fig. 6.4b is controlled by the pier shear failure) soil uncertainties significantly influence the dispersion of the demands.

In conclusion, the fragility evaluation is conducted: 1) with a robust and detailed numerical model; 2) using the site specific spectrum for Komárom considering soil type C; 3) applying 50 tri-directional selected ground motions at each intensity level; 4) incorporating the uncertainties listed in Table 6.3.

## 6.6 Parametric fragility analysis of PMG-I bridges

### 6.6.1 Calculated demands

Besides MSA, Cloud Analysis is often used in literature to create analytical fragility curves, where unscaled recorded ground motions are applied for NLTHA. If the maximal structural responses are plotted against a selected IM, a cloud of points is obtained (GM selection is usually arbitrary; see Fig. 6.5c-d). MSA can be regarded as a special Cloud

Analysis, where the maximal structural responses form into line (see Fig. 6.5a-b) at the chosen conditioning IM levels (PGA in this study).

With regression analysis, a Probabilistic Seismic Demand Model (PSDM) can be obtained providing the median ( $S_D$ ) and the lognormal standard deviation (LNSTD) ( $\beta_D$ ) of the demands as the function of the IM. Typically, a power law is used to describe the PSDM (e.g. Nielson 2005, Padgett 2007, Avşar 2011) with  $a$  and  $b$  constants:

$$S_D = a IM^b, \quad (6.5)$$

The fragility function can be obtained with the median ( $S_C$ ) and LNSTD of the capacity ( $\beta_C$ ):

$$P[(D > C_{LS})|IM] = \Phi\left(\frac{\ln(S_D/S_C)}{\sqrt{\beta_C^2 + \beta_D^2}}\right). \quad (6.6)$$

The presented power law leads to a linear approximation of median values in the log-log space and assumes a constant LNSTD. The advantage of MSA is that median and LNSTD values can be calculated at each IM level providing a better estimation for the PSDM.

Calculated demands of the W14S3P04L30 configuration are illustrated in Fig. 6.5a-b. In some cases (e.g. pier shear forces) the linear approximation is correct; however it is not appropriate to describe elements with high plastic deformations at higher intensity levels (e.g. the reinforcing steel strains). Moreover, the slope of the linear curve in the log-log space is highly dependent on the intensity levels considered. If only records with lower intensities are applied during the analysis, the linear approximation underestimates the demands at higher IM levels. On the other hand, too high dispersion is assumed at low intensity due to the constant LNSTD along the entire IM range if the plastic deformations are dominant.

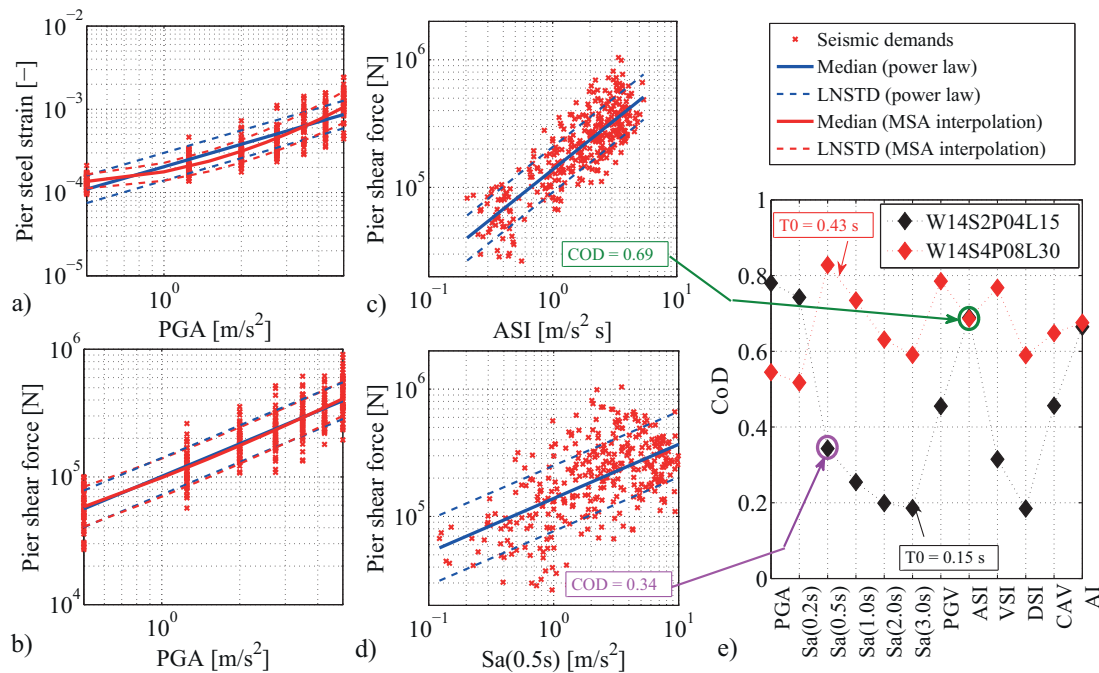


Fig. 6.5 a-d) Structural responses against various IMs for the W14S2P04L15 configuration. e) Coefficient of determination values showing the appropriateness of different IMs.

### 6.6.2 *Optimal intensity measure*

Theoretically, the calculated probability of failure is independent of the chosen IM if hazard compatible ground motions are selected with the GCIM approach. However, the appropriateness of other IMs is evaluated to provide guidance in case of arbitrary record selection (e.g. for Cloud Analysis). The PSDM from Eq.(6.5) is applied and the coefficient of determination (CoD) of the regression is used for comparison. Higher CoD values represent more appropriate IMs. For instance, ASI with a CoD value of 0.69 is a better estimator of the seismic demands than  $S_a(0.5s)$  (COD = 0.34) for the W14S2P04L15 configuration (Fig. 6.5c-d). CoD values of other IMs for pier shear forces (other demands have the same tendencies) are presented in Fig. 6.5e for the stiffest and most flexible examined PMG-I bridges.

The optimal IM is highly correlated with the first fundamental period of the structure. PGA, ASI and the Arias intensity represent well the demands of relatively stiff bridges ( $T_0=0.15s$ ); while with the increase of the fundamental period ( $T_0=0.43s$ ),  $S_a$  values close to  $T_0$  as well as PGV and VSI become more dominant. Note also that ASI and Arias intensity (AI) perform well for both configurations.

### 6.6.3 *Fragility curves*

Component fragility curves in Fig. 6.6 illustrate a general damage mechanism for PMG-I bridges. It is highly possible that the abutment joint yields and even transverse yielding of the abutment is expected to occur prior to the pier damage, while the damage of the backfill soil has nearly zero possibility in the observed PGA range. Therefore the fragility of the system in LS1 is driven by the abutment joints. It is considered that after the joints yield, the bridge is still functional and LS2 is associated with the ultimate deformation capacity of the joint rebars. The probability that the joints reach LS2 is lower, pier flexural damage related to the spalling of concrete layers is dominant, while pier shear failure is possible as well. Collapse of the bridge is definitely caused by the pier shear failure. After the failure of the joint, frictional forces still develop sufficiently preventing the superstructure from unseating (measured with the joint deformations) in LS3.

The results for the whole system in Fig. 6.6 indicate that the simple boundaries of the system fragility curves (blue dashed line for the upper bound and the most vulnerable component fragility curve for the lower bound) are relatively close to each other if one component dominantly governs the failure (see LS1 in Fig. 6.6a, for instance). As expected, system fragilities derived with MC simulation fall between the estimated simple boundaries. Considering no correlation between the component capacities results in higher probabilities

compared to the full correlation estimation. In reality, correlation between component capacities may be relatively high and system fragility should be between the two assumptions.

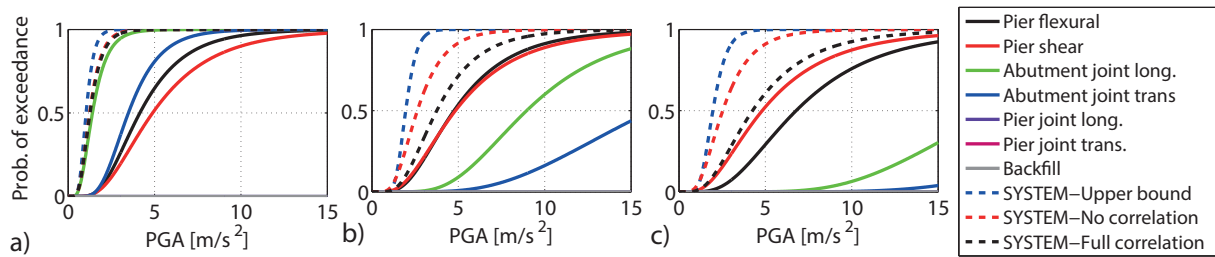


Fig. 6.6 a) Component and system fragility curves for the W14S3P04L30 configuration for: a) LS1; b) LS2; c) LS3 (full correlation in capacity).

In Fig. 6.7a system fragility curves are compared for different deck widths. The result contradicts the one observed in the preliminary analysis that 14 and 20 m width results are nearly the same while those of 8 m width are always higher. Indeed, component fragilities have this tendency (note the component fragility curves for shear failure - SH), however during the compilation of the system fragility curves the number of fragile components are also taken into account, while in the case of intensity based safety check, each element is checked individually. If the component fragilities are close to each other in case of different widths, the system fragility may be worse for wider bridges with more piers. It is important that in the MC simulations all the components have to be included (e.g.  $P_i$  component probabilities of each pier), since the probability of failure increases with the number of possibly critical components.

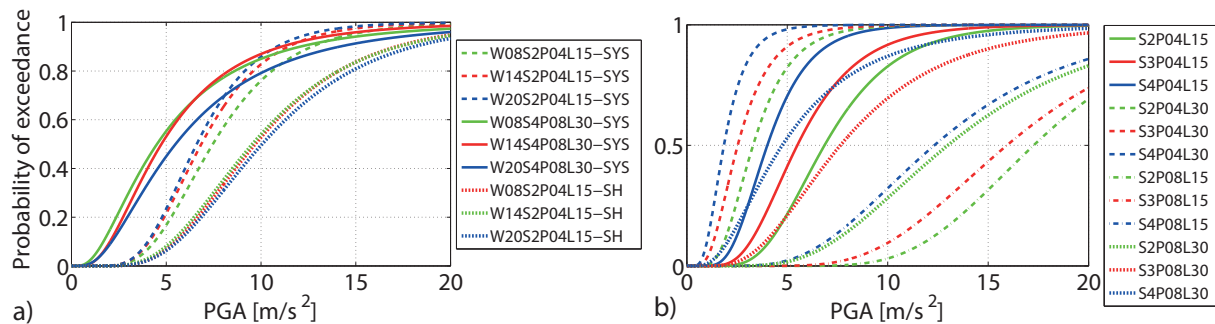


Fig. 6.7 a) System (SYS) fragility curves for different widths. Pier shear failure (SH) are also presented for the S2P04L15 configuration. b) LS3 system fragility curves of W14 bridges (full correlation in capacity).

Fig. 6.7b shows system fragility curves of all W14 bridges for LS3 (Appendix G summarizes the median and LNSTD values for all the bridges and limit states). Although the bridges represent the same bridge class, significant difference can be observed for different layouts due to the various most relevant parameters such as span length and pier height. Median values range between  $1.5 \text{ m/s}^2$  and  $20 \text{ m/s}^2$  and the LNSTD of the fragility curve is typically 0.25-0.45. Fig. 6.7 also confirms that pier height significantly, while the span length

moderately affect the fragility of the structure. It is apparent that the deck width is a less important structural attribute in case of PMG-I bridges.

### 6.7 Fragility analysis of portfolio bridges

#### 6.7.1 Optimal intensity measure

It is shown for PMG-I bridges that the optimal IM is highly correlated with the first fundamental period (see Fig. 6.8c) of the structure. Fig. 6.8a-b illustrate the CoD values for BR01, BR12 and BR19. BR01 is a PMG-I bridge with low fundamental periods in both longitudinal (0.34 s) and transverse (0.15 s) directions. It is confirmed that PGA, ASI and the Arias intensity represent well the demands of relatively stiff bridges.

BR12 is a 7-span non-integrated PMG-NI bridge with 2 fix bearings at the two middle piers and elastomeric bearings elsewhere. This configuration has higher fundamental periods (1.05 and 0.83 s), therefore the demands can be represented well by the Sa value close to 1.0 s as well as PGV and VSI. Both longitudinal and transverse displacements have the same tendency, since the fundamental periods in the two directions are close to each other. In Fig. 6.8b, a concrete box girder bridge (BR19) is presented. In this case, the optimal CoD values are separated, which stems from the high difference in the fundamental periods in the two directions (3.9 s and 0.95 s). Accordingly, optimal values are Sa values over 3.0 s and DSI for demands caused dominantly by the longitudinal vibration (e.g. longitudinal displacement), while the demands caused by transverse vibration (transverse displacement, shear force at piers non-restrained in the longitudinal direction) can be described well by Sa values around 1.0 s, PGV and VSI. However, components that are influenced by vibrations of both directions (e.g. shear forces of piers with longitudinally fixed bearings) highest CoD values can be found between the dominantly longitudinal and transverse vibration values.

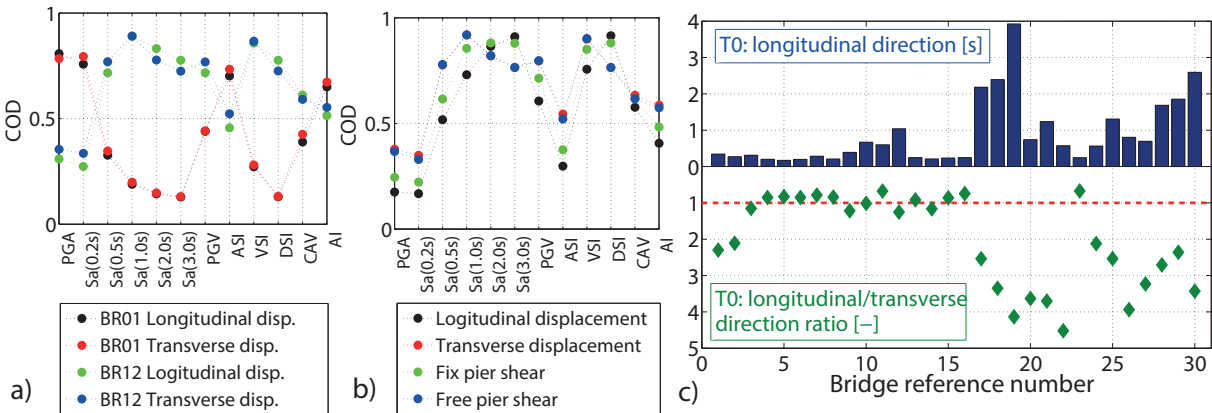


Fig. 6.8 Optimal intensity measure comparison: a) BR01 and BR12; b) BR19. c) Fundamental periods of the portfolio bridges (see also Appendix C).

## 6.7.2 Fragility curves

### 6.7.2.1 PMG-I bridges

BR01-BR08 are PMG-I bridges where all joints are Type 2 monolithic joint. Their behavior is the same in most cases as the ones presented in the previous section: LS1 is reached with the yielding of the abutment joint; LS2 is either pier flexural or shear failure, while collapse is caused by shear failure of the pier (see the BR07 bridge in Fig. 6.9).

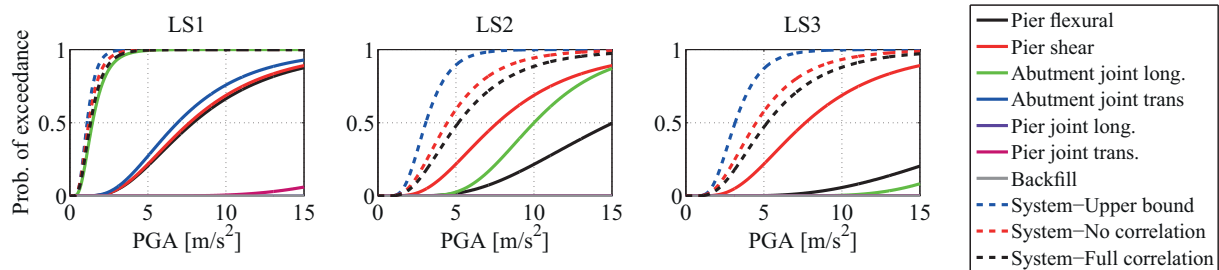


Fig. 6.9 Fragility curves for the BR07 (PMG-I) bridge.

However, BR04 is an exception. Even though it has relatively high piers leading to low shear forces, the shear reinforcement is high ( $\phi 16/150$ ) compared to the other configurations. LS1-LS3 of BR04 are shown in Fig. 6.10. Similarly to other PMG-I bridges, the abutment joint resistance is inadequate, this component controls LS1 and LS2. However in LS3 the bridge is more likely to suffer flexural failure, and due to the high shear resistance, a ductile behavior can be achieved. The unseating of the superstructure (related to joint deformations in LS3) is possible, but the probability is far lower than the probability of flexural failure.

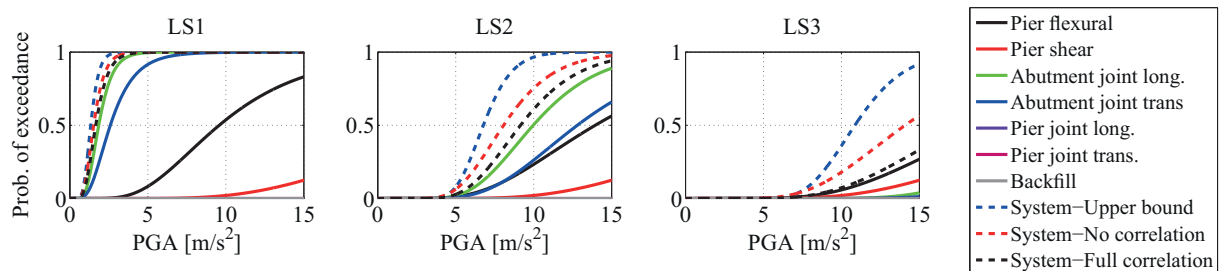


Fig. 6.10 Fragility curves for the BR04 (PMG-I) bridge.

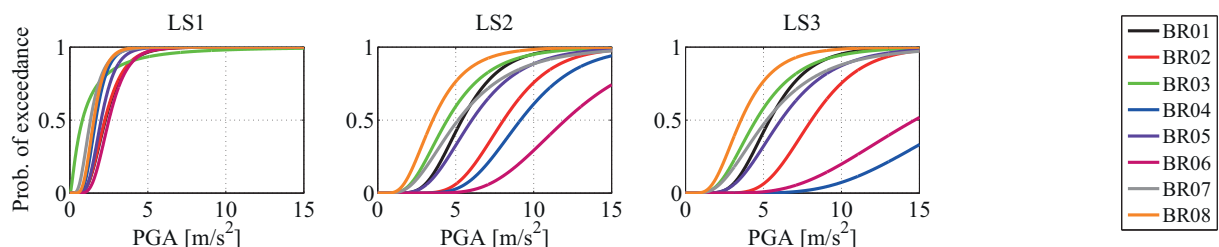


Fig. 6.11 System fragility curves (full correlation in capacity) for PMG-I bridges.

In Fig. 6.11 system fragility curves are illustrated. LS1 fragility curves show the same tendency, except for BR03 where the abutment joint is more likely to yield. This is the only configuration with low ( $\phi 16/200$  instead of  $\phi 16/150$ ) shear reinforcement of this joint. For

most bridges LS2 and LS3 are nearly identical since shear failure dominates before other components reach LS2 or LS3.

### 6.7.2.2 PMG-NI bridges

The other type of precast multi-girder bridge (PMG-NI; BR09-12) is constructed with elastomeric bearings at some piers to provide free movements in case of longer bridges; and monolithic joint Type 2 is applied at specific piers to provide restraint in the two horizontal directions. These bridges are more flexible (Fig. 6.8c) with increased fundamental periods in both directions. For this reason, one would expect lower seismic demands, however the lower base shear force is distributed on fewer piers. The high vulnerability of PMG-NI bridges is illustrated in Fig. 6.12; pier shear failure develops prior to any other component damage.

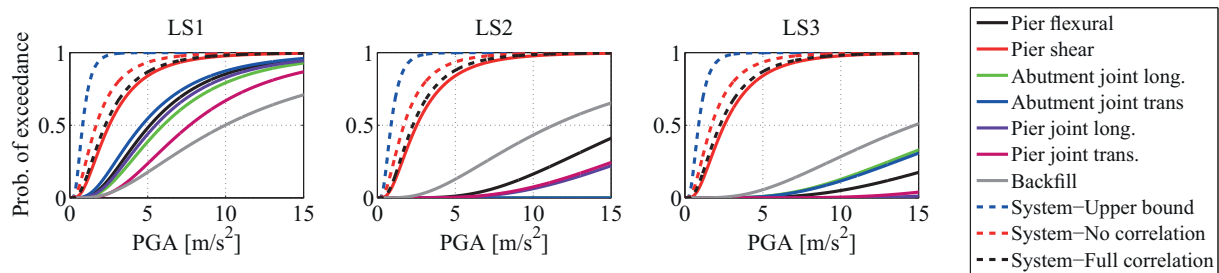


Fig. 6.12 Fragility curves for the BR10 (PMG-NI) bridge.

This is confirmed by the system fragility curves (Fig. 6.13). No significant difference in the system fragilities of different limit states can be observed.

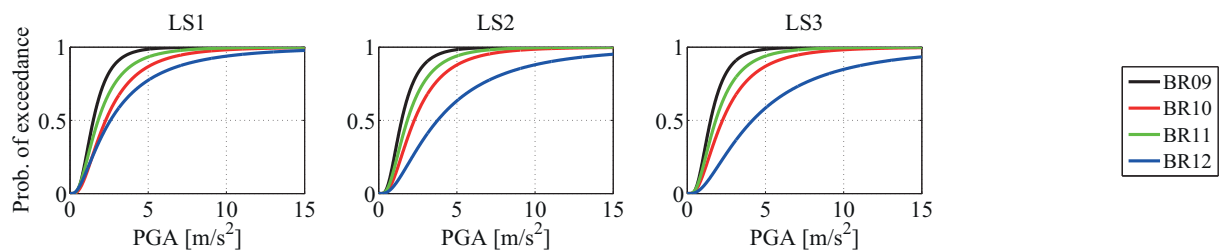


Fig. 6.13 System fragility curves (full correlation in capacity) for PMG-NI bridges.

The component fragility curves provide some additional information about the bridge performance. Besides the piers, there are other components that may be vulnerable because of the structural layout. Typically, monolithic joints are created in the middle piers, while on the abutments, elastomeric bearing and expansion joints are constructed. If pounding occurs, it increases the probability that the backfill soil reaches a given damage limit state. There is also higher probability of unseating because of the excessive movements compared to integrate PMG-I bridges. Fig. 6.12 shows that the backfill failure and unseating would be more likely than pier flexural failure in LS3, if shear resistance was sufficient.

### 6.7.2.3 SLAB bridges

It is shown in Chapter 5 that SLAB bridges may be characterized by the same behavior as PMG-I bridges, except that higher demands are calculated due to the integrated monolithic joint Type 1. According to the component fragility curves (Fig. 6.14), this similar behavior can be confirmed: LS1 is associated with abutment joint yielding while pier shear failure is dominant in LS3 (and also in LS2) for the examined slab bridges as well (see also Fig. 6.15).

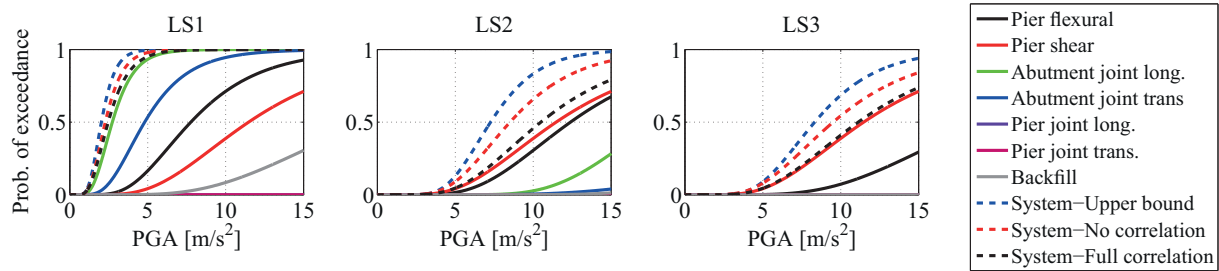


Fig. 6.14 Fragility curves for the BR13 (SLAB) bridge.

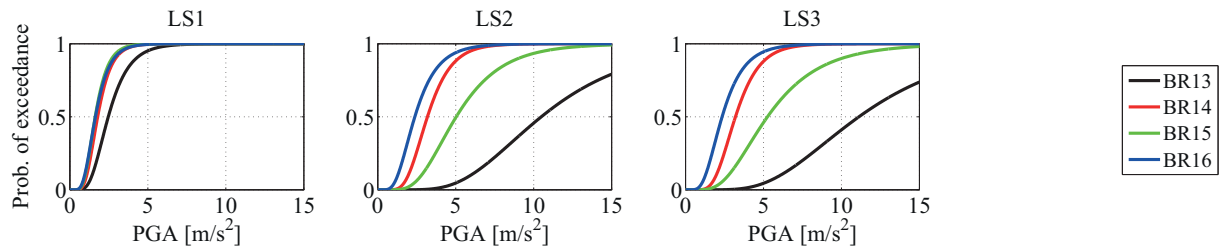


Fig. 6.15 System fragility curves (full correlation in capacity) for SLAB bridges.

### 6.7.2.4 RC-B bridges

Results for RC-B bridges (BR17-19) are illustrated in Fig. 6.16 and 6.17. The component fragility curves illustrate well the development of component damage. LS1 is initiated by the yielding of the piers, and also in LS2 spalling of the outer concrete layer of piers is more likely at lower intensities (assumed to be the important portion of the fragility curve). However, it seems that the shear resistance is still insufficient. Even for more flexible continuous girders (see fundamental periods in Fig. 6.8c), collapse is caused by the shear failure of the pier.

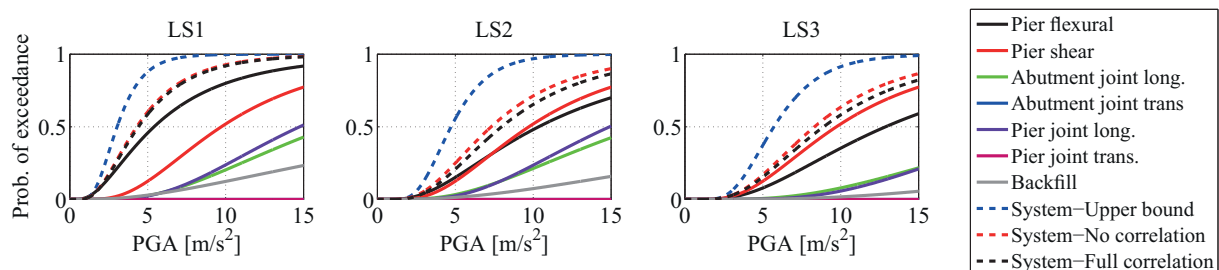


Fig. 6.16 Fragility curves for the BR17 (RC-B) bridge.

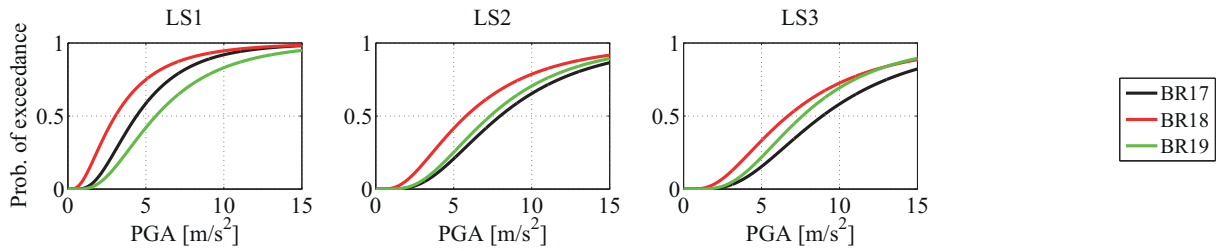


Fig. 6.17 System fragility curves (full correlation in capacity) for RC-B bridges.

#### 6.7.2.5 Composite bridges (COMP-I and COMP-B)

Similar behavior is observed in case of composite girders (Fig. 6.18). The system fragility curves in Fig. 6.19 indicate that there are two composite box girders (BR24 and 25) that are clearly not designed for seismic loads, pier shear failure controls all three LSs.

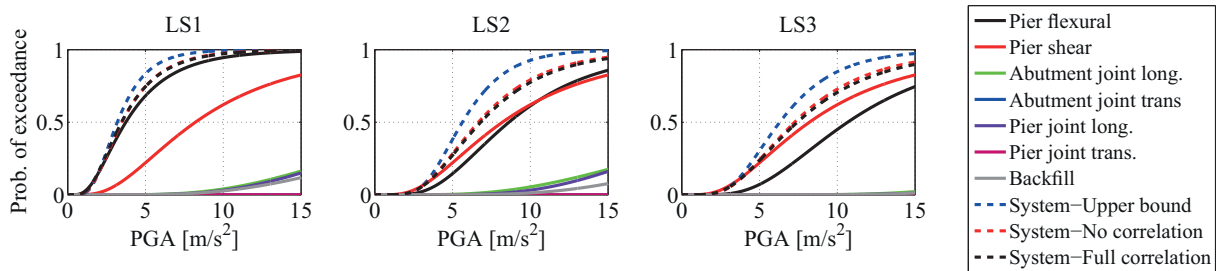


Fig. 6.18 Fragility curves for the BR20 (COMP-I) bridge.

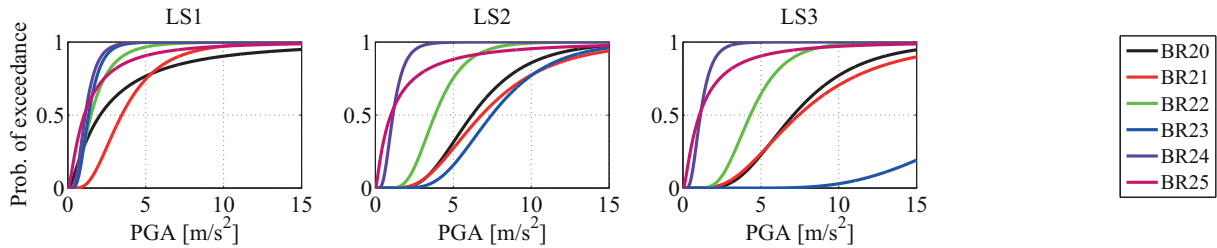


Fig. 6.19 System fragility curves (full correlation in capacity) for COMP bridges.

BR23 should be highlighted having special construction technology and layout: monolithic Type 2 joints are used at the abutments, while the piers are restrained in the longitudinal direction, and free movements can develop in the transverse direction (Fig. 6.20). Due to the supporting role of the abutment-backfill soil system, seismic pier demands are minimal in the longitudinal direction, besides, negligible horizontal forces are transferred to the pier by bearing friction in the transverse direction. Accordingly, the critical components are the abutment joints in LS1 and LS2, and it is also possible that failure is caused by unseating of the superstructure (see Ab. joint. trans. in Fig. 6.21). Note that the pier shear reinforcement is high ( $\phi 16/100$  instead of the typical  $\phi 12/150$ ) which – compared to the developing shear forces – indicates that pier shear failure is not expected. This configuration may be an economical solution for highway bridges with a total length up to 100 m.

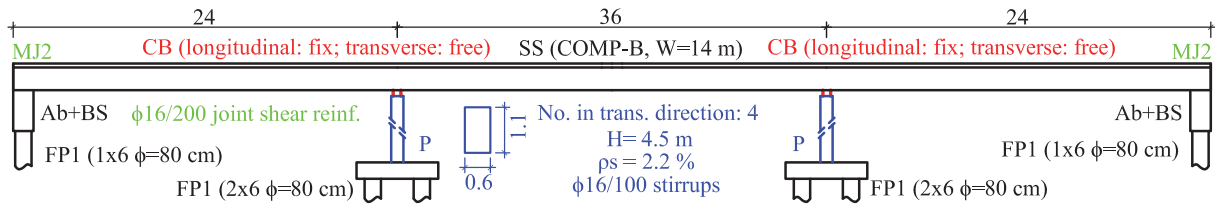


Fig. 6.20 BR23 configuration with special bearing arrangement.

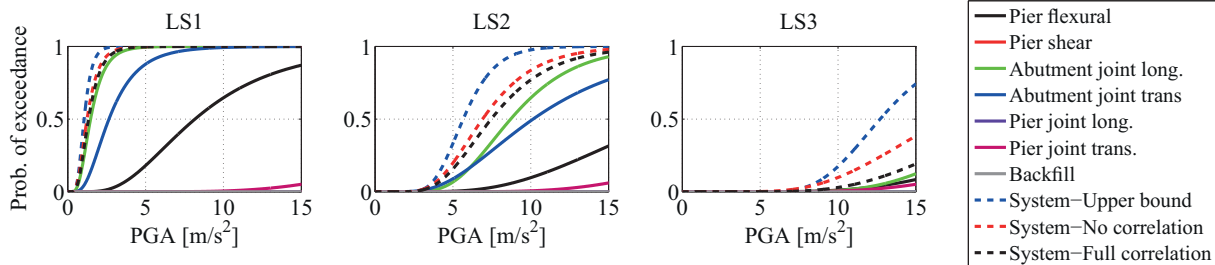


Fig. 6.21 Fragility curves for the BR23 COMP-B bridge.

### 6.7.2.6 Steel bridges (STEEL-I and STEEL-B)

Results for steel girders are shown in Fig. 6.22 and 6.23. Fig. 6.22 illustrates that steel girders typically have an optimal behavior: pier flexural damage characterize all three damage limit states, energy dissipation due to the cyclic behavior of the piers can be utilized until collapse. It is also shown that even though the fundamental periods imply flexible structures, the developing longitudinal displacements are not large enough to cause unseating (measured with joint deformations), pier failure is always more likely to occur.

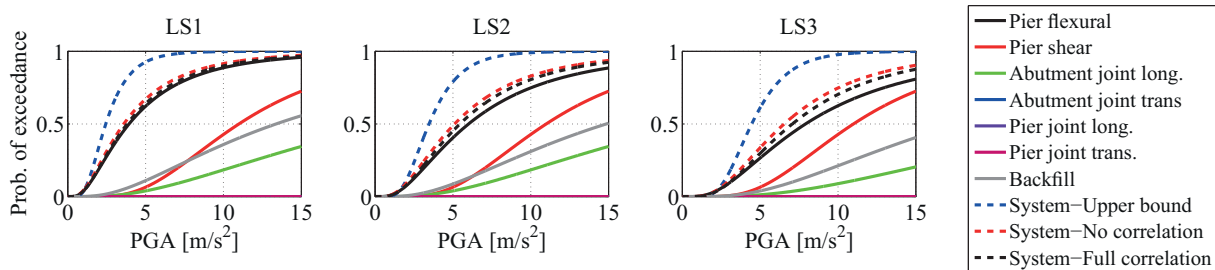


Fig. 6.22 Fragility curves for the BR30 (STEEL-B) bridge.

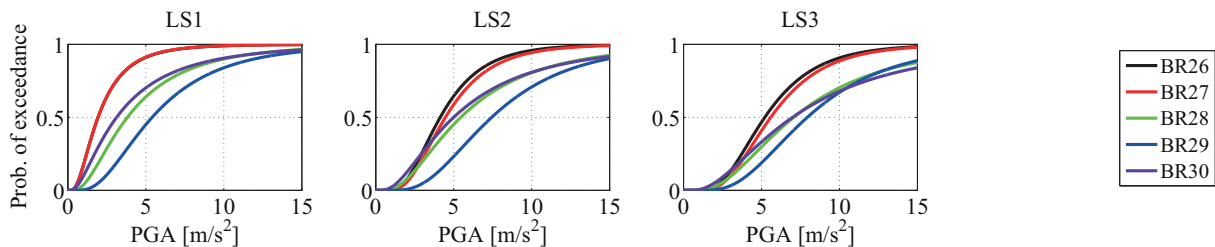


Fig. 6.23 System fragility curves (full correlation in capacity) for STEEL bridges.

## 6.8 Calculated reliability of the structures

### 6.8.1 Introduction

The  $\beta$  reliability index (see Eq.(6.3)) for 50 year reference period is calculated using the hazard curve for Komárom (area of highest seismicity in Hungary; see Fig. 6.1b) for soil type

C for general comparison of the seismic performance and to highlight possibly critical configurations. To provide a range of possible reliability index values in Hungary, the lowest seismic area of Debrecen (see hazard curve in Fig. 6.1b) is also investigated in case of the portfolio bridges.

The target reliability index is not unique and varies from code to code. EC0 specifies a target value only for ULS and Serviceability LS as 3.8 and 1.5, respectively for structures with moderate consequences of failure (RC2 class). In the Joint Committee on Structural Safety Model Code (JCSS 2001) it is proposed that the relative cost of safety measure (RCSM) should be also taken into account in the target reliability. It is stated that due to the large uncertainty in seismic loads, a lower reliability class should be used. A value of 1.98, 3.21 and 3.46 are proposed for large, normal and small RCSM, respectively, thus a 1.98 target is adopted in this study to highlight structures that possibly need strengthening and retrofit.

### 6.8.2 Reliability of PMG-I bridges

The parametric results for PMG-I bridges are presented in Fig. 6.24 and Table 6.3 where  $\beta$  related to the most vulnerable component is also indicated to show the weakest element of the system.

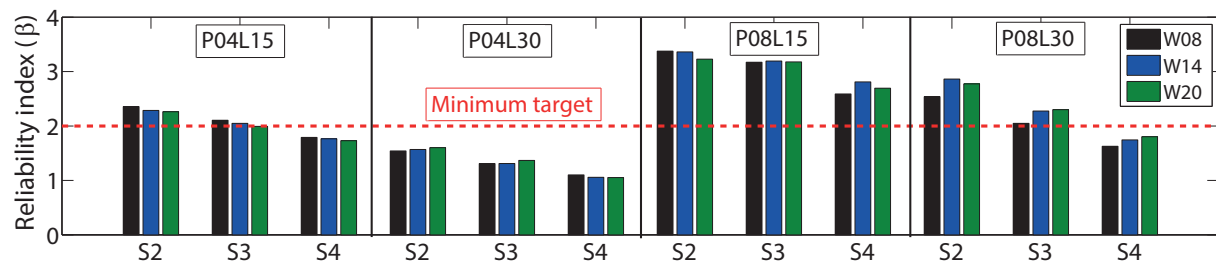


Fig. 6.24 PMG-I bridge reliability indices ( $\beta$ ) for collapse (Komárom area; no correlation in capacity).

Table 6.3 Reliability indices ( $\beta$ ) of W14 PMG-I bridges for Komárom. The weakest element of the system: AJL - abutment joint longitudinal direction; SH – pier shear failure; FL – pier flexural failure.

Correlation (capacity) Configuration	LS1				LS2				LS3				
	No $\beta$	Full $\beta$	Weakest comp. $\beta$	Name	No $\beta$	Full $\beta$	Weakest comp. $\beta$	Name	No $\beta$	Full $\beta$	Weakest comp. $\beta$	Name	
W14 P04 L15	S2	1.49	1.50	1.62	AJL	2.36	2.59	2.59	SH	2.29	2.55	2.55	SH
	S3	1.40	1.40	1.49	AJL	2.13	2.47	2.50	SH	2.05	2.42	2.47	SH
	S4	1.20	1.20	1.28	AJL	1.86	2.22	2.26	SH	1.77	2.20	2.22	SH
P04 L30	S2	0.83	0.83	0.90	AJL	1.59	1.84	1.94	SH	1.57	1.86	1.91	SH
	S3	0.74	0.75	0.83	AJL	1.36	1.65	1.78	SH	1.31	1.70	1.76	SH
	S4	0.60	0.61	0.69	AJL	1.09	1.31	1.46	FL	1.06	1.36	1.44	SH
P08 L15	S2	1.44	1.44	1.61	AJL	3.33	3.56	3.65	SH	3.36	3.62	3.63	SH
	S3	1.26	1.26	1.41	AJL	2.96	3.00	3.05	AJL	3.19	3.54	3.62	SH
	S4	1.02	1.02	1.13	AJL	2.67	2.72	2.79	AJL	2.81	3.20	3.30	SH
P08 L30	S2	0.74	0.74	0.81	AJL	2.52	2.56	2.68	AJL	2.86	3.11	3.22	SH
	S3	0.69	0.69	0.76	AJL	2.09	2.18	2.30	FL	2.27	2.53	2.61	FL
	S4	0.55	0.55	0.62	AJL	1.61	1.72	1.77	FL	1.74	1.92	2.05	FL

The probability of failure is increasing with the length of the bridge and it is higher in case of low piers. The first damage possibly occurs at the abutment joint, while the weakest

component in LS2 depends on the actual layout. For lower piers, shear failure is dominant meaning that the bridge collapses before other components could reach LS3. At higher piers LS2 is reached at the abutment joint or at the pier (spalling of concrete) for shorter or longer spans, respectively. In most cases, the collapse is caused by the shear failure of the piers, however in case of more flexible configurations (with higher piers and longer spans) it is possible that pier flexural failure is dominant. The reliability indices associated with different deck widths show little difference, and the results are in accordance with the ones presented in Fig. 6.7a and explained earlier. If the conservative Komárom area is considered, the minimum target value for collapse cannot be reached with low piers over a 45 m total bridge length, while bridges with high piers are critical only over ~100 m total length.

### 6.8.3 Reliability of the portfolio bridges

The possible range of reliability indices for the portfolio bridges are presented in Fig. 6.25, where the upper and lower bounds are related to the area of Debrecen and Komárom, respectively. Reliability indices and the weakest components are also summarized for the Komárom area in Table 6.4. The reliability is highly dependent on many structural attributes (see Table 3.4), thus only some concluding remarks can be made regarding the reliability of different structural types.

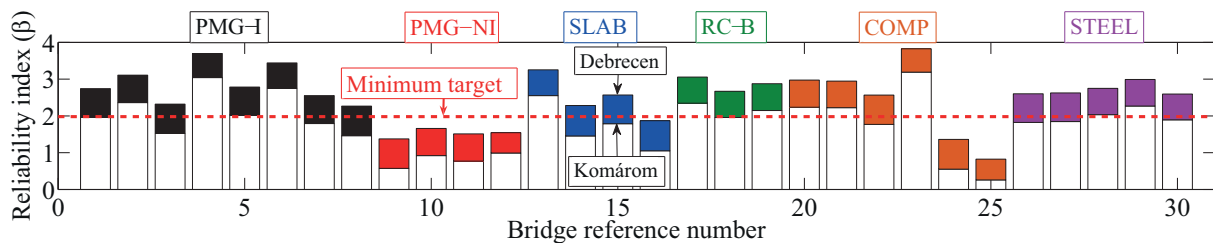


Fig. 6.25 Range of reliability indices ( $\beta$ ) related to collapse of the portfolio bridges (no correlation in capacity).

PMG-I bridges are critical (considering the area of Komárom) if the total length is over 80 m which is in line with the observation made in the parametric fragility analysis if we consider that the pier height is at least 5.5 m for the examined bridges. Pier shear failure is dominant, however 1500-2000 mm<sup>2</sup>/m pier shear reinforcement seems to be sufficient (see shear reinforcements in Table 3.4) to achieve the minimum target reliability except for the longest BR08 bridge with circular cross section ( $D=0.8$  m) and  $\phi 10/100$  stirrups.

PMG-NI bridges perform worse, the calculated reliability index highlights the high vulnerability of these bridges, especially for shear failure. Some decrease of the base shear force can be achieved with this system due to the increased fundamental periods (see Fig. 6.8c). However this base shear force is distributed on fewer piers (for instance, BR12 is 8-span bridge, but it has only 2 longitudinally restrained supports in the middle), while in the

transverse direction these restrained piers carry the horizontal loads. Moreover, in case of the examined bridges, the applied shear reinforcement is even lower than in case of fully integrated PMG-I bridges. The number of PMG-NI bridges contributes with only some percent to the total bridge inventory, however they are mostly important longer highway bridges (e.g. BR11 is a 240 m long bridge over a valley).

Table 6.4 Calculated reliability indices ( $\beta$ ) of the portfolio bridges for Komárom. The weakest components: AJL, ABT - abutment joint longitudinal and transverse direction; SH – pier shear failure; FL – pier flexural failure)

Correlation (capacity) Configuration	No	LS1			No	LS2			No	LS3			
		Full $\beta$	Weakest comp. $\beta$	Name		Full $\beta$	Weakest comp. $\beta$	Name		Full $\beta$	Weakest comp. $\beta$	Name	
PMG BR	1	1.15	1.25	1.32	AJL	1.96	2.07	2.12	SH	1.96	2.07	2.12	SH
	2	1.15	1.24	1.33	AJL	2.36	2.53	2.53	SH	2.36	2.52	2.53	SH
	3	0.18	0.31	0.36	AJL	1.53	1.81	1.86	SH	1.52	1.82	1.86	SH
	4	0.93	1.00	1.09	AJL	2.52	2.65	2.71	AJL	3.04	3.26	3.31	FL
	5	1.08	1.16	1.19	AJL	2.01	2.15	2.19	SH	2.02	2.15	2.19	SH
	6	1.25	1.36	1.41	AJL	2.69	2.92	3.02	SH	2.75	2.98	3.02	SH
	7	0.71	0.78	0.85	AJL	1.80	1.90	1.92	SH	1.79	1.90	1.92	SH
	8	0.85	0.93	0.96	AJL	1.46	1.61	1.67	SH	1.46	1.62	1.67	SH
PMG-NI	9	0.58	0.86	0.93	SH	0.58	0.84	0.93	SH	0.57	0.86	0.93	SH
	10	0.91	1.14	1.20	SH	0.92	1.15	1.20	SH	0.92	1.13	1.20	SH
	11	0.73	0.97	1.06	SH	0.77	0.99	1.06	SH	0.77	0.99	1.06	SH
	12	0.77	1.15	1.25	FL	0.95	1.45	1.56	SH	0.99	1.51	1.56	SH
SLAB	13	1.27	1.32	1.41	AJL	2.50	2.67	2.71	SH	2.55	2.69	2.71	SH
	14	0.98	1.05	1.09	AJL	1.45	1.57	1.61	SH	1.45	1.58	1.61	SH
	15	0.90	0.97	1.01	AJL	1.76	1.95	1.98	SH	1.79	1.95	1.98	SH
	16	0.84	0.97	1.00	AJL	1.06	1.27	1.31	SH	1.05	1.26	1.31	SH
RC-B	17	1.72	1.74	1.80	FL	2.20	2.27	2.35	FL	2.35	2.37	2.44	SH
	18	1.31	1.34	1.35	FL	1.84	1.89	1.95	FL	1.96	2.02	2.08	SH
	19	1.84	1.94	1.99	FL	2.03	2.19	2.31	SH	2.15	2.26	2.31	SH
COMP-I	20	0.87	0.87	0.88	FL	2.12	2.15	2.28	FL	2.24	2.26	2.32	SH
	21	1.57	1.55	1.58	FL	2.17	2.18	2.22	SH	2.22	2.22	2.22	SH
	22	0.76	0.83	0.84	FL	1.62	1.73	1.94	FL	1.77	1.85	1.96	SH
COMP-B	23	0.74	0.80	0.87	AJL	2.31	2.37	2.52	AJT	3.19	3.44	3.56	FL
	24	0.55	0.65	0.68	SH	0.55	0.65	0.68	SH	0.55	0.65	0.68	SH
	25	0.26	0.48	0.52	SH	0.26	0.41	0.52	SH	0.26	0.48	0.52	SH
STEEL-I	26	0.94	1.02	1.04	FL	1.63	1.73	1.81	FL	1.82	1.95	2.10	FL
	27	0.88	1.02	1.08	FL	1.62	1.80	1.89	FL	1.85	2.03	2.25	FL
STEEL-B	28	1.47	1.51	1.52	FL	1.77	1.82	1.85	FL	2.03	2.09	2.10	FL
	29	1.86	1.88	1.92	FL	2.19	2.23	2.41	SH	2.27	2.31	2.41	SH
	30	0.93	1.28	1.33	FL	1.61	1.69	1.73	FL	1.89	1.97	2.01	FL

Generally, some slab bridges perform considerably worse than PMG-I bridges. Shear failure is dominant again as it is shown in the parametric study. Besides, shear reinforcement is low (e.g. BR14 has only  $\phi 10/200$  stirrups); it is estimated that slab bridges would reach the minimal target reliability (even for Komárom) up to 80 m total length if a minimum of  $\sim 2500$  mm<sup>2</sup>/m pier shear reinforcement was applied.

Continuous girder bridges with conventional bearings perform well (even a large span river bridge, BR29), especially steel girders that are shown to behave in an optimal way suffering pier flexural damage with the highest probability in each damage limit state. BR23 should be highlighted since it is already shown in the fragility analysis that the highest performance can be achieved with this bridge system and configuration. The piers are restrained only in the longitudinal direction where most of the base shear force is transmitted to the stiffer

abutment-backfill soil system. The piers are basically isolated, slight and extensive damages are associated with abutment joint failure. Although, the collapse possibly occurs with superstructure unseating, the displacements are moderated by the pier and the frictional forces. The calculated reliability is over 3.1 even for the highly seismic area of Komárom.

Focus should be laid on two composite box girder bridges with 3 and 9 spans which are clearly not designed for seismic actions. Both configurations employ two circular piers in the transverse direction without tie beams and with low shear reinforcements ( $\phi 16/200$  and  $\phi 12/200$ ). The total length is 115 m and 416 m for BR24 and BR25, respectively, while the number of restrained supports in the longitudinal direction is 1 and 2. This means that one pier supports half of the mass of 115 m and 208 m superstructure. Moreover, torsion develops from the transverse vibration causing additional longitudinal shear forces in the pier pairs at the longitudinal restrained supports. This configuration is a typical example where mere strengthening is not a reasonable option, the whole bridge behavior should be altered, conceptual seismic retrofit design should be performed (see later in Section 7).

## 6.9 Comparison of intensity and reliability based evaluation methods

Fig. 6.25 shows that the reliability index is highly dependent on the considered design site. The difference in the reliability index is 0.55-0.85; e.g. the  $\beta$  of the BR15 slab bridge is  $\sim 2.6$  and  $\sim 1.9$  if it is built in Komárom and Debrecen, respectively. Note that the bridge configuration is fixed (e.g. reinforcements, cross sections, capacities etc.), thus the results illustrate possible reliability indices of non-seismically designed bridges.

Table 6.4 shows that a high portion of the examined bridges are highly vulnerable to pier shear forces. To estimate what reliability level can be attained with seismic design according to EC8-2, the following procedure is carried out. An intensity based evaluation using MMRSA is conducted to calculate DC ratios associated with pier shear failure at the design PGA level ( $\lambda_{50}=10\%$ ) for all portfolio bridges. The standard shear resistance is computed per EC8-2. The next step is to assign the corresponding reliability indices to each configuration and then plot these  $\beta$  values against the DC ratios. The procedure is carried out for the area of Komárom and Debrecen; the results are presented in Fig. 6.26.

As confirmed by Fig. 6.26, the correlation between the reliability and the DC ratio can be described with a logarithmic function. The function does not depend on the actual site: the fitted curve represents well both Komárom and Debrecen. With seismic design ( $DC \leq 1.0$ ), a reliability of index of  $\sim 2$  can be reached. Note that an additional increase in the safety of the structure is introduced with the application of MMRSA providing conservative estimates of

seismic demands. For comparison, seismic demands are also calculated with a more rigorous approach using the median demands at the design PGA level determined during MSA. The decreased demands lead to decreased DC ratios, the fitted logarithmic curve is shifted to the left. In conclusion, if the bridge is designed for seismic demands calculated with more sophisticated methods, the reliability index may fall below 1.75.

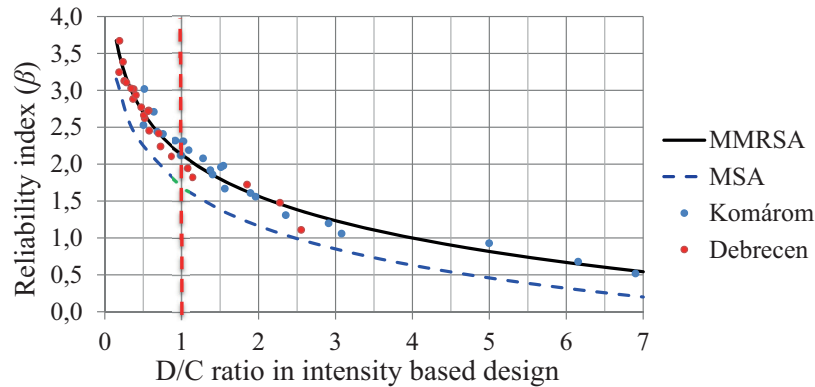


Fig. 6.26 Reliability index againsts the DC ratios calculated at the design PGA level.

The curve can also be used to estimate the required DC ratio for a specific  $\beta$  value. For instance, to reach a 1.98 minimum target value with sophisticated analysis method, the DC ratio should be lower than 0.75 meaning that the piers should be overstrengthened by ~30%. This additional factor may be incorporated in  $\gamma_{Bd}$  (applied to avoid brittle shear failure). Another approach is to increase the return period and thusly the intensity of the design earthquake. In EC8-3, the return period of this earthquake is 2450 years for full collapse, while in case of the design of new bridges the no-collapse criteria of EC8-2 specifies 475 years. This should be clarified and harmonized with the target reliability index for seismic loads. Moreover, the target reliability is also an open question. The determination of the target  $\beta$  should be based on rational economic calculations taking into account the consequences and the relative cost of safety measure.

## 6.10 Application of fragility curves

One of the most important outcome of the study (besides the establishment of an automatic seismic performance evaluation framework) is the determination of fragility curves for several different bridge structures. These fragility curves can be applied for both pre- and post-earthquake situations.

### 6.10.1 Pre-earthquake actions and prioritization of retrofit strategies

One approach to prioritize bridges in pre-earthquake situations is to calculate the probability of system failure. A list of bridges with the worst performance can be created while other aspects can be taken into account such as the actual condition and importance of

the bridge. Component fragility curves and reliability indices help in the decision for retrofit strategies. The calculation of the probability requires the hazard curve of each bridge site (which may be a time-consuming process to create). Another approach is to simply compare the conditional probability (fragility curve values) at the design PGA level (return period of 475 years) where only the PGA value of the bridge site is needed. This approach is illustrated in Fig. 6.27a, where histogram for LS1 conditional probability of all the PMG-I bridges in the inventory is shown.

*6.10.2 Post-earthquake evaluation of bridges*

Fragility curves are also useful tools to estimate the damage state of the bridge inventory after a seismic event. The real earthquake scenario can be simulated estimating the magnitude of the event. Calculating the source-to-site distances and using the GMPE (e.g. Akkar and Bommer 2010) the governing PGA value can be calculate for each bridge. Fragility curves can be used to determine the potential damage state of the bridges near the epicenter, which can be used for decision making during emergency route planning (e.g. if the collapse of a main bridge is probable, alternative routes can be designed to reach important areas).

Such a simulated scenario is illustrated in Fig. 6.27b showing extensive damage of several bridges in case of a magnitude 6.0 earthquake, while collapse of some bridges near the epicenter is also possible. The map also gives an insight about the radius of the area with potential extensive damages. It can be concluded that the diameter is around 20-25 km in case of a high magnitude event; while at ~30-35 km distance, the PGA level is under 1.0 m/s<sup>2</sup> which implies only slight damage of bridges according to the fragility results of the examined structures. These simulations can also be used in a pre-earthquake phase in order to work out plans in advance.

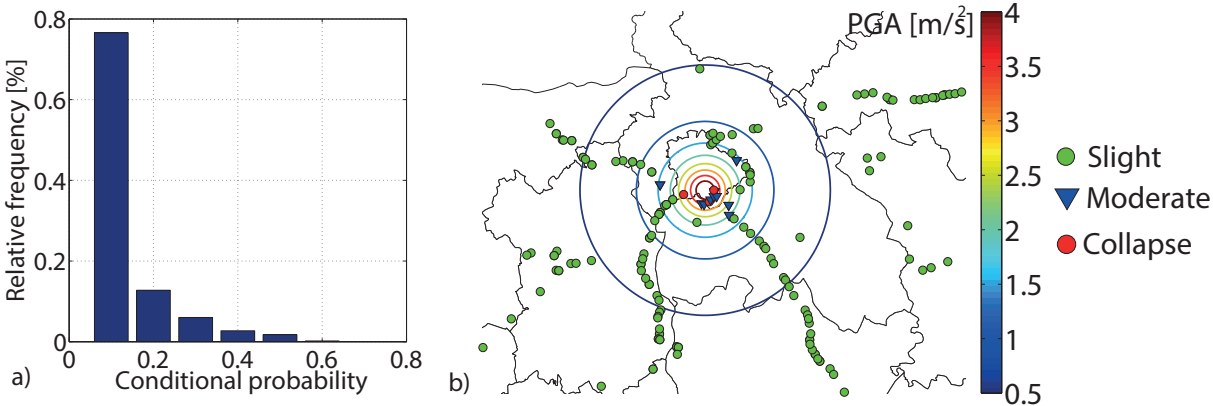


Fig. 6.27 a) System conditional probability in LS1 for PMG-I bridges considering a design seismic event. b) Simulation of a magnitude 6.0 earthquake scenario in the area of Budapest.

## 6.11 Summary

In this chapter, fragility evaluation of a wide range of different integral PMG-I bridge layouts and fragility analysis of 30 representative bridges are conducted. Detailed numerical models and hazard consistent ground motions are used for MSA. The effect of different modeling and analysis assumptions are highlighted; optimal intensity measures are investigated for various bridge configurations. Component fragility curves show that the monolithic joints of PMG-I and SLAB bridges are likely to suffer damage; while collapse is initiated by pier shear failure in most cases. More favorable ductile flexural failure is observed only in case of more flexible PMG-I and STEEL bridges. Comparing the reliability indices indicates the better performance of PMG-I and girder bridges with conventional bearings, while typically certain SLAB bridges and PMG-I bridges have worse behavior. The range of possible reliability indices is presented considering the highest and lowest seismic area of Hungary. It is shown that seismic design leads to a reliability index of  $\sim 2.0$ . Two typical applications of the fragility curves are illustrated. Unfortunately, due to the lack of data, the regional evaluation can be carried out only for PMG-I bridges. For this reason, extension of the database is a primary task in the future. I summarized the results of the fragility analyses in my Thesis IV.

The reliability indices highlight that several bridges do not reach the acceptable reliability level. Evaluation of possible retrofit methods for the vulnerable configurations are presented in the following chapter.

## Chapter 7

# Proposed Retrofit Methods and Design Concepts

### 7.1 Possible retrofit methods

There are two basic approaches to retrofit a bridge:

- 1) conventional strengthening where the sole purpose is to increase the capacity;
- 2) application of anti-seismic devices to alter the seismic behavior.

The latter aims to decrease the seismic demand with the alteration of the fundamental period, redistribution of seismic load and energy dissipation. These approaches are briefly presented in the following sections highlighting possible solutions for vulnerable bridges in Hungary.

#### 7.1.1 Conventional strengthening methods

The main purpose of pier strengthening is to create confinement to increase the shear and flexural resistance, and the ductility of the element. The confinement can be: steel jacket, concrete overlay, Carbon Fiber Reinforced Polymer (CFRP) or external post-tensioning; applied on portions or the full height of the pier (see Fig. 7.1).

Fragility curves and the calculated component reliabilities confirm that flexural behavior is mostly sufficient, but shear capacity shall be improved for several examined bridges. Using CFRP may be an economical choice for PMG-I, PMG-NI and SLAB bridges with standard pier cross sections (e.g. 0.6x0.9 m). The construction is relatively simple compared to other retrofit techniques (steel jacket or concrete overlay), however those methods have the benefit of increasing the flexural capacity and ductility, needed for bridges with inadequate flexural resistance. Concrete overlay can also be used for bridges where the efficiency of CFRP may be drastically decreased due to the cross-section size and proportions (e.g. river bridges).



Fig. 7.1 Pier retrofit with: a) steel jacket; b) concrete overlay; c) CFRP strips; d) post-tensioning (Padgett 2007).

According to the fragility analysis, bridges with Type 2 monolithic joints may suffer joint shear failure because of the inadequate shear reinforcement. Additional rebars can be applied

by drilling holes in the concrete, positioning the reinforcement and finally injecting the holes. This requires information on the exact location of existing reinforcements. Moreover, the cost is relatively high, since during the procedure the pavement has to be removed and then rebuilt.



Fig.7.2 a) Retrainer cable bar; b) retractor bar; c) bumper block; d) shock transmission unit (Padgett 2007).

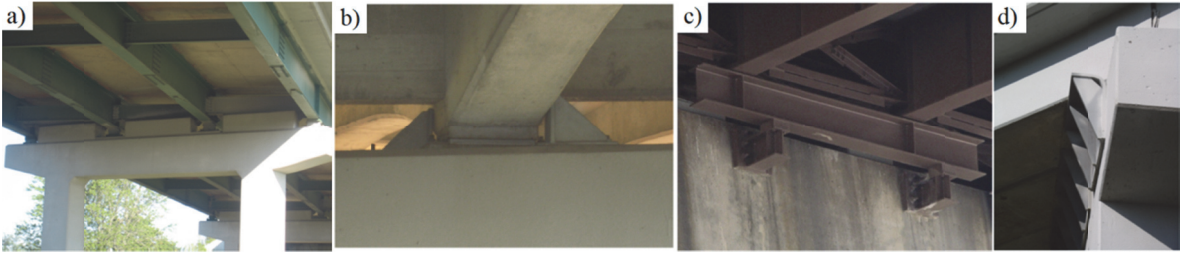


Fig. 7.3 a) Shear keys; b) keeper plate; c-d) seat extenders (Padgett 2007).

Excessive displacements should be avoided, since they may damage the expansion joints and may cause unseating. The following devices can control the longitudinal displacements (see Fig. 7.2): retractor cable; retractor bar; bumper block or shock transmission unit (STU; which works only for high velocity movements during earthquakes, while it lets displacements to develop in case of thermal expansion, for instance). Excessive transverse movements can be blocked by: shear keys or keeper plates (Fig. 7.3a-b). Another approach is to let the superstructure move freely, while the seating surface is extended to prevent the superstructure from falling off. Extension can be done with steel or RC cantilevers (Fig. 7.3c-d). The application of these devices is not essential in Hungary, since excessive displacements are not observed in case of the examined bridges.

7.1.2 Application of anti-seismic devices

The application of anti-seismic devices may be beneficial in the case where the acceptable reliability can only be achieved by fundamentally changing the seismic behavior, e.g. the amount of conventional strengthening is not acceptable (for example, the available space limits the cross section of highway overpass bridges) or extremely costly (e.g. the retrofit of river bridge piers and foundations). Anti-seismic devices are classified by EN 15129 (CEN 2010) as follows: 1) rigid connection devices with either permanent connection (e.g. conventional bearings) or temporary connection (e.g. shock transmission units; see Fig. 7.2d); 2) displacement dependent devices (linear or nonlinear); 3) velocity dependent devices (such

as fluid viscous or spring fluid dampers); 4) seismic isolators (SI) (e.g. elastomeric, lead rubber or sliding bearings). The application of different anti-seismic devices is illustrated with several examples in (Simon et al. 2013; Simon and Vigh 2013b).

### 7.2 Evaluation of possible retrofit methods

To evaluate the effectiveness of different retrofit methods, fragility analysis is conducted for various retrofitted configurations of two example bridges (BR03 and BR24). These two bridges represent typical configurations with typical problems considering the Hungarian road bridge stock: 1) an integral highway overpass bridge with inadequate monolithic joints and pier shear resistance (BR03); 2) a typical continuous girder bridge with conventional bearings where the structural layout is unfavorable and the pier shear resistance is insufficient. The bridges require different strategies due to their fundamentally different seismic behavior. The main goal is to reach a target reliability index of  $\sim 2$  for the area of Komárom.

#### 7.2.1 Conventional strengthening

BR03 is a PMG-I bridge (Fig. 7.4) with insufficient shear reinforcement and highly vulnerable abutment joints. The first damage of such PMG-I bridges is usually caused by the failure of the abutment joints. Based on the results of the parametric preliminary study,  $2\phi 25/100$  shear reinforcement is sufficient to prevent failure and even yielding of the joints. MSA is carried out with the retrofitted (RF1) joint; the joint deformation demands in case of the original and retrofitted configuration are illustrated in Fig. 7.5a. Yielding threshold of the joint deformation is determined at 2 mm which is reached around  $1 \text{ m/s}^2$  and  $5 \text{ m/s}^2$  before and after retrofit meaning that the median of the component fragility curve is shifted to the right towards a PGA value around  $5 \text{ m/s}^2$ .

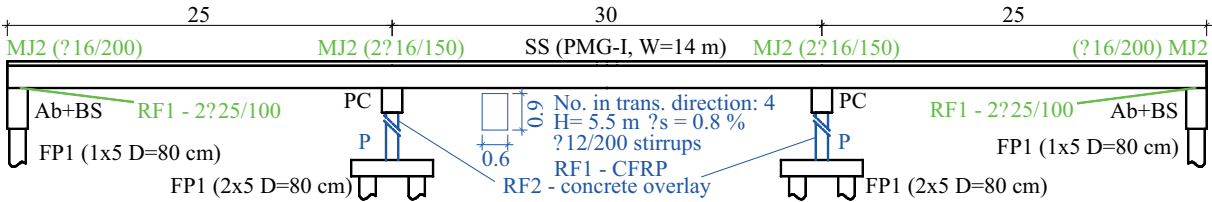


Fig. 7.4 Configuration and characteristics of the BR03 bridge. RF1 and RF2 retrofit strategies are also indicated.

As part of the retrofit design (RF1), the second step is to increase the pier shear resistance (possibly with CFRP). Shear failure is the dominant failure mode, thus the system fragility is close to the shear failure component fragility curve. Assuming that the dispersion of the fragility function does not change significantly, we can calculate the median value needed to reach a minimum target  $\beta$ . The required PGA level is  $\sim 5.5 \text{ m/s}^2$  which can be used to estimate the associated pier shear demands by observing the demands against the PGA (see Fig. 7.5b).

The median shear resistance should be  $\sim 850$  kN instead of the original  $\sim 750$  kN. This increase can be reached easily with CFRP (or  $\phi 16/150$  shear reinforcement in case of newly designed bridges). The calculated reliability index for the retrofitted structure (RF1) is 2.01.

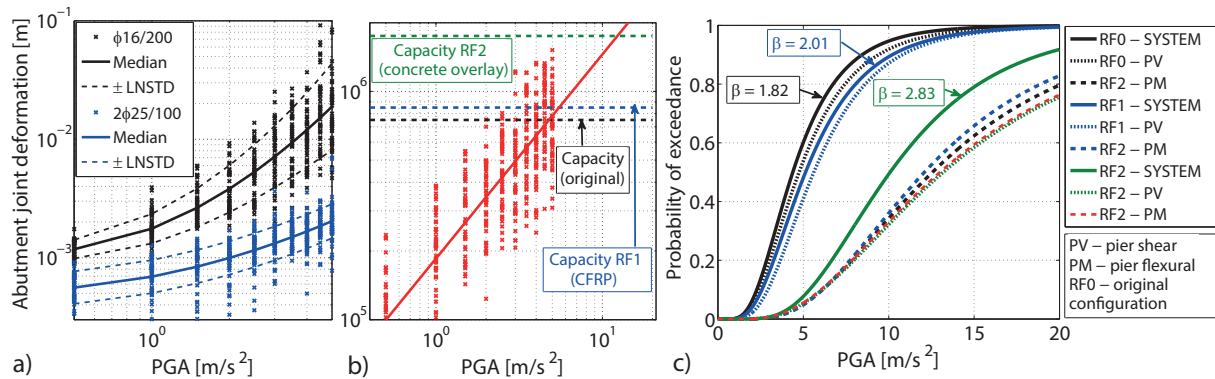


Fig. 7.5 Retrofit of the BR03 bridge. a) Abutment joint deformation demands before and after retrofit (RF1). b) Median pier shear demands. c) Fragility curves for LS3 for the original and two retrofit (RF1 and RF2) versions.

Unfortunately, the governing failure mode is still the pier shear failure (Fig. 7.5c). In order to obtain dominant flexural collapse, the fragility curve should be shifted towards the median of the flexural collapse fragility curve (or beyond if the dispersion of the shear fragility is higher). Two issues should be taken into account; the strengthening: 1) increases the pier stiffness, thus the pier demands; 2) and increases the flexural capacity. The increased demands can be estimated easily (demands are proportional to the square root of the stiffness); while the increase of the flexural capacity should be minimized (e.g. applying only minimal longitudinal reinforcement in case of concrete overlay). According to Fig. 7.5b and c, the median shear resistance should be  $\sim 1750$  kN. This increase may be hard to reach with CFRP retrofit, concrete overlay should be applied (the increase is a rational goal during design, since  $\phi 16/100$  reinforcement can provide the required resistance). The required resistance is calculated based on the initial stiffness and flexural capacity, since the bridge is flexible, the increase of the demands can be neglected, while the concrete overlay can be created to cause minimal flexural capacity increase. The RF2 leads to a 2.83 reliability index.

### 7.2.2 Application of anti-seismic devices

The other example is a COMP-B bridge (BR24; see Fig. 7.6) designed without any consideration of the seismic effect; it is a highly vulnerable layout. The DC ratio for pier shear failure is more than 4 (calculated with median MSA demands at the design PGA level), while the calculated  $\beta$  index is only 0.65 for Komárom. To achieve a minimum target reliability, the median shear resistance of  $\sim 2950$  kN should be increased to  $\sim 13000$  kN (the estimation is carried out in the same way as it is shown for BR03). This increase is extremely high (at least  $\phi 32/100$  shear reinforcement is needed), it can be done only with significant strengthening



efficiently to  $\sim 500$  kN in both directions. (Note that due to the hardening effect, isolator forces and thusly the transferred horizontal forces are usually higher than the yielding force).

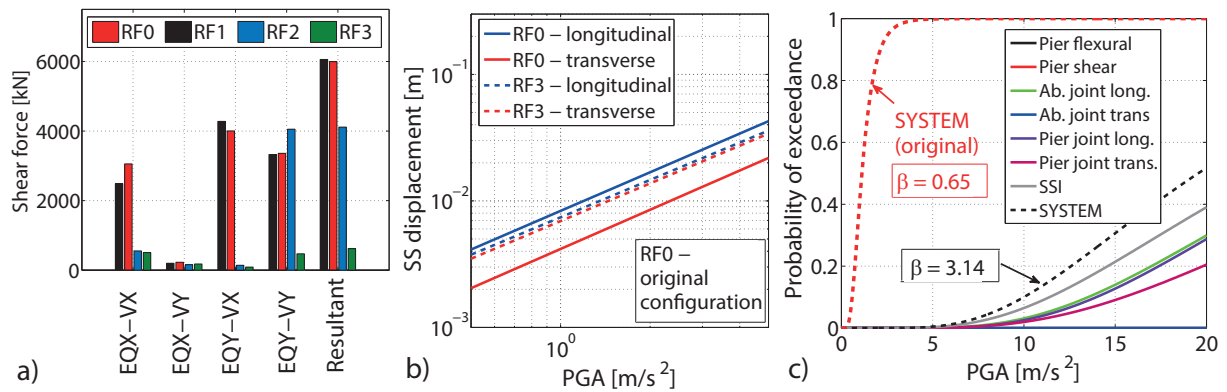


Fig. 7.7 a) Comparison of pier shear demands for different retrofit strategies. b) Median superstructure displacements. c) Fragility curves of the retrofitted configuration for collapse.

Fig. 7.7b depicts the median longitudinal and transverse displacements obtained with MSA for the original and the retrofit version RF3. One would expect that such drastic decrease in the transferred lateral forces with the yielding of the isolator considerably increases the displacements of the superstructure. The natural period elongation caused by the application of isolation devices would indeed lead to higher displacements, however the mitigating effect of the damping of the isolators should also be taken into account. In the longitudinal direction displacements are even decreased because the participation of more piers in the vibration increases the stiffness of the vibrating system compared to the original version (where only one pier support is restrained in this direction). In the transverse direction, the combined effect of the natural period elongation and damping of the isolators results in greater displacements. However, note that these displacements remain small, they are around 1 cm at the design PGA level in both directions.

Component fragility curves for LS3 of the retrofitted version (RF3) are illustrated in Fig. 7.7c, confirming the increased displacements and probability of unseating. Due to pounding, damage of the backfill soil is also more likely compared to the original configuration. With the isolation, the seismic demands of the piers are mitigated to a very low level which results in low probabilities of pier failure. The calculated reliability index of the retrofitted RF3 configuration is 3.14 showing that using seismic isolation devices can be an effective and economic solution. Significant decrease in the seismic demand of the substructure can be achieved, costly strengthening of piers, abutments and more importantly the foundations can be avoided. Moreover, the application of these devices can be easily carried out by replacing existing conventional bearings by lifting of the superstructure. The procedure usually does not

require any further strengthening or design, since bearing replacement is a planned intervention during the lifetime of a bridge.

### 7.3 Simplified analysis method for conceptual retrofit design

It is shown that the application of seismic isolators is a cost-effective retrofit solution if higher reliability can be achieved only with the alteration of the seismic behavior. The design of such devices is a complex task. Their non-linear behavior and the energy dissipation should be taken into consideration directly with NLTHA. However, seismic analysis is typically carried out with linear MMRSA in practice, therefore there is a need for a methodology where the complex behavior can be followed at least approximately with linear characteristics. Such method, the equivalent linear analysis procedure is proposed by EC8-2.

#### 7.3.1 Equivalent linear analysis method

Behavior of the most commonly applied seismic isolators (SI; lead rubber bearings, friction based bearings etc.) may be approximated with a bi-linear characteristic (Fig. 7.8), as suggested by EN 15129 and EC8-2. The required parameters are: initial stiffness ( $K_e$ ), the post-yield stiffness ( $K_p$ ) and yielding strength ( $F_y$ ). The equivalent linear characteristic is expressed with effective stiffness ( $K_{eff}$ ) and effective damping ( $\xi_{eff}$ ), to consider the non-linear behavior and the energy dissipation of the SIs, respectively.

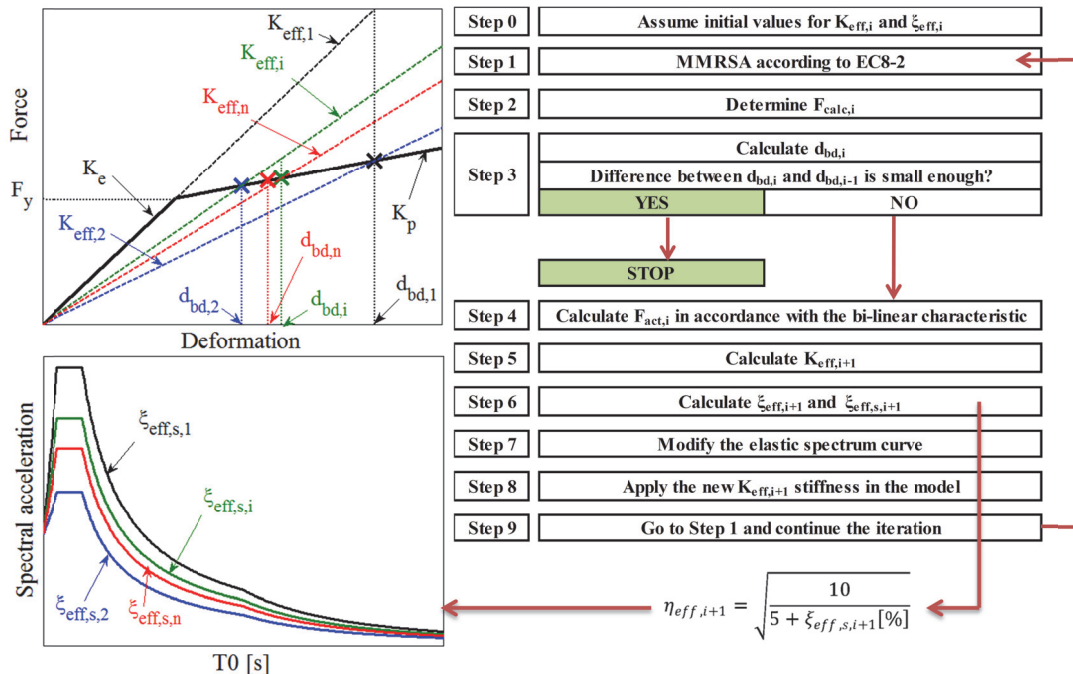


Fig. 7.8 Flowchart of the iteration procedure for equivalent linear analysis.

Equivalent linear analysis (ELA) should be carried out with iteration (Fig. 7.8) to arrive at compatible forces and deformations. In each iteration step, MMRSA is completed with  $K_{eff}$  of

the non-linear components and  $\xi_{\text{eff},s}$  of the system. With the obtained deformations ( $d_{\text{bd},i}$ ) the effective properties are updated. The deformation compatible force  $F_{\text{act},i}$  is:

$$F_{\text{act},i} = F_y + K_p(d_{\text{bd},i} - d_y) \quad (7.1)$$

assuming that  $d_{\text{bd},i}$  is greater than the yielding deformation ( $d_y$ ). The updated effective stiffness ( $K_{\text{eff},i+1}$ ) is the secant stiffness corresponding to the calculated deformation level:

$$K_{\text{eff},i+1} = \frac{F_{\text{act},i}}{d_{\text{bd},i}} \quad (7.2)$$

while the effective damping of one isolator unit is described per EC8-2 as follows:

$$\xi_{\text{eff}} = \frac{4(F_y - K_p d_y)(d_{\text{bd}} - d_y)}{2\pi K_{\text{eff}} d_{\text{bd}}^2} \quad (7.3)$$

The system damping is calculated as the sum of the effective damping of the isolator units. The last step is to modify the elastic response spectrum via the modification factor:

$$\eta_{\text{eff},i} = \sqrt{\frac{10}{5 + \xi_{\text{eff},s,i}[\%]}} \quad (7.4)$$

The iteration is continued until the difference in  $d_{\text{bd},i}$  is less than a predefined tolerance<sup>8</sup>.

### 7.3.2 Limitations of the equivalent linear method

Accuracy of the ELA method has already been evaluated by several researchers concluding that the determination of the effective damping is critical and in several cases it is overestimated. New conclusions were made that the accuracy depends not only on the ductility ratio of the SI ( $\mu$  = the deformation demand divided by the  $d_y$  yielding deformation), but the effective period of the structure and the frequency characteristics of the ground motion. Several new formulations were proposed by various authors, based on either modifying the original equation (Hwang et al. 1996; Dicleli and Buddaram 2007; Liu et al. 2014; Zordan et al. 2014) or creating formulae considering datasets from non-linear analyses (Iwan and Gates 1979; Hwang et al. 1994; Jara et al. 2012; Liu and Zhang 2016).

The mentioned studies focus on the evaluation of a simple SDOF system. As part of this research, the feasibility of the ELA for real structures is investigated through 3 typical (RC-B, COMP-I and STEEL-B) continuous girder bridge examples (see details in Simon and Vigh 2013c). Besides Eq.(7.3), the effective damping is calculated by four other codes as well for comparison: 1) AASHTO code providing the same formula as Eq.(7.3); 2) JPWRI manual (JPWRI 1992); 3) Caltrans94 method (Hwang et al. 1994); 4) Caltrans96 method (Hwang et al. 1996). Fig. 7.9 shows the effective damping ratios calculated by the discussed four methods. Increasing the post-elastic stiffness ( $K_p/K_e$  ratio), the elastic energy associated with  $K_{\text{eff}}$  is higher for the same deformation, thus the corresponding effective damping is lower. At

---

<sup>8</sup> 5% per EC8-2, however, 1% is applied in this study.

lower ductility ratios (<15; possibly the case of moderate seismicity) the highest effective damping is provided by the EC/AASHTO code, followed by the JPWRI, Caltrans 96 and Caltrans94 methods. Accordingly, high variance of the results is expected; lower internal forces may be obtained with AASHTO/EC and JPWRI, and higher ones from Caltrans94 and 96 for moderate earthquakes. Note that at lower ductility, Eq.(7.3) provides an effective damping ratio up to 0.4, while the proposed limitation for ELA method by EC8-2 is 0.3.

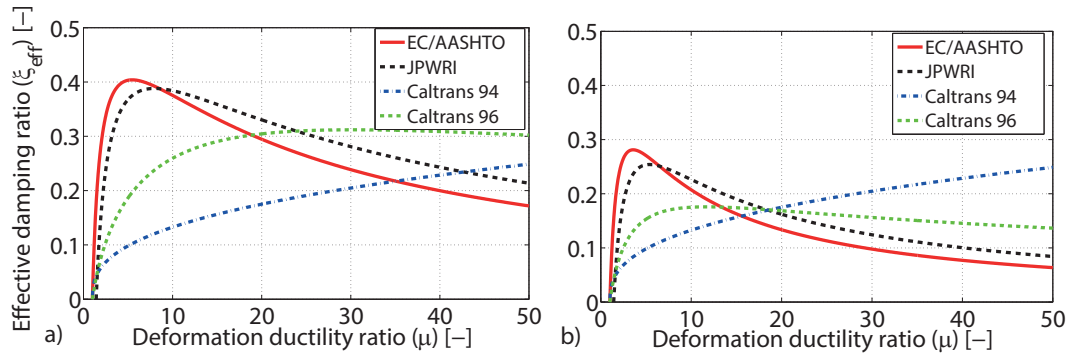


Fig. 7.9 Effective damping ratios calculated with different codes.  $K_p/K_c$  of 0.05 (a), 0.15 (b).

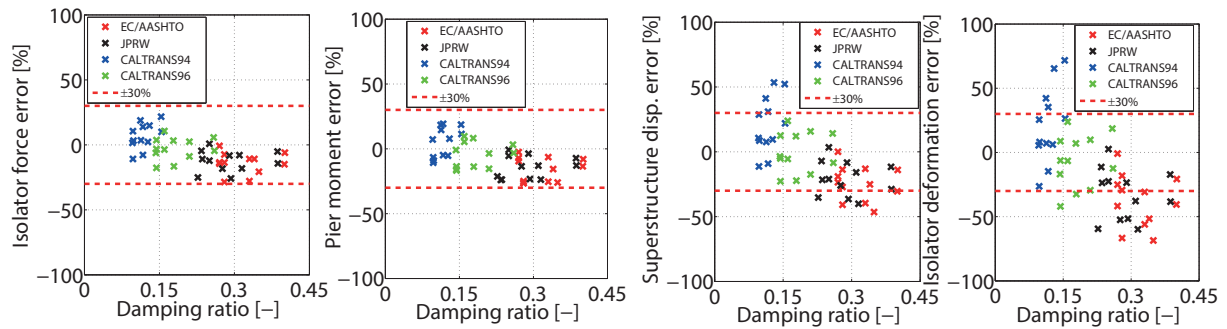


Fig. 7.10 Accuracy of the ELA method compared to NLTHA results. Error is calculated as  $ELA/NLTHA-1$  in % for isolator force, pier moment, superstructure displacement and isolator deformation.

The evaluation is carried out as follows. A total number of 48 ELA is performed with iteration (three bridges; response spectrum with soil type C and E, PGA value of 1.0 and 1.4  $m/s^2$ ; four effective damping determination methods). NLTHA is conducted with 7 artificial ground motions (for each standard spectrum) and the averages of the results are considered as the exact solution per EC8-2. Finally, the two methods are compared by calculating the relative error of the ELA.

Fig. 7.10 shows the results for 4 main responses characterizing the local behavior of the isolator and the global behavior of the whole structure in the dominant longitudinal direction. The observed ductility ratios are under 15. Accordingly, EC/AASHTO underestimates (-signed error) the demands, while Caltrans94 method is too conservative (+ signed error) in most cases. The most reasonable results can be obtained with the Caltrans96 method (error is under 30-40% for all demands). Although displacements and deformations may have an error up to ~50 and ~75%, all methods are applicable to predict the internal forces of the system

components with an accuracy of  $\pm 30\%$ . Note also that this accuracy is valid even for damping ratios over the 0.3 limit.

In the preliminary phase, the aim of the conceptual design is to compare different strategies mainly to decrease the demands of the substructure. The iterative MMRSA is time-efficient, the experience is that only 5-6 iteration steps are needed for compatible internal force solution. Based on the results, the following 6 step procedure is suggested for conceptual retrofit design: 1) if conventional strengthening is not a cost-efficient option, select isolator units with proper characteristics (e.g. yielding force should be higher than the isolator force from service loading); 2) set out strategies with different isolator arrangements and characteristics; 3) carry out iterative MMRSA according to Fig. 7.8 using the EC/ASHTOO (or the more accurate CALTRANS 96) method to determine the effective damping ratio (ignore the 0.3 limit); 4) increase the governing internal forces with a factor of 1.3; 5) compare the different strategies; 6) select the most favorable retrofit version and check the internal forces and displacements with NLTHA.

### *7.3.3 Conceptual seismic retrofit design of M0 Háros highway bridge*

The suggested conceptual retrofit design procedure is used for a real bridge project. As part of the research, an existing highway bridge over the Danube River for the M0 Highway at Háros is examined. The main structural attributes and the configuration of the structure are shown in Fig. 7.11. The bridge was built in 1990 without seismic design. The composite girder of the river bridge has to be replaced due to the ageing of the deck. The replacement results in a new structure, thus seismic performance has to be evaluated according to EC8-2. Since some piers and bearings do not satisfy the standard seismic requirements, seismic retrofit is needed.

The main goal of the conceptual seismic retrofit design is to keep the original piers and foundations, and to achieve a cost-effective solution. There are two alternatives: 1) conventional retrofit methods strengthening the critical members; 2) mitigation of the seismic demand. The first approach leads to increased demands on construction materials, human resources and thus to significant expenses assigned to strengthening of immersed piers and foundations. On the contrary, an effective demand mitigation method may assure to keep the original substructure in its existing form. Such methods can be: a) using more sophisticated modeling techniques (e.g. taking into account the actual, cracked pier stiffness); b) redistribution of internal forces with the rearrangement of fixed bearings; c) using seismic isolators to isolate the substructure from the superstructure.

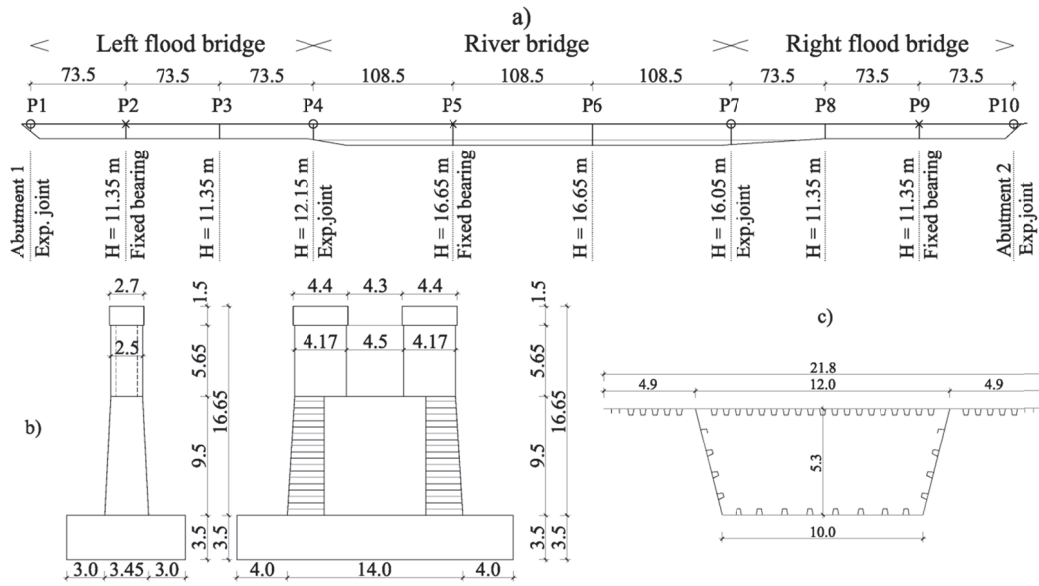


Fig. 7.11 Configuration of the existing M0 Háros Highway Bridge. a) side-view of the bridge; b) side-views of pier P5; c) cross-section of the river bridge girder.

Table 7.1 Retrofit versions. “+” marks fixed bearing in the corresponding direction; SI1-SI4 are showing the application of seismic isolators. V1 – original version. V9 – final retrofitted version.

Ver.	Direction	Piers									Abut. P10	Pier stiffness				
		Abut. P1	P2	P3	P4/1	P4/2	P5	P6	P7/1	P7/2			P8	P9		
V1	Long.		+				+									
	Trans.	+	+	+	+	+	+	+	+	+	+	+	+	+	+	100%
V2	Long.		+				+									
	Trans.	+	+	+	+	+	+	+	+	+	+	+	+	+	+	50%
V3	Long.		+				+	+	+							
	Trans.	+	+	+	+	+	+	+	+	+	+	+	+	+	+	100%
V4	Long.		+				+	+	+							
	Trans.	+	+	+	+	+	+	+	+	+	+	+	+	+	+	50%
V5	Long.		+				SI1									
	Trans.	+	+	+	+	+	+	+	+	+	+	+	+	+	+	100%
V6	Long.	SI1					SI1									
	Trans.	+	+	+	+	+	+	+	+	+	+	+	+	+	+	100%
V7	Long.	SI1					SI1									
	Trans.	+	+	+	+	+	SI3	SI3		+		+	+	+	+	100%
V8	Long.	SI1					SI1									
	Trans.	+	+	+	+	+	SI3	SI3	SI4	SI5	+	+	+	+	+	100%
V9	Long.	SI1					SI1	SI1	SI1							
	Trans.	+	+	+	+	+	SI3	SI3	SI4	SI5	+	+	+	+	+	100%

Isolator properties

SI1 –  $F_y = 1200$  kN;  $K_e = 250$  kN/mm;  $K_p = 15$  kN/mm. SI2 –  $F_y = 3300$  kN;  $K_e = 1400$  kN/mm;  $K_p = 75$  kN/mm.

SI3 –  $F_y = 5100$  kN;  $K_e = 2200$  kN/mm;  $K_p = 115$  kN/mm. SI4 –  $F_y = 1815$  kN;  $K_e = 750$  kN/mm;  $K_p = 40$  kN/mm.

SI5 –  $F_y = 1650$  kN;  $K_e = 700$  kN/mm;  $K_p = 40$  kN/mm.

Accordingly, eight demand mitigation methods (Table 7.1) are evaluated and compared on the level of internal forces in the critical elements. To illustrate the steps of the conceptual design, representative results are presented in two figures. Longitudinal and transverse bending moments acting in the bottom section of the piers are compared in Fig. 7.12. Additionally, Fig. 7.13a presents the DC ratios for pier P5, P6 and P7, while the bi-axial bending interaction diagram of the most critical pier P5 is depicted in Fig. 7.13b.

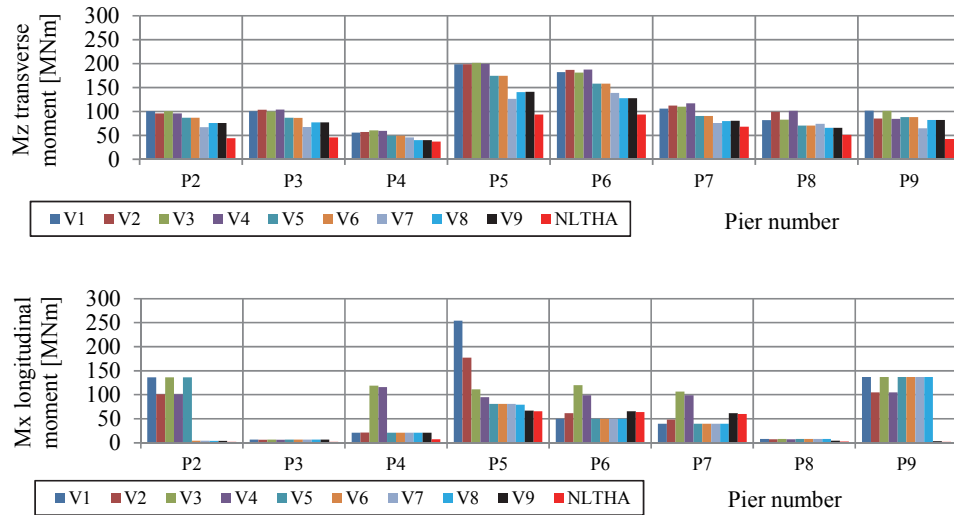


Fig. 7.12 Longitudinal and transverse bending moments of the piers for the examined versions.

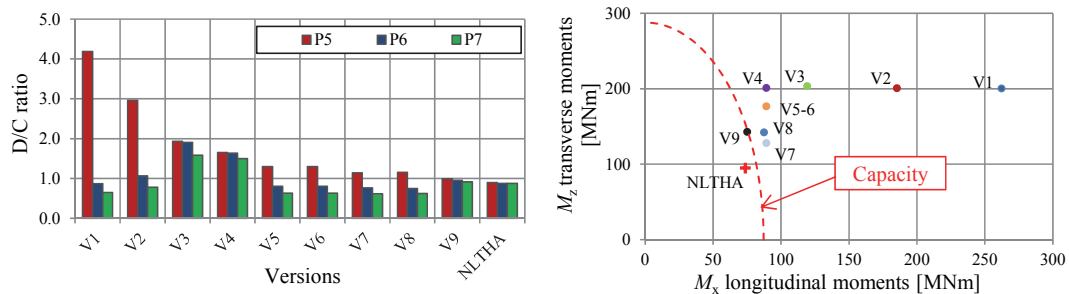


Fig. 7.13 a) Flexural DC ratios of the river bridge piers for the examined versions. b) Bi-axial bending interaction diagram of the most critical pier P5.

Comparison of the ELA and NLTHA is implemented for the last retrofitted configuration (V9) by presenting five different responses in both horizontal directions at pier P5 and P7, and by evaluating the differences of the results (see Table 7.2). The following demands are compared: internal force and deformation of the SI; girder displacement; pier top displacement and pier bending moments in both longitudinal and transverse directions.

Table 7.2 Comparison of ELA and NLTHA results for the final V9 version.  $\Delta$  denotes ELA/NLTHA-1 in %.

Pier #	Longitudinal direction				Transverse direction			
	P5		P7		P5		P7	
Parameter	NLTH	$\Delta\%$	NLTH	$\Delta\%$	NLTH	$\Delta\%$	NLTH	$\Delta\%$
Isolator force (kN)	1397	0	1372	1	4247	21	1542	-6
Isolator deformation (mm)	14.5	25	12.8	31	2	24	2.05	-5
Girder displacement (mm)	22	16	20	23	5.1	22	5.6	-11
Pier top displacement (mm)	9	-20	8.8	-11	3.1	16	4.1	-26
Pier bending moment (kNm)	65582	-22	59715	-20	93592	16	68398	-9

In the longitudinal direction, the force in the SI can be approximated by ELA method with negligible error due to the bi-linear characteristic and low post-yield stiffness of the device. However in case of pier moments, deformations and displacements, the error of the ELA is generally around 20-30%, as expected. The deformation of the SI and thus the girder displacements are overestimated by 16-31%, while the pier top displacements are

underestimated by 10-20%. This underestimation is reflected in the pier moments: typically 20% larger internal forces obtained with NLTHA. These results confirm the previous findings and conclusions.

In the transverse direction, the results are less consistent. The screened values are higher from the ELA compared to the NLTHA in case of pier P5 meaning that even though the equivalent damping ratios may be overestimated, time-history analysis leads to lower demands overall. The tendency is the opposite at pier P7, however the overestimation is not higher than 26% (pier top displacement), and lower than 10% in case of the internal forces (SI force, pier moment). The inconsistent results stem from two origins of uncertainty: 1) calculation of the equivalent damping and the effective stiffness; 2) the analysis method applied. The uncertainty of the ELA method using SDOF system is discussed previously, while it can also be shown that the internal forces obtained with MMRSA and LTHA differ with up to 15% and 40% in the longitudinal and transverse directions, respectively.

In conclusion, using a factor of 1.3 for the increase of the internal forces in the conceptual phase is a rational choice; conservative results are obtained in both directions even for a large-span non-regular bridge configuration. However, NLTHA of the chosen retrofitted version has to be carried out for validation, ELA should be used only in the preliminary phase.

## **7.4 Proposed design concepts**

Based on the preliminary and fragility analyses and the evaluation of retrofit strategies, design concepts can be given for new bridges. One of the main problems with existing bridges is that most of them are not designed for seismic actions. Therefore, the unfavorable behavior stems from the lack of seismic design. Typically, pier shear resistance is insufficient for all bridge types (except for certain steel bridges), and the monolithic joints of SLAB and PMG-I bridges are also critical. It is shown that seismic design carried out in accordance with EC8-2 leads to a minimum acceptable reliability level. Due to their different seismic behavior, bridges with monolithic and bridges with conventional bearings are discussed separately.

### *7.4.1 Bridges with monolithic joints*

PMG-I and SLAB bridges are constructed with monolithic joints at each support. For such structures, seismic analysis should be carried out with a behavior factor of 1.0 using MMRSA; and the effect of the backfill soil and the SSI at the foundations should be included in the numerical model. The use of upper and lower bound estimates of the soil stiffness is recommended to arrive at conservative demands for each bridge component. Details about the modeling and calculation of SSI stiffness can be found in Chapter 4 and 5. Resistance of the

piers and the monolithic joints should be calculated per EC8-2 and EC2, and with the formula presented in Chapter 5. The maximum acceptable PGA results presented in Appendix D highlights the critical components for specific configurations. According to the presented studies, the general layout (e.g. main geometry, pier cross-section) of SLAB and PMG-I bridges can be kept, the required capacity of the piers and the joints can be reached simply with additional reinforcements. Table 7.3 illustrates these estimated required reinforcements considering a typical pier height of 5-6 m and a maximum bridge length of 80-100 m.

Table 7.3 Estimated required reinforcements for SLAB and PMG-I bridges (5-6 m pier height; up to 100 m total length)

	PGA [m/s <sup>2</sup> ]	Pier long. reinf. ratio	Pier shear reinf.	Monolithic joint shear reinforcement
SLAB	0.8	1.2%	φ16/150	2φ20/100
	1.5	2.0%	φ16/100	2φ25/100
PMG-I	0.8	0.8%	φ12/150	2φ16/100
	1.5	1.5%	φ12/100	2φ22/100

#### 7.4.2 Bridges with conventional bearings

The piers of bridges with conventional bearings typically have inadequate shear resistance. Seismic design should be carried out in line with EC8-2 applying either limited ductile ( $q=1.5$ ) or ductile ( $1.5 < q < 3.5$ ) design of the piers. Seismic analysis using MMRSA should be carried out with the above mentioned behavior factors; and SSI at the foundations should be accounted for in the numerical model assuming an upper and a lower estimate for the soil stiffness. The influence of the backfill soil may be neglected to obtain conservative pier demands (pounding decreases these demands and increases the backfill soil demands, but it is shown that the failure of this component is not expected).

Selecting a proper bridge configuration is also part of the seismic design. There are several existing bridges, the seismic behavior of which is unfavorable due to the improperly chosen structural system and layout. For instance, PMG-NI bridges are extremely vulnerable; monolithic joints are constructed only on some piers. It is generally beneficial to draw more piers into the vibration. The application of STUs may be an optimal solution which distributes the seismic load among all piers, but lets the thermal movements develop. One should bear in mind that the piers at which the STU is applied should be designed for the increased demands.

Another issue is the torsion of the supports. Zsarnóczy (2010) showed that pier torsional moments can be neglected, since the torsional capacity is at least an order of magnitude greater. However, if there are multiple piers in the transverse direction, the torsion of the support causes considerable longitudinal shear forces in the piers with longitudinal fixed bearings. This effect is more significant with odd number of supports. A possible solution to avoid this behavior is use one, but more robust pier.

## 7.5 Summary

In this chapter, possible retrofit methods are reviewed and evaluated through fragility analysis for the two most typically critical bridge configurations. It is shown that CFRP strengthening is an optimal solution to moderately increase the shear resistance of PMG-I, PMG-NI and SLAB bridges, while for more significant increase of the shear resistance or in the case of more robust piers, concrete overlay can be used efficiently.

When mere strengthening is not a feasible option (the cost is too high due to the difficult construction, e.g. river bridge piers), seismic isolators should be used to mitigate the pier and foundation demands. It is shown that the reliability level can be increased significantly with seismic isolators, while the probability of unseating remains relatively low.

The design of seismic isolators is a complex task due to their nonlinear behavior and energy dissipation. A simple methodology is proposed for conceptual seismic isolator design which can be applied with the most commonly used linear MMRSA method, therefore is convenient for practicing engineers. I summarized the presented results in my Thesis V.

# Chapter 8

## Summary and Conclusions

### 8.1 Primary results and impact

A comprehensive and rigorous methodology is used in the research to evaluate the seismic performance of typical road bridges in Hungary. The results contribute to three main topics.

#### 1) Seismic analysis and design:

- It is shown that the Type 2 standard spectrum describes well the UHS in Hungary.
- The artificial record generation software is freely available and can be used by engineers for time-history analysis to obtain less conservative seismic demands compared to the most commonly used MMRSA.
- Possible modeling technique of typical bridge types for both linear and nonlinear analysis is suggested, where new modeling approach is presented for the monolithic joints of precast multi-girder bridges.
- The study highlights the critical bridge components and configurations. It also provides design concepts for new bridges.

#### 2) Seismic performance evaluation:

- An automatic seismic performance evaluation framework is established. Nationwide evaluation can be carried out if essential data of each bridge is available.
- The appropriateness of various intensity measures are evaluated for different configurations. Ground motions should be selected with regard to the optimal IM, if the selection is not based on a hazard compatible GCIM procedure.
- An expected structural reliability level is provided by calculating the range of possible reliability indices for typical bridges. It is also shown that with proper seismic design a target reliability of  $\sim 2$  can be achieved.
- The presented fragility curves can be used for decision making in pre- and post-earthquake situations such as retrofit prioritization, emergency routes and recovery planning.

#### 3) Seismic retrofit design:

- It is shown that cost-efficient increase of the pier shear resistance can be obtained with CFRP strengthening for typical precast multi-girder and slab bridges, while concrete overlay can be used for bridges where the efficiency of CFRP may be drastically decreased due to the cross-section size and proportions.

- According to the fragility analysis, bridges with monolithic joints may suffer joint shear failure which is the result of inadequate shear reinforcement.
- It is shown that seismic isolation is an optimal solution for bridges with improper seismic behavior. A time-efficient approach is proposed for conceptual seismic isolation design.

## 8.2 Recommendations for future work

The study showed that the reliability level is low in case of several typical road bridges in Hungary. There is a need for a broader evaluation in order to make economic and financial decisions on a national level. The following task should be carried out to achieve this goal:

- The bridge database shall be extended and the required data shall be collected.
- Site-specific UHS shall be determined for the whole country.
- The developed framework shall be used to evaluate the seismic performance of thousands of bridges in the extended database.
- A possible retrofit strategy shall be worked out based on the results.

Other directions for future work:

- The numerical model shall be further improved. The cyclic behavior and modeling of Type 1 monolithic joints and typical bearings used in Hungary shall be investigated. The developed nonlinear pile foundation model shall be incorporated in the fragility analysis.
- The study raised questions on the target reliability and the design PGA level. This issue is an open question in the literature as well and should be investigated in detail.

## 8.3 New scientific results

### *Thesis I (Simon and Vigh 2013a, 2015c, 2016b)*

I investigated the seismic hazard of Hungary, and carried out comparative evaluation of site specific spectra and Eurocode 8-1 standard spectra.

- I/a I employed a probabilistic seismic hazard analysis procedure and adopted a record selection method based on the general conditional intensity measure approach for Hungarian sites. I also created a freely available artificial record generation program.
- I/b I showed that earthquakes with moderate magnitude ( $<5.5$ ) and small epicentral distance ( $<10$  km) contribute most to the seismic hazard of Hungarian sites at the design intensity level; and that the expected significant duration of ground motions is under 10 s.
- I/c I showed that the Eurocode 8-1 Type 2 standard spectrum describes the site specific spectrum better in Hungary than the Type 1 spectrum.

- I/d I evaluated different intensity measures, and I verified that the seismic response of bridges is highly correlated with the spectral acceleration and the spectral intensity associated with the dominant vibration period controlling the seismic response.

***Thesis II (Simon and Vigh 2015a; Simon et al. 2016)***

I developed an evaluation framework to determine the seismic performance of Hungarian road bridges based on fragility analysis.

- II/a I worked out five separate (database, seismic load generation, numerical model generation, seismic analysis and post-processing) modules in detail, and automatized the evaluation procedure by creating connection between these modules.
- II/b I investigated the applicability of the existing bridge database for the seismic performance evaluation of the whole bridge inventory. I highlighted the shortcomings of the database; and proposed an extended database structure and a strategy for the extension.
- II/c I classified the bridges into 8 bridge classes and characterized their most important structural attributes. I created a portfolio of 30 representative existing bridges.

***Thesis III (Simon and Vigh 2014, 2015b, 2016a)***

I conducted a preliminary parametric study for precast multi-girder and slab bridges with monolithic joints using linear modal response spectrum analysis.

- III/a I developed the linear numerical model of the structures; and proposed a modeling technique for the backfill soil in case of linear modal response spectrum analysis.
- III/b I determined critical configurations and components of typical bridge structures, and showed that the performance of the superstructure, abutment, backfill soil and the foundation is adequate; and that the monolithic joints are critical, especially at the abutments. I also showed that in case of longer (>50 m) bridges, the pier shear or flexural resistance is insufficient for short (<5 m) or high piers (>5 m), respectively.
- III/c I estimated the number of critical integral precast multi-girder and slab bridges in the inventory based on the standard evaluation per Eurocode 8-2.

***Thesis IV (Simon 2012, 2013; Simon and Vigh 2015b, 2016a; Simon et al. 2016)***

I carried out a parametric fragility analysis for precast multi-girder bridges with monolithic joints; and conducted fragility analysis of 30 structures representing typical bridge types of the Hungarian bridge stock.

- IV/a I developed the nonlinear numerical model for each bridge class. I worked out and calibrated a numerical model for the cyclic nonlinear behavior of monolithic joints

with shear reinforcement. I developed a numerical model for pile foundations based on the Beam on Nonlinear Winkler Foundation approach; and proposed parameter definitions in line with Eurocode 7 and Hungarian practice.

IV/b I evaluated the effect of different modeling and analysis assumptions on the seismic response of bridge structures. I showed the importance of modeling the cyclic behavior of monolithic joints and the pounding between bridge components; and showed that the geometric uncertainty is negligible, while the material and soil uncertainties may significantly influence the calculated probability of failure.

IV/c I determined the most vulnerable bridge components using the component fragility curves. I verified that the results for precast multi-girder and slab bridges are in accordance with the conclusions of the preliminary study, and showed that pier shear failure is dominant for several bridge types. I showed that steel bridges with conventional bearings have better behavior, the collapse may be characterized with pier flexural failure.

IV/d I evaluated the reliability of typical road bridges, and compared the seismic performance of the structures based on their reliability index. I showed that an improper structural system and the lack of seismic design may result in an unacceptably low reliability level; and showed that seismic design per EC8-2 leads to a reliability index of around 2.

***Thesis V (Simon and Vigh 2013b, 2013c; Simon et al. 2015)***

I proposed retrofit methods for vulnerable structures and design concepts for new bridges.

V/a I showed that applying monolithic joints at the abutments, and conventional fix and free bearings in the longitudinal and transverse directions at the piers is an optimal configuration for highway overpass bridges up to 100 m total length.

V/b I evaluated retrofit strategies for two representative critical bridges. I showed that carbon fiber reinforced polymer is an economical space-saving solution for pier strengthening when only moderate increase of the reliability is required; while significant increase can be achieved with concrete overlay. In case of an improper structural system, seismic isolation is a cost-efficient retrofit method.

V/c I evaluated the accuracy of the equivalent linear analysis method of Eurocode 8-2 with non-linear time-history analyses; and proposed a methodology for conceptual seismic isolation design, which I verified through the retrofit design of an existing large span river bridge.

## 8.4 Publications of the author on the subject of the thesis

### International journal papers

- Simon J, Vigh LG (2013a) Seismic assessment of an existing Hungarian highway bridge. *Acta Technica Napocensis – Civil Engineering and Architecture* 56(2):43-57
- Simon J, Vigh LG, Horváth A, Pusztai P (2015) Application and assessment of equivalent linear analysis method for conceptual seismic retrofit design of Háros M0 highway bridge. *Periodica Polytechnica – Civil Engineering* 59(2):109-122. doi: 10.3311/PPci.7860
- Simon J, Vigh LG (2016a) Seismic fragility assessment of integral precast multi-span bridges in areas of moderate seismicity. *Bulletin of Earthquake Engineering* (accepted). doi: 10.1007/s10518-016-9947-y

### Hungarian journal papers

- Simon J, Martinovich K, Dani B, Ájpli B, Sapkás Á, Vigh LG (2013) Retrofit methods for bridges – case studies (in Hungarian). *Útügyi Lapok* 1(1) Paper 2
- Simon J, Vigh LG (2015a) Application of the existing road bridge database for the seismic performance evaluation of Hungarian road bridges (in Hungarian). *Útügyi Lapok* 5(1):1-24
- Simon J, Vigh LG (2016b) Determination of seismic load in Hungary: Application of site specific response spectra (in Hungarian). *Vasbetonépítés* (accepted)

### Papers in edited book

- Simon J, Vigh LG, Horváth A (2016) Seismic performance and damage assessment of Hungarian road bridges (in Hungarian). *Scientific Publications of BME Department of Structural Engineering*. pp. 89-98, Budapest, Hungary

### Conference papers

- Simon J (2012) Numerical model development for seismic assessment of continuous girder bridges. *Proc. of the Conference of Junior Researchers in Civil Engineering*. pp. 216-224, Budapest, Hungary
- Simon J, Vigh LG (2012) Seismic assessment of Hungarian highway bridges – A case study. *Proc. of the First international conference for PhD students in Civil Engineering*. pp. 155-162, Cluj-Napoca, Romania
- Simon J, Vigh LG (2013b) Possible seismic retrofit methods for road bridges (in Hungarian). *Építményeink védelme 2013*. pp. 1-14, Ráckeve, Hungary
- Simon J (2013) Parameter identification for dynamic analysis of pile foundation using non-linear p-y method. *Proc. of the Second Conference of Junior Researchers in Civil Engineering*. pp. 161-170, Budapest, Hungary
- Simon J, Vigh LG (2013c) Response spectrum analysis of girder bridges with seismic isolators using effective stiffness. *Int. Conf. on Civil, Structural and Earthquake Engineering*. pp. 1353-1362, Istanbul, Turkey
- Simon J, Vigh LG (2014) Multi modal response spectrum analysis implemented in OpenSees. *OpenSees Days Portugal 2014*. pp. 39-42, Porto, Portugal
- Simon J, Vigh LG (2015b) Preliminary seismic vulnerability assessment of pre-code multi-girder bridges in Hungary. *Earthquake Risk and Engineering towards a Resilient World*, pp. 1-10, Cambridge, UK
- Simon J, Vigh LG (2015c) Seismic vulnerability assessment of existing Hungarian highway bridges using hazard compatible ground motions. *12th Hungarian Conference on Theoretical and Applied Mechanics*. Paper 334. 13 p. Miskolc, Hungary

## References

- AASHTO (2012) Guide specifications for seismic isolation design. Second Edition, American Association of State Highway and Transportation Officials, Washington DC, USA
- Akkar S, Bommer JJ (2010) Empirical equations for the prediction of PGA, PGV and spectral accelerations in Europe, the Mediterranean Region and the Middle East. *Seism Res Lett* 81(2):195-206. doi: 10.1785/gssrl.81.2.195
- ASCE (2014) ASCE 41-13: Seismic evaluation and retrofit of existing buildings. American Society of Civil Engineers
- Aviram A, Mackie KR, Stojadinovic B (2008) Guidelines for nonlinear analysis of bridge structures in California. PEER Report 2008/03, Pacific Earthquake Engineering Research Center, University of California, Berkeley, CA
- Avşar Ö, Yakut A, Caner A (2011) Analytical fragility curves for ordinary highway bridges in Turkey. *Earthq Spectra* 27(4):971–996. doi: 10.1193/1.3651349
- Bada G, Horváth F, Gerner R, Fejes I (1999) Review of the present-day geodynamics of the Pannonian basin: progress and problems. *Geodynamics* 27(4):501-527. doi: 10.1016/S0264-3707(98)00013-1
- Baker JW, Cornell CA (2006) Spectral shape, record selection and epsilon. *Earthq Eng Struct D* 35(9):1077–1095. doi: 10.1002/eqe.571
- Baker JW, Jayaram N (2008) Correlation of spectral acceleration values from NGA ground motion models. *Earthq Spectra* 24(1):299–317. doi: 10.1193/1.2857544
- Baker JW (2008) An introduction to Probabilistic Seismic Hazard Analysis (PSHA), Version 1.3
- Baker JW (2011) Conditional mean spectrum: Tool for ground motion selection. *J Struct Eng* 137(3):322-331. doi: 10.1061/(ASCE)ST.1943-541X.0000215
- Baker JW (2015) Efficient analytical fragility function fitting using dynamic structural analysis. *Earthq Spectra* 31(1): 579-599. doi: 10.1193/021113EQS025M
- Basoz N, Kiremidjian AS (1996) Risk assessment for highway transportation systems. Report No. NCEER-118, John A. Blume Earthquake Engineering Center.
- Billah AHMM, Alam MS (2015) Seismic fragility assessment of highway bridges: a state-of-the-art review. *Struct Infrastruct E* 11(6):1-29. doi: 10.1080/15732479.2014.912243
- Biskinis D, Roupakias G, Fardis MN (2004) Degradation of Shear Strength of RC Members with Inelastic Cyclic Displacements, *ACI Struct J* 101(6):773-783.
- Bommer JJ, Martinez-Pereira A (1999) The effective duration of earthquake strong motion. *J Earthq Eng* 3(2):127–172.
- Borzi B, Ceresa P, Franchin P, Noto F, Calvi GM, Pinto PE (2015) Seismic vulnerability of the Italian roadway bridge stock. *Earthq Spectra* 31(4):2137-2161. doi: 10.1193/070413EQS190M
- Boulanger RW, Curras CJ, Kutter BL, Wilson DW, Abghari A (1990) Seismic soil-pile-structure interaction experiments and analysis. *J Geotech Geoenviron* 125(9):750-759. doi: 10.1061/(ASCE)1090-0241(1999)125:9(750)
- Bradley BA, Cubrinovski M, MacRae GA, Dhakal RP (2009) Ground motion prediction equation for SI based on spectral acceleration prediction. *B Seismol Soc Am* 99(1):277-285. doi: 10.1785/0120080044

- Bradley BA (2010a) A generalized conditional intensity measure approach and holistic ground-motion selection. *Earthq Eng Struct D* 39(12):1321–1342. doi: 10.1002/eqe.995
- Bradley BA (2010b) Site-specific and spatially distributed ground-motion prediction of acceleration spectrum intensity. *B Seismol Soc Am* 100(2):792–801. doi: 10.1785/0120090157
- Bradley BA (2011a) Empirical equations for the prediction of displacement spectrum intensity and its correlation with other intensity measures. *Soil Dyn Earthq Eng* 31(8):1182–1191. doi: 10.1016/j.soildyn.2011.04.007
- Bradley BA (2011b) Empirical correlation of PGA, spectral accelerations and spectrum intensities from active shallow crustal earthquakes. *Earthq Eng Struct D* 40(15):1707–1721. doi: 10.1002/eqe.1110
- Bradley BA (2011c) Correlation of significant duration with amplitude and cumulative intensity measures and its use in ground motion selection. *J Earthq Eng* 15(6):809–832. doi: 10.1080/13632469.2011.557140
- Bradley BA (2012a) A ground motion selection algorithm based on the generalized conditional intensity measure approach. *Soil Dyn Earthq Eng* 40(1):48–61. doi: 10.1016/j.soildyn.2012.04.007
- Bradley BA (2012b) Empirical correlations between peak ground velocity and spectrum-based intensity measures. *Earthq Spectra* 28(1):17–35. doi: 10.1193/1.3675582
- Bradley BA (2012c) Empirical correlations between cumulative absolute velocity and amplitude-based ground motion intensity measures. *Earthq Spectra* 28(1):37–54. doi: 10.1193/1.3675580
- Bradley BA (2012d) The seismic demand hazard and importance of the conditioning intensity measure. *Earthq Eng Struct D* 2012; 41(11):1417–1437. DOI: 10.1002/eqe.2221
- Caltrans (2013) Caltrans seismic design criteria. California Department of Transportation, Sacramento, CA, Version 1.7.
- Campbell KW, Bozorgnia Y (2010) A ground motion prediction equation for the horizontal component of cumulative absolute velocity (CAV) based on the PEER-NGA strong motion database. *Earthq Spectra* 26(3):635–650
- CEN (2005) MSZ EN 1337-3:2005. Structural bearings. Part 3: Elastomeric bearings
- CEN (2008a) MSZ EN 1998-1 Eurocode 8: Design of structures for earthquake resistance. Part 1: General rules, seismic actions and rules for buildings.
- CEN (2008b) MSZ EN 1998-1 Eurocode 8: Design of structures for earthquake resistance. Part 2: Bridges.
- CEN (2009a) MSZ EN 1998-5. Eurocode 8: Design of structures for earthquake resistance. Part 5: Foundations, retaining structures and geotechnical aspects
- CEN (2009b) MSZ EN 1992-2 Eurocode 2: Design of concrete structures. Part 2: Concrete bridges. Design and detailing rules.
- CEN (2010) MSZ EN 15129. Anti-seismic devices.
- CEN (2011a) MSZ EN 1998-3 Eurocode 8: Design of structures for earthquake resistance. Part 3: Assessment and retrofitting of buildings.
- CEN (2011b) MSZ EN 1990-1 Eurocode 0: Basis of structural design.
- CEN (2015) MSZ EN 1997-1:2004/A1:2015. Eurocode 7: Geotechnical design. Part 1: General rules.
- Chandramohan R, Baker JW, Deierlein GG (2015) Quantifying the influence of ground motion duration on structural collapse capacity using spectrally equivalent records. *Earthq Spectra*. (in press).
- Choi E, DesRoches R, Nielson B (2004) Seismic fragility of typical bridges in moderate seismic zones. *Eng Struct* 26(2):187–199. doi: 10.1016/j.engstruct.2003.09.006

- Cornell CA (1968) Engineering seismic risk analysis. *B Seismol Soc Am* 58(5): 1583-1606
- Dicleli M, Mansour MY (2003) Seismic retrofitting of highway bridges in Illinois using friction pendulum seismic isolation bearings and modeling procedures. *Eng Struct* 25(9):1139-1156 doi: 10.1016/S0141-0296(03)00062-2
- Dicleli M, Buddaram S (2007) Comprehensive evaluation of equivalent linear analysis method for seismic-isolated structures represented by SDOF systems. *Eng Struct* 29(1):1653–1663. doi: 10.1016/j.engstruct.2006.09.013
- Du W, Wang G (2012) A simple ground-motion prediction model for cumulative absolute velocity and model validation. *Earthq Eng Struct D* 42(8):1189–1202. doi: 10.1002/eqe.2266
- Duncan MJ, Mokwa RL (2001) Passive earth pressure: theories and tests. *J Geotech Geoenviron* 127(3):248-257. doi: 10.1061/(ASCE)1090-0241(2001)127:3(248)
- Dutta A (1999) On energy based seismic analysis and design of highway bridges. PhD thesis, State University of New York at Buffalo
- EFEHR (2015) European Facility for Earthquake Hazard and Risk website (<http://www.efehr.org/>).
- Elnashai AS, Di Sarno L (2008) Fundamentals of earthquake engineering. Wiley and Sons, UK.
- Ellingwood BR (1998) Issues related to structural aging in probabilistic risk assessment of nuclear power plants. *Reliab Eng Syst Safe* 62(3):171-183. doi: 10.1016/S0951-8320(98)00018-0
- Eröz M, DesRoches R (2008) Bridge seismic response as a function of the Friction Pendulum System (FPS) modeling assumptions, *Eng Struct* 30(11):3204-3212. doi: 10.1016/j.engstruct.2008.04.032
- ÉTK (1978) MI-04.133-78: Technical guideline for seismic design (in Hungarian). Építésügyi Tájékoztatási Központ, Budapest
- ÉVM (1972) Technical specification. ME 95-72 (in Hungarian). Építésügyi és Városfejlesztési Minisztérium, Budapest
- Fennema J, Laman J, Linzell D (2005) Predicted and Measured Response of an Integral Abutment Bridge. *J Bridge Eng* 10(6):666-677. doi: 10.1061/(ASCE)1084-0702(2005)10:6(666)
- FHWA (2002) National Bridge Inventory Data
- FIB (2008) Bulletin 43: Structural connections for precast concrete buildings. International Federation for Structural Concrete.
- Gasparini DA, Vanmarcke EH (1976) Simulated earthquakes compatible with prescribed response spectra. Massachusetts Institute of Technology, Publication No. R76-4, Cambridge, Massachusetts
- Ghosh G, Singh Y, Thakkar SK (2011) Seismic response of a continuous bridge with bearing protection devices. *Eng Struct* 33(4):1149-1156. doi: 10.1016/j.engstruct.2010.12.033
- Goel RK, Chopra AK (1995) Evaluation of abutment stiffness in a short bridge overcrossing during strong ground shaking. Proc. of the Fourth US Conference on Lifeline Earthquake Engineering, Technical Council on Lifeline Earthquake Engineering Monograph No. 6, August.
- Goldberg DE (1989) Genetic algorithm in search, optimization, and machine learning. Boston: Kluwer Academic Publishers.
- Gutenberg B, Richter CF (1944) Frequency of earthquakes in California. *B Seismol Soc Am* 34(4):185-188

- Haque MN, Bhuiyan AR, Alam MJ (2010) Seismic response analysis of base isolated highway bridge: Effectiveness of using laminated rubber bearings. IABSE-JSCE Joint Conference on Advances in Bridge Engineering-II, August 8-10, 2010, Dhaka, Bangladesh
- HSI (1986a) MSZ-15021-1. Design of load bearing structures of buildings. Design loads for buildings. Hungarian Standards Institution.
- HSI (1986b) MSZ-07-3701. Statical calculation of road bridges. Hungarian Standards Institution.
- HSI (1987) MSZ-15002. Mechanic design of the foundation of buildings. Hungarian Standards Institution.
- HSI (1990) MSZ-07-2306. Design of railway bridges. Hungarian Standards Institution.
- HSI (1998a) MSZ ENV 1998-1-1:1998. Eurocode 8:Design provisions for earthquake resistance of structures. Part 1.1: General rules. Seismic actions and general requirements for structures. Hungarian Standards Institution.
- HSI (2008) National Annex to MSZ EN 1998-1:2008. Hungarian Standards Institute. (in Hungarian).
- Horváth F (1988) Neotectonic behavior of the Alpine-Mediterranean region. The Pannonian Basin – A study in basin evolution, AAPG Memoir 45:49-51
- HTA (2015) Integrated Bridge Database. Hungarian Transport Administration
- Hwang JS, Sheng LH, Gates JH (1994) Practical analysis of bridges on isolation bearings with bi-linear hysteresis characteristics. *Earthq Spectra* 10(4):705-727. doi: 10.1193/1.1585794
- Hwang JS, Chiou JM, Sheng LH, Gates JH (1996) A refined model for base-isolated bridges with bi-linear hysteretic bearings. *Earthq Spectra* 12(2):245-273. doi: 10.1193/1.1585879
- Hwang H, Jernigan JB, Lin Y (2000) Evaluation of seismic damage to Memphis bridges and highway systems. *J Bridge Eng* 5(4):322–330. doi: 10.1061/(ASCE)1084-0702(2000)5:4(322)
- Iwan WD, Gates NC (1979) The effective period and damping of a class of hysteretic structures. *Earthq Eng Struct D* 7(3):199-211. doi: 10.1002/eqe.4290070302
- Jalayer F, Cornell CA (2009) Alternative nonlinear demand estimation methods for probability-based seismic assessments. *Earthq Eng Struct D* 38(8):951-972. doi: 10.1002/eqe.876
- Jara M, Jara JM, Olmos BA, Casas JR (2012) Improved procedure for equivalent linearization of bridges supported on hysteretic isolators. *Eng Struct* 35(1):99-106. doi: 10.1016/j.engstruct.2011.10.028
- Jayaram N, Baker JW (2008) Statistical tests of the joint distribution of spectral acceleration values. *B Seismol Soc Am*, 98(5):2231–2243. doi: 10.1785/0120070208
- Jayaram N, Lin T, Baker JW (2011) A computationally efficient ground-motion selection algorithm for matching a target response spectrum mean and variance. *Earthq Spectra* 2011;27(3):797–815.
- JCSS (2001) Probabilistic model code – Part 1: Basis of design. Joint Committee on Structural Safety
- Jernigan JB, Hwang H (2002) Development of Bridge Fragility Curves. 7th US National Conference on Earthquake Engineering, Boston, Mass. EERI
- JPWRI (1992) Manual for Menshin design of highway bridges. Public Works Research Institute, Japan
- Kempton JJ, Stewart JP (2006) Prediction equations for significant duration of earthquake ground motions considering site and near-source effects. *Earthq Spectra* 22(4):985-1013. doi: 10.1193/1.2358175
- Kent DC, Park R (1971) Flexural members with confined concrete. *J Struct Div ASCE* 97(7):1969-1990

- Kibboua A, Bechtoula H, Mehani Y, Naili M (2014) Vulnerability assessment of reinforced concrete bridge structures in Algiers using scenario earthquakes. *B Earthq Eng* 12(2):807–827. doi: 10.1007/s10518-013-9523-7.
- Liu T, Zordan T, Briseghella B, Zhang Q (2014) An improved equivalent linear model of seismic isolation system with bilinear behavior. *Eng Struct* 61(1):113-126. doi: 10.1016/j.engstruct.2014.01.013
- Liu T, Zhang Q (2016) AP/VP specific equivalent viscous damping model for base-isolated buildings characterized by SDOF systems. *Eng Struct* 111(1):36-47. doi:10.1016/j.engstruct.2015.12.024
- Lowes LN, Mitra N, Altoontash A (2003) A beam-column joint model for simulating the earthquake response of reinforced concrete frames. PEER-2003/10 Pacific Earthquake Engineering Research Center, University of California, Berkeley, CA
- Maroney BH (1995) Large scale bridge abutment tests to determine stiffness and ultimate strength under seismic loading. PhD thesis, Dept. of Civil Engineering, University of California Davis, CA.
- McKenna F, Scott MH, Fenves GL (2010) Nonlinear Finite-Element Analysis Software Architecture Using Object Composition. *J Comput Civil Eng* 24(1):97-105. doi: 10.1061/(ASCE)CP.1943-5487.0000002
- Moschonas IF, Kappos AJ, Panetsos P, Papadopoulos V, Makarios T, Thanopoulos P (2009) Seismic fragility curves for Greek bridges: methodology and case studies. *B Earthq Eng* 7(2):439-468. doi: 10.1007/s10518-008-9077-2
- Naito CJ, Moehle JP, Mosalam KM (2001) Experimental and computation evaluation of reinforced concrete bridge beam-column connections for seismic performance. PEERC Report 2001;08:1–232.
- NIBS (National Institute of Building Sciences) (1999) Earthquake loss estimation methodology: HAZUS99 (SR2). Technical manual, Federal Emergency Management Agency, Washington, DC
- Nielson BG (2005) Analytical fragility curves for highway bridges in moderate seismic zones. PhD dissertation, School of Civil and Environmental Engineering, Georgia Institute of Technology.
- Nielson BG, DesRoches R (2006) Influence of modeling assumptions on the seismic response of multi-span simply supported steel girder bridges in moderate seismic zones. *Eng Struct* 28(8):1083-1092. doi: 10.1016/j.engstruct.2005.12.014
- Nowak AS, Collins KR (2000) Reliability of structures. USA: The McGraw-Hill Companies, Inc.
- Padgett JE (2007) Seismic vulnerability assessment of retrofitted bridges using probabilistic methods, PhD Dissertation, 2007, School of Civil and Environmental Engineering - Georgia Institute of Technology
- Padgett JE, DesRoches R (2008) Three-dimensional nonlinear seismic performance evaluation of retrofit measures for typical steel girder bridges. *Eng Struct* 30(7):1869-1878. doi: 10.1016/j.engstruct.2007.12.011
- Papageorgiou A, Halldorsson B, Dong G (2000) Target acceleration spectra compatible time histories. University of Buffalo, Dept. of Civil, Structural and Environmental Engineering, NY
- PEER (2015) NGA-West2 database: Shallow crustal earthquakes in active tectonic regimes. Pacific Earthquake Engineering Research Center, University of California, Berkeley, CA.
- Priestley MJN, Seible F, Calvi GM (1996) Seismic Design and Retrofit of Bridges, John Wiley & Sons, Inc., New York, NY
- Psycharis NI, Mouzakis PH (2012) Shear resistance of pinned connections of precast members to monotonic and cyclic loading. *Eng Struct* 41(1):413–427. doi: 10.1016/j.engstruct.2012.03.051

- Rezaeian S, Der Kiureghian A (2010) Stochastic modeling and simulation of ground motions for performance-based earthquake engineering. PEER Report 2010/02, Pacific Earthquake Engineering Research Center, University of California, Berkeley, CA
- Romstad K, Ketter B, Maroney BH (1995) Large scale bridge abutment tests to determine stiffness and ultimate strength under seismic loading. PhD thesis, Dept. of Civil Engineering, University of California Davis, CA.
- Saadeghvaziri MA, Yazdani-Motlagh AR, Rashidi S (2000) Effects of soil–structure interaction on longitudinal seismic response of MSSS bridges. *Soil Dyn Earthq Eng* 20(1):231-242. doi: 10.1016/S0267-7261(00)00056-7
- Scott BD, Park R, Priestley MJN (1982) Stress-strain behavior of concrete confined by overlapping hoops at low and high strain rates. *ACI Struct J* 79(1):13-27.
- Shamsabadi A, Rollins K, Kapuskar M (2007) Nonlinear soil–abutment–bridge structure interaction for seismic performance-based design. *J Geotech Geoenviron* 133(6):707-720. doi: 10.1061/(ASCE)1090-0241(2007)133:6(707)
- Szeidovitz Gy (1990) Determination of epicentral intensity and depth of historical earthquakes in the Komárom Mór area (in Hungarian), p. 139, MTA, Budapest, Hungary
- Szepesházi R (2011) Pile design according to EC7. PhD Theses (in Hungarian), University of Miskolc, Hungary
- Taucer FF, Spacone E, Filippou FC (1991) A fiber beam-column element for seismic response analysis of reinforced concrete structures. Report No. UCB/EERC- 91/17, Earthquake Engineering Research Center, College of Engineering, University of California, Berkeley, CA
- Tavares DH, Padgett JE, Paultre P (2012) Fragility curves of typical as-built highway bridges in eastern Canada. *Eng Struct* 40(1):107-118. doi: 10.1016/j.engstruct.2012.02.019
- Timosidis D, Megalooikonomou KG, Pantazopoulou SJ (2015) Monolithic reinforced concrete bridge joints under cyclic excitation. *Eng Struct* 101(1):477–493. doi: 10.1016/j.engstruct.2015.08.004
- Timosidis D, Pantazopoulou SJ (2009) Analytical modeling of monolithic joints in concrete bridges. *B Earthq Eng* 7(2):411–438. doi: 10.1007/s10518-008-9102-5
- Tóth L, Mónus P, Zsíros T, Kiszely M (2004) Micro-seismic monitoring of seismoactive areas in Hungary. *Studi Geologici Camerti, Special Issue: Proceedings of the workshop COST Action 625 "Active faults: analysis, processes and monitoring"*
- Tóth L, Győri E, Mónus P and Zsíros T (2006) Seismic hazard in the Pannonian Region. *The Adria Microplate: GPS Geodesy, Tectonics, and Hazards*, Springer Verlag, NATO ARW Series 61(1):369-84. doi: 10.1007/1-4020-4235-3\_25
- ÚT (2004) *Útügyi Műszaki Előírás ÚT 2-3.401 Közúti hidak tervezése, Általános előírások* (in Hungarian). Magyar Útügyi Társaság
- Vamvatsikos D, Cornell CA (2002) Incremental Dynamic Analysis. *Earthq Eng Struct D* 31(3):491–514. doi: 10.1002/eqe.141
- Vanmarcke EH, Fenton GA, Heredia-Zavoni E (1990) SIMQKE-II: conditioned earthquake ground motion simulator: user's manual, version 2.1, Princeton University. 25 pages
- Vigh A, Kollár L (2006) Approximate analysis of bridges for the routing and permitting procedures of overweight vehicle. *J Bridge Eng* 11(3):282-292. doi: 10.1061/(ASCE)1084-0702(2006)11:3(282)

- Vigh LG, Dunai L, Kollár L (2006) Numerical and design considerations of earthquake resistant design of two Danube bridges. 1st European Conference on Earthq Eng and Seismology, Switzerland, Paper 1420.
- Vigh LG, Rózsás Á, Zsarnóczay Á, Balogh T, Morais EC, Simon J (2016) Reliability analysis of structures subjected to extreme loads (in Hungarian). Scientific Publications of BME Department of Structural Engineering. pp. 119-128, Budapest, Hungary
- Wang G (2011) A ground motion selection and modification method capturing response spectrum characteristics and variability of scenario earthquakes. *Soil Dyn Earthq Eng* 2011;31(4):611–25
- Wei Z, Yuan W, Cheung P, Cao X, Rong Z (2011) Seismic performance of continuous girder bridges using cable-sliding friction aseismic bearing. *Procedia Engineering* 14(1):914-921. doi: 10.1016/j.proeng.2011.07.115
- Wilson JC (1988) Stiffness of non-skew monolithic bridge abutments for seismic analysis. *Earthq Eng Struct D* 16(6):867- 883. doi: 10.1002/eqe.4290160608
- Wilson JC, Tan BS (1990) Bridge abutments: formulation of simple model for earthquake response analysis. *J Eng Mech ASCE* 116(8):1828-1837. doi: 10.1061/(ASCE)0733-9399(1990)116:8(1828)
- Wilson P, Elgamal A (2010) Large scale passive earth pressure load-displacement tests and numerical simulation. *J Geotech Geoenviron* 136(12):1634-1643. doi: 10.1061/(ASCE)GT.1943-5606.0000386
- Wolf JP (1985) *Dynamic soil-structure interaction*. Prentice-Hall, Inc., New Jersey
- Zhang J, Makris N (2002) Kinematic response functions and dynamic stiffnesses of bridge embankments. *Earthq Eng Struct Dyn* 31:1933–1966 doi: 10.1002/eqe.196
- Zhu P, Abe M, Fujino Y (2002) Modeling three dimensional non-linear seismic performance of elevated bridges with emphasis on pounding of girders. *Earthq Eng Struct D* 31(11):1891-1913. doi: 10.1002/eqe.194
- Zordan T, Liu T, Briseghella B, Zhang Q (2014) Improved equivalent viscous damping model for base-isolated structures with lead rubber bearings. *Eng Struct* 75(1):340-352. doi: 10.1016/j.engstruct.2014.05.044
- Zsarnóczay Á (2010) Seismic performance analysis of common bridge types in Hungary (in Hungarian). M.Sc. thesis, Department of Structural Engineering, Budapest University of Technology and Economics, Budapest
- Zsarnóczay Á, Vigh LG, Kollár L (2014) Seismic Performance of Conventional Girder Bridges in Moderate Seismic Regions. *J Bridge Eng* 19(5), 9 p. Paper 04014001. doi: 10.1061/(ASCE)BE.1943-5592.0000536
- Zsíros T (2000) Seismicity and seismic hazard of the Pannonian Basin: Hungarian earthquake catalogue (456-1995) (in Hungarian). MTA FK GGKI, Budapest, p. 495. ISBN 9638381159

*Appendix A: Ground motion prediction and correlation equations,  
calculation of intensity measures*

**A1. Ground motion prediction equations and correlation equations**

Table A1 presents the ground motion prediction equations (GMPE) and correlation equations applied for the generalized conditioned intensity measure (GCIM) record selection procedure. All empirical formulae were derived using shallow crustal earthquake data. Therefore they are assumed to be valid for Hungarian circumstances.

Ground motion prediction equations:

- AB10 (Akkar and Bommer 2010);
- BR09 (Bradley et al. 2009);
- BR10b (Bradley 2010b);
- BR11a (Bradley 2011a);
- DW12 (Du and Wang 2012);
- KS06 (Kempton and Stewart 2006).

Correlations:

- BJ08 (Baker and Jayaram 2008);
- BR11b (Bradley 2011b);
- BR11c (Bradley 2011c);
- BR12b (Bradley 2012b);
- BR12c (Bradley 2012c);

Table A1 References to the applied ground motion prediction equations and correlation equations.

GMPE	IM	Sa	PGA	PGV	ASI	VSI	DSI	CAV	D <sub>S75</sub>	D <sub>S95</sub>
AB2010	Sa	BJ08	BR11b	BR12b	BR11b	BR11b	BR11a	BR12c	BR11c	BR11c
AB2010	PGA	-	-	BR12b	BR11b	BR11b	BR11a	BR12c	BR11c	BR11c
AB2010	PGV	-	-	-	BR12b	BR12b	BR11a	BR12c	BR11c	BR11c
BR10b	ASI	-	-	-	-	BR11b	BR11a	BR12c	BR11c	BR11c
BR09	SI	-	-	-	-	-	BR11a	BR12c	BR11c	BR11c
BR11a	DSI	-	symmetric	-	-	-	-	BR12c	BR11c	BR11c
DW12	CAV	-	-	-	-	-	-	-	BR11c	BR11c
KS06	D <sub>S75</sub>	-	-	-	-	-	-	-	-	BR11c
KS06	D <sub>S95</sub>	-	-	-	-	-	-	-	-	-

Sa: spectral acceleration; PGA: peak ground acceleration; PGV: peak ground velocity; ASI: acceleration spectrum intensity; VSI – velocity spectrum intensity; DSI: displacement spectrum intensity; CAV: cumulative absolute velocity; D<sub>S75</sub> and D<sub>S95</sub>: significant duration determined between 5-75% (D<sub>S75</sub>) and 5-95% (D<sub>S95</sub>) of the cumulative Arias intensity (AI).

## A2. Calculation of ground motion intensity measures

The calculation of PGA, PGV, Sa, ASI, VSI, DSI, CAV, AI,  $D_{s575}$  and  $D_{s595}$  of a ground motion (GM) is presented in the following equations.

PGA is the maximum absolute value of the acceleration time series  $a(t)$  of the GM:

$$PGA = \max(|a(t)|). \quad (A.1)$$

PGV is the maximum absolute value of the velocity time series  $v(t)$  of the GM:

$$PGV = \max(|v(t)|). \quad (A.2)$$

Sa is the spectral acceleration (AS) value calculated with 5% damping at vibration period T:

$$Sa(T) = AS(T, 0.05). \quad (A.3)$$

ASI, VSI and DSI are obtained by integrating the acceleration (AS), velocity (VS) and displacement (DS) spectra with 5% damping in the range of 0.1-0.5s, 0.1-2.5s and 2.0-5.0s vibration periods, respectively:

$$ASI = \int_{0.1s}^{0.5s} AS(T, 0.05)dT, \quad (A.4)$$

$$VSI = \int_{0.1s}^{2.5s} VS(T, 0.05)dT, \quad (A.5)$$

$$DSI = \int_{2.0s}^{5.0s} DS(T, 0.05)dT. \quad (A.6)$$

CAV is defined as the integral of the absolute value of the acceleration time series:

$$CAV = \int_0^{t^{max}} |a(t)|dt. \quad (A.7)$$

The definition of the Arias intensity is as follows:

$$AI = \frac{\pi}{2g} \int_0^{t^{max}} a(t)^2 dt. \quad (A.8)$$

Significant duration is defined as:

$$D_{sxy} = t_y - t_x, \quad (A.9)$$

$$x, y = \frac{100\%}{AI} \int_0^{t^{x,y}} a(t)^2 dt, \quad (A.10)$$

where  $t_x$  and  $t_y$  the times at which x and y percent of the total Arias intensity occur. The values for  $D_{s575}$  and  $D_{s595}$  are  $x, y = 5\%, 75\%$  and  $x, y = 5\%, 95\%$ , respectively.

## *Appendix B: Extension of the existing road bridge database*

### **B.1 Three-phase data collection**

Fig. B1 shows the original, while Fig. B2 illustrates the extended structure of the existing road bridge database. A three-phase extension is worked out and presented in the following sections.

#### **Extension Phase 1 (EP-1)**

In EP-1, the most important data that should be collected is the type (single or multi column, wall-type etc.) and height of the piers. The existing database lacks this parameter, it only stores the vertical underclearance for bridges over roads. For bridges crossing other obstacles such as rivers or valleys, not even this underclearance is defined. The seismic response is highly influenced by the type and dimensions of the abutment in case of shorter bridges, or bridges with integrate monolithic joints (e.g. precast multi-girder bridges on highways). Therefore minimal description of the abutments is necessary. In this phase, revision of existing and uploading of missing data should be performed (e.g. description of expansion joints, bearing types, foundation types etc.). At the end of EP-1 the following bridges can be analyzed: straight bridges with one or more spans and one girder, where cross-sections are only assumed based on simplified calculations or observations on typical bridge plans. With EP-1 KL-1 can be achieved which is sufficient for bridge classification and the analysis of typical bridge types.

#### **Extension Phase 2 (EP-2)**

In accordance with KL-2, in this phase the global geometry is refined. Bridges with multiple superstructures are included; the important parameter here is the distance between them. The skew angle and the alignment of the bearings can be modeled. Since the cross-section of the structural elements should be defined in this level, different parameters depending on the cross-section type may be needed. For instance, two constants are required to define a rectangular, one for a circular and multiple (top flange thickness and width, web thickness and height etc.) for a steel box cross-section. The bearing properties and the size of existing expansion joints should also be input for the database. To increase the accuracy of the model, the foundation type and different attributes are required for different foundations such as the size of the shallow foundation or number, length and layout of piles for pile foundation. In order to determine proper seismic loads, soil classification should be carried out for the site of the bridge. The material properties should be obtained from plans to achieve KL-2. After

EP-2, sufficient data is provided to carry out a regional seismic performance evaluation based on individual analysis of bridges. This way, for each bridge an individual fragility curve and seismic risk can be calculated, and reliable comparison can be made between bridges in the inventory.

### **Extension Phase 3 (EP-3)**

EP-3 is about including bridges with curvature in plan and describing the structural elements more precisely. For the former point, the exact locations of the supports and the curvature of the superstructure between them have to be defined. The structural elements are divided into segments following any important change in cross-section. The bearing or monolithic joint properties should be specified in a way to obtain reliable force-deformation relationship (material properties, sizes, number of steel plates in an elastomeric bearing etc.). Both material properties of the structural elements and the soil should be defined with in-situ tests.

### **B.2 Extended structure of the database**

The extended structure is illustrated with the entity relationships diagram (Fig. B2), where existing data is marked with black, while the first, second and third extensions are marked with green, blue and red. Table names, the primary keys and foreign keys are indicated with bold, underlined and italic fonts, respectively. On the line representing the relationship between two tables the degree of relationship (cardinality) is also shown (e.g. a bridge has at least two supports and maximum n supports). In cases when multiple alternatives can be chosen depending on the actual arrangement of the bridge (e.g. cross-section type of the superstructure or the pier) only one example is given. Certainly, introducing new items (e.g. new cross-sections such as steel box section with new constants) requires the definition of new tables, but the relationship structure remains the same.

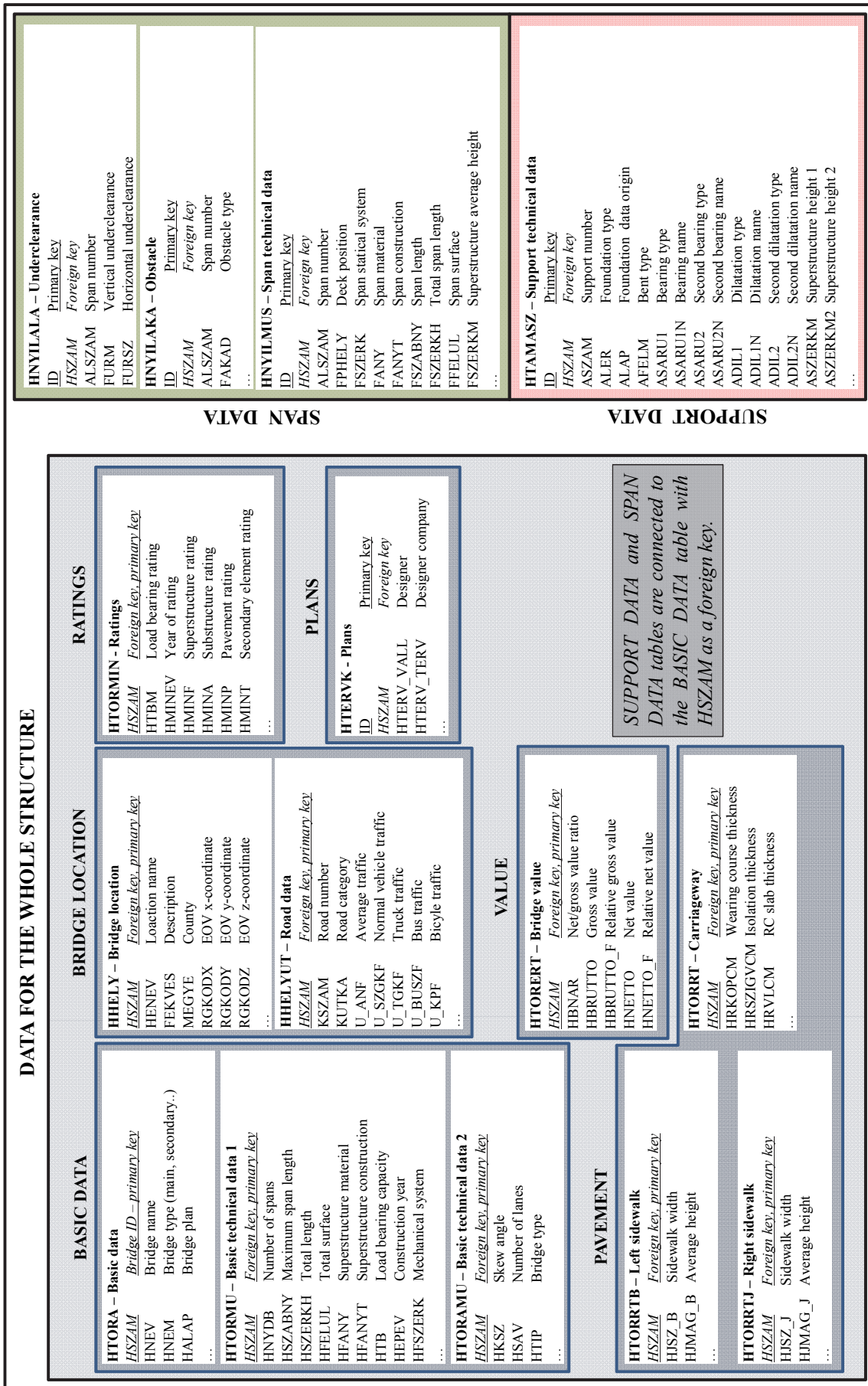


Fig. B1 Structure of the existing bridge database.

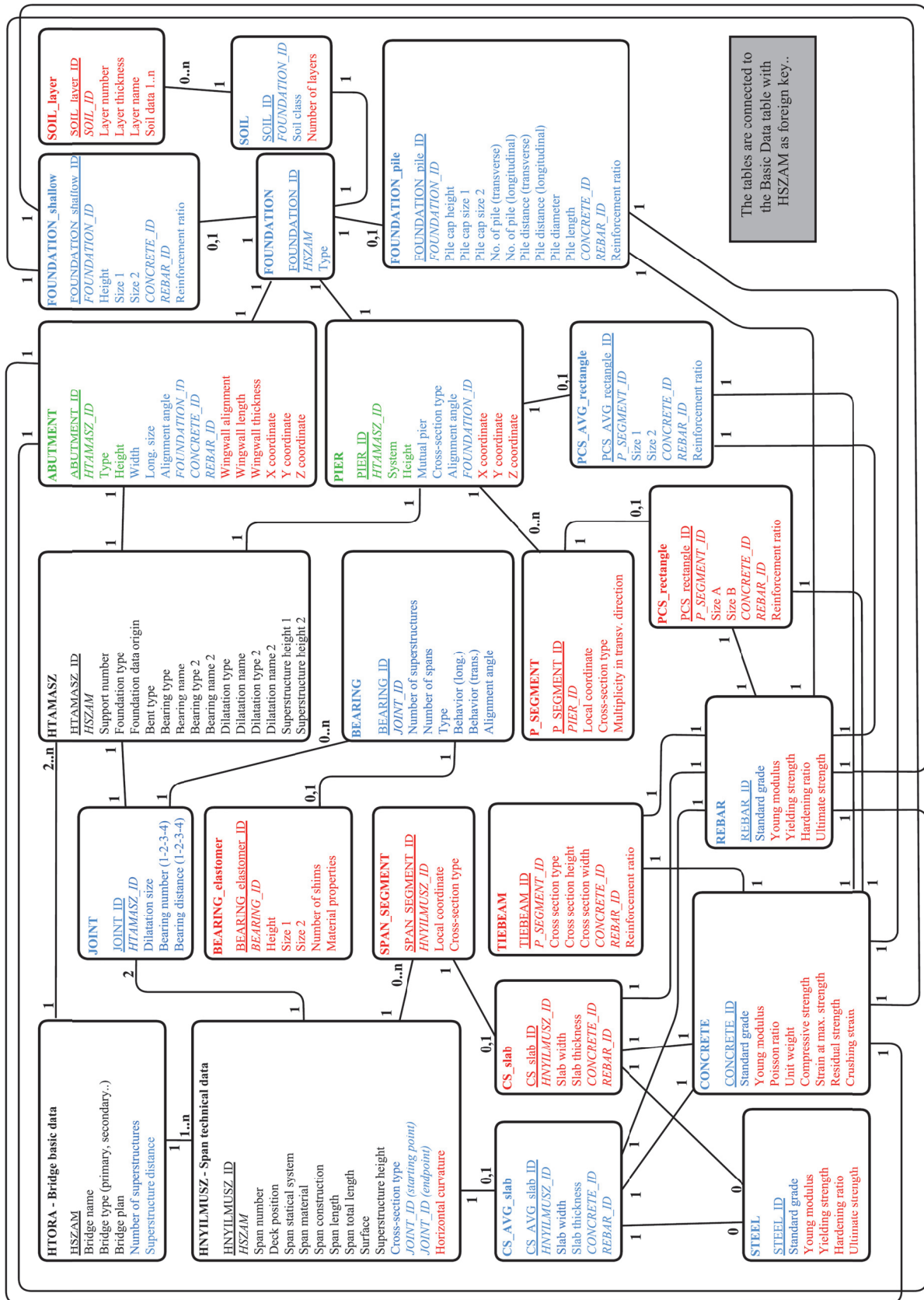


Fig. B2 Three-phase extension of the existing database (black). Phase 1: green; phase 2: blue; phase 3: red.

## *Appendix C: Fundamental periods of the examined bridges*

In the following tables, fundamental periods (in seconds) are presented for the dominant vibration mode in the longitudinal (X), transverse (Y) and vertical (Z) directions, respectively. Since only slight difference is observed in case of PMG-I and SLAB bridges for different widths, only the results for 14 m deck width are presented.

Table C1 Fundamental periods [s] of the portfolio bridges.

PORTFOLIO BRIDGES														
Configuration	X	Y	Z	Configuration	X	Y	Z	Configuration	X	Y	Z			
BR	1	0.34	0.15	0.27	BR	11	0.60	0.89	0.48	BR	21	1.24	0.33	0.68
	2	0.27	0.13	0.23		12	1.04	0.83	0.14		22	0.57	0.13	0.40
	3	0.31	0.27	0.27		13	0.25	0.27	0.19		23	0.24	0.36	0.37
	4	0.20	0.23	0.26		14	0.21	0.18	0.13		24	0.56	0.27	0.41
	5	0.17	0.21	0.12		15	0.23	0.27	0.16		25	1.31	0.52	0.32
	6	0.20	0.23	0.13		16	0.25	0.33	0.12		26	0.80	0.20	0.57
	7	0.28	0.36	0.22		17	2.18	0.86	0.27		27	0.69	0.21	0.59
	8	0.21	0.25	0.14		18	2.39	0.71	0.30		28	1.69	0.62	0.69
	9	0.39	0.32	0.49		19	3.93	0.95	0.24		29	1.85	0.79	1.10
	10	0.67	0.66	0.24		20	0.74	0.20	0.48		30	2.59	0.76	0.99

Table C2 Fundamental periods [s] of single span PMG-I and SLAB bridges.

PMG-I - W14					SLAB - W14				
Configuration	X	Y	Z	Configuration	X	Y	Z		
SI P00 L05	0.07	0.06	0.04	SI P00 L05	0.07	0.06	0.07		
L10	0.10	0.08	0.10	L10	0.12	0.08	0.12		
L15	0.11	0.09	0.17	L15	0.17	0.11	0.17		
L20	0.13	0.11	0.25	L20	0.22	0.13	0.22		
L25	0.15	0.12	0.34	L25	0.28	0.16	0.28		
L30	0.17	0.14	0.45	L30	0.33	0.19	0.33		

Table C3 Fundamental periods [s] of multi-span PMG-I bridges.

PMG-I - W14																	
Configuration			X	Y	Z	Configuration			X	Y	Z	Configuration			X	Y	Z
S2	P02	L05	0.07	0.06	0.03	S3	P02	L05	0.07	0.06	0.03	S4	P02	L05	0.07	0.06	0.02
		L10	0.10	0.08	0.06			L10	0.10	0.08	0.07			L10	0.11	0.08	0.06
		L15	0.16	0.10	0.11			L15	0.13	0.10	0.13			L15	0.14	0.11	0.11
		L20	0.24	0.12	0.16			L20	0.16	0.12	0.19			L20	0.17	0.12	0.16
		L25	0.33	0.14	0.22			L25	0.18	0.13	0.26			L25	0.21	0.14	0.21
		L30	0.20	0.15	0.29			L30	0.23	0.15	0.34			L30	0.22	0.16	0.28
P04	L05	L05	0.08	0.07	0.03	P04	L05	L05	0.09	0.07	0.03	P04	L05	L05	0.10	0.08	0.03
		L10	0.12	0.10	0.07			L10	0.13	0.10	0.08			L10	0.14	0.11	0.06
		L15	0.17	0.12	0.11			L15	0.16	0.13	0.13			L15	0.18	0.15	0.11
		L20	0.25	0.14	0.18			L20	0.20	0.16	0.20			L20	0.22	0.18	0.16
		L25	0.34	0.17	0.22			L25	0.23	0.19	0.27			L25	0.30	0.22	0.22
		L30	0.45	0.19	0.29			L30	0.26	0.22	0.36			L30	0.39	0.25	0.29
P06	L05	L05	0.08	0.08	0.03	P06	L05	L05	0.09	0.08	0.03	P06	L05	L05	0.10	0.09	0.03
		L10	0.12	0.10	0.07			L10	0.13	0.11	0.08			L10	0.15	0.13	0.07
		L15	0.17	0.13	0.11			L15	0.17	0.14	0.14			L15	0.20	0.17	0.11
		L20	0.25	0.15	0.18			L20	0.20	0.18	0.20			L20	0.24	0.23	0.16
		L25	0.35	0.18	0.22			L25	0.27	0.22	0.27			L25	0.30	0.29	0.22
		L30	0.45	0.22	0.29			L30	0.27	0.27	0.36			L30	0.39	0.35	0.29
P08	L05	L05	0.09	0.08	0.03	P08	L05	L05	0.10	0.09	0.03	P08	L05	L05	0.11	0.10	0.03
		L10	0.12	0.10	0.07			L10	0.13	0.12	0.08			L10	0.16	0.14	0.07
		L15	0.18	0.13	0.11			L15	0.17	0.15	0.14			L15	0.20	0.19	0.11
		L20	0.26	0.16	0.18			L20	0.21	0.19	0.20			L20	0.24	0.26	0.16
		L25	0.35	0.19	0.22			L25	0.27	0.24	0.27			L25	0.30	0.34	0.22
		L30	0.46	0.23	0.29			L30	0.27	0.30	0.36			L30	0.40	0.43	0.29
P10	L05	L05	0.09	0.08	0.03	P10	L05	L05	0.10	0.09	0.03	P10	L05	L05	0.11	0.10	0.03
		L10	0.12	0.10	0.07			L10	0.14	0.12	0.08			L10	0.16	0.14	0.07
		L15	0.18	0.13	0.11			L15	0.17	0.15	0.14			L15	0.20	0.20	0.11
		L20	0.26	0.16	0.18			L20	0.21	0.20	0.20			L20	0.25	0.28	0.16
		L25	0.35	0.19	0.23			L25	0.27	0.25	0.27			L25	0.30	0.38	0.22
		L30	0.46	0.24	0.29			L30	0.28	0.32	0.36			L30	0.40	0.48	0.29



## Appendix D: MAPGA values for PMG-I and SLAB bridges

The following tables illustrate maximum acceptable PGA values based on the parametric analysis for PMG-I and SLAB bridges.

Notation: SS1, SS2 – superstructure failure for sagging and hogging bending moments, respectively; B1, B2 – monolithic joint failure at the abutment and pier; F1, F2 – Pile compressive failure at the abutment and pier; SSI – backfill soil failure; AB – abutment failure; PM, PV – pier flexural and shear failure. SL – span length [m]; PH – pier height [m].

Table D1 MAPGA values for single span PMG-I bridges.

3.6	3.3	3.2	3.2	3.2	3.1	3.7	3.2	3.2	3.2	3.2	3.2	3.7	3.1	3.2	3.2	3.2	3.2	0	SS1
0.5	0.8	0.8	0.9	1.0	1.2	0.5	0.7	0.7	0.8	0.9	1.0	0.4	0.6	0.7	0.8	0.9	1.0	0	SS2
6.3	2.2	1.1	0.7	0.4	0.3	6.7	2.4	1.2	0.7	0.5	0.4	6.7	2.4	1.2	0.7	0.5	0.4	0	B1
14.6	8.6	5.6	4.1	3.1	2.4	13.6	8.2	5.5	4.0	3.1	2.4	13.4	8.0	5.5	4.0	3.1	2.4	0	F1
73.6	32.2	16.9	11.0	7.7	5.7	65.3	29.3	15.9	10.5	7.4	5.5	61.7	28.1	15.4	10.2	7.2	5.4	0	SSI
86.7	43.1	25.1	17.8	13.4	10.5	74.6	37.6	22.6	16.0	12.0	9.4	69.5	35.7	21.5	15.2	11.5	9.0	0	AB
5	10	15	20	25	30	5	10	15	20	25	30	5	10	15	20	25	30	SL/PH	COMP
SI - PMG-I																			

Table D2 MAPGA values for single span SLAB bridges.

3.6	3.3	3.1	3.0	2.9	2.8	2.8	3.4	3.2	3.0	3.0	2.9	2.8	3.4	3.2	3.0	3.0	2.9	0	SS1
1.1	1.0	0.8	0.7	0.6	0.5	1.0	0.8	0.6	0.5	0.5	0.4	1.0	0.7	0.5	0.5	0.4	0.4	0	SS2
5.4	1.8	0.9	0.5	0.4	0.3	6.0	1.8	0.9	0.5	0.4	0.3	6.4	1.7	0.8	0.5	0.3	0.2	0	B1
14.1	8.0	4.8	3.3	2.3	1.7	12.2	7.1	4.1	2.7	1.9	1.4	12.0	6.9	3.9	2.6	1.8	1.3	0	F1
64.2	26.4	14.3	9.3	6.5	4.8	60.8	22.7	12.2	7.7	5.3	3.8	69.7	21.0	11.4	7.1	4.8	3.5	0	SSI
82.8	37.9	22.0	14.9	10.7	8.1	87.5	29.8	17.5	11.4	8.0	6.0	67.3	27.2	15.9	10.3	7.2	5.3	0	AB
5	10	15	20	25	30	5	10	15	20	25	30	5	10	15	20	25	30	SL/PH	COMP
SI - SLAB																			

Table D3 MAPGA values for two-span PMG-I bridges.

3.1	2.1	2.7	2.9	2.9	2.9	3.2	2.4	2.7	2.8	2.9	2.9	3.3	2.6	2.7	2.4	2.9	2.9	2	
3.1	2.1	2.7	2.5	2.9	2.9	3.2	2.3	2.6	2.4	2.8	2.9	3.3	2.2	2.5	2.6	2.8	2.9	4	
2.9	2.1	2.5	2.4	2.8	2.9	3.0	2.2	2.4	2.5	2.8	2.9	3.1	2.2	2.3	2.6	2.7	2.9	6	SS1
2.7	2.0	2.5	2.3	2.8	2.9	2.8	2.2	2.3	2.5	2.7	2.9	2.9	2.1	2.3	2.6	2.7	2.9	8	
2.6	2.0	2.4	2.3	2.8	2.9	2.7	2.1	2.3	2.5	2.7	2.9	2.8	2.1	2.2	2.6	2.7	2.9	10	
3.0	3.4	3.4	3.3	3.5	3.7	3.0	3.5	3.0	3.1	3.6	3.8	3.1	3.5	3.3	2.4	3.6	3.8	2	
3.9	3.7	3.3	2.7	3.8	4.0	3.9	3.8	3.6	2.6	3.7	4.0	4.0	3.8	3.7	3.0	3.6	4.0	4	
3.7	3.7	3.1	2.6	3.8	4.0	3.8	3.8	3.6	2.8	3.7	4.1	3.9	3.8	3.7	3.1	3.4	4.1	6	SS2
3.4	3.7	3.2	2.5	3.8	4.0	3.6	3.7	3.5	2.8	3.7	4.1	3.6	3.7	3.6	3.1	3.4	4.1	8	
2.9	3.6	3.2	2.5	3.8	4.0	3.2	3.7	3.5	2.7	3.7	4.1	3.2	3.7	3.6	3.0	3.4	4.1	10	
4.7	1.7	0.8	0.5	0.4	0.3	5.0	1.8	0.9	0.6	0.4	0.3	4.8	1.7	0.9	0.6	0.4	0.3	2	
3.5	1.4	0.7	0.5	0.3	0.3	3.7	1.4	0.8	0.5	0.4	0.3	3.7	1.4	0.8	0.5	0.4	0.3	4	
3.1	1.3	0.7	0.4	0.3	0.2	3.3	1.3	0.8	0.5	0.3	0.3	3.4	1.3	0.8	0.5	0.4	0.3	6	B1
2.9	1.2	0.7	0.4	0.3	0.2	3.1	1.3	0.7	0.5	0.3	0.3	3.2	1.3	0.8	0.5	0.3	0.3	8	
2.9	1.2	0.6	0.4	0.3	0.2	3.1	1.3	0.7	0.5	0.3	0.3	3.2	1.3	0.8	0.5	0.3	0.3	10	
14.6	7.7	5.4	4.2	3.5	2.9	13.9	7.8	5.4	3.9	3.2	2.7	13.7	8.1	5.5	3.7	3.2	2.7	2	
13.7	7.1	4.9	3.6	3.1	2.6	13.4	7.2	4.9	3.4	2.9	2.5	13.4	7.3	5.0	3.6	2.9	2.4	4	
13.1	6.8	4.6	3.3	2.8	2.5	12.9	6.8	4.6	3.3	2.7	2.3	13.0	7.0	4.7	3.5	2.8	2.3	6	F1
12.5	6.6	4.5	3.2	2.7	2.5	12.5	6.6	4.5	3.3	2.6	2.2	12.7	6.8	4.6	3.4	2.7	2.3	8	
12.2	6.5	4.4	3.2	2.6	2.5	12.2	6.5	4.4	3.2	2.6	2.2	12.5	6.7	4.5	3.4	2.7	2.2	10	
60.9	32.7	15.1	9.7	7.0	5.4	53.6	23.4	13.6	9.0	6.5	4.9	49.7	21.0	12.7	9.0	6.1	4.7	2	
48.4	24.9	12.5	8.6	5.9	4.5	42.9	20.3	11.7	9.3	5.5	4.2	40.4	18.9	11.4	8.0	5.4	4.1	4	
44.6	24.0	12.3	8.9	5.7	4.3	40.0	19.9	11.6	8.4	5.4	4.1	37.9	18.5	11.4	7.7	5.2	4.0	6	SSI
42.5	23.5	12.2	8.9	5.6	4.3	38.3	19.6	11.6	8.3	5.3	4.0	36.5	18.3	11.4	7.6	5.2	3.9	8	
47.2	23.0	12.1	8.8	5.5	4.2	40.3	19.4	11.6	8.3	5.3	4.0	38.0	18.2	11.4	7.6	5.1	3.9	10	
76.1	42.9	20.7	14.3	10.7	8.4	65.2	32.1	18.5	12.8	9.4	7.4	59.6	28.1	17.1	13.3	8.7	6.9	2	
54.6	25.9	16.1	12.6	8.1	6.4	47.4	22.4	14.9	9.9	7.4	5.7	44.2	21.1	14.6	9.4	7.0	5.5	4	
49.2	25.0	16.0	10.9	7.8	6.1	43.4	21.4	15.2	9.6	7.1	5.5	40.8	20.2	15.1	9.1	6.9	5.2	6	AB
46.5	24.5	15.9	10.7	7.7	6.0	41.4	21.0	15.3	9.5	7.0	5.4	39.1	19.9	15.2	9.1	6.8	5.2	8	
47.1	24.2	15.9	10.6	7.6	6.0	40.9	20.8	15.3	9.4	7.0	5.4	38.5	19.6	15.2	9.0	6.8	5.2	10	
11.7	4.9	2.3	1.5	1.1	0.8	11.7	5.0	2.4	1.6	1.1	0.8	11.9	5.0	2.4	1.7	1.1	0.8	2	
29.5	9.8	5.2	3.0	1.9	1.3	29.3	10.2	5.5	3.3	2.2	1.5	33.2	11.0	5.8	3.6	2.4	1.7	4	
61.1	22.5	10.1	5.4	3.1	2.2	63.5	21.0	10.5	6.2	3.9	2.6	48.1	21.8	10.7	6.5	4.3	3.0	6	B2
29.8	38.2	19.4	9.5	5.2	3.7	36.5	33.3	17.6	10.0	6.3	4.2	32.8	27.5	16.1	9.7	6.4	4.5	8	
18.2	22.4	24.9	15.8	8.4	5.8	22.5	23.1	19.2	14.0	9.0	6.0	22.0	21.3	15.7	11.0	7.7	5.6	10	
8.3	4.3	2.1	1.5	1.2	1.0	6.6	3.6	1.7	1.3	1.0	0.8	6.3	3.2	1.6	1.4	1.0	0.8	2	
9.1	4.1	3.0	2.1	1.5	1.1	8.0	3.8	2.8	2.0	1.5	1.1	8.2	3.8	2.8	2.0	1.5	1.1	4	
10.2	5.2	3.8	2.5	1.8	1.4	9.5	5.0	3.8	2.7	2.0	1.5	10.0	5.1	3.9	2.8	2.2	1.6	6	PM
8.9	5.5	4.1	2.9	2.0	1.7	8.8	5.3	4.2	3.1	2.4	1.8	8.8	5.5	4.3	3.3	2.6	2.0	8	
5.5	4.9	3.9	2.9	2.2	1.8	5.4	4.7	3.9	3.1	2.4	1.9	5.3	4.8	4.0	3.2	2.6	2.1	10	
5.7	2.5	1.2	0.8	0.6	0.4	4.6	2.1	1.0	0.7	0.5	0.4	4.6	2.0	1.0	0.7	0.4	0.3	2	
10.5	4.4	2.6	1.6	1.0	0.7	9.4	4.0	2.4	1.5	1.0	0.7	10.2	4.2	2.4	1.5	1.0	0.7	4	
15.2	7.7	4.6	2.7	1.6	1.2	14.8	7.4	4.7	3.0	1.9	1.3	16.6	8.0	5.0	3.2	2.2	1.5	6	PV
13.5	10.5	7.1	4.3	2.6	2.0	14.7	10.7	7.7	5.1	3.4	2.3	16.0	11.5	8.4	5.8	4.1	2.9	8	
8.6	11.1	8.9	6.0	3.9	3.1	7.9	11.2	10.0	7.3	5.2	3.6	7.6	11.7	10.7	8.3	6.2	4.6	10	
21.1	9.2	4.6	3.1	2.3	1.7	20.4	9.1	4.5	3.1	2.3	1.8	20.9	9.2	4.6	3.1	2.4	1.9	2	
23.2	10.0	6.0	3.7	2.7	2.0	23.4	10.3	6.2	3.7	3.0	2.2	24.1	10.6	6.5	4.1	3.1	2.4	4	
24.7	11.6	6.8	4.2	3.2	2.4	25.0	11.7	7.3	4.5	3.5	2.7	25.4	12.0	7.5	4.7	3.6	2.9	6	F2
23.7	12.4	7.4	4.6	3.6	2.8	24.5	12.4	7.8	4.8	3.9	3.0	23.7	12.5	7.9	5.1	3.9	3.2	8	
19.8	12.4	7.7	4.9	3.9	3.1	20.3	12.3	7.9	5.0	4.1	3.3	19.8	12.3	8.0	5.2	4.0	3.3	10	
5	10	15	20	25	30	5	10	15	20	25	30	5	10	15	20	25	30	SL/PH	COMP

S2 - PMG-I

Table D4 MAPGA values for three-span PMG-I bridges.

3.2	3.1	2.5	2.5	2.6	2.5	3.3	3.1	2.1	2.8	2.6	2.7	3.3	3.1	2.6	2.8	2.8	2.7	2	SS1
3.1	3.1	2.7	2.7	2.7	2.5	3.1	3.1	2.7	2.2	2.5	2.6	3.1	3.1	1.9	2.1	2.6	2.6	4	
2.8	3.1	2.8	2.6	2.6	2.4	2.9	3.1	2.3	2.2	2.5	2.6	2.9	3.1	2.5	1.8	2.6	2.7	6	
2.6	3.0	2.8	2.4	2.5	2.4	2.8	3.1	1.9	2.1	2.5	2.6	2.8	3.1	2.6	1.8	2.6	2.7	8	
2.5	2.9	2.8	2.2	2.5	2.4	2.6	3.0	1.8	2.0	2.5	2.6	2.7	3.0	2.7	1.8	2.6	2.7	10	
2.4	3.1	3.3	2.6	2.5	2.3	2.5	3.1	3.0	3.2	2.7	3.1	2.5	3.1	3.2	3.2	3.2	3.0	2	SS2
3.4	3.4	3.2	2.8	2.6	2.5	3.5	3.5	3.4	3.0	2.5	2.5	3.5	3.5	3.1	2.9	2.6	2.6	4	
3.4	3.5	3.3	2.8	2.6	2.3	3.6	3.5	3.4	3.0	2.6	2.6	3.7	3.6	3.1	2.9	2.6	2.7	6	
2.9	3.5	3.3	2.8	2.5	2.2	3.2	3.6	3.0	3.0	2.6	2.7	3.3	3.7	3.2	2.7	2.6	2.7	8	
2.5	3.5	3.3	2.8	2.5	2.2	2.7	3.6	2.7	3.0	2.6	2.7	2.8	3.6	3.2	2.6	2.6	2.6	10	
4.7	1.5	0.8	0.6	0.4	0.3	5.0	1.6	0.9	0.6	0.5	0.4	4.7	1.6	0.9	0.6	0.4	0.3	2	B1
2.8	1.0	0.6	0.4	0.3	0.3	3.0	1.2	0.7	0.5	0.3	0.3	3.0	1.2	0.7	0.5	0.3	0.3	4	
2.3	0.9	0.5	0.4	0.3	0.3	2.5	1.0	0.6	0.4	0.3	0.3	2.5	1.0	0.6	0.4	0.3	0.3	6	
2.0	0.8	0.5	0.3	0.3	0.3	2.2	1.0	0.6	0.4	0.3	0.3	2.3	1.0	0.6	0.4	0.3	0.2	8	
1.9	0.8	0.5	0.3	0.3	0.2	2.1	0.9	0.5	0.4	0.3	0.3	2.1	0.9	0.6	0.4	0.3	0.2	10	
15.2	8.9	6.1	4.6	4.0	3.5	14.5	9.0	5.6	4.5	3.4	3.3	14.3	9.1	6.0	4.4	3.5	3.1	2	F1
13.5	7.7	5.5	4.2	3.3	3.0	13.4	7.9	5.2	3.9	3.0	2.6	13.4	8.2	5.0	3.9	2.9	2.5	4	
12.3	7.0	5.0	3.7	3.1	2.8	12.4	7.4	4.8	3.6	2.7	2.4	12.7	7.7	5.0	3.5	2.7	2.2	6	
11.5	6.7	4.6	3.4	3.0	2.8	11.9	7.0	4.4	3.3	2.5	2.3	12.3	7.4	4.9	3.3	2.6	2.1	8	
11.0	6.5	4.4	3.3	2.9	2.7	11.5	6.8	4.3	3.2	2.4	2.2	12.0	7.2	4.8	3.3	2.5	2.1	10	
63.1	25.1	14.9	10.1	8.3	6.6	55.0	22.1	15.7	9.1	7.1	5.5	50.0	20.6	12.9	8.5	6.3	5.0	2	SSI
40.5	17.7	10.9	7.4	5.9	5.3	35.9	16.2	9.9	6.8	5.2	5.1	33.8	15.4	9.5	6.7	4.9	4.6	4	
34.8	16.1	9.9	6.8	5.3	5.2	31.5	14.9	9.2	6.5	4.7	4.5	30.0	14.3	8.8	7.6	4.6	4.2	6	
31.8	15.4	9.5	6.5	5.1	5.0	29.3	14.3	8.9	6.6	4.6	4.3	28.1	13.8	8.6	8.1	4.4	4.1	8	
30.6	14.9	9.3	6.4	5.0	4.9	28.1	14.0	8.7	6.7	4.5	4.3	27.0	13.5	8.4	7.8	4.4	4.0	10	
79.3	32.5	20.4	14.1	11.4	9.0	69.0	28.4	18.4	12.4	10.4	7.6	62.5	26.3	16.6	11.5	8.6	6.9	2	AB
45.6	20.8	13.0	9.1	6.9	7.3	39.7	18.7	11.6	8.6	6.1	5.5	37.0	17.7	10.9	8.3	5.7	5.1	4	
38.2	18.5	11.6	8.2	6.2	6.1	34.0	16.8	10.5	7.6	5.5	5.1	32.1	16.1	10.0	7.0	5.3	4.8	6	
34.7	17.6	11.1	8.1	6.0	5.9	31.4	16.1	10.1	7.2	5.4	5.0	29.9	15.5	9.7	6.8	5.1	4.7	8	
32.5	17.0	10.8	8.2	5.9	5.8	29.6	15.7	9.9	7.0	5.3	4.9	28.3	15.1	9.5	6.7	5.1	4.7	10	
12.4	4.6	2.4	1.6	1.1	0.8	12.6	4.8	2.5	1.7	1.2	0.9	12.4	4.7	2.5	1.6	1.2	0.9	2	B2
26.6	8.7	4.3	2.5	1.6	1.3	27.5	9.3	4.9	2.9	1.9	1.4	30.8	10.1	5.2	3.2	2.1	1.5	4	
56.7	17.5	7.6	3.9	2.6	2.1	60.2	18.8	9.0	5.1	3.1	2.2	59.5	20.1	9.8	5.8	3.7	2.5	6	
34.9	29.2	12.8	6.2	4.3	3.3	42.4	33.1	15.6	8.3	5.0	3.7	38.0	32.2	16.1	9.2	5.8	4.0	8	
20.3	21.4	18.2	9.5	6.6	4.9	24.5	25.1	23.3	12.6	7.5	5.4	23.9	22.7	18.7	12.5	8.1	5.6	10	
8.2	3.4	2.1	1.6	1.2	0.9	6.6	2.8	1.7	1.3	1.2	0.8	6.2	2.7	1.6	1.2	1.0	0.7	2	PM
8.0	3.7	2.3	1.6	1.2	1.0	7.1	3.4	2.1	1.5	1.1	0.9	7.1	3.4	2.1	1.5	1.1	0.9	4	
8.9	4.6	2.8	1.8	1.4	1.2	8.3	4.4	2.8	1.9	1.4	1.1	8.7	4.5	2.9	2.1	1.6	1.2	6	
8.2	4.9	3.2	2.1	1.7	1.5	8.0	4.9	3.3	2.3	1.7	1.5	8.4	5.0	3.4	2.5	2.0	1.5	8	
5.7	4.6	3.2	2.3	1.9	1.6	5.6	4.6	3.4	2.5	1.9	1.7	5.6	4.7	3.5	2.7	2.2	1.8	10	
6.0	2.4	1.3	0.9	0.6	0.5	4.9	1.9	1.0	0.7	0.5	0.4	4.7	1.9	1.0	0.6	0.5	0.3	2	PV
9.6	4.0	2.2	1.3	0.9	0.7	8.6	3.6	2.0	1.2	0.8	0.6	9.1	3.7	2.0	1.3	0.9	0.6	4	
13.2	6.5	3.5	2.0	1.4	1.1	12.8	6.3	3.7	2.2	1.4	1.0	14.3	6.7	3.9	2.5	1.6	1.1	6	
14.1	8.8	5.2	3.0	2.3	1.8	14.7	9.2	5.9	3.7	2.3	1.8	15.9	9.8	6.5	4.3	2.8	1.9	8	
9.0	9.6	6.8	4.3	3.4	2.8	8.9	10.3	8.0	5.4	3.6	3.0	8.8	9.9	8.7	6.4	4.5	3.2	10	
23.2	9.5	5.2	3.4	2.5	1.8	22.6	9.3	5.1	3.5	2.6	1.9	23.0	9.6	5.4	3.6	2.6	2.0	2	F2
23.8	10.4	5.9	3.7	2.6	2.1	24.3	10.8	6.3	4.1	2.8	2.1	25.3	11.4	6.4	4.3	3.0	2.4	4	
24.8	12.0	6.8	4.2	3.0	2.3	25.8	12.6	7.3	4.8	3.3	2.6	26.7	13.0	7.7	5.0	3.6	2.8	6	
24.3	12.9	7.6	4.7	3.5	2.7	25.4	13.5	7.8	5.3	3.7	3.0	26.0	13.8	8.4	5.6	4.0	3.1	8	
20.7	13.0	8.0	5.2	3.8	2.9	21.7	13.6	8.2	5.6	4.0	3.3	20.4	13.8	8.7	5.8	4.2	3.3	10	
5	10	15	20	25	30	5	10	15	20	25	30	5	10	15	20	25	30	SL/PH	COMP

S3 - PMG-I

Table D5 MAPGA values for four-span PMG-I bridges.

3.1	2.9	2.5	2.2	2.5	2.6	3.1	3.0	1.8	2.7	2.7	2.5	3.1	3.1	2.5	2.1	2.6	2.6	2	SSI
2.7	2.7	1.9	2.0	2.4	2.5	2.7	2.9	1.8	1.8	2.4	2.2	2.7	2.9	2.0	1.7	2.4	2.3	4	
2.3	2.7	1.7	1.7	2.4	2.2	2.3	2.8	1.9	1.8	2.2	2.2	2.3	2.8	2.1	2.0	2.1	2.3	6	
2.1	2.6	1.7	1.7	2.3	2.3	2.2	2.7	1.9	1.9	2.1	2.3	2.2	2.8	2.1	2.0	2.0	2.4	8	
2.0	2.6	1.7	1.7	2.2	2.3	2.1	2.7	1.9	1.9	2.1	2.3	2.1	2.7	2.1	2.0	1.9	2.4	10	
2.5	2.8	3.1	1.9	2.1	2.5	2.5	2.8	2.9	2.9	3.1	2.2	2.5	2.9	3.1	1.9	3.1	3.0	2	SS2
3.5	3.5	2.7	2.7	2.6	2.1	3.5	3.6	2.8	2.6	2.8	1.9	3.6	3.7	3.2	2.6	2.9	2.2	4	
3.8	3.8	2.6	2.5	2.6	2.0	4.0	3.8	3.0	2.7	2.4	2.0	4.0	3.9	3.3	2.8	2.8	2.5	6	
3.3	3.8	2.6	2.5	2.6	2.2	3.7	3.9	3.1	2.8	1.9	2.4	3.8	3.9	3.4	2.8	2.6	2.5	8	
2.9	3.8	2.6	2.5	2.6	2.2	3.3	3.9	3.1	2.8	2.1	2.4	3.4	3.9	3.4	2.8	2.6	2.5	10	
3.9	1.3	0.7	0.5	0.4	0.3	4.2	1.4	0.8	0.5	0.4	0.3	3.9	1.3	0.7	0.5	0.4	0.3	2	B1
2.0	0.8	0.5	0.3	0.3	0.2	2.2	0.9	0.5	0.4	0.3	0.2	2.2	0.9	0.5	0.4	0.3	0.2	4	
1.6	0.7	0.4	0.3	0.2	0.2	1.8	0.8	0.4	0.3	0.2	0.2	1.8	0.8	0.4	0.3	0.2	0.2	6	
1.4	0.6	0.3	0.3	0.2	0.2	1.6	0.7	0.4	0.3	0.2	0.2	1.6	0.7	0.4	0.3	0.2	0.2	8	
1.2	0.6	0.3	0.3	0.2	0.2	1.4	0.7	0.4	0.3	0.2	0.2	1.5	0.7	0.4	0.3	0.2	0.2	10	
14.5	8.8	7.0	5.1	4.0	3.4	14.0	8.6	5.8	5.1	4.2	3.1	13.8	8.6	5.8	4.3	4.0	3.2	2	F1
12.4	7.4	5.6	4.7	4.1	3.2	12.5	7.1	5.0	4.0	3.7	2.9	12.6	7.5	5.0	3.8	3.3	2.8	4	
10.7	6.6	4.7	4.2	3.9	3.2	11.1	6.5	4.5	3.5	3.1	2.8	11.5	6.8	4.6	3.5	2.9	2.7	6	
9.7	6.0	4.2	3.9	3.8	3.1	10.3	6.1	4.1	3.2	2.8	2.8	10.9	6.5	4.3	3.2	2.7	2.5	8	
9.2	5.7	4.0	3.8	3.6	3.0	9.8	5.9	3.9	3.1	2.8	2.7	10.5	6.3	4.2	3.1	2.6	2.5	10	
56.9	21.9	13.3	12.1	6.6	5.9	49.4	19.7	12.2	8.2	5.9	4.9	44.4	18.2	10.9	7.5	5.5	4.2	2	SSI
31.2	14.1	8.7	6.1	4.6	3.7	27.7	12.9	7.8	6.6	4.0	3.5	26.0	12.3	7.4	6.8	3.8	3.8	4	
25.4	12.3	7.5	6.3	4.0	3.6	23.1	11.5	6.9	5.8	3.7	4.2	22.3	11.0	6.7	5.1	3.6	3.4	6	
22.8	11.6	7.0	6.4	3.8	3.6	21.6	10.9	6.6	5.2	3.6	3.6	21.0	10.5	6.4	4.8	3.6	3.2	8	
21.6	11.1	6.8	6.3	3.8	3.7	20.6	10.5	6.4	5.0	3.6	3.4	20.1	10.2	6.3	4.6	3.6	3.1	10	
70.9	28.0	17.4	13.8	9.2	7.8	61.4	25.0	16.1	10.8	8.1	7.0	55.0	23.0	14.1	9.8	7.5	5.8	2	AB
35.4	16.6	10.2	7.9	5.3	4.6	30.8	14.8	9.1	7.7	4.9	4.7	28.5	14.0	8.5	6.3	4.8	4.3	4	
27.8	14.1	8.7	8.0	4.9	4.7	25.6	12.8	7.9	5.8	4.8	4.1	24.6	12.3	7.5	5.3	4.8	4.0	6	
25.4	13.2	8.3	6.9	4.8	4.4	23.8	12.2	7.5	5.4	4.8	4.0	23.0	11.7	7.2	5.1	4.8	3.9	8	
23.8	12.7	8.0	6.5	4.8	4.2	22.5	11.7	7.3	5.3	4.8	3.9	21.9	11.3	7.0	5.0	4.8	3.9	10	
11.6	3.9	2.0	1.2	0.9	0.7	11.9	4.2	2.2	1.4	1.0	0.8	11.5	4.2	2.1	1.4	1.0	0.7	2	B2
20.4	6.0	2.8	1.7	1.1	1.0	22.1	7.2	3.4	2.0	1.3	0.9	24.5	7.9	3.9	2.2	1.4	1.0	4	
40.0	10.2	4.0	2.4	1.8	1.5	45.1	13.0	5.6	2.9	2.0	1.6	52.0	14.9	6.7	3.6	2.2	1.7	6	
35.0	16.2	5.9	3.7	2.8	2.2	44.6	22.7	9.1	4.6	3.2	2.4	40.4	24.9	11.1	5.6	3.6	2.7	8	
19.8	19.7	8.8	5.5	3.9	3.1	25.7	27.5	14.2	7.0	4.8	3.6	25.0	24.8	16.2	8.3	5.3	3.9	10	
7.5	2.9	1.9	1.4	1.1	0.9	6.2	2.5	1.6	1.1	0.9	0.8	5.7	2.4	1.4	1.0	0.8	0.7	2	PM
6.6	2.9	1.7	1.1	0.8	0.7	5.8	2.7	1.6	1.2	0.8	0.7	5.8	2.7	1.6	1.2	0.8	0.6	4	
7.0	3.4	1.9	1.3	1.0	0.9	6.7	3.4	2.0	1.3	0.9	0.8	7.1	3.6	2.1	1.4	1.0	0.8	6	
6.8	3.7	2.0	1.5	1.2	1.0	6.8	3.9	2.3	1.5	1.2	1.0	7.2	4.1	2.6	1.7	1.3	1.1	8	
5.5	3.6	2.2	1.7	1.3	1.1	5.5	3.9	2.5	1.8	1.4	1.2	5.8	4.1	2.8	1.9	1.5	1.3	10	
5.6	2.0	1.1	0.7	0.5	0.4	4.6	1.7	0.9	0.6	0.4	0.3	4.4	1.7	0.8	0.5	0.4	0.3	2	PV
7.9	2.9	1.5	0.9	0.6	0.5	7.2	2.8	1.4	0.8	0.5	0.4	7.5	2.9	1.5	0.9	0.5	0.4	4	
10.3	4.3	2.0	1.2	1.0	0.8	10.3	4.6	2.2	1.2	0.8	0.7	11.4	5.0	2.6	1.4	0.9	0.7	6	
11.5	5.9	2.7	1.9	1.5	1.2	12.3	6.8	3.5	1.9	1.4	1.1	13.7	7.7	4.2	2.3	1.5	1.2	8	
9.4	7.3	3.8	2.8	2.1	1.7	9.8	8.4	5.0	3.0	2.2	1.8	10.2	9.4	6.1	3.5	2.5	2.0	10	
22.4	8.4	4.9	2.9	2.3	1.7	21.9	8.7	4.9	3.1	2.3	1.9	22.3	9.0	4.9	3.0	2.3	1.9	2	F2
21.4	8.9	4.9	3.0	2.1	1.8	22.1	9.7	5.5	3.6	2.4	1.7	23.1	10.4	5.9	3.8	2.6	1.9	4	
22.0	10.0	5.3	3.4	2.5	2.0	23.6	11.3	6.4	4.0	2.7	2.1	24.8	12.1	7.1	4.5	3.0	2.4	6	
22.0	11.0	5.8	4.0	3.0	2.3	23.8	12.4	7.2	4.6	2.9	2.5	24.8	13.1	7.9	5.1	3.7	2.8	8	
20.1	11.4	6.4	4.5	3.3	2.5	21.8	12.9	7.8	5.1	3.4	2.8	22.5	13.3	8.3	5.4	4.1	3.2	10	
5	10	15	20	25	30	5	10	15	20	25	30	5	10	15	20	25	30	SL/PH	COMP

S4 - PMG-I

Table D6 MAPGA values for two-span SLAB bridges.

3.0	2.3	2.4	2.5	2.5	2.5	3.1	2.3	2.3	2.3	2.1	2.1	3.1	2.2	2.3	2.4	2.4	2.4	2	SS1
3.5	2.2	2.5	2.6	2.5	2.3	3.6	2.5	2.1	2.6	2.6	2.5	3.7	3.0	2.1	2.0	2.1	2.2	4	
3.1	2.4	2.4	2.5	2.5	2.4	3.5	2.7	2.1	2.0	2.1	2.2	3.3	2.5	2.0	1.9	1.9	2.0	6	
2.7	2.1	2.4	2.4	2.4	2.3	2.9	2.3	2.0	1.9	2.0	2.1	2.9	2.3	2.0	1.9	1.9	1.9	8	
2.8	2.1	2.2	2.3	2.3	2.3	2.8	2.1	2.0	1.9	1.9	2.1	3.0	2.2	1.9	1.9	1.9	1.9	10	
3.3	2.8	2.3	2.5	2.6	2.6	3.5	3.1	2.8	2.6	2.6	1.7	3.6	3.2	3.1	3.1	3.1	2.8	2	SS2
3.6	3.0	2.9	3.1	3.0	2.3	3.6	3.6	3.2	3.3	3.4	3.3	3.6	3.6	3.5	3.5	3.5	3.5	4	
3.4	3.3	2.5	2.8	3.1	2.8	3.6	3.6	3.4	3.5	3.5	3.4	3.7	3.7	3.6	3.5	3.5	3.5	6	
3.4	3.3	2.7	2.7	3.1	2.8	3.6	3.6	3.6	3.5	3.5	3.3	3.7	3.8	3.6	3.5	3.5	3.4	8	
3.7	3.5	2.6	2.8	3.1	2.7	3.8	3.7	3.6	3.5	3.4	3.3	3.7	3.8	3.6	3.5	3.5	3.3	10	
5.0	1.7	0.8	0.5	0.4	0.3	5.2	1.7	0.8	0.5	0.3	0.2	4.9	1.5	0.7	0.4	0.3	0.2	2	B1
3.4	1.3	0.6	0.4	0.3	0.2	3.6	1.2	0.6	0.4	0.2	0.2	3.5	1.1	0.6	0.3	0.2	0.2	4	
2.9	1.1	0.6	0.3	0.2	0.2	3.1	1.1	0.6	0.3	0.2	0.2	3.1	1.0	0.5	0.3	0.2	0.2	6	
2.7	1.1	0.5	0.3	0.2	0.2	2.9	1.1	0.6	0.3	0.2	0.2	2.9	1.0	0.5	0.3	0.2	0.2	8	
2.7	1.1	0.5	0.3	0.2	0.2	2.8	1.1	0.5	0.3	0.2	0.2	2.9	1.0	0.5	0.3	0.2	0.2	10	
14.6	7.8	4.7	3.4	2.5	1.9	13.6	6.9	4.0	2.7	1.8	1.3	13.3	6.5	3.8	2.5	1.8	1.3	2	F1
13.4	6.8	4.5	3.2	2.3	1.7	12.9	6.3	3.6	2.6	1.8	1.3	12.8	6.5	3.5	2.2	1.6	1.2	4	
12.8	6.7	4.2	3.0	2.2	1.8	12.5	6.3	3.5	2.3	1.7	1.3	12.5	6.0	3.3	2.2	1.5	1.1	6	
12.1	6.3	4.1	2.9	2.2	1.9	11.9	6.1	3.5	2.3	1.6	1.2	12.0	5.9	3.3	2.1	1.5	1.1	8	
11.8	6.2	4.1	2.9	2.3	1.9	11.6	5.9	3.4	2.2	1.6	1.2	11.8	5.8	3.3	2.1	1.5	1.1	10	
64.7	35.5	17.2	10.2	6.9	5.0	56.6	29.2	14.1	8.3	5.6	4.3	50.6	25.4	11.5	6.6	4.4	3.1	2	SSI
47.1	23.7	11.6	7.5	5.3	4.3	41.8	17.9	9.4	5.7	3.9	3.0	38.9	15.0	9.6	5.3	3.5	2.8	4	
42.5	18.8	10.4	6.7	4.7	3.6	37.9	15.9	10.1	5.7	3.8	2.9	35.7	15.2	10.3	5.8	3.7	2.9	6	
40.6	20.6	10.5	6.6	4.6	3.5	36.2	17.3	10.5	5.9	3.8	3.0	34.3	15.6	10.0	5.9	3.8	3.0	8	
43.7	20.7	10.5	6.5	4.6	3.5	36.9	18.1	10.5	5.9	3.8	3.0	36.7	15.8	9.8	5.9	3.8	3.0	10	
89.3	50.5	27.1	16.4	11.5	8.7	76.2	42.0	20.0	12.3	8.6	6.8	66.8	35.7	16.0	9.6	6.6	4.9	2	AB
56.3	31.1	16.1	10.4	7.4	5.6	48.5	22.7	13.0	7.8	5.4	4.4	44.1	18.4	10.3	7.9	5.4	4.5	4	
48.4	24.9	13.7	9.2	6.6	5.0	42.2	18.2	12.5	8.5	5.6	4.7	39.1	16.7	10.3	7.6	5.7	4.7	6	
44.8	28.9	14.5	9.3	6.6	5.0	39.3	18.0	12.5	8.8	5.9	4.8	36.8	16.5	10.2	7.2	5.9	4.8	8	
44.4	28.0	14.8	9.4	6.6	5.0	38.1	18.3	12.5	8.7	6.0	4.8	36.6	16.5	10.1	7.1	5.9	4.8	10	
32.2	11.0	5.1	3.2	2.2	1.6	25.6	8.2	3.6	2.2	1.5	1.1	17.6	5.2	2.3	1.3	0.9	0.6	2	B2
59.0	20.4	10.4	6.0	3.7	2.7	50.6	18.9	8.6	5.0	3.2	2.3	41.8	13.6	6.5	4.6	3.0	2.1	4	
90.3	35.7	23.8	12.2	7.3	5.4	85.3	34.4	18.0	13.2	8.2	5.9	77.9	28.3	15.4	10.3	7.7	5.7	6	
89.9	55.2	43.1	22.6	14.0	10.1	88.2	50.4	32.4	24.2	16.7	12.6	83.0	46.6	29.0	20.3	15.9	12.4	8	
67.8	67.6	61.3	36.4	23.8	17.1	69.1	60.8	47.6	38.1	28.7	22.8	79.4	58.9	43.9	33.1	27.5	22.4	10	
7.2	3.5	1.8	1.2	0.8	0.6	5.9	2.8	1.4	1.0	0.7	0.5	4.3	1.9	1.0	0.6	0.4	0.2	2	PM
8.2	3.5	1.7	1.1	0.7	0.6	7.0	3.0	1.7	1.0	0.7	0.5	5.9	2.3	1.3	1.1	0.7	0.4	4	
10.0	4.0	2.7	1.5	1.0	0.8	8.8	3.7	2.2	1.8	1.2	0.9	7.8	3.2	2.0	1.5	1.2	0.7	6	
9.8	5.1	3.8	2.1	1.4	1.1	9.0	4.3	2.8	2.2	1.7	1.4	7.1	3.8	2.5	1.9	1.5	1.0	8	
7.0	5.4	4.4	2.7	1.9	1.4	6.9	4.4	3.2	2.5	2.0	1.7	6.5	4.0	2.8	2.1	1.7	1.1	10	
4.6	1.6	0.7	0.5	0.3	0.2	3.7	1.2	0.5	0.3	0.2	0.2	2.5	0.7	0.3	0.2	0.1	0.1	2	PV
8.4	2.9	1.5	0.9	0.5	0.4	7.3	2.7	1.2	0.7	0.5	0.3	6.0	1.9	0.9	0.7	0.4	0.3	4	
12.9	5.1	3.4	1.8	1.0	0.8	12.2	4.9	2.6	1.9	1.2	0.8	11.2	4.1	2.2	1.5	1.1	0.8	6	
12.9	7.9	6.2	3.2	2.0	1.4	12.6	7.2	4.6	3.5	2.4	1.8	11.9	6.7	4.2	2.9	2.3	1.8	8	
9.7	9.7	8.8	5.2	3.4	2.5	9.9	8.7	6.8	5.5	4.1	3.3	11.4	8.4	6.3	4.7	3.9	3.2	10	
20.5	7.8	3.9	2.5	1.7	1.3	19.5	7.3	3.2	2.0	1.3	1.0	20.4	7.3	3.4	2.0	1.3	0.9	2	F2
21.8	8.5	4.4	2.7	1.8	1.3	21.4	8.3	4.1	2.4	1.6	1.2	22.3	8.2	4.2	2.7	1.8	1.3	4	
23.0	9.5	5.0	3.2	2.2	1.7	22.8	9.0	4.7	3.0	2.0	1.5	23.2	9.1	4.8	3.0	2.0	1.5	6	
22.4	10.3	5.6	3.5	2.5	1.9	22.4	9.5	5.1	3.2	2.2	1.6	21.1	9.5	5.1	3.1	2.2	1.6	8	
19.5	10.5	5.8	3.7	2.7	2.1	20.1	9.6	5.3	3.3	2.3	1.7	18.3	9.6	5.2	3.2	2.2	1.6	10	
5	10	15	20	25	30	5	10	15	20	25	30	5	10	15	20	25	30	SL/PH	COMP

S2 - SLAB

Table D7 MAPGA values for three-span SLAB bridges.

3.3	2.5	2.6	2.6	2.6	2.5	3.3	2.8	1.9	2.4	2.5	2.5	3.4	3.0	2.2	1.8	1.7	2.1	2	SS1
3.7	3.0	2.6	2.3	1.9	2.2	3.7	3.0	2.9	2.6	1.7	2.3	3.8	3.2	2.9	2.7	2.6	2.5	4	
3.5	3.0	2.5	2.6	2.4	2.0	3.6	3.1	2.9	2.7	2.5	2.4	3.6	3.0	2.9	2.7	2.6	2.6	6	
3.2	2.8	2.6	2.4	2.4	2.2	3.4	3.0	2.9	2.7	2.6	2.5	3.4	3.0	2.9	2.8	2.7	2.6	8	
2.9	2.7	2.6	2.4	2.4	2.3	3.0	2.9	2.9	2.7	2.6	2.5	3.2	2.9	2.9	2.8	2.7	2.6	10	
2.9	2.8	2.9	2.5	2.1	1.8	2.8	2.7	2.6	3.0	2.9	2.7	2.7	2.7	3.1	2.7	2.6	2.8	2	SS2
2.8	3.0	2.9	2.8	2.5	2.5	2.8	3.0	2.9	2.8	2.4	2.6	2.9	3.2	3.1	2.9	2.8	2.6	4	
3.2	3.1	2.9	2.8	2.6	2.2	3.2	3.2	3.1	2.9	2.7	2.5	3.4	3.4	3.2	3.0	2.9	2.8	6	
3.6	3.3	2.9	2.9	2.7	2.5	3.6	3.3	3.1	2.9	2.8	2.6	3.8	3.5	3.2	3.0	2.9	2.9	8	
2.9	3.3	2.9	2.9	2.7	2.5	3.1	3.5	3.2	3.0	2.8	2.7	3.4	3.6	3.3	3.1	2.9	2.9	10	
5.4	1.8	0.9	0.6	0.5	0.4	5.8	1.7	0.8	0.5	0.4	0.3	5.3	1.5	0.7	0.4	0.3	0.2	2	B1
3.0	1.0	0.6	0.4	0.3	0.2	3.2	1.0	0.5	0.3	0.2	0.2	3.0	1.0	0.5	0.3	0.2	0.2	4	
2.2	0.8	0.5	0.3	0.2	0.2	2.4	0.9	0.5	0.3	0.2	0.2	2.4	0.8	0.4	0.3	0.2	0.1	6	
1.9	0.8	0.4	0.3	0.2	0.2	2.1	0.8	0.4	0.3	0.2	0.2	2.1	0.8	0.4	0.2	0.2	0.1	8	
1.7	0.7	0.4	0.3	0.2	0.2	1.9	0.8	0.4	0.2	0.2	0.2	2.0	0.7	0.4	0.2	0.2	0.1	10	
15.7	8.8	5.5	3.8	2.7	2.0	14.7	7.9	4.4	3.1	2.2	1.7	14.3	7.7	4.2	2.7	1.9	1.5	2	F1
13.6	7.4	5.1	3.6	2.5	2.1	13.2	6.9	4.2	2.9	1.9	1.6	13.1	6.9	4.0	2.6	1.9	1.4	4	
12.2	6.8	4.6	3.3	2.7	2.1	12.2	6.5	4.0	2.7	2.0	1.6	12.3	6.5	3.8	2.5	1.8	1.4	6	
11.4	6.6	4.5	3.3	2.8	2.3	11.6	6.3	3.9	2.6	2.0	1.7	12.0	6.4	3.8	2.5	1.7	1.4	8	
10.9	6.4	4.3	3.3	2.8	2.3	11.3	6.2	3.8	2.6	2.0	1.7	11.8	6.3	3.7	2.4	1.7	1.4	10	
73.2	30.7	17.2	11.5	8.2	6.2	65.0	24.8	14.3	8.6	5.8	4.2	56.2	20.4	11.2	7.2	5.9	3.4	2	SSI
43.0	18.4	10.9	7.4	5.7	3.8	38.2	15.6	8.6	5.4	3.7	3.0	34.7	13.6	7.3	4.5	3.2	2.7	4	
34.8	15.5	9.0	5.8	4.3	3.7	31.2	13.2	7.2	4.5	3.2	2.7	29.1	11.9	6.4	3.9	3.0	2.5	6	
30.8	14.3	8.3	5.4	3.9	3.2	28.0	12.2	6.7	4.2	3.1	2.6	26.5	11.3	6.1	3.7	2.9	2.4	8	
28.3	13.6	7.9	5.1	3.7	3.1	26.0	11.7	6.5	4.1	3.1	2.6	25.4	10.9	5.9	3.6	2.9	2.4	10	
95.1	43.0	26.1	18.1	13.5	10.7	83.7	33.8	20.1	13.1	9.1	6.8	71.4	27.2	15.5	10.2	7.7	5.4	2	AB
50.7	23.4	14.5	9.8	7.8	5.5	44.2	19.3	11.1	7.2	5.0	4.3	39.3	16.4	9.1	5.7	4.4	3.8	4	
38.8	18.5	11.2	7.5	5.4	4.5	34.2	15.4	8.8	5.6	4.4	3.8	31.4	13.7	7.6	4.9	4.0	3.5	6	
33.7	16.7	10.2	6.8	4.9	4.3	30.1	14.1	8.0	5.1	4.2	3.6	28.2	12.8	7.1	4.7	3.9	3.4	8	
30.5	15.8	9.7	6.5	4.8	4.2	27.7	13.4	7.7	4.9	4.1	3.5	27.1	12.4	6.9	4.6	3.9	3.3	10	
34.8	13.4	6.6	4.2	2.9	2.1	27.8	9.2	4.4	2.6	1.7	1.2	17.7	5.2	2.5	1.5	1.0	0.7	2	B2
51.2	18.9	9.6	5.5	3.5	2.8	43.5	15.0	7.7	4.4	2.8	2.1	34.0	11.2	5.8	3.4	2.3	1.7	4	
75.3	33.2	16.5	8.8	6.4	5.1	69.2	29.0	15.4	8.8	5.9	4.7	61.7	24.6	13.3	8.0	5.4	4.4	6	
90.7	51.0	27.1	15.5	11.2	8.7	88.3	47.8	27.7	16.3	11.7	9.2	85.9	43.9	25.6	16.2	11.5	9.2	8	
76.2	64.6	39.7	24.9	18.0	13.8	81.2	64.3	42.5	26.7	20.4	16.1	89.2	61.8	40.9	27.6	20.5	16.8	10	
8.2	3.7	2.1	1.5	1.1	0.9	6.8	2.8	1.7	1.1	0.8	0.6	4.7	1.7	1.0	0.7	0.4	0.3	2	PM
7.2	2.9	1.6	1.0	0.7	0.5	6.1	2.4	1.4	0.9	0.6	0.5	4.9	1.9	1.1	0.7	0.5	0.3	4	
8.0	3.5	1.9	1.1	0.8	0.7	7.1	3.1	1.8	1.1	0.9	0.7	6.3	2.7	1.6	1.1	0.8	0.6	6	
8.4	4.3	2.3	1.4	1.1	0.9	7.7	3.9	2.3	1.5	1.2	1.0	7.2	3.5	2.2	1.5	1.2	0.9	8	
7.3	4.8	2.8	1.8	1.4	1.1	7.0	4.3	2.8	1.8	1.5	1.3	6.6	3.9	2.5	1.9	1.4	1.1	10	
5.0	1.9	1.0	0.6	0.4	0.3	4.0	1.3	0.6	0.4	0.3	0.2	2.5	0.7	0.4	0.2	0.1	0.1	2	PV
7.3	2.7	1.4	0.8	0.5	0.4	6.2	2.1	1.1	0.6	0.4	0.3	4.9	1.6	0.8	0.5	0.3	0.2	4	
10.8	4.8	2.4	1.3	0.9	0.7	9.9	4.1	2.2	1.3	0.9	0.7	8.8	3.5	1.9	1.1	0.8	0.6	6	
13.0	7.3	3.9	2.2	1.6	1.2	12.7	6.9	4.0	2.3	1.7	1.3	12.3	6.3	3.7	2.3	1.6	1.3	8	
10.9	9.3	5.7	3.6	2.6	2.0	11.6	9.2	6.1	3.8	2.9	2.3	12.8	8.9	5.9	4.0	2.9	2.4	10	
23.4	9.4	4.8	3.1	2.1	1.6	22.3	8.0	4.1	2.4	1.6	1.2	22.8	7.8	3.9	2.4	1.5	1.1	2	F2
22.3	9.0	4.8	2.9	1.9	1.5	22.2	8.3	4.3	2.6	1.6	1.3	23.4	8.7	4.5	2.7	1.8	1.4	4	
23.1	10.1	5.3	3.2	2.3	1.8	23.4	9.6	5.0	3.0	2.1	1.6	24.5	10.0	5.3	3.2	2.2	1.6	6	
22.9	10.9	5.9	3.6	2.7	2.1	23.5	10.4	5.6	3.4	2.4	1.8	23.4	10.7	5.7	3.5	2.4	1.8	8	
21.1	11.2	6.3	4.0	2.9	2.3	22.1	10.8	5.9	3.6	2.6	1.9	20.6	10.8	5.9	3.7	2.5	1.9	10	
5	10	15	20	25	30	5	10	15	20	25	30	5	10	15	20	25	30	SL/PH	COMP

S3 - SLAB

Table D8 MAPGA values for four-span SLAB bridges.

3.3	2.1	2.4	2.3	2.3	2.4	3.3	2.5	1.8	2.4	2.4	2.1	3.4	2.6	1.9	1.8	2.4	2.5	2	SSI
3.7	2.9	2.1	2.3	1.8	2.2	3.7	2.9	2.8	2.4	1.9	1.7	3.7	3.1	2.7	2.5	2.3	2.2	4	
3.4	2.9	2.3	1.8	1.8	2.0	3.5	2.9	2.7	2.4	2.2	2.1	3.4	2.8	2.7	2.5	2.4	2.3	6	
3.1	2.6	2.2	1.9	1.7	1.8	3.2	2.7	2.6	2.4	2.2	2.2	3.2	2.7	2.6	2.5	2.4	2.4	8	
2.7	2.5	2.1	1.9	1.7	1.8	2.8	2.6	2.5	2.3	2.2	2.2	3.0	2.6	2.6	2.4	2.4	2.4	10	
2.9	2.6	2.6	2.1	2.6	2.4	2.9	2.6	2.4	2.7	2.2	1.8	2.8	2.7	2.7	2.5	2.7	2.5	2	SS2
2.7	2.7	2.8	2.6	2.7	2.4	2.6	2.7	2.8	2.7	2.8	2.2	2.8	3.1	3.0	3.0	3.2	3.2	4	
2.9	2.9	2.9	2.6	2.4	2.2	2.9	3.0	2.9	3.0	3.2	3.2	3.2	3.3	3.1	3.3	3.5	3.5	6	
3.3	3.1	3.0	2.8	2.4	2.0	3.4	3.2	3.1	3.2	3.5	3.4	3.6	3.6	3.3	3.4	3.6	3.6	8	
3.4	3.3	3.2	2.7	2.5	2.0	3.6	3.5	3.2	3.3	3.5	3.5	3.7	3.8	3.4	3.5	3.7	3.7	10	
4.7	1.8	0.9	0.6	0.4	0.3	5.1	1.5	0.8	0.5	0.4	0.3	4.5	1.2	0.6	0.4	0.3	0.2	2	B1
2.3	0.8	0.5	0.3	0.3	0.2	2.4	0.8	0.5	0.3	0.2	0.2	2.3	0.7	0.4	0.2	0.2	0.2	4	
1.6	0.6	0.4	0.3	0.2	0.2	1.8	0.7	0.4	0.2	0.2	0.2	1.7	0.6	0.3	0.2	0.2	0.1	6	
1.3	0.6	0.3	0.2	0.2	0.2	1.5	0.6	0.3	0.2	0.2	0.1	1.5	0.6	0.3	0.2	0.2	0.1	8	
1.2	0.5	0.3	0.2	0.2	0.2	1.4	0.6	0.3	0.2	0.2	0.1	1.4	0.5	0.3	0.2	0.2	0.1	10	
15.4	8.9	6.1	4.1	2.9	2.1	14.5	7.7	4.8	3.5	2.4	1.7	13.9	7.3	4.2	2.9	2.3	1.7	2	F1
12.5	7.3	5.4	3.8	2.7	2.2	12.3	6.3	4.1	3.0	2.2	1.7	12.3	6.1	3.7	2.5	1.9	1.6	4	
10.7	6.4	4.7	3.6	2.8	2.3	10.9	5.7	3.7	2.7	2.2	1.8	11.2	5.6	3.4	2.3	1.8	1.5	6	
9.7	6.0	4.3	3.6	2.8	2.3	10.1	5.4	3.5	2.6	2.2	1.8	10.6	5.5	3.3	2.2	1.8	1.5	8	
9.2	5.7	4.2	3.6	2.8	2.3	9.7	5.3	3.3	2.6	2.2	1.8	10.3	5.4	3.2	2.1	1.8	1.5	10	
70.2	29.2	17.4	11.9	7.7	5.6	62.6	23.2	17.6	8.4	5.6	4.1	52.9	19.0	10.3	7.5	4.2	3.1	2	SSI
35.1	15.6	9.2	6.1	5.8	3.4	31.3	13.2	7.2	4.5	3.2	2.7	27.9	11.3	5.9	3.6	2.9	2.4	4	
26.2	12.2	7.0	4.7	3.5	3.1	23.6	10.4	5.6	3.5	2.8	2.4	22.2	9.3	4.9	3.3	2.6	2.2	6	
22.6	10.9	6.2	4.2	3.3	2.9	21.2	9.4	5.1	3.3	2.7	2.3	20.3	8.6	4.6	3.1	2.5	2.1	8	
20.9	10.2	5.8	3.9	3.2	2.8	19.8	8.9	4.8	3.2	2.6	2.2	19.3	8.3	4.4	3.1	2.5	2.1	10	
90.6	41.1	24.8	17.4	12.7	9.2	80.1	31.5	21.7	12.2	8.5	6.3	66.8	25.2	14.3	10.5	6.2	4.8	2	AB
41.9	20.0	12.4	8.3	6.0	4.8	36.7	16.5	9.4	6.1	4.6	3.9	31.9	13.7	7.5	4.8	4.0	3.4	4	
29.2	14.7	8.9	5.9	4.6	4.0	26.5	12.2	6.9	4.6	3.9	3.3	24.7	10.7	5.8	4.2	3.5	3.0	6	
25.2	12.8	7.7	5.1	4.3	3.7	23.4	10.8	6.1	4.4	3.6	3.1	22.3	9.7	5.3	4.1	3.4	2.9	8	
23.0	11.9	7.2	4.9	4.1	3.6	21.6	10.1	5.7	4.2	3.5	3.0	20.9	9.3	5.1	4.0	3.3	2.8	10	
34.2	10.8	6.1	3.6	2.4	1.7	27.3	8.0	4.1	2.4	1.6	1.1	16.8	4.7	2.2	1.4	0.9	0.6	2	B2
42.4	14.2	6.8	3.9	2.8	2.2	36.4	12.0	5.7	3.1	2.0	1.7	27.9	9.1	4.4	2.4	1.6	1.3	4	
58.1	21.8	9.4	6.0	4.7	3.8	55.0	21.3	9.7	5.4	4.0	3.2	49.3	18.9	9.1	5.0	3.7	2.9	6	
72.8	32.4	14.2	9.7	7.3	5.9	73.9	35.0	16.4	10.0	7.3	5.6	71.4	34.0	17.1	10.2	7.5	5.7	8	
73.1	43.7	21.7	14.8	10.9	8.6	76.4	49.4	25.3	16.6	12.1	9.2	80.5	50.7	28.1	17.8	13.3	10.2	10	
8.3	3.5	1.9	1.3	0.9	0.7	6.9	2.6	1.5	1.0	0.7	0.5	4.6	1.6	0.9	0.6	0.4	0.2	2	PM
5.9	2.2	1.2	0.7	0.5	0.4	5.1	1.9	1.0	0.6	0.5	0.4	4.0	1.6	0.9	0.5	0.4	0.3	4	
6.1	2.5	1.2	0.8	0.6	0.6	5.6	2.3	1.2	0.8	0.6	0.5	5.0	2.1	1.2	0.8	0.6	0.4	6	
6.6	2.9	1.4	1.0	0.8	0.7	6.3	2.9	1.5	1.1	0.8	0.7	5.9	2.8	1.6	1.1	0.9	0.6	8	
6.4	3.3	1.7	1.2	1.0	0.8	6.2	3.4	1.9	1.3	1.1	0.9	6.1	3.2	1.9	1.4	1.1	0.8	10	
4.9	1.6	0.9	0.5	0.3	0.2	3.9	1.1	0.6	0.3	0.2	0.2	2.4	0.7	0.3	0.2	0.1	0.1	2	PV
6.1	2.0	1.0	0.6	0.4	0.3	5.2	1.7	0.8	0.4	0.3	0.2	4.0	1.3	0.6	0.3	0.2	0.2	4	
8.3	3.1	1.3	0.9	0.7	0.5	7.9	3.1	1.4	0.8	0.6	0.5	7.1	2.7	1.3	0.7	0.5	0.4	6	
10.4	4.6	2.0	1.4	1.1	0.8	10.6	5.0	2.3	1.4	1.0	0.8	10.2	4.9	2.5	1.5	1.1	0.8	8	
10.5	6.3	3.1	2.1	1.6	1.2	10.9	7.1	3.6	2.4	1.7	1.3	11.5	7.3	4.0	2.5	1.9	1.5	10	
23.6	8.9	4.6	2.9	2.0	1.5	22.5	7.7	3.9	2.4	1.6	1.1	22.7	7.5	3.8	2.2	1.5	1.1	2	F2
20.2	7.8	4.0	2.5	1.8	1.4	20.3	7.5	3.8	2.2	1.5	1.2	21.5	8.1	4.1	2.4	1.7	1.3	4	
20.4	8.5	4.2	2.8	2.1	1.7	21.3	8.7	4.4	2.7	1.9	1.5	22.8	9.3	4.8	3.0	2.1	1.6	6	
20.5	9.4	4.8	3.2	2.4	1.9	21.7	9.5	5.0	3.2	2.3	1.7	22.9	10.1	5.3	3.4	2.4	1.8	8	
19.8	10.1	5.5	3.7	2.7	2.1	21.0	10.0	5.4	3.5	2.5	1.9	20.2	10.4	5.6	3.6	2.5	1.9	10	
5	10	15	20	25	30	5	10	15	20	25	30	5	10	15	20	25	30	SL/PH	COMP

S4 - SLAB

## *Appendix E: Detailed description of portfolio bridges*

Table E1 Notations for Table E2-E31.

<b><i>Notation</i></b>	
SS.E	Superstructure (SS) material Young modulus [GPa]
SS.G	SS material shear modulus [GPa]
SS.A	SS cross-sectional area [m <sup>2</sup> ]
SS.J	SS torsional inertia [m <sup>3</sup> ]
SS.IY	SS inertia for the horizontal axis [m <sup>4</sup> ]
SS.IZ	SS inertia for the vertical axis [m <sup>4</sup> ]
P.A/PC.A	Pier/cap beam dimension in the transverse direction [m]
P.B/PC.B	Pier/cap beam dimension in the longitudinal direction [m]
P.RO_S/PC.RO_S	Pier/cap beam longitudinal reinforcement ratio [-]
P.S_FI/PC.S_FI	Pier/cap beam stirrup diameter [mm]
P.S_W/PC.S_W	Pier/cap beam stirrup distance [m]
P.EC/PC.EC	Pier/cap beam concrete Young modulus [GPa]
P.GC/PC.GC	Pier/cap beam concrete shear modulus [GPa]
P.FC/PC.FC	Pier/cap beam concrete compressive strength [MPa]
P.FY/PC.FY	Pier/cap beam reinforcing steel yielding strength [MPa]
P.ES/PC.ES	Pier/cap beam reinforcing steel Young modulus [GPa]
B.M1-M7	Dimensions of the bearings [m]
B.FY	Bearing yielding strength [kN]
B.K0	Bearing initial stiffness [kN/mm]
B.K1	Bearing post-yield stiffness [kN/mm]
B.RDX	Calculated bearing capacity in the longitudinal direction [kN]
B.RDY	Calculated bearing capacity in the transverse direction [kN]
F.A	Shallow foundation/pile cap dimension (transverse direction) [m]
F.B	Shallow foundation/pile cap dimension (longitudinal direction) [m]
F.M	Shallow foundation/pile cap height [m]
F.NX	Number of piles (longitudinal direction)
F.NY	Number of piles (transverse direction)
F.L	Pile length [m]
F.AK1	Abutment foundation stiffness (K <sub>x</sub> ) [N/m]
F.AK2	Abutment foundation stiffness (K <sub>y</sub> ) [N/m]
F.AK3	Abutment foundation stiffness (K <sub>z</sub> ) [N/m]
F.AK4	Abutment foundation stiffness (K <sub>xx</sub> ) [Nm/rad]
F.AK5	Abutment foundation stiffness (K <sub>yy</sub> ) [Nm/rad]
F.AK6	Abutment foundation stiffness (K <sub>zz</sub> ) [Nm/rad]
F.PK1	Pier foundation stiffness (K <sub>x</sub> ) [N/m]
F.PK2	Pier foundation stiffness (K <sub>y</sub> ) [N/m]
F.PK3	Pier foundation stiffness (K <sub>z</sub> ) [N/m]
F.PK4	Pier foundation stiffness (K <sub>xx</sub> ) [Nm/rad]
F.PK5	Pier foundation stiffness (K <sub>yy</sub> ) [Nm/rad]
F.PK6	Pier foundation stiffness (K <sub>zz</sub> ) [Nm/rad]

Table E2 Description of BR01 bridge.

<i>Example Bridge #01</i>				
Bridge Name	x			
Year of construction	2007			
Coordinates	x			
Name of road	M0			
<b>Global geometry</b>				
Superstructure type	SS.TYPE	Pre-cast beams - integrated		
Mechanical system	SS.SYSTEM	Continuous girder		
No. of spans	SS.NO_SPAN	2		
Span lengths [m]	SS.SPAN_L	25	25	
Deck width [m]	SS.B1	10.2		
Pier height [m]	P.H	5.5		
Pier number (trans. direction)	P.NO_PIER	3		
Pier distance (trans. dir.) [m]	P.DIST	8		
Skew angle [°]	SS.SKEW	70		
<b>Superstructure</b>				
Material	SS.E, SS.G	35.0	14.6	
Cross-section	SS.A,SS.J,SS.IY,SS.IZ	5.601	0.150	0.721 49.984
Height [m]	SS.HT	1.10		
Height of centroid [m]	SS.H2	0.65		
Bearing distance [m]	SS.B2	10.2		
Lineweight [kg/m]	SS.W	18275		
<b>Piers</b>				
Cross-section	P.A, P.B	0.8	0.8	
Reinforcement	P.RO_S, P.S_FI, P.S_W	1.000	10	0.1
Material	P.EC,P.GC,P.FC,P.FY,P.ES	34.0	14.2	35 500 200
<b>Bearings/joints</b>				
Type	B.TYPE	Monolithic joint		
Dimensions	B.M1, B.M2, B.M3	-		
Material	B.FY, B.K0, B.K1	-	-	-
Capacity	B.RDX, B.RDY	-	-	
Seat length [m]	B.SEAT	0.6		
Fix bearing positions	B.NFIX	All monolithic		
<b>Pier cap beam</b>				
Cross-section	PC.A, PC.B	1.6	1.0	
Reinforcement	PC.RO_S, PC.S_FI, PC.S_W	-	-	-
Material	PC.EC,PC.GC,PC.FC,PC.FY,PC.ES	-	-	- - -
<b>Foundation</b>				
Type	F.TYPE	Pile foundation		
Dimensions of shallow found.	F.A, F.B, F.M	-	-	
Pile foundation layout	F.A, F.B, F.NY, F.NX, F.L	14.4	0	4 1 13
Found. stiffness (abutment)	F.AK1-F.AK6	6.1E9	6.1E9	5.3E8 2.1E10 1.2E10 1.0E13
Found. stiffness (pier)	F.PK1-F.PK6	6.1E9	6.1E9	5.8E8 2.1E10 1.2E10 1.0E13
<b>Notes</b>				
Circular piers D = 80 cm with 16 $\phi$ 20 rebars. SS-SBS joint shear reinforcement: ABUTMENT - $\phi$ 16/15; PIER - 2 $\phi$ 16/15.				
Piles: ABUTMENT - 1x4 (3200 kN); PIER - 1x4 (3500 kN).				

Table E3 Description of BR02 bridge.

<b>Example Bridge #02</b>					
Bridge Name	x				
Year of construction	2005				
Coordinates	x				
Name of road	M0				
<b>Global geometry</b>					
Superstructure type	SS.TYPE	Pre-cast beams - integrate			
Mechanical system	SS.SYSTEM	Continuous girder			
No. of spans	SS.NO_SPAN	2			
Span lengths [m]	SS.SPAN_L	25 25			
Deck width [m]	SS.B1	18			
Pier height [m]	P.H	8			
Pier number (trans. direction)	P.NO_PIER	5			
Pier distance (trans. dir.) [m]	P.DIST	16.2			
Skew angle [°]	SS.SKEW	70			
<b>Superstructure</b>					
Material	SS.E, SS.G	35.0 14.6			
Cross-section	SS.A,SS.J,SS.IY,SS.IZ	9.721 0.240 2.267 259			
Height [m]	SS.HT	1.40			
Height of centroid [m]	SS.H2	0.85			
Bearing distance [m]	SS.B2	18.0			
Lineweight [kg/m]	SS.W	32700			
<b>Piers</b>					
Cross-section	P.A, P.B	0.8 0.8			
Reinforcement	P.RO_S, P.S_FI, P.S_W	2.450 10 0.1			
Material	P.EC,P.GC,P.FC,P.FY,P.ES	34.0 14.2 35 500 200			
<b>Bearings/joints</b>					
Type	B.TYPE	Monolithic joint			
Dimensions	B.M1, B.M2, B.M3	-			
Material	B.FY, B.K0, B.K1	- - -			
Capacity	B.RDX, B.RDY	- -			
Seat length [m]	B.SEAT	0.6			
Fix bearing positions	B.NFIX	All monolithic			
<b>Pier cap beam</b>					
Cross-section	PC.A, PC.B	1.6 1.0			
Reinforcement	PC.RO_S, PC.S_FI, PC.S_W	- - -			
Material	PC.EC,PC.GC,PC.FC,PC.FY,PC.ES	- - - - -			
<b>Foundation</b>					
Type	F.TYPE	Pile foundation			
Dimensions of shallow found.	F.A, F.B, F.M	- -			
Pile foundation layout	F.A, F.B, F.NY, F.NX, F.L	19 0 7 1 18			
Found. stiffness (abutment)	F.AK1-F.AK6	9.2E9 9.2E9 8.4E8 4.0E10 7.9E9 1.0E13			
Found. stiffness (pier)	F.PK1-F.PK6	8.9E9 8.9E9 1.1E9 5.0E10 1.2E10 1.0E13			
<b>Notes</b>					
Circular piers D = 80 cm with 20φ28 rebars. SS-SBS joint shear reinforcement: ABUTMENT - φ16/15; PIER - 2φ16/15. Piles: ABUTMENT - 1x9 (1500 kN); PIER - 1x7 (3000 kN).					

Table E4 Description of BR03 bridge.

<b>Example Bridge #03</b>						
Bridge Name	x					
Year of construction	2008					
Coordinates	x					
Name of road	M31					
<b>Global geometry</b>						
Superstructure type	SS.TYPE	Pre-cast beams - integrated				
Mechanical system	SS.SYSTEM	Continuous girder				
No. of spans	SS.NO_SPAN	3				
Span lengths [m]	SS.SPAN_L	25	30	25		
Deck width [m]	SS.B1	14				
Pier height [m]	P.H	5.5				
Pier number (trans. direction)	P.NO_PIER	4				
Pier distance (trans. dir.) [m]	P.DIST	10.8				
Skew angle [°]	SS.SKEW	90				
<b>Superstructure</b>						
Material	SS.E, SS.G	35.0	14.6			
Cross-section	SS.A,SS.J,SS.IY,SS.IZ	9.004	0.370	1.132	133.7	
Height [m]	SS.HT	1.20				
Height of centroid [m]	SS.H2	0.75				
Bearing distance [m]	SS.B2	14.0				
Lineweight [kg/m]	SS.W	32200				
<b>Piers</b>						
Cross-section	P.A, P.B	0.9	0.6			
Reinforcement	P.RO_S, P.S_FI, P.S_W	0.820	12	0.2		
Material	P.EC,P.GC,P.FC,P.FY,P.ES	34.0	14.2	35	500	200
<b>Bearings/joints</b>						
Type	B.TYPE	Monolithic joint				
Dimensions	B.M1, B.M2, B.M3	-				
Material	B.FY, B.K0, B.K1	-				
Capacity	B.RDX, B.RDY	-				
Seat length [m]	B.SEAT	0.4				
Fix bearing positions	B.NFIX	All monolithic				
<b>Pier cap beam</b>						
Cross-section	PC.A, PC.B	1.6	0.6			
Reinforcement	PC.RO_S, PC.S_FI, PC.S_W	-				
Material	PC.EC,PC.GC,PC.FC,PC.FY,PC.ES	-				
<b>Foundation</b>						
Type	F.TYPE	Pile foundation				
Dimensions of shallow found.	F.A, F.B, F.M	-				
Pile foundation layout	F.A, F.B, F.NY, F.NX, F.L	9.6	0	5	2	11
Found. stiffness (abutment)	F.AK1-F.AK6	1.0E10	1.0E10	1.3E9	2.3E10	8.8E9 1.0E13
Found. stiffness (pier)	F.PK1-F.PK6	1.0E10	1.0E10	1.4E9	2.5E10	8.8E9 1.0E13
<b>Notes</b>						
Piers with 14 φ20 rebars. SS-SBS joint shear reinforcement: ABUTMENT - φ16/20; PIER - 2φ16/15. Piles: ABUTMENT - 1x5 (2000 kN); PIER - 2x5 (2300 kN).						

Table E5 Description of BR04 bridge.

<b>Example Bridge #04</b>						
Bridge Name	x					
Year of construction	2015					
Coordinates	x					
Name of road	M35					
<b>Global geometry</b>						
Superstructure type	SS.TYPE	Pre-cast beams - integrated				
Mechanical system	SS.SYSTEM	Continuous girder				
No. of spans	SS.NO_SPAN	3				
Span lengths [m]	SS.SPAN_L	18	30	18		
Deck width [m]	SS.B1	14				
Pier height [m]	P.H	9				
Pier number (trans. direction)	P.NO_PIER	3				
Pier distance (trans. dir.) [m]	P.DIST	10.8				
Skew angle [°]	SS.SKEW	76				
<b>Superstructure</b>						
Material	SS.E, SS.G	35.0	14.6			
Cross-section	SS.A,SS.J,SS.IY,SS.IZ	7.903	0.197	1.849	#####	
Height [m]	SS.HT	1.40				
Height of centroid [m]	SS.H2	0.90				
Bearing distance [m]	SS.B2	14.0				
Lineweight [kg/m]	SS.W	28950				
<b>Piers</b>						
Cross-section	P.A, P.B	0.9	0.6			
Reinforcement	P.RO_S, P.S_FI, P.S_W	1.160	16	0.15		
Material	P.EC,P.GC,P.FC,P.FY,P.ES	34.0	14.2	35	500	200
<b>Bearings/joints</b>						
Type	B.TYPE	Monolithic joint				
Dimensions	B.M1, B.M2, B.M3	-				
Material	B.FY, B.K0, B.K1	-				
Capacity	B.RDX, B.RDY	-				
Seat length [m]	B.SEAT	0.45				
Fix bearing positions	B.NFIX	All monolithic				
<b>Pier cap beam</b>						
Cross-section	PC.A, PC.B	1.3	0.8			
Reinforcement	PC.RO_S, PC.S_FI, PC.S_W	-				
Material	PC.EC,PC.GC,PC.FC,PC.FY,PC.ES	-				
<b>Foundation</b>						
Type	F.TYPE	Pile foundation				
Dimensions of shallow found.	F.A, F.B, F.M	-				
Pile foundation layout	F.A, F.B, F.NY, F.NX, F.L	12	2.4	6	2	15
Found. stiffness (abutment)	F.AK1-F.AK6	6.1E9	6.1E9	1.0E13	2.4E10	5.3E9 1.0E13
Found. stiffness (pier)	F.PK1-F.PK6	1.2E10	1.2E10	1.0E13	4.8E10	1.4E10 1.0E13
<b>Notes</b>						
Piers with 20 $\phi$ 20 rebars. SS-SBS joint shear reinforcement: ABUTMENT - $\phi$ 16/15; PIER - 2 $\phi$ 16/15. Piles: ABUTMENT - 1x6 (3000 kN); PIER - 2x6 (3000 kN).						

Table E6 Description of BR05 bridge.

<b>Example Bridge #05</b>					
Bridge Name	x				
Year of construction	2014				
Coordinates	x				
Name of road	M3				
<b>Global geometry</b>					
Superstructure type	SS.TYPE	Pre-cast beams - integrated			
Mechanical system	SS.SYSTEM	Continuous girder			
No. of spans	SS.NO_SPAN	4			
Span lengths [m]	SS.SPAN_L	13	18	18	13
Deck width [m]	SS.B1	10			
Pier height [m]	P.H	5.5			
Pier number (trans. direction)	P.NO_PIER	3			
Pier distance (trans. dir.) [m]	P.DIST	8.4			
Skew angle [°]	SS.SKEW	70			
<b>Superstructure</b>					
Material	SS.E, SS.G	35.0	14.6		
Cross-section	SS.A,SS.J,SS.IY,SS.IZ	4.622	0.118	0.588	38.902
Height [m]	SS.HT	1.10			
Height of centroid [m]	SS.H2	0.65			
Bearing distance [m]	SS.B2	10.0			
Lineweight [kg/m]	SS.W	17745			
<b>Piers</b>					
Cross-section	P.A, P.B	0.9	0.6		
Reinforcement	P.RO_S, P.S_FI, P.S_W	1.050	12	0.15	
Material	P.EC,P.GC,P.FC,P.FY,P.ES	34.0	14.2	35	500 200
<b>Bearings/joints</b>					
Type	B.TYPE	Monolithic joint			
Dimensions	B.M1, B.M2, B.M3	-			
Material	B.FY, B.K0, B.K1	-			
Capacity	B.RDX, B.RDY	-			
Seat length [m]	B.SEAT	0.7			
Fix bearing positions	B.NFIX	All monolithic			
<b>Pier cap beam</b>					
Cross-section	PC.A, PC.B	1.7	0.8		
Reinforcement	PC.RO_S, PC.S_FI, PC.S_W	-			
Material	PC.EC,PC.GC,PC.FC,PC.FY,PC.ES	-			
<b>Foundation</b>					
Type	F.TYPE	Pile foundation			
Dimensions of shallow found.	F.A, F.B, F.M	-			
Pile foundation layout	F.A, F.B, F.NY, F.NX, F.L	16.8	0	7	1 11
Found. stiffness (abutment)	F.AK1-F.AK6	5.1E9	5.1E9	1.0E13	8.0E9 4.4E9 1.0E13
Found. stiffness (pier)	F.PK1-F.PK6	7.1E9	7.1E9	1.0E13	1.8E10 6.2E9 1.0E13
<b>Notes</b>					
Piers with 18 φ20 rebars. SS-SBS joint shear reinforcement: ABUTMENT - φ16/15; PIER - 2φ16/15. Piles: ABUTMENT - 1x5 (1000 kN); PIER - 1x7 (1200 kN).					

Table E7 Description of BR06 bridge.

<b>Example Bridge #06</b>					
Bridge Name	x				
Year of construction	2015				
Coordinates	x				
Name of road	M35				
<b>Global geometry</b>					
Superstructure type	SS.TYPE	Pre-cast beams - integrated			
Mechanical system	SS.SYSTEM	Continuous girder			
No. of spans	SS.NO_SPAN	4			
Span lengths [m]	SS.SPAN_L	15	17.5	17.5	15
Deck width [m]	SS.B1	15			
Pier height [m]	P.H	7.5			
Pier number (trans. direction)	P.NO_PIER	4			
Pier distance (trans. dir.) [m]	P.DIST	12.6			
Skew angle [°]	SS.SKEW	70			
<b>Superstructure</b>					
Material	SS.E, SS.G	35.0	14.6		
Cross-section	SS.A,SS.J,SS.IY,SS.IZ	6.158	0.151	0.768	#####
Height [m]	SS.HT	1.10			
Height of centroid [m]	SS.H2	0.70			
Bearing distance [m]	SS.B2	15.0			
Lineweight [kg/m]	SS.W	24635			
<b>Piers</b>					
Cross-section	P.A, P.B	0.9	0.6		
Reinforcement	P.RO_S, P.S_FI, P.S_W	1.050	12	0.15	
Material	P.EC,P.GC,P.FC,P.FY,P.ES	34.0	14.2	35	500 200
<b>Bearings/joints</b>					
Type	B.TYPE	Monolithic joint			
Dimensions	B.M1, B.M2, B.M3	-			
Material	B.FY, B.K0, B.K1	-			
Capacity	B.RDX, B.RDY	-			
Seat length [m]	B.SEAT	0.7			
Fix bearing positions	B.NFIX	All monolithic			
<b>Pier cap beam</b>					
Cross-section	PC.A, PC.B	1.6	0.8		
Reinforcement	PC.RO_S, PC.S_FI, PC.S_W	-	-	-	
Material	PC.EC,PC.GC,PC.FC,PC.FY,PC.ES	-	-	-	-
<b>Foundation</b>					
Type	F.TYPE	Pile foundation			
Dimensions of shallow found.	F.A, F.B, F.M	-			
Pile foundation layout	F.A, F.B, F.NY, F.NX, F.L	12	0	6	1 17
Found. stiffness (abutment)	F.AK1-F.AK6	5.1E9	5.1E9	1.0E13	8.7E9 4.4E9 1.0E13
Found. stiffness (pier)	F.PK1-F.PK6	6.1E9	6.1E9	1.0E13	1.3E10 5.3E9 1.0E13
<b>Notes</b>					
Piers with 18 $\phi$ 20 rebars. SS-SBS joint shear reinforcement: ABUTMENT - $\phi$ 20/15; PIER - 2 $\phi$ 16/15. Piles: ABUTMENT - 1x5 (1000 kN); PIER - 1x6 (1200 kN).					

Table E8 Description of BR07 bridge.

<b>Example Bridge #07</b>						
Bridge Name	x					
Year of construction	2005					
Coordinates	x					
Name of road	M7					
<b>Global geometry</b>						
Superstructure type	SS.TYPE	Pre-cast beams - integrated				
Mechanical system	SS.SYSTEM	Continuous girder				
No. of spans	SS.NO_SPAN	4				
Span lengths [m]	SS.SPAN_L	19	22	22	19	
Deck width [m]	SS.B1	9				
Pier height [m]	P.H	8				
Pier number (trans. direction)	P.NO_PIER	2				
Pier distance (trans. dir.) [m]	P.DIST	5.2				
Skew angle [°]	SS.SKEW	90				
<b>Superstructure</b>						
Material	SS.E, SS.G	35.0	14.6			
Cross-section	SS.A,SS.J,SS.IY,SS.IZ	3.638	0.105	0.397	22.179	
Height [m]	SS.HT	1.10				
Height of centroid [m]	SS.H2	0.70				
Bearing distance [m]	SS.B2	9.0				
Lineweight [kg/m]	SS.W	14710				
<b>Piers</b>						
Cross-section	P.A, P.B	0.9	0.6			
Reinforcement	P.RO_S, P.S_FI, P.S_W	3.000	12	0.2		
Material	P.EC,P.GC,P.FC,P.FY,P.ES	34.0	14.2	35	500	200
<b>Bearings/joints</b>						
Type	B.TYPE	Monolithic joint				
Dimensions	B.M1, B.M2, B.M3	-				
Material	B.FY, B.K0, B.K1	-				
Capacity	B.RDX, B.RDY	-				
Seat length [m]	B.SEAT	0.6				
Fix bearing positions	B.NFIX	All monolithic				
<b>Pier cap beam</b>						
Cross-section	PC.A, PC.B	1.6	0.8			
Reinforcement	PC.RO_S, PC.S_FI, PC.S_W	-	-	-		
Material	PC.EC,PC.GC,PC.FC,PC.FY,PC.ES	-	-	-	-	-
<b>Foundation</b>						
Type	F.TYPE	Pile foundation				
Dimensions of shallow found.	F.A, F.B, F.M	-	-			
Pile foundation layout	F.A, F.B, F.NY, F.NX, F.L	7.2	2.4	4	2	17
Found. stiffness (abutment)	F.AK1-F.AK6	4.1E9	4.1E9	1.0E13	8.0E9	3.5E9 1.0E13
Found. stiffness (pier)	F.PK1-F.PK6	8.2E9	8.2E9	1.0E13	1.4E10	8.4E9 1.0E13
<b>Notes</b>						
Piers with 26 $\phi$ 28 rebars. SS-SBS joint shear reinforcement: ABUTMENT - $\phi$ 20/20; PIER - 2 $\phi$ 16/20. Piles: ABUTMENT - 1x4 (2500 kN); PIER - 2x4 (1900 kN).						

Table E9 Description of BR08 bridge.

<b>Example Bridge #08</b>						
Bridge Name	x					
Year of construction	2006					
Coordinates	x					
Name of road	M0					
<b>Global geometry</b>						
Superstructure type	SS.TYPE	Pre-cast beams - integrated				
Mechanical system	SS.SYSTEM	Continuous girder				
No. of spans	SS.NO_SPAN	6				
Span lengths [m]	SS.SPAN_L	11	15	17	17	15 11
Deck width [m]	SS.B1	12				
Pier height [m]	P.H	6				
Pier number (trans. direction)	P.NO_PIER	3				
Pier distance (trans. dir.) [m]	P.DIST	8.3				
Skew angle [°]	SS.SKEW	90				
<b>Superstructure</b>						
Material	SS.E, SS.G	35.0	14.6			
Cross-section	SS.A,SS.J,SS.IY,SS.IZ	5.208	0.900	0.423	60.145	
Height [m]	SS.HT	0.90				
Height of centroid [m]	SS.H2	0.55				
Bearing distance [m]	SS.B2	12.0				
Lineweight [kg/m]	SS.W	20232				
<b>Piers</b>						
Cross-section	P.A, P.B	0.8	0.8			
Reinforcement	P.RO_S, P.S_FI, P.S_W	1.000	10	0.1		
Material	P.EC,P.GC,P.FC,P.FY,P.ES	34.0	14.2	35	500	200
<b>Bearings/joints</b>						
Type	B.TYPE	Monolithic joint				
Dimensions	B.M1, B.M2, B.M3	-				
Material	B.FY, B.K0, B.K1	-				
Capacity	B.RDX, B.RDY	-				
Seat length [m]	B.SEAT	0.4				
Fix bearing positions	B.NFIX	All monolithic				
<b>Pier cap beam</b>						
Cross-section	PC.A, PC.B	1.3	0.8			
Reinforcement	PC.RO_S, PC.S_FI, PC.S_W	-	-	-		
Material	PC.EC,PC.GC,PC.FC,PC.FY,PC.ES	-	-	-	-	-
<b>Foundation</b>						
Type	F.TYPE	Pile foundation				
Dimensions of shallow found.	F.A, F.B, F.M	-	-			
Pile foundation layout	F.A, F.B, F.NY, F.NX, F.L	9.6	0	5	1	17
Found. stiffness (abutment)	F.AK1-F.AK6	4.1E9	4.1E9	1.0E13	5.7E9	3.5E9 1.0E13
Found. stiffness (pier)	F.PK1-F.PK6	5.1E9	5.1E9	1.0E13	1.1E10	4.4E9 1.0E13
<b>Notes</b>						
Piers D = 80 cm with 16 $\phi$ 20 rebars. SS-SBS joint shear reinforcement: ABUTMENT - $\phi$ 16/20; PIER - 2 $\phi$ 16/20. Piles: ABUTMENT - 1x4 (1200 kN); PIER - 1x5 (1700 kN).						

Table E10 Description of BR09 bridge.

<b>Example Bridge #09</b>					
Bridge Name	x				
Year of construction	2008				
Coordinates	x				
Name of road	M43				
<b>Global geometry</b>					
Superstructure type	SS.TYPE	Pre-cast beams - non-integrated			
Mechanical system	SS.SYSTEM	Continuous girder			
No. of spans	SS.NO_SPAN	3			
Span lengths [m]	SS.SPAN_L	35	45	35	
Deck width [m]	SS.B1	14			
Pier height [m]	P.H	4.5			
Pier number (trans. direction)	P.NO_PIER	4			
Pier distance (trans. dir.) [m]	P.DIST	12			
Skew angle [°]	SS.SKEW	60			
<b>Superstructure</b>					
Material	SS.E, SS.G	35.0	14.6		
Cross-section	SS.A,SS.J,SS.IY,SS.IZ	8.982	0.306	3.435	137.88
Height [m]	SS.HT	1.75			
Height of centroid [m]	SS.H2	1.00			
Bearing distance [m]	SS.B2	14.0			
Lineweight [kg/m]	SS.W	29795			
<b>Piers</b>					
Cross-section	P.A, P.B	1.2	1.2		
Reinforcement	P.RO_S, P.S_FI, P.S_W	0.868	12	0.2	
Material	P.EC,P.GC,P.FC,P.FY,P.ES	34.0	14.2	35	500 200
<b>Bearings/joints</b>					
Type	B.TYPE	Monolithic joint and rubber bearings			
Dimensions	B.M1, B.M2, B.M3	400	500	180	
Material	B.FY, B.K0, B.K1	-	-	-	
Capacity	B.RDX, B.RDY	-	-	-	
Seat length [m]	B.SEAT	0.95			
Fix bearing positions	B.NFIX	At the piers			
<b>Pier cap beam</b>					
Cross-section	PC.A, PC.B	2.4	1.0		
Reinforcement	PC.RO_S, PC.S_FI, PC.S_W	-	-	-	
Material	PC.EC,PC.GC,PC.FC,PC.FY,PC.ES	-	-	-	-
<b>Foundation</b>					
Type	F.TYPE	Pile foundation			
Dimensions of shallow found.	F.A, F.B, F.M	-	-		
Pile foundation layout	F.A, F.B, F.NY, F.NX, F.L	14.4	2.4	7	2 25
Found. stiffness (abutment)	F.AK1-F.AK6	1.0E10	1.0E10	1.0E13	2.7E10 1.1E10 1.0E13
Found. stiffness (pier)	F.PK1-F.PK6	1.4E10	1.4E10	1.0E13	6.3E10 1.6E10 1.0E13
<b>Notes</b>					
Piers D = 120 cm with 20 $\phi$ 25 rebars. SS-SBS joint: ABUTMENT - bearing with 73 mm movement capacity; PIER - 2 $\phi$ 16/20. Piles: ABUTMENT - 2x5 (2500 kN); PIER - 2x7 (2500 kN). Dilatation: at the abutments with 30 mm					

Table E11 Description of BR10 bridge.

<b>Example Bridge #10</b>		
Bridge Name	x	
Year of construction	2006	
Coordinates	x	
Name of road	M3	
<b>Global geometry</b>		
Superstructure type	SS.TYPE	Pre-cast beams - non-integrated
Mechanical system	SS.SYSTEM	Continuous girder
No. of spans	SS.NO_SPAN	5
Span lengths [m]	SS.SPAN_L	25 32 33 32 25
Deck width [m]	SS.B1	14
Pier height [m]	P.H	7
Pier number (trans. direction)	P.NO_PIER	4
Pier distance (trans. dir.) [m]	P.DIST	12.3
Skew angle [°]	SS.SKEW	60
<b>Superstructure</b>		
Material	SS.E, SS.G	35.0 14.6
Cross-section	SS.A,SS.J,SS.IY,SS.IZ	8.574 0.267 2.059 136.43
Height [m]	SS.HT	1.45
Height of centroid [m]	SS.H2	0.90
Bearing distance [m]	SS.B2	14.0
Lineweight [kg/m]	SS.W	29535
<b>Piers</b>		
Cross-section	P.A, P.B	1.2 1.2
Reinforcement	P.RO_S, P.S_FI, P.S_W	0.667 10 0.15
Material	P.EC,P.GC,P.FC,P.FY,P.ES	34.0 14.2 35 500 200
<b>Bearings/joints</b>		
Type	B.TYPE	Monolithic joint and rubber bearings
Dimensions	B.M1, B.M2, B.M3	400 500 180
Material	B.FY, B.K0, B.K1	- - -
Capacity	B.RDX, B.RDY	- -
Seat length [m]	B.SEAT	1
Fix bearing positions	B.NFIX	Two middle piers
<b>Pier cap beam</b>		
Cross-section	PC.A, PC.B	1.6 1.0
Reinforcement	PC.RO_S, PC.S_FI, PC.S_W	- - -
Material	PC.EC,PC.GC,PC.FC,PC.FY,PC.ES	- - - - -
<b>Foundation</b>		
Type	F.TYPE	Pile foundation
Dimensions of shallow found.	F.A, F.B, F.M	- -
Pile foundation layout	F.A, F.B, F.NY, F.NX, F.L	10.8 3.6 4 1 14
Found. stiffness (abutment)	F.AK1-F.AK6	8.2E9 8.2E9 1.0E13 1.9E10 9.4E9 1.0E13
Found. stiffness (pier)	F.PK1-F.PK6	6.1E9 6.1E9 1.0E13 2.6E10 1.2E10 1.0E13
<b>Notes</b>		
Piers D = 120 cm with 24 $\phi$ 20 rebars. SS-SBS joint: rubber bearing with 73 mm movement capacity; fix - 2 $\phi$ 16/10 shear reinforcement. Piles: ABUTMENT - 2x4 (3200 kN); PIER - 1x4 (5300 kN). Dilatation: at the abutments with 50 mm		

Table E12 Description of BR11 bridge.

<b>Example Bridge #11</b>						
Bridge Name	x					
Year of construction	2009					
Coordinates	x					
Name of road	M6					
<b>Global geometry</b>						
Superstructure type	SS.TYPE	Pre-cast beams - non-integrated				
Mechanical system	SS.SYSTEM	Continuous girder				
No. of spans	SS.NO_SPAN	6				
Span lengths [m]	SS.SPAN_L	30	45	45	45	30
Deck width [m]	SS.B1	14				
Pier height [m]	P.H	7				
Pier number (trans. direction)	P.NO_PIER	3				
Pier distance (trans. dir.) [m]	P.DIST	10.5				
Skew angle [°]	SS.SKEW	90				
<b>Superstructure</b>						
Material	SS.E, SS.G	35.0	14.6			
Cross-section	SS.A,SS.J,SS.IY,SS.IZ	9.414	0.325	3.615	142.63	
Height [m]	SS.HT	1.75				
Height of centroid [m]	SS.H2	1.00				
Bearing distance [m]	SS.B2	14.0				
Lineweight [kg/m]	SS.W	32155				
<b>Piers</b>						
Cross-section	P.A, P.B	1.2	1.2			
Reinforcement	P.RO_S, P.S_FI, P.S_W	1.040	12	0.1		
Material	P.EC,P.GC,P.FC,P.FY,P.ES	34.0	14.2	35	500	200
<b>Bearings/joints</b>						
Type	B.TYPE	Monolithic joint and rubber bearings				
Dimensions	B.M1, B.M2, B.M3	400	500	180		
Material	B.FY, B.K0, B.K1	-	-	-		
Capacity	B.RDX, B.RDY	-	-			
Seat length [m]	B.SEAT	1				
Fix bearing positions	B.NFIX	Three middle piers				
<b>Pier cap beam</b>						
Cross-section	PC.A, PC.B	1.6	1.0			
Reinforcement	PC.RO_S, PC.S_FI, PC.S_W	-	-	-		
Material	PC.EC,PC.GC,PC.FC,PC.FY,PC.ES	-	-	-	-	-
<b>Foundation</b>						
Type	F.TYPE	Pile foundation				
Dimensions of shallow found.	F.A, F.B, F.M	-	-			
Pile foundation layout	F.A, F.B, F.NY, F.NX, F.L	12	4.8	5	3	14
Found. stiffness (abutment)	F.AK1-F.AK6	1.0E10	1.0E10	1.0E13	2.7E10	1.1E10 1.0E13
Found. stiffness (pier)	F.PK1-F.PK6	1.5E10	1.5E10	1.0E13	4.0E10	2.2E10 1.0E13
<b>Notes</b>						
Piers D = 120 cm with 24 $\phi$ 25 rebars. SS-SBS joint: rubber bearing with 73 mm movement capacity; fix - 2 $\phi$ 16/10 shear reinforcement. Piles: ABUTMENT - 2x5 (2500 kN); PIER - 3x5 (2500 kN). Dilatation: at the abutments with 65 mm						

Table E13 Description of BR12 bridge.

<b>Example Bridge #12</b>					
Bridge Name	x				
Year of construction	2015				
Coordinates	x				
Name of road	M76				
<b>Global geometry</b>					
Superstructure type	SS.TYPE	Pre-cast beams - non-integrated			
Mechanical system	SS.SYSTEM	Continuous girder			
No. of spans	SS.NO_SPAN	7			
Span lengths [m]	SS.SPAN_L	20	5x24	20	
Deck width [m]	SS.B1	14			
Pier height [m]	P.H	7			
Pier number (trans. direction)	P.NO_PIER	4			
Pier distance (trans. dir.) [m]	P.DIST	10.8			
Skew angle [°]	SS.SKEW	90			
<b>Superstructure</b>					
Material	SS.E, SS.G	35.0	14.6		
Cross-section	SS.A,SS.J,SS.IY,SS.IZ	8.168	0.263	1.103	130.77
Height [m]	SS.HT	1.15			
Height of centroid [m]	SS.H2	0.65			
Bearing distance [m]	SS.B2	14.0			
Lineweight [kg/m]	SS.W	28850			
<b>Piers</b>					
Cross-section	P.A, P.B	0.9	0.9		
Reinforcement	P.RO_S, P.S_FI, P.S_W	1.086	12	0.2	
Material	P.EC,P.GC,P.FC,P.FY,P.ES	34.0	14.2	35	500 200
<b>Bearings/joints</b>					
Type	B.TYPE	Monolithic joint and rubber bearings			
Dimensions	B.M1, B.M2, B.M3	400	500	140	
Material	B.FY, B.K0, B.K1	-	-	-	
Capacity	B.RDX, B.RDY	-	-	-	
Seat length [m]	B.SEAT	0.55			
Fix bearing positions	B.NFIX	Two middle piers			
<b>Pier cap beam</b>					
Cross-section	PC.A, PC.B	1.4	0.8		
Reinforcement	PC.RO_S, PC.S_FI, PC.S_W	-	-	-	
Material	PC.EC,PC.GC,PC.FC,PC.FY,PC.ES	-	-	-	-
<b>Foundation</b>					
Type	F.TYPE	Pile foundation			
Dimensions of shallow found.	F.A, F.B, F.M	-	-	-	
Pile foundation layout	F.A, F.B, F.NY, F.NX, F.L	7.2	2.4	4	2 10
Found. stiffness (abutment)	F.AK1-F.AK6	8.2E9	8.2E9	1.0E13	1.6E10 8.9E9 1.0E13
Found. stiffness (pier)	F.PK1-F.PK6	8.2E9	8.2E9	1.0E13	1.8E10 9.2E9 1.0E13
<b>Notes</b>					
Piers with 28φ20 rebars. SS-SBS joint: rubber bearing with 65 mm movement capacity; fix - 2φ16/20 shear reinforcement. Piles: ABUTMENT - 2x4 (2500 kN); PIER - 2x4 (3000 kN). Dilatation: at the abutments with 50 mm					

Table E14 Description of BR13 bridge.

<b>Example Bridge #13</b>		
Bridge Name	x	
Year of construction	2009	
Coordinates	x	
Name of road	M31	
<b>Global geometry</b>		
Superstructure type	SS.TYPE	Cast in-situ concrete slab
Mechanical system	SS.SYSTEM	Continuous girder
No. of spans	SS.NO_SPAN	2
Span lengths [m]	SS.SPAN_L	25 25
Deck width [m]	SS.B1	9
Pier height [m]	P.H	8.5
Pier number (trans. direction)	P.NO_PIER	2
Pier distance (trans. dir.) [m]	P.DIST	3.6
Skew angle [°]	SS.SKEW	90
<b>Superstructure</b>		
Material	SS.E, SS.G	34.0 14.2
Cross-section	SS.A,SS.J,SS.IY,SS.IZ	6.343 4.214 1.550 22.84
Height [m]	SS.HT	1.55
Height of centroid [m]	SS.H2	0.85
Bearing distance [m]	SS.B2	3.6
Lineweight [kg/m]	SS.W	19650
<b>Piers</b>		
Cross-section	P.A, P.B	0.9 0.6
Reinforcement	P.RO_S, P.S_FI, P.S_W	2.000 12 0.15
Material	P.EC,P.GC,P.FC,P.FY,P.ES	34.0 14.2 35 500 200
<b>Bearings/joints</b>		
Type	B.TYPE	-
Dimensions	B.M1, B.M2, B.M3	- - -
Material	B.FY, B.K0, B.K1	- - -
Capacity	B.RDX, B.RDY	- -
Seat length [m]	B.SEAT	0.9
Fix bearing positions	B.NFIX	All monolithic
<b>Pier cap beam</b>		
Cross-section	PC.A, PC.B	None -
Reinforcement	PC.RO_S, PC.S_FI, PC.S_W	- - -
Material	PC.EC,PC.GC,PC.FC,PC.FY,PC.ES	- - - - -
<b>Foundation</b>		
Type	F.TYPE	Shallow foundation
Dimensions of shallow found.	F.A, F.B, F.M	AB: 8.75 2.80 P: 9.00 4.00
Pile foundation layout	F.A, F.B, F.NY, F.NX, F.L	- - - - -
Found. stiffness (abutment)	F.AK1-F.AK6	1.1E9 1.0E9 1.3E9 1.6E10 4.5E9 3.0E10
Found. stiffness (pier)	F.PK1-F.PK6	1.3E9 1.2E9 1.5E9 2.1E10 7.7E9 3.5E10
<b>Notes</b>		
Piers with 22φ25 rebars. SS-SBS joint: ABUTMENT: 16/10 shear reinforcement; PIER: longitudinal reinforcement + cast in-situ concrete. Shallow foundation: ABUTMENT: 8.75x2.8 m PIER: 9x4 m.		

Table E15 Description of BR14 bridge.

<b>Example Bridge #14</b>						
Bridge Name	x					
Year of construction	2009					
Coordinates	x					
Name of road	M31					
<b>Global geometry</b>						
Superstructure type	SS.TYPE	Cast in-situ concrete slab				
Mechanical system	SS.SYSTEM	Continuous girder				
No. of spans	SS.NO_SPAN	4				
Span lengths [m]	SS.SPAN_L	13	23	23	13	
Deck width [m]	SS.B1	15				
Pier height [m]	P.H	6				
Pier number (trans. direction)	P.NO_PIER	3				
Pier distance (trans. dir.) [m]	P.DIST	10				
Skew angle [°]	SS.SKEW	45				
<b>Superstructure</b>						
Material	SSE, SS.G	34.0	14.2			
Cross-section	SS.A,SS.J,SS.IY,SS.IZ	10.370	5.578	1.827	134.87	
Height [m]	SS.HT	1.35				
Height of centroid [m]	SS.H2	0.72				
Bearing distance [m]	SS.B2	10.0				
Lineweight [kg/m]	SS.W	34780				
<b>Piers</b>						
Cross-section	P.A, P.B	2.5	0.9			
Reinforcement	P.RO_S, P.S_FI, P.S_W	0.785	10	0.2		
Material	P.EC,P.GC,P.FC,P.FY,P.ES	34.0	14.2	35	500	200
<b>Bearings/joints</b>						
Type	B.TYPE	-				
Dimensions	B.M1, B.M2, B.M3	-	-	-		
Material	B.FY, B.K0, B.K1	-	-	-		
Capacity	B.RDX, B.RDY	-	-			
Seat length [m]	B.SEAT	1				
Fix bearing positions	B.NFIX	All monolithic				
<b>Pier cap beam</b>						
Cross-section	PC.A, PC.B	None	-			
Reinforcement	PC.RO_S, PC.S_FI, PC.S_W	-	-	-		
Material	PC.EC,PC.GC,PC.FC,PC.FY,PC.ES	-	-	-	-	-
<b>Foundation</b>						
Type	F.TYPE	Pile foundation				
Dimensions of shallow found.	F.A, F.B, F.M	-	-	-	-	-
Pile foundation layout	F.A, F.B, F.NY, F.NX, F.L	19.2	0	9	1	14
Found. stiffness (abutment)	F.AK1-F.AK6	5.1E9	5.1E9	1.0E13	1.2E10	4.4E9 1.0E13
Found. stiffness (pier)	F.PK1-F.PK6	9.2E9	9.2E9	1.0E13	5.1E10	7.9E9 1.0E13
<b>Notes</b>						
Piers with 3x12φ25 rebars. SS-SBS joint: ABUTMENT: 16/20 shear reinforcement; PIER: longitudinal reinforcement + cast in-situ concrete. Pile: Abutment: 1x5 (2000 kN); Pier: 1x9 (2000 kN).						

Table E16 Description of BR15 bridge.

<i>Example Bridge #15</i>						
Bridge Name	x					
Year of construction	2004					
Coordinates	x					
Name of road	M0					
<b>Global geometry</b>						
Superstructure type	SS.TYPE	Cast in-situ concrete slab				
Mechanical system	SS.SYSTEM	Continuous girder				
No. of spans	SS.NO_SPAN	4				
Span lengths [m]	SS.SPAN_L	12	22	22	12	
Deck width [m]	SS.B1	12				
Pier height [m]	P.H	6.5				
Pier number (trans. direction)	P.NO_PIER	2				
Pier distance (trans. dir.) [m]	P.DIST	7.6				
Skew angle [°]	SS.SKEW	80				
<b>Superstructure</b>						
Material	SS.E, SS.G	34.0	14.2			
Cross-section	SS.A,SS.J,SS.IY,SS.IZ	8.040	3.023	0.899	70.06	
Height [m]	SS.HT	1.15				
Height of centroid [m]	SS.H2	0.57				
Bearing distance [m]	SS.B2	7.6				
Lineweight [kg/m]	SS.W	26200				
<b>Piers</b>						
Cross-section	P.A, P.B	0.9	0.6			
Reinforcement	P.RO_S, P.S_FI, P.S_W	1.164	12	0.2		
Material	P.EC,P.GC,P.FC,P.FY,P.ES	34.0	14.2	35	500	200
<b>Bearings/joints</b>						
Type	B.TYPE	-				
Dimensions	B.M1, B.M2, B.M3	-	-	-		
Material	B.FY, B.K0, B.K1	-	-	-		
Capacity	B.RDX, B.RDY	-	-			
Seat length [m]	B.SEAT	1				
Fix bearing positions	B.NFIX	All monolithic				
<b>Pier cap beam</b>						
Cross-section	PC.A, PC.B	None	-			
Reinforcement	PC.RO_S, PC.S_FI, PC.S_W	-	-	-		
Material	PC.EC,PC.GC,PC.FC,PC.FY,PC.ES	-	-	-	-	-
<b>Foundation</b>						
Type	F.TYPE	Pile foundation				
Dimensions of shallow found.	F.A, F.B, F.M	-	-	-	-	-
Pile foundation layout	F.A, F.B, F.NY, F.NX, F.L	7.2	1.8	5	2	10
Found. stiffness (abutment)	F.AK1-F.AK6	6.1E9	6.1E9	1.0E13	2.0E10	3.0E9 1.0E13
Found. stiffness (pier)	F.PK1-F.PK6	7.7E9	7.7E9	1.0E13	1.3E10	4.9E9 1.0E13
<b>Notes</b>						
Piers with 20φ20 rebars. SS-SBS joint: ABUTMENT: 16/15 shear reinforcement; PIER: longitudinal reinforcement + cast in-situ concrete. Pile: Abutment: 1x8 (1500 kN); Pier: 2x5 (1700 kN).						

Table E17 Description of BR16 bridge.

Example Bridge #16							
Bridge Name	x						
Year of construction	2004						
Coordinates	x						
Name of road	M0						
<b>Global geometry</b>							
Superstructure type	SS.TYPE	Cast in-situ concrete slab					
Mechanical system	SS.SYSTEM	Continuous girder					
No. of spans	SS.NO_SPAN	6					
Span lengths [m]	SS.SPAN_L	12	14	18	18	14	12
Deck width [m]	SS.B1	13					
Pier height [m]	P.H	8					
Pier number (trans. direction)	P.NO_PIER	3					
Pier distance (trans. dir.) [m]	P.DIST	7.2					
Skew angle [°]	SS.SKEW	70					
<b>Superstructure</b>							
Material	SS.E, SS.G	34.0	14.2				
Cross-section	SS.A,SS.J,SS.IY,SS.IZ	8.556	2.511	0.765	88.14		
Height [m]	SS.HT	1.05					
Height of centroid [m]	SS.H2	0.55					
Bearing distance [m]	SS.B2	7.2					
Lineweight [kg/m]	SS.W	29050					
<b>Piers</b>							
Cross-section	P.A, P.B	0.6	0.6				
Reinforcement	P.RO_S, P.S_FI, P.S_W	2.780	10	0.1			
Material	P.EC,P.GC,P.FC,P.FY,P.ES	34.0	14.2	35	500	200	
<b>Bearings/joints</b>							
Type	B.TYPE	-					
Dimensions	B.M1, B.M2, B.M3	-	-	-			
Material	B.FY, B.K0, B.K1	-	-	-			
Capacity	B.RDX, B.RDY	-	-				
Seat length [m]	B.SEAT	1					
Fix bearing positions	B.NFIX	All monolithic					
<b>Pier cap beam</b>							
Cross-section	PC.A, PC.B	None	-				
Reinforcement	PC.RO_S, PC.S_FI, PC.S_W	-	-	-			
Material	PC.EC,PC.GC,PC.FC,PC.FY,PC.ES	-	-	-	-	-	
<b>Foundation</b>							
Type	F.TYPE	Pile foundation					
Dimensions of shallow found.	F.A, F.B, F.M	-	-	-	-	-	
Pile foundation layout	F.A, F.B, F.NY, F.NX, F.L	9.6	0	5	1	16	
Found. stiffness (abutment)	F.AK1-F.AK6	4.1E9	4.1E9	1.0E13	8.0E9	3.5E9 1.0E13	
Found. stiffness (pier)	F.PK1-F.PK6	5.1E9	5.1E9	1.0E13	1.4E10	4.4E9 1.0E13	
<b>Notes</b>							
D=0.6 m piers with 16φ25 rebars. SS-SBS joint: ABUTMENT: 20/20 shear reinforcement; PIER: longitudinal reinforcement + cast in-situ concrete. Pile: Abutment: 1x4 (2500 kN); Pier: 1x5 (2700 kN).							

Table E18 Description of BR17 bridge.

<i>Example Bridge #17</i>						
Bridge Name	x					
Year of construction	2010					
Coordinates	x					
Name of road	M0					
<b>Global geometry</b>						
Superstructure type	SS.TYPE	Reinforced concrete box girder				
Mechanical system	SS.SYSTEM	Continuous girder				
No. of spans	SS.NO_SPAN	5				
Span lengths [m]	SS.SPAN_L	34	34	34	34	34
Deck width [m]	SS.B1	11				
Pier height [m]	P.H	14				
Pier number (trans. direction)	P.NO_PIER	1				
Pier distance (trans. dir.) [m]	P.DIST	0				
Skew angle [°]	SS.SKEW	90				
<b>Superstructure</b>						
Material	SS.E, SS.G	34.0	14.2			
Cross-section	SS.A,SS.J,SS.IY,SS.IZ	6.683	13.380	6.110	47.19	
Height [m]	SS.HT	2.50				
Height of centroid [m]	SS.H2	1.50				
Bearing distance [m]	SS.B2	4.8				
Lineweight [kg/m]	SS.W	27800				
<b>Piers</b>						
Cross-section	P.A, P.B	6	2			
Reinforcement	P.RO_S, P.S_FI, P.S_W	0.5	16	0.2		
Material	P.EC,P.GC,P.FC,P.FY,P.ES	34.0	14.2	35	500	200
<b>Bearings/joints</b>						
Type	B.TYPE	Conventional bearings				
Dimensions	B.M1, B.M2, B.M3	-	-	-		
Material	B.FY, B.K0, B.K1	-	-	-		
Capacity	B.RDX, B.RDY	-	-			
Seat length [m]	B.SEAT	1.1				
Fix bearing positions	B.NFIX	1 (support 4)				
<b>Pier cap beam</b>						
Cross-section	PC.A, PC.B	None				
Reinforcement	PC.RO_S, PC.S_FI, PC.S_W	-	-	-		
Material	PC.EC,PC.GC,PC.FC,PC.FY,PC.ES	-	-	-	-	-
<b>Foundation</b>						
Type	F.TYPE	Pile foundation				
Dimensions of shallow found.	F.A, F.B, F.M	-	-	-	-	-
Pile foundation layout	F.A, F.B, F.NY, F.NX, F.L	7.2	7.2	3	3	20
Found. stiffness (abutment)	F.AK1-F.AK6	2.3E9	2.3E9	1.5E9	1.6E10	6.9E9 1.0E13
Found. stiffness (pier)	F.PK1-F.PK6	2.6E9	2.6E9	1.7E9	1.2E10	1.2E10 1.0E13
<b>Notes</b>						
Conventional bearings. Pile: Abutment: 2x4 (1800 kN); Pier: 3x3 (3000 kN). Reinf. ratio is only 0.45%.						

Table E19 Description of BR18 bridge.

<b>Example Bridge #18</b>						
Bridge Name	x					
Year of construction	2010					
Coordinates	x					
Name of road	M0					
<b>Global geometry</b>						
Superstructure type	SS.TYPE	Reinforced concrete box girder				
Mechanical system	SS.SYSTEM	Continuous girder				
No. of spans	SS.NO_SPAN	6				
Span lengths [m]	SS.SPAN_L	37.5	50	50	50	37.5
Deck width [m]	SS.B1	13.5				
Pier height [m]	P.H	15				
Pier number (trans. direction)	P.NO_PIER	1				
Pier distance (trans. dir.) [m]	P.DIST	0				
Skew angle [°]	SS.SKEW	90				
<b>Superstructure</b>						
Material	SS.E, SS.G	34.0	14.2			
Cross-section	SS.A,SS.J,SS.IY,SS.IZ	9.660	30.800	18.060	90.28	
Height [m]	SS.HT	3.85				
Height of centroid [m]	SS.H2	2.55				
Bearing distance [m]	SS.B2	4.4				
Lineweight [kg/m]	SS.W	32500				
<b>Piers</b>						
Cross-section	P.A, P.B	4.9	2			
Reinforcement	P.RO_S, P.S_FI, P.S_W	0.45	12	0.2		
Material	P.EC,P.GC,P.FC,P.FY,P.ES	34.0	14.2	35	500	200
<b>Bearings/joints</b>						
Type	B.TYPE	Conventional bearings				
Dimensions	B.M1, B.M2, B.M3	-	-	-		
Material	B.FY, B.K0, B.K1	-	-	-		
Capacity	B.RDX, B.RDY	-	-			
Seat length [m]	B.SEAT	1.4				
Fix bearing positions	B.NFIX	1 (suppoert 4)				
<b>Pier cap beam</b>						
Cross-section	PC.A, PC.B	None	-			
Reinforcement	PC.RO_S, PC.S_FI, PC.S_W	-	-	-		
Material	PC.EC,PC.GC,PC.FC,PC.FY,PC.ES	-	-	-	-	-
<b>Foundation</b>						
Type	F.TYPE	Pile foundation				
Dimensions of shallow found.	F.A, F.B, F.M	-	-	-	-	-
Pile foundation layout	F.A, F.B, F.NY, F.NX, F.L	9.6	7.2	5	4	20
Found. stiffness (abutment)	F.AK1-F.AK6	5.2E9	5.2E9	2.3E9	4.8E10	1.9E10 1.0E13
Found. stiffness (pier)	F.PK1-F.PK6	5.7E9	5.7E9	3.1E9	4.8E10	3.4E10 1.0E13
<b>Notes</b>						
Conventional bearings. Pile: Abutment: 3x6 (2000 kN); Pier: 4x5 (2500 kN). Reinf. ratio is only 0.45%						

Table E20 Description of BR19 bridge.

<i>Example Bridge #19</i>						
Bridge Name	x					
Year of construction	2010					
Coordinates	x					
Name of road	M7					
<b>Global geometry</b>						
Superstructure type	SS.TYPE	Reinforced concrete box girder				
Mechanical system	SS.SYSTEM	Continuous girder				
No. of spans	SS.NO_SPAN	7				
Span lengths [m]	SS.SPAN_L	36	5x45	36		
Deck width [m]	SS.B1	17				
Pier height [m]	P.H	24				
Pier number (trans. direction)	P.NO_PIER	1				
Pier distance (trans. dir.) [m]	P.DIST	0				
Skew angle [°]	SS.SKEW	90				
<b>Superstructure</b>						
Material	SS.E, SS.G	34.0	14.2			
Cross-section	SS.A,SS.J,SS.IY,SS.IZ	11.210	39.410	19.810	187.00	
Height [m]	SS.HT	3.50				
Height of centroid [m]	SS.H2	2.30				
Bearing distance [m]	SS.B2	6.5				
Lineweight [kg/m]	SS.W	36485				
<b>Piers</b>						
Cross-section	P.A, P.B	6	2.8			
Reinforcement	P.RO_S, P.S_FI, P.S_W	1.0	12	0.15		
Material	P.EC,P.GC,P.FC,P.FY,P.ES	34.0	14.2	35	500	200
<b>Bearings/joints</b>						
Type	B.TYPE	Conventional bearings				
Dimensions	B.M1, B.M2, B.M3	-	-	-		
Material	B.FY, B.K0, B.K1	-	-	-		
Capacity	B.RDX, B.RDY	-	-			
Seat length [m]	B.SEAT	1.1				
Fix bearing positions	B.NFIX	1 (support 5)				
<b>Pier cap beam</b>						
Cross-section	PC.A, PC.B	None				
Reinforcement	PC.RO_S, PC.S_FI, PC.S_W	-	-	-		
Material	PC.EC,PC.GC,PC.FC,PC.FY,PC.ES	-	-	-	-	-
<b>Foundation</b>						
Type	F.TYPE	Pile foundation				
Dimensions of shallow found.	F.A, F.B, F.M	-	-	-	-	-
Pile foundation layout	F.A, F.B, F.NY, F.NX, F.L	7.2	14.4	3	6	18
Found. stiffness (abutment)	F.AK1-F.AK6	3.4E9	3.4E9	1.5E9	3.2E10	9.2E9 1.0E13
Found. stiffness (pier)	F.PK1-F.PK6	5.2E9	5.2E9	3.4E9	6.7E10	2.4E10 1.0E13
<b>Notes</b>						
Conventional bearings. Pile: Abutment: 2x6 (2000 kN); Pier: 3x6 (3000 kN). Reinf. ratio is 1%.						

Table E21 Description of BR20 bridge.

Example Bridge #20						
Bridge Name	x					
Year of construction	2004					
Coordinates	x					
Name of road	M3					
<b>Global geometry</b>						
Superstructure type	SS.TYPE	Composite girder				
Mechanical system	SS.SYSTEM	Continuous girder				
No. of spans	SS.NO_SPAN	3				
Span lengths [m]	SS.SPAN_L	40	60	40		
Deck width [m]	SS.B1	14				
Pier height [m]	P.H	8				
Pier number (trans. direction)	P.NO_PIER	1				
Pier distance (trans. dir.) [m]	P.DIST	0				
Skew angle [°]	SS.SKEW	70				
<b>Superstructure</b>						
Material	SS.E, SS.G	210.0	80.8			
Cross-section	SS.A,SS.J,SS.IY,SS.IZ	0.962	0.150	1.200	14.52	
Height [m]	SS.HT	3.30				
Height of centroid [m]	SS.H2	2.50				
Bearing distance [m]	SS.B2	7.3				
Lineweight [kg/m]	SS.W	21300				
<b>Piers</b>						
Cross-section	P.A, P.B	7.3	1.4			
Reinforcement	P.RO_S, P.S_FI, P.S_W	0.4	20	0.2		
Material	P.EC,P.GC,P.FC,P.FY,P.ES	34.0	14.2	35	500	200
<b>Bearings/joints</b>						
Type	B.TYPE	Conventional bearings				
Dimensions	B.M1, B.M2, B.M3	-	-	-		
Material	B.FY, B.K0, B.K1	-	-	-		
Capacity	B.RDX, B.RDY	-	-			
Seat length [m]	B.SEAT	0.5				
Fix bearing positions	B.NFIX	1 (support 2)				
<b>Pier cap beam</b>						
Cross-section	PC.A, PC.B	None				
Reinforcement	PC.RO_S, PC.S_FI, PC.S_W	-	-	-		
Material	PC.EC,PC.GC,PC.FC,PC.FY,PC.ES	-	-	-	-	-
<b>Foundation</b>						
Type	F.TYPE	Pile foundation				
Dimensions of shallow found.	F.A, F.B, F.M	-	-	-	-	-
Pile foundation layout	F.A, F.B, F.NY, F.NX, F.L	4.8	24	2	10	22
Found. stiffness (abutment)	F.AK1-F.AK6	7.2E9	7.2E9	2.5E9	2.1E11	2.9E10 1.0E13
Found. stiffness (pier)	F.PK1-F.PK6	7.2E9	7.2E9	3.0E9	2.5E11	3.0E10 1.0E13
<b>Notes</b>						
Conventional bearings. Pile: Abutment: 2x10 (2000 kN); Pier: 2x10 (3000 kN). Pier reinf. ratio is only 0.4%. Expansion joint 35 and 65 mm at the abutments.						

Table E22 Description of BR21 bridge.

<i>Example Bridge #21</i>						
Bridge Name	x					
Year of construction	2010					
Coordinates	x					
Name of road	M6					
<b>Global geometry</b>						
Superstructure type	SS.TYPE	Composite girder				
Mechanical system	SS.SYSTEM	Continuous girder				
No. of spans	SS.NO_SPAN	3				
Span lengths [m]	SS.SPAN_L	75	90	75		
Deck width [m]	SS.B1	14				
Pier height [m]	P.H	7				
Pier number (trans. direction)	P.NO_PIER	1				
Pier distance (trans. dir.) [m]	P.DIST	0				
Skew angle [°]	SS.SKEW	90				
<b>Superstructure</b>						
Material	SS.E, SS.G	210.0	80.8			
Cross-section	SS.A,SS.J,SS.IY,SS.IZ	0.940	0.150	1.098	15.35	
Height [m]	SS.HT	2.90				
Height of centroid [m]	SS.H2	2.20				
Bearing distance [m]	SS.B2	8.0				
Lineweight [kg/m]	SS.W	19700				
<b>Piers</b>						
Cross-section	P.A, P.B	12	3.3			
Reinforcement	P.RO_S, P.S_FI, P.S_W	0.2	16	0.15		
Material	P.EC,P.GC,P.FC,P.FY,P.ES	34.0	14.2	35	500	200
<b>Bearings/joints</b>						
Type	B.TYPE	Conventional bearings				
Dimensions	B.M1, B.M2, B.M3	-	-	-		
Material	B.FY, B.K0, B.K1	-	-	-		
Capacity	B.RDX, B.RDY	-	-	-		
Seat length [m]	B.SEAT	0.5				
Fix bearing positions	B.NFIX	1 (support 2)				
<b>Pier cap beam</b>						
Cross-section	PC.A, PC.B	None	-			
Reinforcement	PC.RO_S, PC.S_FI, PC.S_W	-	-	-		
Material	PC.EC,PC.GC,PC.FC,PC.FY,PC.ES	-	-	-	-	-
<b>Foundation</b>						
Type	F.TYPE	Pile foundation				
Dimensions of shallow found.	F.A, F.B, F.M	-	-	-	-	-
Pile foundation layout	F.A, F.B, F.NY, F.NX, F.L	7.2	16.8	3	7	20
Found. stiffness (abutment)	F.AK1-F.AK6	4.6E9	4.6E9	2.0E9	7.0E10	1.2E10 1.0E13
Found. stiffness (pier)	F.PK1-F.PK6	6.0E9	6.0E9	3.9E9	1.0E11	2.8E10 1.0E13
<b>Notes</b>						
Conventional bearings. Pile: Abutment: 2x8 (2000 kN); Pier: 3x7 (3000 kN). Pier reinf. ratio is only 0.15%. Expansion joint 120 mm.						

Table E23 Description of BR22 bridge.

<b>Example Bridge #22</b>					
Bridge Name	x				
Year of construction	2004				
Coordinates	x				
Name of road	Main road No. 3				
<b>Global geometry</b>					
Superstructure type	SS.TYPE	Composite girder			
Mechanical system	SS.SYSTEM	Continuous girder			
No. of spans	SS.NO_SPAN	4			
Span lengths [m]	SS.SPAN_L	35	45	45	35
Deck width [m]	SS.B1	11			
Pier height [m]	P.H	4.5			
Pier number (trans. direction)	P.NO_PIER	2			
Pier distance (trans. dir.) [m]	P.DIST	6.5			
Skew angle [°]	SS.SKEW	90			
<b>Superstructure</b>					
Material	SS.E, SS.G	210.0	80.8		
Cross-section	SS.A, SS.J, SS.IY, SS.IZ	0.720	0.120	0.360	9.57
Height [m]	SS.HT	2.30			
Height of centroid [m]	SS.H2	2.20			
Bearing distance [m]	SS.B2	6.5			
Lineweight [kg/m]	SS.W	18200			
<b>Piers</b>					
Cross-section	P.A, P.B	2.4	1.2		
Reinforcement	P.RO_S, P.S_FI, P.S_W	0.50	16	0.15	
Material	P.EC, P.GC, P.FC, P.FY, P.ES	34.0	14.2	35	500 200
<b>Bearings/joints</b>					
Type	B.TYPE	Conventional bearings			
Dimensions	B.M1, B.M2, B.M3	-	-	-	
Material	B.FY, B.K0, B.K1	-	-	-	
Capacity	B.RDX, B.RDY	-	-		
Seat length [m]	B.SEAT	0.5			
Fix bearing positions	B.NFIX	1 (support 3)			
<b>Pier cap beam</b>					
Cross-section	PC.A, PC.B	None -			
Reinforcement	PC.RO_S, PC.S_FI, PC.S_W	-	-	-	
Material	PC.EC, PC.GC, PC.FC, PC.FY, PC.ES	-	-	-	-
<b>Foundation</b>					
Type	F.TYPE	Pile foundation			
Dimensions of shallow found.	F.A, F.B, F.M	-	-	-	-
Pile foundation layout	F.A, F.B, F.NY, F.NX, F.L	7.2	24	3	10 13
Found. stiffness (abutment)	F.AK1-F.AK6	8.6E9	8.6E9	5.3E9	2.7E11 3.8E10 1.0E13
Found. stiffness (pier)	F.PK1-F.PK6	8.6E9	8.6E9	4.7E9	2.4E11 3.6E10 1.0E13
<b>Notes</b>					
Conventional bearings. Pile: Abutment: 3x10 (2800 kN); Pier: 3x10 (2500 kN). Pier reinf. ratio is only 0.45%.					
Expansion joint 80 mm.					

Table E24 Description of BR23 bridge.

<i>Example Bridge #23</i>						
Bridge Name	x					
Year of construction	2012					
Coordinates	x					
Name of road	M4					
<b>Global geometry</b>						
Superstructure type	SS.TYPE	Composite box girder				
Mechanical system	SS.SYSTEM	Continuous girder				
No. of spans	SS.NO_SPAN	3				
Span lengths [m]	SS.SPAN_L	24	36	24		
Deck width [m]	SS.B1	14				
Pier height [m]	P.H	4.5				
Pier number (trans. direction)	P.NO_PIER	4				
Pier distance (trans. dir.) [m]	P.DIST	12				
Skew angle [°]	SS.SKEW	60				
<b>Superstructure</b>						
Material	SS.E, SS.G	210.0	80.8			
Cross-section	SS.A,SS.J,SS.IY,SS.IZ	1.310	0.570	0.290	18.72	
Height [m]	SS.HT	1.30				
Height of centroid [m]	SS.H2	1.00				
Bearing distance [m]	SS.B2	12.0				
Lineweight [kg/m]	SS.W	23700				
<b>Piers</b>						
Cross-section	P.A, P.B	1.1	0.6			
Reinforcement	P.RO_S, P.S_FI, P.S_W	2.24	16	0.1		
Material	P.EC,P.GC,P.FC,P.FY,P.ES	34.0	14.2	35	500	200
<b>Bearings/joints</b>						
Type	B.TYPE	Conventional bearings + shear reinforcement				
Dimensions	B.M1, B.M2, B.M3	-	-	-		
Material	B.FY, B.K0, B.K1	-	-	-		
Capacity	B.RDX, B.RDY	-	-			
Seat length [m]	B.SEAT	0.5				
Fix bearing positions	B.NFIX	4 (support 1-2-3-4)				
<b>Pier cap beam</b>						
Cross-section	PC.A, PC.B	None				
Reinforcement	PC.RO_S, PC.S_FI, PC.S_W	-	-	-		
Material	PC.EC,PC.GC,PC.FC,PC.FY,PC.ES	-	-	-	-	-
<b>Foundation</b>						
Type	F.TYPE	Pile foundation				
Dimensions of shallow found.	F.A, F.B, F.M	-	-	-	-	-
Pile foundation layout	F.A, F.B, F.NY, F.NX, F.L	4.8	14.4	2	6	10
Found. stiffness (abutment)	F.AK1-F.AK6	1.7E9	1.7E9	9.4E8	1.9E10	3.5E9 1.0E13
Found. stiffness (pier)	F.PK1-F.PK6	3.4E9	3.4E9	1.9E9	3.9E10	9.8E9 1.0E13
<b>Notes</b>						
Conventional bearings + $\phi$ 16/20 shear reinforcement at the abutments. Pile: Abutment: 1x6 (2500 kN); Pier: 2x6 (2500 kN). Pier reinf. ratio is 2.24%.						

Table E25 Description of BR24 bridge.

<b>Example Bridge #24</b>					
Bridge Name	x				
Year of construction	2012				
Coordinates	x				
Name of road	M4				
<b>Global geometry</b>					
Superstructure type	SS.TYPE	Composite box girder			
Mechanical system	SS.SYSTEM	Continuous girder			
No. of spans	SS.NO_SPAN	3			
Span lengths [m]	SS.SPAN_L	35	45	35	
Deck width [m]	SS.B1	14			
Pier height [m]	P.H	5.5			
Pier number (trans. direction)	P.NO_PIER	2			
Pier distance (trans. dir.) [m]	P.DIST	7			
Skew angle [°]	SS.SKEW	60			
<b>Superstructure</b>					
Material	SS.E, SS.G	210.0	80.8		
Cross-section	SS.A,SS.J,SS.IY,SS.IZ	1.020	0.330	0.620	15.03
Height [m]	SS.HT	2.25			
Height of centroid [m]	SS.H2	2.00			
Bearing distance [m]	SS.B2	7.0			
Lineweight [kg/m]	SS.W	22000			
<b>Piers</b>					
Cross-section	P.A, P.B	1.6	1.6		
Reinforcement	P.RO_S, P.S_FI, P.S_W	0.80	16	0.2	
Material	P.EC,P.GC,P.FC,P.FY,P.ES	34.0	14.2	35	500 200
<b>Bearings/joints</b>					
Type	B.TYPE	Conventional bearings			
Dimensions	B.M1, B.M2, B.M3	-	-	-	
Material	B.FY, B.K0, B.K1	-	-	-	
Capacity	B.RDX, B.RDY	-	-	-	
Seat length [m]	B.SEAT	0.6			
Fix bearing positions	B.NFIX	1 (support C)			
<b>Pier cap beam</b>					
Cross-section	PC.A, PC.B	1.4	1.4		
Reinforcement	PC.RO_S, PC.S_FI, PC.S_W	0.8	12	0.2	
Material	PC.EC,PC.GC,PC.FC,PC.FY,PC.ES	34.0	14.2	35	500 200
<b>Foundation</b>					
Type	F.TYPE	Pile foundation			
Dimensions of shallow found.	F.A, F.B, F.M	-	-	-	-
Pile foundation layout	F.A, F.B, F.NY, F.NX, F.L	7.2	12	3	5 16
Found. stiffness (abutment)	F.AK1-F.AK6	4.0E9	4.0E9	1.3E9	3.9E10 1.0E10 1.0E13
Found. stiffness (pier)	F.PK1-F.PK6	4.3E9	4.3E9	1.8E9	2.9E10 1.6E10 1.0E13
<b>Notes</b>					
Conventional bearings. Pile: Abutment: 2x7 (1500 kN); Pier: 3x5 (1900 kN). Pier reinf. ratio is 0.8%. Expansion joint 50 and 90 mm at the abutments.					

Table E26 Description of BR25 bridge.

<b>Example Bridge #25</b>					
Bridge Name	x				
Year of construction	2013				
Coordinates	x				
Name of road	M4				
<b>Global geometry</b>					
Superstructure type	SS.TYPE	Composite box girder			
Mechanical system	SS.SYSTEM	Continuous girder			
No. of spans	SS.NO_SPAN	9			
Span lengths [m]	SS.SPAN_L	40	7-48	40	
Deck width [m]	SS.B1	14			
Pier height [m]	P.H	6.5			
Pier number (trans. direction)	P.NO_PIER	2			
Pier distance (trans. dir.) [m]	P.DIST	7			
Skew angle [°]	SS.SKEW	80			
<b>Superstructure</b>					
Material	SS.E, SS.G	210.0	80.8		
Cross-section	SS.A,SS.J,SS.IY,SS.IZ	1.020	0.330	0.620	15.03
Height [m]	SS.HT	2.25			
Height of centroid [m]	SS.H2	2.00			
Bearing distance [m]	SS.B2	7.0			
Lineweight [kg/m]	SS.W	22000			
<b>Piers</b>					
Cross-section	P.A, P.B	1.4	1.4		
Reinforcement	P.RO_S, P.S_FI, P.S_W	0.40	12	0.2	
Material	P.EC,P.GC,P.FC,P.FY,P.ES	34.0	14.2	35	500 200
<b>Bearings/joints</b>					
Type	B.TYPE	Conventional bearings			
Dimensions	B.M1, B.M2, B.M3	-	-	-	
Material	B.FY, B.K0, B.K1	-	-	-	
Capacity	B.RDX, B.RDY	-	-		
Seat length [m]	B.SEAT	0.6			
Fix bearing positions	B.NFIX	2 (support 5 6)			
<b>Pier cap beam</b>					
Cross-section	PC.A, PC.B	0.8	1.0		
Reinforcement	PC.RO_S, PC.S_FI, PC.S_W	1.000	12	0.2	
Material	PC.EC,PC.GC,PC.FC,PC.FY,PC.ES	34.0	14.2	35	500 200
<b>Foundation</b>					
Type	F.TYPE	Pile foundation			
Dimensions of shallow found.	F.A, F.B, F.M	-	-	-	-
Pile foundation layout	F.A, F.B, F.NY, F.NX, F.L	4.8	9.6	2	4 25
Found. stiffness (abutment)	F.AK1-F.AK6	2.3E9	2.3E9	1.5E9	1.6E10 6.9E9 1.0E13
Found. stiffness (pier)	F.PK1-F.PK6	2.3E9	2.3E9	1.5E9	1.6E10 6.9E9 1.0E13
<b>Notes</b>					
Conventional bearings. Pile: Abutment: 2x4 (3000 kN); Pier: 2x4 (3000 kN). Pier reinf. ratio is 0.4%. Expansion joint 150 mm at the abutments.					

Table E27 Description of BR26 bridge.

<i>Example Bridge #26</i>						
Bridge Name	x					
Year of construction	2012					
Coordinates	x					
Name of road	M4					
<b>Global geometry</b>						
Superstructure type	SS.TYPE	Steel girder				
Mechanical system	SS.SYSTEM	Continuous girder				
No. of spans	SS.NO_SPAN	5				
Span lengths [m]	SS.SPAN_L	50	50	50	50	50
Deck width [m]	SS.B1	14				
Pier height [m]	P.H	5.5				
Pier number (trans. direction)	P.NO_PIER	2				
Pier distance (trans. dir.) [m]	P.DIST	9				
Skew angle [°]	SS.SKEW	90				
<b>Superstructure</b>						
Material	SS.E, SS.G	210.0	80.8			
Cross-section	SS.A,SS.J,SS.IY,SS.IZ	1.050	0.010	0.570	14.44	
Height [m]	SS.HT	2.10				
Height of centroid [m]	SS.H2	1.60				
Bearing distance [m]	SS.B2	9.0				
Lineweight [kg/m]	SS.W	15500				
<b>Piers</b>						
Cross-section	P.A, P.B	2	1.2			
Reinforcement	P.RO_S, P.S_FI, P.S_W	1.25	16	0.15		
Material	P.EC,P.GC,P.FC,P.FY,P.ES	34.0	14.2	35	500	200
<b>Bearings/joints</b>						
T type	B.TYPE	Conventional bearings				
Dimensions	B.M1, B.M2, B.M3	-	-	-		
Material	B.FY, B.K0, B.K1	-	-	-		
Capacity	B.RDX, B.RDY	-	-	-		
Seat length [m]	B.SEAT					
Fix bearing positions	B.NFIX	2 (support 5 6)				
<b>Pier cap beam</b>						
Cross-section	PC.A, PC.B	None				
Reinforcement	PC.RO_S, PC.S_FI, PC.S_W	-	-	-		
Material	PC.EC,PC.GC,PC.FC,PC.FY,PC.ES	-	-	-	-	-
<b>Foundation</b>						
Type	F.TYPE	Pile foundation				
Dimensions of shallow found.	F.A, F.B, F.M	-	-	-	-	-
Pile foundation layout	F.A, F.B, F.NY, F.NX, F.L	7.2	14.4	3	6	18
Found. stiffness (abutment)	F.AK1-F.AK6	2.3E9	2.3E9	1.0E9	1.2E10	6.2E9 1.0E13
Found. stiffness (pier)	F.PK1-F.PK6	5.2E9	5.2E9	3.4E9	6.7E10	2.4E10 1.0E13
<b>Notes</b>						
Conventional bearings. Pile: Abutment: 2x4 (2000 kN); Pier: 3x6 (3000 kN). Pier reinf. ratio is 1.25%. Expansion joint 150 mm at the abutments.						

Table E28 Description of BR27 bridge.

<i>Example Bridge #27</i>						
Bridge Name	x					
Year of construction	2012					
Coordinates	x					
Name of road	M4					
<b>Global geometry</b>						
Superstructure type	SS.TYPE	Steel girder				
Mechanical system	SS.SYSTEM	Continuous girder				
No. of spans	SS.NO_SPAN	9				
Span lengths [m]	SS.SPAN_L	22.5	3-45	60	3-45	22.5
Deck width [m]	SS.B1	14				
Pier height [m]	P.H	5.5				
Pier number (trans. direction)	P.NO_PIER	2				
Pier distance (trans. dir.) [m]	P.DIST	9				
Skew angle [°]	SS.SKEW	90				
<b>Superstructure</b>						
Material	SSE, SSG	210.0	80.8			
Cross-section	SS.A,SS.J,SS.IY,SS.IZ	1.050	0.010	0.570	14.44	
Height [m]	SS.HT	2.10				
Height of centroid [m]	SS.H2	1.60				
Bearing distance [m]	SS.B2	9.0				
Lineweight [kg/m]	SS.W	15500				
<b>Piers</b>						
Cross-section	P.A, P.B	2	1.2			
Reinforcement	P.RO_S, P.S_FI, P.S_W	1.25	16	0.15		
Material	P.EC,P.GC,P.FC,P.FY,P.ES	34.0	14.2	35	500	200
<b>Bearings/joints</b>						
Type	B.TYPE	Conventional bearings				
Dimensions	B.M1, B.M2, B.M3	-	-	-		
Material	B.FY, B.K0, B.K1	-	-	-		
Capacity	B.RDX, B.RDY	-	-	-		
Seat length [m]	B.SEAT					
Fix bearing positions	B.NFIX	2 (support 5 6)				
<b>Pier cap beam</b>						
Cross-section	PC.A, PC.B	None -				
Reinforcement	PC.RO_S, PC.S_FI, PC.S_W	-	-	-		
Material	PC.EC,PC.GC,PC.FC,PC.FY,PC.ES	-	-	-	-	-
<b>Foundation</b>						
Type	F.TYPE	Pile foundation				
Dimensions of shallow found.	F.A, F.B, F.M	-	-	-	-	-
Pile foundation layout	F.A, F.B, F.NY, F.NX, F.L	7.2	14.4	3	6	18
Found. stiffness (abutment)	F.AK1-F.AK6	2.3E9	2.3E9	1.0E9	1.2E10	6.2E9 1.0E13
Found. stiffness (pier)	F.PK1-F.PK6	5.2E9	5.2E9	3.4E9	6.7E10	2.4E10 1.0E13
<b>Notes</b>						
Conventional bearings. Pile: Abutment: 2x4 (2000 kN); Pier: 3x6 (3000 kN). Pier reinf. ratio is 1.25%. Expansion joint 200 mm at the abutments.						

Table E29 Description of BR28 bridge.

<b>Example Bridge #28</b>					
Bridge Name	x				
Year of construction	2012				
Coordinates	x				
Name of road	Main road no. 86				
<b>Global geometry</b>					
Superstructure type	SS.TYPE	Steel box girder			
Mechanical system	SS.SYSTEM	Continuous girder			
No. of spans	SS.NO_SPAN	2			
Span lengths [m]	SS.SPAN_L	80	80		
Deck width [m]	SS.B1	15			
Pier height [m]	P.H	11.5			
Pier number (trans. direction)	P.NO_PIER	2			
Pier distance (trans. dir.) [m]	P.DIST	5			
Skew angle [°]	SS.SKEW	90			
<b>Superstructure</b>					
Material	SS.E, SS.G	210.0	80.8		
Cross-section	SS.A,SS.J,SS.IY,SS.IZ	1.150	1.880	1.200	16.41
Height [m]	SS.HT	2.80			
Height of centroid [m]	SS.H2	2.00			
Bearing distance [m]	SS.B2	5.0			
Lineweight [kg/m]	SS.W	16500			
<b>Piers</b>					
Cross-section	P.A, P.B	1.5	1.5		
Reinforcement	P.RO_S, P.S_FI, P.S_W	1.30	16	0.15	
Material	P.EC,P.GC,P.FC,P.FY,P.ES	34.0	14.2	35	500 200
<b>Bearings/joints</b>					
Type	B.TYPE	Conventional bearings			
Dimensions	B.M1, B.M2, B.M3	-	-	-	
Material	B.FY, B.K0, B.K1	-	-	-	
Capacity	B.RDX, B.RDY	-	-	-	
Seat length [m]	B.SEAT				
Fix bearing positions	B.NFIX	1 (support 2)			
<b>Pier cap beam</b>					
Cross-section	PC.A, PC.B	1.5	1.5		
Reinforcement	PC.RO_S, PC.S_FI, PC.S_W	1.000	20	0.2	
Material	PC.EC,PC.GC,PC.FC,PC.FY,PC.ES	34.0	14.2	35	500 200
<b>Foundation</b>					
Type	F.TYPE	Pile foundation			
Dimensions of shallow found.	F.A, F.B, F.M	-	-	-	-
Pile foundation layout	F.A, F.B, F.NY, F.NX, F.L	4.8	12	2	5 10
Found. stiffness (abutment)	F.AK1-F.AK6	3.6E9	3.6E9	1.3E9	3.4E10 1.4E10 1.0E13
Found. stiffness (pier)	F.PK1-F.PK6	3.6E9	3.6E9	1.3E9	3.4E10 1.4E10 1.0E13
<b>Notes</b>					
Conventional bearings. Pile: Abutment: 2x5 (2500 kN); Pier: 2x5 (2500 kN). Pier reinf. ratio is 1.3%. Expansion joint 100 mm at the abutments.					

Table E30 Description of BR29 bridge.

<i>Example Bridge #29</i>					
Bridge Name	x				
Year of construction	1990				
Coordinates	x				
Name of road	M0				
<b>Global geometry</b>					
Superstructure type	SS.TYPE	Steel box girder			
Mechanical system	SS.SYSTEM	Continuous girder			
No. of spans	SS.NO_SPAN	3			
Span lengths [m]	SS.SPAN_L	110	110	110	
Deck width [m]	SS.B1	22			
Pier height [m]	P.H	16.5			
Pier number (trans. direction)	P.NO_PIER	1			
Pier distance (trans. dir.) [m]	P.DIST	0			
Skew angle [°]	SS.SKEW	90			
<b>Superstructure</b>					
Material	SS.E, SS.G	210.0	80.8		
Cross-section	SS.A,SS.I,SS.IY,SS.IZ	0.860	2.500	4.150	19.20
Height [m]	SS.HT	5.20			
Height of centroid [m]	SS.H2	3.20			
Bearing distance [m]	SS.B2	9.0			
Lineweight [kg/m]	SS.W	17500			
<b>Piers</b>					
Cross-section	P.A, P.B	13	3.5		
Reinforcement	P.RO_S, P.S_FI, P.S_W	0.15	16	0.25	
Material	P.EC,P.GC,P.FC,P.FY,P.ES	32.0	12.3	30	500 200
<b>Bearings/joints</b>					
Type	B.TYPE	Conventional bearings			
Dimensions	B.M1, B.M2, B.M3	-	-	-	
Material	B.FY, B.K0, B.K1	-	-	-	
Capacity	B.RDX, B.RDY	-	-	-	
Seat length [m]	B.SEAT	0.5			
Fix bearing positions	B.NFIX	1 (support 2)			
<b>Pier cap beam</b>					
Cross-section	PC.A, PC.B	-	-		
Reinforcement	PC.RO_S, PC.S_FI, PC.S_W	-	-	-	
Material	PC.EC,PC.GC,PC.FC,PC.FY,PC.ES	-	-	-	-
<b>Foundation</b>					
Type	F.TYPE	Pile foundation			
Dimensions of shallow found.	F.A, F.B, F.M	-	-	-	-
Pile foundation layout	F.A, F.B, F.NY, F.NX, F.L	4.8	12	2	5 25
Found. stiffness (abutment)	F.AK1-F.AK6	4.3E9	4.3E9	8.3E8	4.2E10 2.3E10 1.0E13
Found. stiffness (pier)	F.PK1-F.PK6	4.3E9	4.3E9	1.7E9	6.3E10 2.5E10 1.0E13
<b>Notes</b>					
Conventional bearings. Pile: Abutment: 2x5 (2000 kN); Pier: 2x5 (4000 kN). Pier reinf. ratio is 0.15%. Expansion joint 70 and 140 mm at the abutments.					

Table E31 Description of BR30 bridge.

<i>Example Bridge #30</i>						
Bridge Name	x					
Year of construction	2012					
Coordinates	x					
Name of road	Main road no. 86					
<b>Global geometry</b>						
Superstructure type	SS.TYPE	Steel box girder				
Mechanical system	SS.SYSTEM	Continuous girder				
No. of spans	SS.NO_SPAN	8				
Span lengths [m]	SS.SPAN_L	6	6-80	60		
Deck width [m]	SS.B1	14				
Pier height [m]	P.H	11				
Pier number (trans. direction)	P.NO_PIER	2				
Pier distance (trans. dir.) [m]	P.DIST	5.5				
Skew angle [°]	SS.SKEW	90				
<b>Superstructure</b>						
Material	SS.E, SS.G	210.0	80.8			
Cross-section	SS.A,SS.J,SS.IY,SS.IZ	1.140	1.75	0.950	16.30	
Height [m]	SS.HT	2.50				
Height of centroid [m]	SS.H2	1.80				
Bearing distance [m]	SS.B2	5.5				
Lineweight [kg/m]	SS.W	16500				
<b>Piers</b>						
Cross-section	P.A, P.B	1.5	1.5			
Reinforcement	P.RO_S, P.S_FI, P.S_W	1.30	16	0.15		
Material	P.EC,P.GC,P.FC,P.FY,P.ES	34.0	13.1	35	500	200
<b>Bearings/joints</b>						
Type	B.TYPE	Conventional bearings				
Dimensions	B.M1, B.M2, B.M3	-	-	-		
Material	B.FY, B.K0, B.K1	-	-	-		
Capacity	B.RDX, B.RDY	-	-	-		
Seat length [m]	B.SEAT					
Fix bearing positions	B.NFIX	1 (support 5)				
<b>Pier cap beam</b>						
Cross-section	PC.A, PC.B	1.5	1.5			
Reinforcement	PC.RO_S, PC.S_FI, PC.S_W	1.000	20	0.2		
Material	PC.EC,PC.GC,PC.FC,PC.FY,PC.ES	34.0	13.1	35	500	200
<b>Foundation</b>						
Type	F.TYPE	Pile foundation				
Dimensions of shallow found.	F.A, F.B, F.M	-	-	-	-	-
Pile foundation layout	F.A, F.B, F.NY, F.NX, F.L	7.2	9.6	3	4	10
Found. stiffness (abutment)	F.AK1-F.AK6	2.9E9	2.9E9	8.8E8	1.9E10	1.1E10 1.0E13
Found. stiffness (pier)	F.PK1-F.PK6	4.3E9	4.3E9	1.5E9	3.1E10	2.3E10 1.0E13
<b>Notes</b>						
Conventional bearings. Pile: Abutment: 2x4 (2200 kN); Pier: 3x4 (2500 kN). Pier reinf. ratio is 1.3%. Expansion joint 350 mm at the abutments.						

## *Appendix F: Damage limit states for the examined bridges*

Median capacity values for LS1-LS3 limit states of PMG-I bridges (for the parametric study) and of portfolio bridges are shown in Table F1 and F3, respectively (COV values are presented in Table 6.2). Further details about Bearing 1 and 2 associated with each bridge class is shown in Table F2.

Table F1 Median capacity values of PMG-I bridges for LS1-LS3 damage limit states.

Configuration	Pier						Bearing 1 - deformation [m]						Bearing 2 - deformation [m]						Backfill				
	Shear [kN]			Flexural [%]			Longitudinal			Transverse			Longitudinal			Transverse			Deformation [m]				
	LS1	LS2	LS3	LS1	LS2	LS3	LS1	LS2	LS3	LS1	LS2	LS3	LS1	LS2	LS3	LS1	LS2	LS3	LS1	LS2	LS3		
W08 P04 L15	S2	784	784	784	0.28	0.30	0.38	0.002	0.05	0.5	0.002	0.05	0.8	0.002	0.05	0.3	0.002	0.05	0.45	0.03	0.06	0.3	
		S3	784	784	784	0.28	0.30	0.38	0.002	0.05	0.5	0.002	0.05	0.8	0.002	0.05	0.3	0.002	0.05	0.45	0.03	0.06	0.3
		S4	784	784	784	0.28	0.30	0.38	0.002	0.05	0.5	0.002	0.05	0.8	0.002	0.05	0.3	0.002	0.05	0.45	0.03	0.06	0.3
	P04 L30	S2	873	873	873	0.28	0.30	0.38	0.002	0.05	0.5	0.002	0.05	0.8	0.002	0.05	0.3	0.002	0.05	0.45	0.03	0.06	0.3
		S3	873	873	873	0.28	0.30	0.38	0.002	0.05	0.5	0.002	0.05	0.8	0.002	0.05	0.3	0.002	0.05	0.45	0.03	0.06	0.3
		S4	873	873	873	0.28	0.30	0.38	0.002	0.05	0.5	0.002	0.05	0.8	0.002	0.05	0.3	0.002	0.05	0.45	0.03	0.06	0.3
	P08 L15	S2	757	757	757	0.28	0.30	0.38	0.002	0.05	0.5	0.002	0.05	0.8	0.002	0.05	0.3	0.002	0.05	0.45	0.03	0.06	0.3
		S3	757	757	757	0.28	0.30	0.38	0.002	0.05	0.5	0.002	0.05	0.8	0.002	0.05	0.3	0.002	0.05	0.45	0.03	0.06	0.3
		S4	757	757	757	0.28	0.30	0.38	0.002	0.05	0.5	0.002	0.05	0.8	0.002	0.05	0.3	0.002	0.05	0.45	0.03	0.06	0.3
P08 L30	S2	801	801	801	0.28	0.30	0.38	0.002	0.05	0.5	0.002	0.05	0.8	0.002	0.05	0.3	0.002	0.05	0.45	0.03	0.06	0.3	
	S3	801	801	801	0.28	0.30	0.38	0.002	0.05	0.5	0.002	0.05	0.8	0.002	0.05	0.3	0.002	0.05	0.45	0.03	0.06	0.3	
	S4	801	801	801	0.28	0.30	0.38	0.002	0.05	0.5	0.002	0.05	0.8	0.002	0.05	0.3	0.002	0.05	0.45	0.03	0.06	0.3	
W14 P04 L15	S2	800	800	800	0.28	0.30	0.37	0.002	0.05	0.5	0.002	0.05	0.8	0.002	0.05	0.3	0.002	0.05	0.45	0.03	0.06	0.3	
		S3	800	800	800	0.28	0.30	0.37	0.002	0.05	0.5	0.002	0.05	0.8	0.002	0.05	0.3	0.002	0.05	0.45	0.03	0.06	0.3
		S4	800	800	800	0.28	0.30	0.37	0.002	0.05	0.5	0.002	0.05	0.8	0.002	0.05	0.3	0.002	0.05	0.45	0.03	0.06	0.3
	P04 L30	S2	915	915	915	0.28	0.30	0.37	0.002	0.05	0.5	0.002	0.05	0.8	0.002	0.05	0.3	0.002	0.05	0.45	0.03	0.06	0.3
		S3	915	915	915	0.28	0.30	0.37	0.002	0.05	0.5	0.002	0.05	0.8	0.002	0.05	0.3	0.002	0.05	0.45	0.03	0.06	0.3
		S4	915	915	915	0.28	0.30	0.37	0.002	0.05	0.5	0.002	0.05	0.8	0.002	0.05	0.3	0.002	0.05	0.45	0.03	0.06	0.3
	P08 L15	S2	765	765	765	0.28	0.30	0.37	0.002	0.05	0.5	0.002	0.05	0.8	0.002	0.05	0.3	0.002	0.05	0.45	0.03	0.06	0.3
		S3	765	765	765	0.28	0.30	0.37	0.002	0.05	0.5	0.002	0.05	0.8	0.002	0.05	0.3	0.002	0.05	0.45	0.03	0.06	0.3
		S4	765	765	765	0.28	0.30	0.37	0.002	0.05	0.5	0.002	0.05	0.8	0.002	0.05	0.3	0.002	0.05	0.45	0.03	0.06	0.3
P08 L30	S2	822	822	822	0.28	0.30	0.37	0.002	0.05	0.5	0.002	0.05	0.8	0.002	0.05	0.3	0.002	0.05	0.45	0.03	0.06	0.3	
	S3	822	822	822	0.28	0.30	0.37	0.002	0.05	0.5	0.002	0.05	0.8	0.002	0.05	0.3	0.002	0.05	0.45	0.03	0.06	0.3	
	S4	822	822	822	0.28	0.30	0.37	0.002	0.05	0.5	0.002	0.05	0.8	0.002	0.05	0.3	0.002	0.05	0.45	0.03	0.06	0.3	
W20 P04 L15	S2	809	809	809	0.28	0.30	0.36	0.002	0.05	0.5	0.002	0.05	0.8	0.002	0.05	0.3	0.002	0.05	0.45	0.03	0.06	0.3	
		S3	809	809	809	0.28	0.30	0.36	0.002	0.05	0.5	0.002	0.05	0.8	0.002	0.05	0.3	0.002	0.05	0.45	0.03	0.06	0.3
		S4	809	809	809	0.28	0.30	0.36	0.002	0.05	0.5	0.002	0.05	0.8	0.002	0.05	0.3	0.002	0.05	0.45	0.03	0.06	0.3
	P04 L30	S2	939	939	939	0.28	0.30	0.36	0.002	0.05	0.5	0.002	0.05	0.8	0.002	0.05	0.3	0.002	0.05	0.45	0.03	0.06	0.3
		S3	939	939	939	0.28	0.30	0.36	0.002	0.05	0.5	0.002	0.05	0.8	0.002	0.05	0.3	0.002	0.05	0.45	0.03	0.06	0.3
		S4	939	939	939	0.28	0.30	0.36	0.002	0.05	0.5	0.002	0.05	0.8	0.002	0.05	0.3	0.002	0.05	0.45	0.03	0.06	0.3
	P08 L15	S2	769	769	769	0.28	0.30	0.36	0.002	0.05	0.5	0.002	0.05	0.8	0.002	0.05	0.3	0.002	0.05	0.45	0.03	0.06	0.3
		S3	769	769	769	0.28	0.30	0.36	0.002	0.05	0.5	0.002	0.05	0.8	0.002	0.05	0.3	0.002	0.05	0.45	0.03	0.06	0.3
		S4	769	769	769	0.28	0.30	0.36	0.002	0.05	0.5	0.002	0.05	0.8	0.002	0.05	0.3	0.002	0.05	0.45	0.03	0.06	0.3
P08 L30	S2	835	835	835	0.28	0.30	0.36	0.002	0.05	0.5	0.002	0.05	0.8	0.002	0.05	0.3	0.002	0.05	0.45	0.03	0.06	0.3	
	S3	835	835	835	0.28	0.30	0.36	0.002	0.05	0.5	0.002	0.05	0.8	0.002	0.05	0.3	0.002	0.05	0.45	0.03	0.06	0.3	
	S4	835	835	835	0.28	0.30	0.36	0.002	0.05	0.5	0.002	0.05	0.8	0.002	0.05	0.3	0.002	0.05	0.45	0.03	0.06	0.3	

Table F2 Explanation of Bearing 1 and 2 associated with different bridge classes.

Bridge	Bearing 1	Bearing 2	BR
PMG-I	Monolithic joint Type 2 at the abutments	Monolithic joint Type 2 at the piers	1-8
PMG-NI	Elastomeric bearing at some piers and the abutments	Monolithic joint Type 2 at other piers	9-12
SLAB	Monolithic joint Type 1 at the abutments	Monolithic joint Type 2 at the piers	12-16
BR23	Monolithic joint Type 2 at the abutments	Conventional bearings at the piers	23
OTHER	Conventional bearings at the abutments	Conventional bearings at the piers	Other

Table F3 Median capacity values of portfolio bridges for LS1-LS3 damage limit states.

BR	Pier						Bearing 1 - deformation [m]						Bearing 2 - deformation [m]						Backfill		
	Shear [kN]			Flexural [%]			Longitudinal			Transverse			Longitudinal			Transverse			Deformation [m]		
	LS1	LS2	LS3	LS1	LS2	LS3	LS1	LS2	LS3	LS1	LS2	LS3	LS1	LS2	LS3	LS1	LS2	LS3	LS1	LS2	LS3
01	905	905	905	0.28	0.30	0.40	0.002	0.05	0.5	0.002	0.05	0.45	0.002	0.05	0.4	0.002	0.05	0.4	0.03	0.06	0.3
02	877	877	877	0.28	0.30	0.39	0.002	0.05	0.5	0.002	0.05	0.45	0.002	0.05	0.4	0.002	0.05	0.4	0.03	0.06	0.3
03	743	743	743	0.28	0.30	0.38	0.002	0.05	0.45	0.002	0.05	0.45	0.002	0.05	0.45	0.002	0.05	0.45	0.03	0.06	0.3
04	1295	1295	1295	0.28	0.30	0.38	0.002	0.05	0.5	0.002	0.05	0.45	0.002	0.05	0.45	0.002	0.05	0.45	0.03	0.06	0.3
05	800	800	800	0.28	0.30	0.36	0.002	0.05	0.55	0.002	0.05	0.55	0.002	0.05	0.55	0.002	0.05	0.45	0.03	0.06	0.3
06	781	781	781	0.28	0.30	0.36	0.002	0.05	0.5	0.002	0.05	0.5	0.002	0.05	0.5	0.002	0.05	0.45	0.03	0.06	0.3
07	658	658	658	0.28	0.30	0.37	0.002	0.05	0.5	0.002	0.05	0.3	0.002	0.05	0.45	0.002	0.05	0.45	0.03	0.06	0.3
08	872	872	872	0.28	0.30	0.47	0.002	0.05	0.45	0.002	0.05	0.6	0.002	0.05	0.4	0.002	0.05	0.4	0.03	0.06	0.3
09	1460	1460	1460	0.28	0.30	0.48	0.075	0.45	0.45	0.075	0.6	0.6	0.075	0.45	0.4	0.002	0.05	0.4	0.03	0.06	0.3
10	1178	1178	1178	0.28	0.30	0.39	0.075	0.45	0.45	0.075	0.6	0.6	0.075	0.45	0.4	0.002	0.05	0.4	0.03	0.06	0.3
11	2140	2140	2140	0.28	0.30	0.40	0.075	0.45	0.45	0.075	0.6	0.6	0.075	0.45	0.4	0.002	0.05	0.4	0.03	0.06	0.3
12	850	850	850	0.28	0.30	0.36	0.065	0.45	0.45	0.065	0.6	0.6	0.065	0.45	0.4	0.002	0.05	0.4	0.03	0.06	0.3
13	835	835	835	0.28	0.30	0.38	0.002	0.05	0.4	0.002	0.05	2.4	0.002	0.05	0.4	x	x	x	0.03	0.06	0.3
14	2800	2800	2800	0.28	0.30	0.38	0.002	0.05	0.5	0.002	0.05	2.5	0.002	0.05	0.4	x	x	x	0.03	0.06	0.3
15	745	745	745	0.28	0.30	0.38	0.002	0.05	0.5	0.002	0.05	4.3	0.002	0.05	0.4	x	x	x	0.03	0.06	0.3
16	635	635	635	0.28	0.30	0.39	0.002	0.05	0.5	0.002	0.05	3.25	0.002	0.05	0.4	x	x	x	0.03	0.06	0.3
17	11780	11780	11780	0.28	0.30	0.36	0.5	0.5	1	0.5	0.5	5.5	0.5	0.5	1	0.5	0.5	3	0.03	0.06	0.3
18	11800	11800	11800	0.28	0.30	0.39	0.5	0.5	1.4	0.5	0.5	7	0.5	0.5	1	0.5	0.5	2.5	0.03	0.06	0.3
19	12500	12500	12500	0.28	0.30	0.37	0.5	0.5	1	0.5	0.5	8.5	0.5	0.5	1.4	0.5	0.5	3	0.03	0.06	0.3
20	21100	21100	21100	0.28	0.30	0.37	0.5	0.5	0.9	0.5	0.5	7	0.5	0.5	0.9	0.5	0.5	4.5	0.03	0.06	0.3
21	92300	92300	92300	0.28	0.30	0.40	0.5	0.5	1.3	0.5	0.5	7	0.5	0.5	0.9	0.5	0.5	4	0.03	0.06	0.3
22	6300	6300	6300	0.28	0.30	0.37	0.5	0.5	0.5	0.5	0.5	5.5	0.5	0.5	0.6	0.5	0.5	1.2	0.03	0.06	0.3
23	2100	2100	2100	0.28	0.30	0.38	0.002	0.05	0.5	0.002	0.05	7	0.002	0.05	0.5	x	x	0.55	0.03	0.06	0.3
24	2950	2950	2950	0.28	0.30	0.38	0.5	0.5	0.5	0.5	0.5	7	0.5	0.5	0.8	0.5	0.5	0.8	0.03	0.06	0.3
25	1750	1750	1750	0.28	0.30	0.43	0.5	0.5	0.6	0.5	0.5	7	0.5	0.5	0.7	0.5	0.5	0.7	0.03	0.06	0.3
26	7700	7700	7700	0.28	0.30	0.37	0.5	0.5	0.6	0.5	0.5	7	0.5	0.5	0.6	0.5	0.5	1	0.03	0.06	0.3
27	7700	7700	7700	0.28	0.30	0.38	0.5	0.5	0.6	0.5	0.5	7	0.5	0.5	0.6	0.5	0.5	1	0.03	0.06	0.3
28	7350	7350	7350	0.28	0.30	0.38	0.5	0.5	1	0.5	0.5	7	0.5	0.5	0.75	0.5	0.5	0.75	0.03	0.06	0.3
29	33600	33600	33600	0.28	0.30	0.40	0.5	0.5	1	0.5	0.5	11	0.5	0.5	1.85	0.5	0.5	1.75	0.03	0.06	0.3
30	7250	7250	7250	0.28	0.30	0.39	0.5	0.5	1	0.5	0.5	7	0.5	0.5	0.75	0.5	0.5	1.75	0.03	0.06	0.3

## *Appendix G: Fragility parameters of the examined bridges*

The following tables illustrate the system fragility curve parameters (median:  $\theta_{fr}$ ; dispersion:  $\beta_{fr}$ ) based on the parametric fragility analysis of PMG-I bridges (Table G1), and the fragility analysis of portfolio bridges (Table G2).

Table G1 Fragility curve parameters for PMG-I bridges.

Correlation Configuration	LS1				LS2				LS3				
	No		Full		No		Full		No		Full		
	$\theta_{fr}$	$\beta_{fr}$											
W08 P04 L15 S2	2.95	0.36	2.95	0.36	7.72	0.39	9.25	0.42	7.46	0.41	9.25	0.46	
	2.66	0.35	2.66	0.35	6.15	0.41	8.41	0.43	5.91	0.45	9.17	0.54	
	2.20	0.32	2.21	0.33	4.38	0.39	5.80	0.42	4.10	0.41	5.95	0.49	
	P04 L30 S2	1.31	0.39	1.31	0.39	3.25	0.42	4.00	0.45	3.28	0.49	4.36	0.54
		1.26	0.38	1.26	0.38	2.61	0.48	3.54	0.52	2.52	0.50	3.78	0.57
		1.12	0.45	1.13	0.46	2.05	0.52	2.52	0.54	2.01	0.55	2.73	0.60
	P08 L15 S2	2.66	0.35	2.66	0.35	16.45	0.26	18.71	0.27	19.16	0.37	24.34	0.41
		2.23	0.32	2.23	0.32	10.85	0.22	11.14	0.22	15.64	0.36	20.24	0.37
		1.61	0.35	1.61	0.35	8.87	0.35	10.28	0.33	10.01	0.47	14.96	0.55
	P08 L30 S2	1.18	0.38	1.18	0.38	7.22	0.39	7.70	0.38	9.44	0.46	11.36	0.48
		1.08	0.42	1.08	0.42	5.39	0.55	5.90	0.54	6.33	0.59	8.01	0.61
		1.02	0.60	1.02	0.60	3.95	0.76	4.30	0.78	4.51	0.77	5.29	0.80
W14 P04 L15 S2	2.91	0.37	2.92	0.37	7.14	0.36	9.39	0.41	6.85	0.40	9.49	0.46	
	2.60	0.34	2.60	0.34	5.80	0.39	8.18	0.39	5.50	0.43	8.80	0.51	
	2.09	0.36	2.09	0.36	4.33	0.38	6.37	0.40	4.01	0.41	6.91	0.50	
	P04 L30 S2	1.36	0.38	1.37	0.39	3.28	0.38	4.25	0.39	3.30	0.45	4.62	0.47
		1.24	0.43	1.26	0.44	2.63	0.47	3.75	0.51	2.53	0.51	4.26	0.59
		1.04	0.46	1.06	0.47	1.89	0.45	2.55	0.52	1.85	0.48	2.79	0.57
	P08 L15 S2	2.72	0.34	2.72	0.34	16.25	0.25	20.06	0.27	17.26	0.29	23.29	0.35
		2.20	0.32	2.20	0.32	11.39	0.23	11.91	0.24	15.93	0.36	22.03	0.36
		1.70	0.35	1.70	0.35	9.18	0.29	9.55	0.29	12.32	0.45	18.16	0.45
	P08 L30 S2	1.24	0.39	1.24	0.39	8.28	0.35	8.65	0.35	12.99	0.45	15.54	0.40
		1.16	0.44	1.16	0.44	5.98	0.48	6.58	0.48	7.64	0.53	10.23	0.54
		1.00	0.58	1.00	0.58	4.08	0.67	4.67	0.68	4.75	0.66	5.97	0.67
W20 P04 L15 S2	2.93	0.38	2.94	0.39	6.91	0.36	9.56	0.40	6.61	0.39	9.73	0.45	
	2.59	0.36	2.59	0.35	5.43	0.38	8.11	0.38	5.07	0.40	8.58	0.47	
	2.00	0.37	2.00	0.37	4.09	0.36	6.39	0.38	3.85	0.41	7.01	0.49	
	P04 L30 S2	1.35	0.39	1.35	0.39	3.37	0.36	4.65	0.39	3.38	0.43	5.15	0.47
		1.30	0.43	1.31	0.44	2.70	0.41	3.90	0.44	2.63	0.45	4.33	0.51
		1.05	0.45	1.07	0.47	1.91	0.44	2.64	0.47	1.84	0.48	2.88	0.54
	P08 L15 S2	2.67	0.35	2.67	0.35	14.93	0.25	18.35	0.25	15.46	0.30	21.20	0.37
		2.24	0.32	2.24	0.32	11.70	0.25	12.06	0.25	15.60	0.35	21.70	0.31
		1.69	0.37	1.69	0.37	8.35	0.31	8.62	0.31	10.53	0.42	15.31	0.38
	P08 L30 S2	1.18	0.42	1.18	0.42	8.31	0.33	8.92	0.33	10.66	0.35	14.17	0.39
		1.19	0.44	1.19	0.44	5.88	0.46	6.36	0.45	8.13	0.56	10.11	0.54
		1.01	0.56	1.00	0.55	4.59	0.71	5.16	0.69	5.49	0.74	7.06	0.76

Table G2 Fragility curve parameters for portfolio bridges.

Correlation Configuration	LS1				LS2				LS3			
	No		Full		No		Full		No		Full	
	$\theta_{fr}$	$\beta_{fr}$										
BR 01	2.01	0.39	2.28	0.43	4.70	0.34	5.39	0.37	4.70	0.34	5.39	0.37
02	1.99	0.38	2.24	0.43	6.69	0.27	8.07	0.31	6.73	0.27	8.08	0.31
03	0.65	1.35	0.81	1.22	3.15	0.44	4.46	0.49	3.16	0.46	4.52	0.50
04	1.53	0.36	1.66	0.37	8.08	0.31	9.16	0.32	14.09	0.37	17.83	0.40
05	1.82	0.33	2.01	0.37	5.08	0.38	6.04	0.42	5.20	0.40	6.11	0.43
06	2.22	0.37	2.50	0.37	9.66	0.33	12.04	0.34	10.90	0.39	14.70	0.45
07	1.21	0.47	1.32	0.50	4.45	0.51	5.16	0.55	4.51	0.53	5.21	0.56
08	1.40	0.37	1.54	0.38	2.89	0.43	3.53	0.49	2.90	0.44	3.56	0.47
09	1.03	0.50	1.49	0.55	1.03	0.51	1.47	0.58	1.02	0.50	1.49	0.55
10	1.69	0.72	2.28	0.71	1.70	0.71	2.28	0.67	1.71	0.71	2.25	0.71
11	1.34	0.73	1.80	0.68	1.39	0.69	1.83	0.65	1.40	0.71	1.82	0.65
12	1.81	1.26	2.59	0.88	2.56	1.32	3.77	0.83	2.84	1.37	4.17	0.85
13	2.28	0.39	2.47	0.43	8.52	0.40	10.49	0.44	9.51	0.46	11.13	0.47
14	1.61	0.34	1.78	0.39	2.74	0.34	3.19	0.38	2.75	0.34	3.21	0.38
15	1.48	0.38	1.63	0.39	4.00	0.42	5.04	0.46	4.20	0.44	5.26	0.50
16	1.40	0.42	1.64	0.43	1.84	0.45	2.38	0.48	1.82	0.45	2.35	0.47
17	4.30	0.58	4.40	0.59	7.30	0.56	7.98	0.57	8.32	0.53	8.90	0.57
18	2.89	0.73	3.04	0.74	5.36	0.66	5.80	0.69	6.22	0.67	6.69	0.67
19	5.13	0.62	5.64	0.60	6.13	0.58	7.34	0.57	6.64	0.53	7.62	0.54
20	2.04	1.19	2.08	1.21	5.94	0.44	6.21	0.45	6.68	0.43	7.09	0.46
21	3.49	0.54	3.46	0.56	6.67	0.50	6.82	0.51	7.26	0.53	7.43	0.55
22	1.35	0.65	1.49	0.66	3.34	0.37	3.82	0.39	3.91	0.37	4.33	0.40
23	1.24	0.46	1.34	0.46	6.90	0.38	7.46	0.40	16.92	0.41	21.27	0.40
24	0.99	0.51	1.12	0.50	0.99	0.49	1.13	0.50	0.99	0.48	1.12	0.50
25	0.76	1.33	1.06	1.18	0.76	1.34	0.99	1.37	0.75	1.33	1.06	1.19
26	1.73	0.68	1.94	0.71	3.58	0.46	4.14	0.51	4.32	0.43	5.21	0.49
27	1.59	0.68	1.94	0.70	3.53	0.46	4.47	0.51	4.41	0.42	5.59	0.48
28	3.60	0.74	3.82	0.75	5.11	0.70	5.45	0.71	6.54	0.64	7.07	0.65
29	5.26	0.62	5.40	0.62	7.06	0.54	7.44	0.54	7.51	0.51	7.94	0.52
30	2.55	1.37	3.13	0.89	4.51	0.79	5.00	0.80	6.14	0.74	6.99	0.77

## *Appendix H: New scientific results in Hungarian*

### ***I. Tézis (Simon and Vigh 2013a, 2015c, 2016b)***

Megvizsgáltam Magyarország szeizmikus veszélyeztetettségét és összehasonlító vizsgálatot végeztem helyszíni és az Eurocode 8-1 által javasolt szabványos spektrumok között.

- I/a Egy valószínűségi szeizmikus veszélyeztetettségi vizsgálati rendszert és egy általános feltételes intenzitásjellemző alapú rekordkiválasztó rendszert alkalmaztam magyarországi körülményekre, valamint létrehoztam egy ingyenesen hozzáférhető, mesterséges rekord generáló programot.
- I/b Megmutattam, hogy magyarországi helyszínek esetén a tervezési szinthez tartozó veszélyeztetettséghez mérsékelt magnitúdójú (<5.5) és kis epicentrális távolságú (<10 km) földrengések járulnak hozzá leginkább, valamint hogy a várható szignifikáns rengésidő 10 s alatt van.
- I/c Ráműtattam, hogy magyarországi helyszínek esetén az Eurocode 8-1 által javasolt 2-es típusú spektrum jobban jellemzi a tényleges helyszíni spektrumot, mint az 1-es típusú spektrum.
- I/d A különböző intenzitásjellemzők elemzésével igazoltam, hogy a hidak szerkezeti válaszait a szerkezeti választ döntően meghatározó rezgés periódusidejéhez rendelhető spektrális gyorsulás és a spektrális intenzitás írja le legjobban.

### ***II. Tézis (Simon and Vigh 2015a; Simon et al. 2016)***

Kidolgoztam egy törekenységi vizsgálat alapú kiértékelő keretrendszert magyarországi közúti hidak szeizmikus teljesítőképességének meghatározására.

- II/a Részletesen kidolgoztam 5 különálló (adatbázis, szeizmikus teher előállító, numerikus modell generáló, szeizmikus analízis és kiértékelő) modult, melyek összekapcsolásával automatizáltam a kiértékelési folyamatot.
- II/b Elemeztem az adatbázis alkalmazhatóságát a teljes hídállomány szeizmikus teljesítőképességének kiértékelése szempontjából. Kimutattam a meglévő adatbázis hiányosságait, majd ajánlatot tettem az adatbázis kibővítésének stratégiájára.
- II/c A teljes hídállományt megfelelően jellemző 8 típusszerkezetet határoztam meg, és jellemeztem a típusszerkezetek legfontosabb szerkezeti paramétereit. Létrehoztam egy 30 reprezentatív hídból álló hídportfóliót.

### **III. Tézis (Simon and Vigh 2014, 2015b, 2016a)**

Közelítő lineáris modális válaszspektrumon alapuló paraméteres vizsgálatot hajtottam végre monolit kapcsolatú sűrűbordás és lemezhidakra.

- III/a Kidolgoztam a szerkezetek lineáris numerikus modelljét és javaslatot tettem a háttöltés hatásának modellezésére lineáris modális válaszspektrum analízis esetén.
- III/b Meghatároztam a kritikus kialakítások és komponensek körét tipikus hídszerkezetek esetén, és megmutattam, hogy a felszerkezet, a hídfő, a háttöltés és az alapozás viselkedése megfelelő; a monolit kapcsolatok teherbírása elégtelen, főleg a hídfő-felszerkezet kapcsolat esetén. Tipikus pillérvasalást feltételezve megmutattam, hogy hosszabb hidaknál (>50 m) alacsonyabb pillérek (<5 m) esetén a nyírási, míg magasabb pillérek (>5 m) esetén a hajlítási teherbírás kritikus.
- III/c Az Eurocode 8-2 szerinti szabványos kiértékelés alapján egy előzetes becslést adtam a kritikus sűrűbordás és lemezhidak számára.

### **IV. Tézis (Simon 2012, 2013; Simon and Vigh 2015b, 2016a; Simon et al. 2016)**

Paraméteres törékenységi vizsgálatot hajtottam végre monolit kapcsolatú sűrűbordás hidakra, valamint elvégeztem 30 olyan meglévő szerkezet törékenységi vizsgálatát, melyek jól reprezentálják a hídállomány tipikus hídszerkezeteit.

- IV/a Kidolgoztam az egyes típus szerkezetek nemlineáris numerikus modelljét. Kidolgoztam és kalibráltam a nyírási vasalással ellátott monolit kapcsolat ciklikus numerikus modelljét. Nemlineáris Winkler-ágyazású gerendamodellen alapuló cölöpalapozási modellt hoztam létre, melynek paramétereinek felvételére az Eurocode 7-tel és a magyar tervezési elvekkel összhangban adtam javaslatot.
- IV/b Elemeztem a különböző modellezési és analízissel kapcsolatos feltételezések szerkezeti válaszokra gyakorolt hatását. Rámutattam a monolit kapcsolat ciklikus viselkedésének és az ütközések modellezésének a fontosságára. Megmutattam, hogy a geometriai bizonytalanság elhanyagolható, míg az anyagjellemzők és a talajjellemzők bizonytalansága jelentősen befolyásolhatja a számított tönkremeneteli valószínűséget.
- IV/c A komponens törékenységi görbék alapján meghatároztam a kritikus hídkomponensek körét. Igazoltam a paraméteres vizsgálat következtetéseit monolit kapcsolatú sűrűbordás és lemezhidakra, valamint megmutattam, hogy a pillér nyírási tönkremenetele domináns számos híd típus esetén. Rámutattam, hogy a hagyományos sarus acél gerendahidak viselkedése kedvezőbb, hajlítási tönkremenetel jellemezhető.

IV/d Kiértékeltem tipikus közúti hidak megbízhatóságát, a megbízhatósági index alapján összehasonlítottam az egyes szerkezetek szeizmikus teljesítőképességét. Megmutattam, hogy a nem megfelelő szerkezeti kialakítás és a szeizmikus tervezés hiánya extrém alacsony megbízhatósági indexet eredményezhet, valamint hogy az EC8-2 alapú tervezéssel 2 körüli megbízhatósági index érhető el.

***V. Tézis (Simon and Vigh 2013b, 2013c; Simon et al. 2015)***

Javaslatot tettem a kritikus szerkezetek megerősítési módjaira, valamint új szerkezetek tervezéséhez tervezési koncepciókat adtam meg.

V/a Ráműtattam, hogy a hídfőknél monolit kapcsolat, a pilléreknel hosszirányú fix és keresztirányban mozgó saruk alkalmazása optimális kialakítás maximum 100 méteres autópálya felüljáró hidak esetén.

V/b Kiértékeltem két reprezentatív kritikus híd megerősítési módszereit. Megmutattam, hogy a pillérek szénszál erősítésű polimeres erősítése optimális, helytakarékos megoldás olyan esetben, amikor a megbízhatóság kis mértékű növelése szükséges, míg beton köpenyezéssel jelentős növekedés érhető el. Nem megfelelő szerkezeti kialakítás esetén a szeizmikus szigetelés költséghatékony megoldás.

V/c Értékeltem az Eurocode 8-2 által javasolt ekvivalens lineáris analízis módszer pontosságát nemlineáris időtörténeti analízis segítségével; és javaslatot tettem a módszer módosított alkalmazására szeizmikus szigetelések koncepcionális tervezéséhez, melynek alkalmazhatóságát igazoltam egy valós hídmegerősítés során.

